The Effect of Nanoscale and Micron Sized Alumina and Cobalt Chromium Particles on Plasma Membrane Integrity

Ruth Thurza Craven

Submitted in accordance with the requirements for the degree of

Doctor of Philosophy

The University of Leeds

School of Mechanical Engineering

October 2016

The candidate confirms that the work submitted is her own and that appropriate credit has been given where reference has been made to the work of others.

Acknowledgements

There are a number of people I would like to thank during my PhD studies. I would like to express my sincere gratitude to all my supervisors, Prof. Joanne Tipper, Dr. Lars Jeuken and Dr. Sophie Williams whose complementary knowledge and skills made this project possible. I would like to thank Prof. Tipper for all her help and support. Even during the never ending string of negative experimental results she was unrelenting in her guidance and encouragement, which was a testament to her patience and professionalism. Thank you to Dr. Jeuken for his innovative ideas and extensive expertise, which really helped guide this project. I would also like to thank Dr. Williams for her help, especially with the engineering side of my project. Her advice, sense of fun and thought provoking questions really helped me throughout my project.

During my PhD project I worked in a number of laboratories. First I would like to thank Prof. Eileen Ingham's research group, past and present, for their support, in particular Dr. Chris Brown, Dr. Iraklis Papageorgiou and Mrs Sha Zhang. I would also like to thank Dr. Daniel Thomas and the technical team for keeping the laboratory running so efficiently. I would like to express my gratitude to Dr. Jeuken's research group for all their help, especially Mrs. Riitta Partanen for her kindness and patience. I would also like to express my gratitude to the MNP laboratory in Physics, with special thanks to Dr. Ben Shepherd for his advice on QCM-D. Lastly, I would like to express my appreciation to Phil Wood and the technical team in Mechanical Engineering for their help whilst using the pin-on-plate wear rig.

I would also like to thank my peers during my time at Leeds. In particular, Rachel Pallen, Liam Lawlor, the "Sheffield Lot" and the members of my office for their support and constant supply of food. Their unwavering sense of humour helped me keep things in perspective and they were a joy to work with.

I would also like to sincerely thank past supervisors and mentors for encouraging me to undertake my PhD studies, with a special thank you to Prof. Ingham for her support and kindness. I am extremely grateful and honoured to have worked in her group.

I would like to thank my family and friends for all their help. To my parents, Robert and Margaret and sisters, Helen and Mary; thank you for all the encouragement and for listening to me when things got tough. And of course thank you to my husband, Philip. I am very grateful for all the love and support he gave me over the past 5 years. His advice, compassion and his belief in me this made this all possible. Finally to my beautiful daughter, Elizabeth, whilst this thesis maybe a bit beyond your reading ability at the moment; I dedicate it to you.

Abstract

Under optimum conditions, alumina ceramic-on-ceramic and cobalt chromium (CoCr) metal-on-metal prostheses have low wear rates with the generation of predominately nanoscale wear particles. Delayed type IV hypersensitivity reactions and pseudotumours have been reported in patients with metal-on-metal prostheses. *In vitro* studies have revealed that CoCr, and to a lesser extent, alumina wear particles induce cytotoxic, genotoxic, and pro-inflammatory responses. Little is known about the mechanism of how the wear particles induce toxic effects, in particular how particles interact with the cell membrane. The aim of this study was to determine if CoCr and alumina particles were able to damage the cell membrane with toxic consequences or whether they passed through the membrane and exerted toxic effects intracellularly.

Cobalt chromium (mode size 40 – 49 nm) nanoscale particles were generated using a pin-on-plate tribometer and compared against commercially available micron sized CoCr (mode size 2 – 3 μm) particles. Micron sized alumina (mode size 400 – 450 nm) particles were isolated *via* filtration methods and nanoscale alumina (mode size 30 – 39 nm) particles were obtained from a commercially available source. All particle stocks were characterised using TEM, EDX, and compared against the published literature. The effect of the particles on the integrity of a model membrane was assessed using vesicle leakage assays. None of the particle types tested induced extensive vesicle leakage, even in the presence of 10% (v/v) serum, or with isolated membrane proteins incorporated into the lipid vesicles. Particle binding to a solid supported bilayer lipid membrane (sBLM) was assessed using quartz crystal microbalance with dissipation (QCM-D) methods. Weak interactions with the membrane were observed by an increase in the dissipation measurements. In the presence of serum and with isolated primary fibroblast membrane proteins within the sBLM, nanoscale and micron sized alumina particles bound to the membrane at particle concentrations of 10 and 100 $\mu g.ml^{-1}$. However, this did not occur for the nanoscale and micron sized CoCr particles. These results demonstrated that the

formation of a protein corona and the presence of membrane proteins are critical for alumina particle binding to a model membrane system. However, membrane binding does not necessarily correlate to particle toxicity. Further experiments, such as investigating if the particles are actively taken up by the cells, is required to understand the interaction of nanoscale a micron sized CoCr particles with the cell membrane.

Table of Contents

List of Tables

List of Figures

List of Abbreviations

Al_2O_3	Alumina
ALVAL	Aseptic lymphocytic vasculitis-associated lesions
ANOVA	One way analysis of variance
ARMD	Adverse reaction to metal debris
ASR™	Acetabular surface replacement
ATP	Adenosine triphosphate
BCA	Bicinchoninic acid
BSA	Bovine serum albumin
CF	Carboxylfluorescein
CO_2	Carbon dioxide
CoCr	Cobalt-chromium
CPS	Counts per second
CRP	C reactive protein
DDSA	Dodecenylsuccinic anhydride
DMEM	Dulbecco's modified eagles medium
DMP30	2,4,6-Tris(dimethylaminomethyl)phenol
DMSO	Dimethyl sulphoxide
DMT-1	Divalent metal transporter 1
DPBS	Dulbecco's phosphate buffered saline
DTT	Dithiothreitol
EDTA	Ethylenediaminetetraacetic acid
EDX	Energy-dispersive X-ray spectroscopy
ESR	Erythrocyte sedimentation rate
EtO	Ethylene oxide
FCS	Foetal calf serum
FEGSEM	Field emission gun scanning electron microscopy

HA	Hydroxyapatite
HCl	Hydrogen chloride
HEK293	Embryonic kidney cell line
HFB	Human fibroblast
HIF-1	Hypoxia-inducible factor-1
HL-60	Human promyelocytic leukaemia
HSA	Human Serum Albumin
H_2O_2	Hydrogen peroxide
IARC	International Agency for Research on Cancer
IL-6	Interleukin-6
KOH	Potassium hydroxide
LALLS	Low angle laser light scattering
L929	Fibroblast cell line
MAPK	Mitogen-activated protein kinase
MEM	Minimal essential medium
MOPS	3-(N-morpholino)propanesulfonic acid
MHRA	Medicines and Healthcare Products Regulatory Agency
MSD	Minimum significant difference
MTT	3-(4, 5-dimethylthiazol-2-yl)-2, 5 diphenyltetrazolium bromide
NA	Nutrient agar
Na_2SO_4	Sodium sulphate
NO•	Nitrogen oxide
OH•	Hydroxyl radical
OPG	Osteoprotegrin
PBMNC	Peripheral blood mononuclear cell
PCV	Packed cell volume
PGE_2	Prostaglandin E-2
PHD	Prolyl hydroxylases

PMMA	Polymethylmethacrylate
PMSF	Phenylmethanesulfonyl fluoride
POPC	1-palmitoyl-2-oleoyl-sn-glycero-3-phosphocholine
QCM	Quartz crystal microbalance
QCM-D	Quartz crystal microbalance with dissipation
Ra	Surface roughness
RBC	Red blood cell
RhoA	Ras homolog gene family, member A
ROS	Reactive oxygen species
RPMI	Roswell Park Memorial Institute
SAB	Sabouraud dextrose agar
sBLM	Solid supported bilayer lipid membrane
SDS	Sodium dodecyl sulphate
SEM	Scanning electron microscopy
SPR	Surface plasmon resonance
tBLM	Tethered bilayer lipid membrane
TEM	Transmission electron microscopy
THAs	Total hip arthroplasties
THP-1	Monocyte cell line
THRs	Total hip replacements
TJR	Total joint replacement
TNF-α	Tumour necrosis factor-alpha
UHMWPE	Ultra-high molecular weight polyethylene
U937	Histiocyte cell line
ZrO_2	Zirconia

Chapter 1
Introduction

1.1 Introduction

Total hip replacements (THRs) have been used reliably since the 1960s to reduce pain and improve mobility in patients with diseased joints, such as rheumatoid arthritis and osteoarthritis (Charnley and Cupic 1973; Caton and Prudhon 2011). Hip prostheses consist of a head and stem component, which replaces the natural femoral head and the acetabular cup of the pelvis (Figure 1.1) (Charnley and Cupic 1973). The continued success of THRs led to over 83,000 primary hip prostheses being implanted in England and Wales in 2014 (NJR 2015). Materials commonly used as bearing surfaces include ultra-high molecular weight polyethylene (UHMWPE), cobalt-chromium (CoCr), and alumina (Al_2O_3) -based ceramics. The cobalt chromium alloy consists of predominately cobalt with chromium and molybdenum. Alumina matrix composites (AMCs) have also been developed and include alumina toughened zirconia (ATZ) and zirconia toughened alumina (ZTA) (Isaac *et al.* 2006).

The majority of THRs are based upon the design of Sir John Charnley and consist of a low friction UHMWPE acetabular cup articulating against a metal or ceramic femoral head. The survivorship of the Charnley prosthesis has been excellent, with a 92% survival rate after 9 – 10 years, with some implants surviving up to 25 years (Charnley and Cupic 1973; Caton and Prudhon 2011). However, the performance in younger, more active patients has been reported to be less successful, with a reduction in the survival rate to 65% after 13.8 years in patients younger than 21 years (Bessette *et al.* 2003).

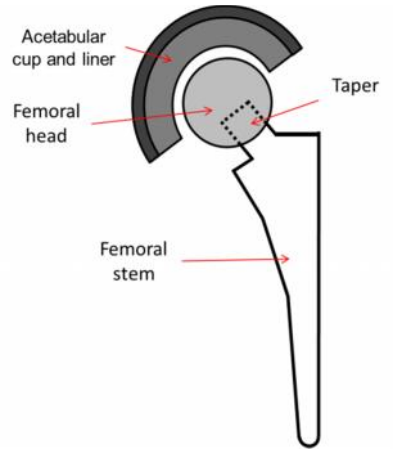

Figure 1.1 – Diagram of the main components of a total hip replacement

The early failure of THRs was partly attributed to UHMWPE wear particles generated and the subsequent biological reaction to them. UHMWPE wear particles have been associated with osteolysis, leading to aseptic loosening (Ingham and Fisher 2000). Osteolysis is proposed to be caused by the engulfment of the UHMWPE wear particles by surrounding macrophages, leading to frustrated phagocytosis and the release of inflammatory mediators. These signals can impact on the remodelling of the surrounding bone and can promote bone resorption (Ingham and Fisher 2000; Ingham and Fisher 2005). Once aseptic loosening is extensive enough to cause significant pain to the patient, then revision surgery is required (Holding *et al.* 2006). The high incidence of osteolysis of 24% for conventional UHMWPE-on-metal THR in patients less than 55 years old, five years after implantation, led to the development of alternative bearing surfaces in order to minimise wear (Mall *et al.* 2011). An increase in the popularity of hard-on-hard bearings occurred during the 1990s, such as the second generation metal-on-metal cobalt-chromium (Co-Cr) and alumina or zirconia (ZrO_2) based ceramic-on-ceramic THRs and hip resurfacing implants (Figure 1.2A&B) (Rieker *et al.* 1998; D'Antonio *et al.* 2012).

Large diameter metal-on-metal THRs and hip resurfacing bearings were introduced more recently to theoretically promote lubrication and hence reduce wear (McMinn 2012). Metal-on-metal hip resurfacing implants have large diameter femoral components (>36 mm) with a redesigned, shortened, femoral stem, thus preserving

patient bone stock (McMinn 2012). Moreover, it was thought that these types of bearings would improve joint mobility, such as range of motion and the reduce risk of dislocation, and therefore were marketed as an attractive alternative for younger patients (McMinn 2012).

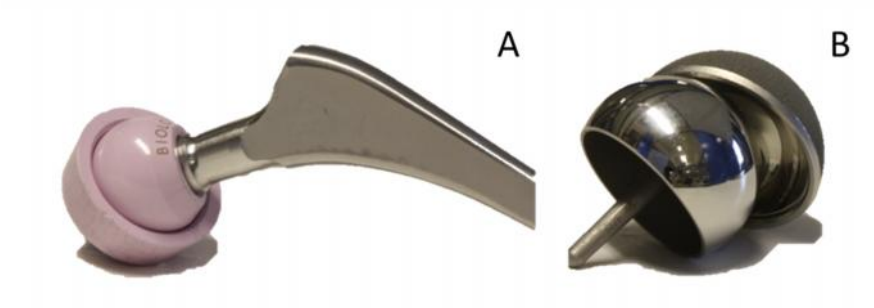

Figure 1.2 – Hard-on-hard total hip replacement bearings – (A) **C**eramic-on-ceramic (zirconia toughened alumina (ZTA) composite) implant. (B) Metal-on-metal hip resurfacing implant.

Recent reports have shown that large diameter CoCr bearings, particularly hip resurfacing implants, are susceptible to accelerated wear (Langton *et al.* 2011). It is thought that the suboptimal surgical implantation causes edge loading and disruption of the lubrication regime (Fisher 2011). Biological consequences, such as pseudotumours, hypersensitivity reactions, and necrosis have been reported in patients with metal-on-metal bearings and have been associated with the CoCr wear particles and ions generated (Willert *et al.* 2005; Pandit *et al.* 2008; Natu *et al.* 2012). This most notably led to the voluntary removal of the hip resurfacing implant, Acetabular Surface Replacement (ASR) by the manufacturer DePuy Synthes due to high early failure rates of 12% at 5 years (Langton *et al.* 2011; NJR 2011). The Medical and Healthcare Products Regulatory Agency (MHRA) have released a number of alerts on the use of large diameter metal-on-metal bearings. In particular, the MHRA released an alert in 2010 stating that all patients with metal-on-metal implants should be monitored closely 5 years post-operatively (MHRA 2010). However, this has been superseded by the MHRA alerts issued in 2012 and 2015 recommending that all patients with metal-on-

metal bearings should be monitored annually for the lifetime of the bearing and the use of metal-on-metal prostheses should be severely limited (MHRA 2012; MHRA 2015).

Following the concerns surrounding metal-on-metal THRs, the number of ceramic-on-ceramic bearings has risen, from 21% of all uncemented THRs in 2003 to 45% in 2011 in England and Wales (NJR 2015). This is due to metal-on-metal THRs often being replaced with ceramic bearings alongside UHWMPE-on-metal or UHWMPE–on-ceramic THRs in England and Wales (NJR 2015). However, ceramic-on-ceramic THRs are less popular in the USA, particularly following the poor longevity of the Mittelmeier prosthesis (Smith & Nephew) (Berry & Lieberman 2012). Historically ceramic-on-ceramic bearings have also been linked with incidences of squeaking or catastrophic failure of the implant (Jarrett *et al.* 2009; D'Antonio *et al.* 2012). Nevertheless, modern ceramic-on-ceramic THRs are rarely associated with osteolysis or other notable adverse tissue reactions (Niche *et al.* 2006; Amanatullah *et al.* 2011).

In vitro cellular studies have demonstrated that CoCr wear particles and ions can induce cytotoxic, genotoxic and inflammatory effects (Germain *et al.* 2003; Brown *et al.* 2006). However, these studies have provided limited information on the precise mechanism of how CoCr wear particles can cause larger scale problems in patients. In particular, little is known about how the particles interact with the cell membrane and subsequent internalisation of the particles. This is especially important as particle entry mechanisms can dictate the subsequent biological consequences of the particles (Canton and Battaglia 2012). Whilst alumina- based ceramic THRs are relatively inert, there are very limited studies on the internalisation and subsequent effects of alumina wear particles (Hashimoto and Imazato 2015). Therefore more research is required to gain a deeper understanding of how wear particles interact with the cell plasma membrane and how this can effect particle toxicity mechanisms.

1.2 Wear

Excessive wear can lead to failure of the total joint replacement (TJR) and adverse biological reactions to the generated wear particles (Fisher 1994; Stewart 2010). Five modes of wear can occur within THRs, which are abrasive, adhesive, fatigue, erosive, and corrosive (Affatato *et al.* 2008). During articulation of the THR bearing surfaces, more than one mode of wear can occur at one time. For UHMWPE components, it is proposed that fatigue and adhesion processes produce most of the wear debris (Fisher *et al.* 1991). Accelerated wear has been reported for polyethylene-on-metal THRs caused by third body wear. The third body wear debris, such as bone cement, can be embedded in the UHMWPE cup and causes roughening of the metal femoral head and subsequently increases asperity contact. Third body wear has also been reported for highly cross-linked UHMWPE prostheses (Kubo *et al.* 2009). Corrosive wear is limited to metallic materials, such as CoCr bearing surfaces, or metallic femoral stems and taper junctions and is described in more detail in Section 1.2.2.1.

Investigating the wear mechanisms of different bearing couples is important in reducing volumetric wear rates and hence survivability of the implant. In addition, the wear mechanisms can influence particle morphology and size. Three modes of lubrication theoretically exist within the THR environment and include boundary, mixed, and fluid-film lubrication. Boundary lubrication occurs when there is asperity contact between the two surfaces, whereas fluid lubrication is when the surfaces are separated by lubricant, causing minimal or no asperity contact. As the name suggests, mixed lubrication is a mixture of boundary and fluid lubrication (Jin *et al.* 2006). Prostheses comprised of UHMWPE-on-metal operate towards a boundary lubrication regime whereas metal-on-metal THRs have been reported to operate in the mixed lubrication regime, with the potential to operate towards the fluid-film lubrication regime. Jin *et al*. (1997) proposed the adapted lubrication theory, which stated that a reduction in wear would be observed with larger diameter heads, with a small radial clearance and low surface roughness. In hard-on-hard bearings, larger diameter heads cause an increase in the sliding distance

and hence increase the sliding speeds, which promote lubrication. Ceramic-on-ceramic THRs have been reported to operate under a mixed lubrication regime. However, due to the hardness of ceramic-on-ceramic THRs, the bearing surfaces are very smooth and therefore have minimal asperity contact and hence generate minimal wear under optimal conditions (Vassiliou *et al.* 2007).

1.2.1.1 Malpositioning of total hip replacements and accelerated wear

Malpositioning occurs when the femoral head component is not centric to the acetabular cup, causing head-to-cup edge contact. Rotational malpositioning of THRs is associated with steep inclination angles, whilst translational malpositioning is caused by the superior translation of the acetabular cup (Nevelos *et al.* 2000; Fisher 2011). Head to acetabular cup contact has been of particular interest for ceramic-on-ceramic and metal-on-metal implants as edge wear patterns have been observed on retrievals (Nevelos *et al.* 2000; Langton *et al.* 2010).

1.2.2 Wear of metal-on-metal total hip replacements

Optimal implantation of metal-on-metal THRs was associated with lower wear rates in comparison to UHMWPE-on-metal THRs. McKellop *et al.* (1996) reported average wear rates from retrieved McKee Farrar, Ring and Müller metal-on-metal THRs of 1.2, 2.3 and 3 mm^3 per year, respectively. Sieber *et al.* (1999) analysed the wear of 118 retreived metal-on-metal Metasul THRs and reported penetration rates of 5 μm^3 per year. Morlock *et al.* (2008) also revealed that retrieved metal-on-metal hip resurfacing implants had a wear rate of less than 1 mm^3 per year when no evidence edge loading was detected. Simulator studies of metal-on-metal THRs, using two directions of motion, that were out of phase, reproduced the wear scars and wear volumes of 1.23 $mm^3/ 10^6$ cycles, which was comparable to retrieval studies (Firkins *et al.* 2001a; Tipper *et al.* 2001).

The wear of metal-on-metal THRs is characterised by two distinct phases, known as the "running-in" phase, followed by the "steady-state" phase (Isaac *et al.* 2006). The running in phase typically occurs during the first million cycles, with a wear rate of 2 – 3 $mm^3/ 10^6$ cycles. Once the transition point of 0.5 million cycles is reached, the wear rate is reduced and eventually falls to a steady state of less than 0.1 $mm^3/ 10^6$ cycles (Dowson *et al.* 2004).

More recently wear rates for metal-on-metal hip resurfacing implants and THRs with large femoral head diameters (i.e. a diameter greater than 36 mm) have been reported to be higher due to edge loading. This has been characterised by high ion levels in the serum of patients with poorly functioning implants (Sampson and Hart 2012). Wear rates of 11.02 mm^3 per year have been reported for poorly functioning ASR™ implants, which is significantly higher than well-functioning implants (Lord *et al.* 2011). A major concern with the high wear rates is the dissemination of nanoscale wear particles from their site of release to other parts of the body. Indeed CoCr wear particles have been observed in the kidney, spleen, and distant lymph nodes (Case *et al.* 1994; Urban *et al.* 2004). Therefore there are concerns about the systemic effects of long-term exposure to CoCr wear particles and released ions.

The high failure rate of large diameter metal-on-metal implants is thought to be due to a number of factors, however rotational and translational malpositioning have been implicated (Fisher 2011). In particular, the ASR™ implant was reported to have cup coverage of only 160 degrees (Underwood *et al.* 2011). Truncated cup coverage reduces the tolerance to rotational and translational malpositioning and edge contact, and therefore there is an increase in contact stress and a disruption of the lubrication (Fisher 2011). These factors are thought to be the main contributors to the high wear rates observed for large diameter metallic bearings (Sariali *et al.* 2008; Sariali *et al.* 2009).

Variable wear rates associated with failed metal-on-metal implants are thought to be caused by factors other than acetabular cup angle alone (De Haan *et al.* 2008). Translational malpositioning has also been implicated for metal-on-metal bearings, which would elevate wear rates. Williams *et al.* (2013) revealed that the introduction of translational malpositioning elevated the wear rates of 36 mm large head diameter metal-on-metal THRs from 0.6 ± 0.18 $mm^3/10^6$ cycles under standard simulator conditions to 1.32 ± 0.91 $mm^3/10^6$ cycles under adverse simulator conditions. Furthermore Leslie *et al.* (2009) demonstrated a 17 fold increase in wear for metal-on-metal hip resurfacing implants at a high acetabular cup angle of 55° when tested under translational malpositioning conditions. Interestingly, these authors observed a greater variation in the wear of the implants when positioned at higher cup angles in comparison to standard conditions. In addition, Al-Hajjar *et al.* (2013b) also reported an increase in wear of 28 mm and 36 mm diameter metal-on-metal THRs when translational malpositioning was introduced alongside acetabular cup angles of 45° and 65°. In addition, the generation of a stripe wear corresponding to edge contact was observed in these implants. However, whilst the introduction of translational malpositioning increased the wear rates for the large head diameters of 36 mm, no significant difference in wear was observed between the two inclination angles.

1.2.2.1 Corrosion and ion release

The long-term survivability of hip implants containing metal components is also dependent on the resistance to corrosion (Yan *et al.* 2006). Metal corrosion can occur at the bearing surface of metallic components, at the stem: cement interface and any modular junctions of the stem component (Goldberg and Gilbert 2003). Most THRs contain metallic components such as a femoral stem and taper. Therefore corrosive wear can occur in all types of THRs, regardless of the composition of the THR bearing surfaces. Alongside this, wear at the taper junction, which predominately produces CoCr wear particles and ions, can occur. Retrieval studies have reported extensive

taper fretting and corrosion both at the head-neck and cone-taper interface, which is currently an increasing area of research within the field of THR wear (Langton *et al.* 2011; Cooper *et al.* 2012; Meyer *et al.* 2012; Rehmer *et al.* 2012; Baxmann *et al.* 2013). Furthermore, the metal wear particles generated can subsequently corrode, releasing metal ions (Billi and Campbell 2010).

Corrosion occurs during the simultaneous action of mechanical wear and corrosion on the metal surface (Virtanen *et al.* 2008). In hip implants, CoCr bearing surfaces are protected from corrosion by the formation of a chromium oxide (CrO_3) rich passive film. This passive film makes the CoCr alloy highly resistant to corrosion (Yan *et al.* 2006). During tribocorrosion of metal-on-metal implants, the mechanical action of the bearings articulating against one another can cause a localised breakdown of the passive film. This causes the surface to be exposed to the corrosive biological fluids and a shift from a passive to an active regime occurs (Yan *et al.* 2006). However, re-passivation can occur, which restores the passive film. Nevertheless, the constant breakdown and re-passivation of the film can lead to accelerated corrosion (Metikos-Hukovic and Babic 2007). Whilst the presence of proteins has been reported to promote lubrication and wear in metal-on-metal bearings, proteins can increase corrosion by the dissolution of the Cr ions causing the ions to form complexes with the proteins (Yan *et al.* 2006).

1.2.2.1.1 Chromium ion release from bearing surfaces

Chromium ions can exist as Cr(VI) and Cr (III),whereby Cr(VI) can undergo two mechanisms of reduction to Cr(III) as shown in Figure 1.3 (O'Brien 2003). The reduction process also causes the formation of radicals and as such Cr(VI) is classed as a group one human carcinogen by the International Agency for Research on Cancer (IARC) (O'Brien 2003).

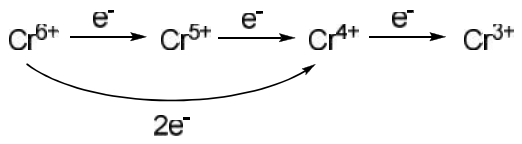

Figure 1.3 – Intracellular reduction of chromium ions. (O'Brien 2003)

Merritt and Brown (1995) reported high levels of chromium ions in red blood cells (RBCs) in comparison to serum samples from patients with metal-on-metal THRs or CoCr alloy containing knee prostheses. The authors hypothesised that Cr(VI) was the most likely ion to be released from the bearing surfaces of metal-on-metal THRs in comparison to Cr(III). However, Walter *et al.* (2008) compared the chromium ion levels of whole blood, serum, plasma and RBCs from patients with well-functioning Birmingham hip resurfacing implants. Higher concentrations of chromium ions were measured in the serum and plasma fractions in comparison to the RBC fraction and the authors proposed that Cr(III) rather than Cr(VI) was released from the bearing surface. *In vitro* spiking of blood with Cr(VI) and Cr (III) ions revealed that Cr(III) accumulated in the serum fraction whereas Cr(VI) was detected in RBCs (Sidaginamale *et al.* 2013). Hart *et al.* (2010) reported the presence of Cr(III) in periprosthetic tissues of patients who had received metal-on-metal prostheses using synchroton x-ray analysis. Chromium (VI) was not detected in any of the samples. Interestingly, no difference in chromium ion species was detected across the four different types of metal-on-metal implants used in this study.

1.2.3 Wear of ceramic-on-ceramic total hip replacements

High survivorship rates of 97% are reported or ceramic-on-ceramic THRs at 10 years after implantation (D'Antonio *et al.* 2012). This is attributed to the low wear of the bearing surfaces, with retrievals of alumina ceramic THRs typically generating volumetric wear rates of less than 1 – 5 mm^3 per year (Nevelos *et al.* 1999).

Historically, ceramic-on-ceramic THRs have been associated with fractures, causing catastrophic failure of the implant. A number of ceramic bearing materials have been introduced to reduce the risk of fracture and this has included increasing the toughness through the inclusion of zirconia within the ceramic composite. This has led to the development of alumina toughened zirconia (ATZ) and zirconia toughened alumina (ZTA) composites. In addition, the use of hot isostatic pressing (HIPed) of alumina methods has been introduced to reduce the grain size and hence improve the toughness of the material (Stewart *et al.* 2003; Stewart 2010). However, Tipper *et al.* (2002) reported no significant difference in wear between 28 mm diameter non-HIPed and HIPed ceramic-on-ceramic THRs. In contrast, alumina matrix composites (AMC) THRs significantly improved the wear rates in comparison to HIPed alumina, following the bedding in wear period (Stewart *et al.* 2003). Furthermore, ATZ have been reported to produce 12 fold less wear (0.06 ± 0.004 $mm^3/10^6$ cycles) than alumina-on-alumina THRs (0.74 ± 1.73 $mm^3/10^6$ cycles. The same study also revealed ZTA THRs generated fivefold less wear (0.14 ± 0.1 $mm^3/10^6$ cycles) in comparison to alumina-on-alumina THRs (Al-Hajjar *et al.* 2013c).

Retrieval studies of ceramic-on-ceramic THRs revealed an elliptical stripe on the femoral head and on the rim of the acetabular cup (Nevelos *et al.* 1999; Esposito *et al.* 2012). Fluoroscopy studies of patients with THRs revealed that during heel strike, the femoral head translated superiorly, with the head coming into contact with the edge of the cup, which occurred in 50% of patients tested (Lombardi *et al.* 2000). Nevelos *et al*. (2000) reproduced the wear stripe observed in the retrieval studies *via* the introduction of translational malpositioning conditions into hip simulator testing.

Simulator studies have demonstrated that translational malpositioning can significantly increase ceramic-on-ceramic wear rates (Stewart *et al.* 2003; Williams *et al.* 2007; Al-Hajjar *et al.* 2010; Al-Hajjar *et al.* 2013a). Al-Hajjar *et al.* (2010) reported an increase in wear for AMC ceramic-on-ceramic prostheses, under translational malpositioning conditions in comparison to standard gait conditions. However, increases in the cup

inclination angle from 55º to 65º did not significantly affect the wear with measured wear rates of 1.13 mm^3/ 10^6 cycles and 1.1 mm^3/ 10^6 cycles reported, respectively.

1.3 Wear Particle Characterisation

Particle characterisation *in vivo* and *in vitro* can be used to determine and predict the biological responses to the wear debris *in vivo*. This is especially important as the biological response to wear particles is largely dependent on particle size and volume (Green *et al.* 1998).

1.3.1 Characterisation of cobalt-chromium wear particles

Wear particles from metal-on-metal THRs have been reported to be nanoscale in size from both retrieval and simulator studies (Doorn *et al.* 1998; Firkins *et al.* 2001b; Brown *et al.* 2007). Doorn *et al*. (1998) isolated CoCr wear particles from the periprosthetic tissues of 13 patients undergoing revision THR surgery. The medians of the particle sizes of the different samples ranged from 51 to 116 nm, with an average of 81 nm. The particles were also observed to be round in morphology, with some shard-like particles. Simulator studies have reported CoCr wear particles to be slightly smaller, with a mean size of less than 40 nm, with no shard-like particles detected (Firkins *et al.* 2001b; Brown *et al.* 2007).

The discrepancies in particle size and morphology between studies are often caused by the isolation method. Isolating CoCr wear particles from serum is particularly challenging due to their small size and low wear volumes. Metallic particles have a tendency to aggregate and also corrode, particularly at high temperatures and aggressive pH levels (Catelas *et al.* 2001a). Moreover, alkaline and acidic digestion protocols commonly employed in particle isolation have been reported to alter the morphology, shape, and composition of CoCr wear particles (Catelas *et al.* 2001b).

Particle preparation for TEM analysis has been shown to cause aggregation, thus causing particle size inaccuracies (Firkins *et al.* 2001b). A number of isolation methods have been developed, including Brown *et al*. (2007), which involved a multiple step enzymatic digestion protocol. However, enzymatic digestion has been reported to affect particle size and induce aggregation (Catelas *et al.* 2001a; Lu *et al.* 2012). Lu *et al*. (2012) developed a freeze dry method, which removed most of the water from the serum, followed by enzyme digestion. However, the method also involved repeated centrifugation steps, which may lead to a particle loss. In addition, Billi *et al*. (2012) optimised an isolation method involving an ultracentrifugation process, which deposits the particles onto a silicon wafer. However, retrieval of the particles from the wafer is not possible for further particle experiments.

Characterisation of CoCr wear particles generated under adverse conditions has received increased attention due to the high early failure rates of metal-on-metal bearings. Leslie *et al*. (2009) reported an increase in particle size under translational malpositioning conditions. Under standard conditions, the mode particle size was 20 – 29 nm, but increased to 30 – 39 nm under translational malpositioning. However the particle morphology was reported to be the same under both conditions. Xia *et al*. (2011) reported larger (20 – 500 nm), needle shaped particles from periprosthetic tissues from patients suffering from pseudotumours (section 1.5.1.2). In addition, Goode *et al*. (2012) revealed a wide CoCr wear particle size distribution of a few nanometres to 5 µm in length from periprosthetic tissues of a patient with a failed ASR implant.

1.3.2 Characterisation of alumina ceramic wear particles

A limited number of studies have been published on the particle characterisation of alumina ceramic wear particles from THRs. The low wear rates of ceramic-on-ceramic wear particles means it is technically very difficult to isolate particles under normal wear

conditions. Alumina ceramic wear particles from periprosthetic tissues were reported to have a wide size range of 5 – 90 nm when visualised using TEM and 0.05 – 3.2 µm size distribution when analysed using SEM (Hatton *et al.* 2002). It is thought that the large size distribution was caused by the introduction of translational malpositioning. Tipper *et al.* (2002) observed alumina wear particles generated from wear simulators, under standard gait conditions, to be 2 – 27.5 nm in diameter when visualised by TEM. However, when translational malpositioning conditions were introduced, the particle diameters increased to 0.02 – 1 µm. These authors proposed that during standard gait conditions, alumina wear particles were generated by relief wear, thus producing smaller particles. When translational malpositioning occurred, the head component came into contact with the rim of the cup and generated larger, irregular sized alumina particles by grain fracture. This was further confirmed by Affatato *et al*. (2012), who analysed the wear surface of 6 retrieved alumina ceramic-on-ceramic THRs by SEM, 13 years after implantation. The areas of high wear on the femoral head and acetabular cup were characterised by large granular, pitted surfaces. However, in unworn areas, the surface appears to be smooth, with minimal defects.

1.4 Biocompatibility of total hip replacements

Numerous studies have evaluated the biocompatibility of alumina and CoCr wear particles including adverse reactions reported in patients with THRs and *in vitro* cell studies on the toxic potential of the particles. Alumina and CoCr wear particles were hypothesised to induce fewer incidences of osteolysis than conventional UHMWPE due to the low wear rates and the wear particles produced being predominantly nanoscale in size. The implication was that the particles were outside the “critical size range” of 0.3 to 10 µm, and therefore would not promote osteolysis (Green *et al.* 1998). Osteolysis is largely associated with the engulfment of UHMWPE wear particles by macrophages, causing frustrated phagocytosis and the release of pro-inflammatory mediators, such as tumour necrosis factor-alpha (TNF-α), interleukin-1β (IL-1β), IL-6,

IL-8, monocyte chemo-attractant protein (MCP)-1, prostaglandin E-2 (PGE_2), and macrophage inflammatory protein (MIP)-1 (Green *et al.* 1998; Ingham and Fisher 2000; Ingham and Fisher 2005; Liu *et al.* 2015; Singh *et al.* 2015). The secreted pro-inflammatory mediators are able to influence osteoclast differentiation and promote bone-resorbing activity and osteolysis (Fuller *et al.* 2002; Peng *et al.* 2015). Nevertheless, alumina, and in particular CoCr, wear particles have been associated with alternative biological reactions which are discussed in the following sections.

1.4.1 Patient reported effects of ceramic-on-ceramic bearings

In comparison to UHWMPE-on-metal and metal-on-metal THRs, ceramic-on-ceramic prostheses have not been as strongly associated with adverse effects in patients. Incidences of aseptic loosening with ceramic-on-ceramic were coupled with high wear rates caused by severe malpositioning of the implant (D'Antonio *et al.* 2014). In particular the Mittelmeier THR was associated with loosening of the implant and an absence of osteointegration, leading to poor survivorship (Garcia-Cimbrelo *et al.* 1996).

Ceramic-on-ceramic THRs have also been associated with catastrophic failure of the implant due to the brittle nature of the material. However, improvements of the purity, density, reduction in porosity and grain size of the ceramic components have improved the incidence of fracture (Hannouche *et al.* 2003). Another complication has been the detection of an audible squeak in less than 1 – 4.2% of patients with a ceramic-on-ceramic THR. The possible causes of this phenomenon as not clear, but THR design, malpositioning and altered lubrication have been proposed (D'Antonio *et al.* 2014; Owen *et al.* 2014).

1.4.2 Patient reported effects of CoCr alloy metal-on-metal bearings

Patient complications associated with metal-on-metal and ceramic-on-ceramic bearings have been reported. Of particular concern have been the reported complications associated with large diameter metal-on-metal bearings. These include pseudotumours, delayed type IV hypersensitivity type reactions, and necrosis of the periprosthetic tissues (Pandit *et al.* 2008; Hart *et al.* 2009; Natu *et al.* 2012). However, the nomenclature of these tissue responses varies between studies and may also be referred as metallois, adverse local tissue reaction (ALTR), adverse reaction to metal debris (ARMD) and acute lymphocytic vasculitis and associated lesions (ALVAL), making direct comparisons between studies difficult (Gill *et al.* 2012). For clarification the terms pseudotumour, delayed type IV hypersensitivity reactions and ALVAL are only used to describe adverse reactions to metal-on-metal implants.

1.4.2.1 Cobalt and chromium ion levels in patients with metal-on-metal prostheses

The presence of elevated levels of Co and Cr ions in the blood, urine, and organs of patients with metal-on-metal THRs have been reported (Sargeant and Goswami 2007; Walter *et al.* 2008). Elevated Co and Cr ion levels have been reported in the joint fluid of patients with metal-on-metal implants (De Smet *et al.* 2008; Langton *et al.* 2010). Langton *et al.* (2010) reported a large range of elevated Cr (~1000 µg/L to 46,000 µg/L) and Co (~1000 µg/L to 10,000 µg/L) levels in patients. However, De Smet *et al.* (2008) demonstrated a correlation between blood serum Co and Cr ion concentrations and hip joint fluid ion concentrations. In addition, serum levels have been shown to increase as the inclination angle of metal resurfacing implants increases (De Haan *et al.* 2008). Sidaginamale *et al.* (2013) reported that Co ion concentrations equal or greater than 5.04 µg/L from whole blood samples demonstrated 93% sensitivity and 96% specificity from abnormal wear (greater than $3mm^3$ per year).These results suggested that serum Co and Cr ion concentrations are an indicator of implant wear. Consequently this led to

the MHRA guidelines stating 7 µg/L as the threshold level for acceptable Co and Cr blood ion levels. However, large variations in whole blood and serum ion concentrations have been reported (Davda *et al.* 2011; Renner *et al.* 2016). This is further compounded by the contamination of samples such as collecting the blood sample in the incorrect blood sample tube (Moyer & Sierra 2011). Ion concentrations lower than the threshold set by the MHRA have been associated with delayed type IV hypersensitivity reactions and pseudotumours (Hallab *et al.* 2010; Sampson and Hart 2012). Ion concentrations of either Cr or Co at 4 µg/L have been reported to have 90% specificity for detecting adverse reactions to metal-on-metal prostheses (Haddad *et al.* 2011). This indicates that patient-specific responses to the Co and Cr ions may occur, which vary across individuals, rather than a biological effect occurring when a threshold level of metal ions has been achieved.

1.4.2.2 Pseudotumours

Pseudotumours are described as a mass or a fluid-filled cyst around the hip prosthesis (Engh *et al.* 2006; Engh Jr *et al.* 2010). This phenomenon is a major concern with large diameter metal-on-metal bearings. Pandit *et al*. (2008) were the first to use the term pseudotumour associated with metal-on-metal replacements after observing soft tissue masses, which were extensively necrotic and infiltrated with lymphocytes in 17 female patients. Furthermore, large volumes of metal wear debris were observed in the necrotic tissue, thus suggesting an association with metal wear particles. Clinical presentation of pseudotumours is varied and pain around the hip can range from slight discomfort to functional impairment. The board spectrum of pseudotumour characteristics has led to the development of a classification system using MRI, as explained in Table 1.1 (Hauptfleisch *et al.* 2012). The highly invasive nature of pseudotumours has potential catastrophic consequences with nerve damage, dislocation, and extensive soft tissue damage being reported (Grammatopoulos *et al.* 2009; van der Veen *et al.* 2015).

Table 1.1 – Classification system for pseudotumours. Magnetic resonance imaging is used to classify pseudotumours, ranging from thin walled cysts (type 1) to predominantly solid masses which have minimal cyst lesions (type 3) (Hauptfleisch *et al.* 2012).

Classification	Description
1	Thin-walled cystic mass (cyst wall <3 mm)
2	Thick-walled cystic mass (cyst wall >3mm)
3	Mostly consists of a solid mass

Histological analysis of pseudotumours demonstrated an association with metal wear particles (Pandit *et al.* 2008). Indeed a correlation between high wear levels, elevated blood Co and Cr levels and pseudotumour prevalence has been reported (Hart *et al.* 2009; Langton *et al.* 2010; Davda *et al.* 2011). In contrast, pseudotumours have also been reported in patients with low wear. Matties *et al*. (2012) found that 40% of patients with a pseudotumour had wear rates less than 5 µm per year in a cohort of 103 patients with metal-on-metal hips. In addition, 40% of patients with pseudotumours had Co and Cr blood levels less than the threshold limit of 7 µg/L. Interestingly the authors reported no association between adverse cup positioning and pseudotumour prevalence. In addition to this, asymptomatic patients with pseudotumours have been observed (Kwon *et al.* 2011; Hart *et al.* 2012).

1.4.2.3 Hypersensitivity reaction and aseptic lymphocytic vasculitis-associated lesions

Incidences of patients suffering from a painful hip, shortly after implantation of a metal-on-metal bearing have been reported in the absence of infection (Blumenfeld *et al.* 2010). Extensive surface ulceration and the presence of wear debris within the periprosthetic tissue have been observed (Davies *et al.* 2005; Blumenfeld *et al.* 2010). This suggests that an immunological response, more specifically a delayed type IV hypersensitivity reaction may be associated with early implant failure. Type IV

hypersensitivity is characterised by a delayed reaction (1 – 3 days) including T lymphocytes which are activated by antigen presenting cells (Janeway *et al.* 2005).

Hypersensitivity reactions are thought to be due to the wear particles or the released ions forming immunocomplexes with native proteins, which subsequently initiate an immune response. The most common reported metal sensitisation is to nickel. The next most potent allergens are cobalt and chromium, whereby chromium is found to show cross reactivity with cobalt and nickel (Hallab *et al.* 2010). The frequency of hypersensitivity reactions in failed metal-on-metal implants is low and ranges from 0.3 – 1.0% (Engh Jr *et al.* 2010).

1.4.2.3.1 Histological evidence for hypersensitivity reactions

Willert *et al.* (2005) observed lymphocyte infiltration, occasionally with plasma cells, in the periprosthetic tissues of 19 patients with suspected hypersensitivity reactions. The lymphocyte infiltration was found to be distinctly different between the different layers of the tissue, whereby in the inner layer of the neocapsule, the lymphocyte infiltration was diffusely distributed. In contrast, in the deeper intermediate vascular layers, the lymphocytes surrounded post-capillary venules walls. High endothelial venules (a capillary venous swelling to enable lymphocytes in the blood to enter the lymph nodes) were also detected. The differences in lymphocyte infiltration in the deeper tissue layers was also observed by Natu *et al.* (2012) and Davies *et al.* (2005). However, these studies also observed the presence of plasma cells, B cells, and fibrin exudation, which are not characteristic of a type IV hypersensitivity reaction. Nevertheless, Willert *et al.* (2005) hypothesised that a form of hypersensitivity reaction was likely to be occurring, as patients who received another metal implant following early failure of the primary implant did not report any alleviation of symptoms. In contrast, the patients who received a polyethylene-on-metal or polyethylene-on-ceramic implant reported symptoms had been relieved. The term aseptic lymphocytic vasculitis-associated

lesions (ALVAL) is also used extensively to described this form of immunological reaction.

1.4.2.3.2 Potential mechanisms of delayed type IV hypersensitivity reactions and pseudotumours

The pathogenesis of delayed type IV hypersensitivity reactions and pseudotumours has been of much debate. *In vitro* experiments have demonstrated CoCr wear particles and associated ions can promote cytokine release, which includes interleukin-6 (IL-6), IL-8, and tumour necrosis factor-α (TNF-α) as shown in Table 1.2 (Granchi *et al.* 1999; Trindade *et al.* 2001; Masui *et al.* 2005; Papageorgiou *et al.* 2007; Kaufman *et al.* 2008; Dalal *et al.* 2012; Rose *et al.* 2012; Posada *et al.* 2014; Pearson *et al.* 2015; Posada *et al.* 2015b). However, there is no clear consensus on the cytokines CoCr wear particles can induce in cells, in particular TNF-α, which have been associated with inducing inflammatory reactions. CoCr particles have been reported to induce TNF-α release in osteoblasts, human macrophages, U937 histiocytes and peripheral blood mononuclear cell (PBMNCs) (Granchi *et al.* 1999; Kaufman *et al.* 2008; Dalal *et al.* 2012; Rose *et al.* 2012; Posada *et al.* 2015a).

The conflicting outcomes of the studies may be caused by a number of factors, including cell specificity. Dalal *et al.* (2012) demonstrated that osteoblast cells were more sensitive to CoCr particles in comparison to macrophages and fibroblasts. Furthermore the inconsistencies can be caused by use of large particle sizes, thus particles are not clinically relevant and therefore the *in vivo* biological effects may be underestimated (Trindade *et al.* 2001). Particle retrieval studies from failed prostheses have revealed CoCr wear particles to be nanoscale in size (Doorn *et al.* 1998). Nevertheless, some studies have used micron sized particles, as shown in Table 1.2 , which have been demonstrated to be less cytotoxic and induce a different immunological response (Brown *et al.* 2013).

It is hypothesised that these adverse reactions are linked with osteolysis and aseptic loosening of metal THRs. Korovessis *et al*. (2006) hypothesised that CoCr wear debris activates lymphocytes, which then release IL-2, IFN-γ, and RANKL, which can promote osteoclast activity and inhibit osteoblasts. However, osteolysis is predominately a macrophage response to wear particles, whereas histological analysis of ALVAL has revealed a large lymphocyte response (Natu *et al.* 2012). Further, osteolysis is associated with long-term failures of THRs, whereas delayed type IV hypersensitivity reactions occur shortly after implantation. Therefore, the link between the predominately adaptive immune response of hypersensitivity reactions with the inflammatory response of osteolysis is unlikely.

Pseudotumour formation has also been linked with hypersensitivity reactions. Mahendra *et al*. (2009) analysed tissue samples of pseudotumours and detected plasma cells and perivascular lymphoid aggregates, which was similar to the characteristic histology of hypersensitivity reactions. Campbell *et al*. (2010) analysed periprosthetic tissue, collected during revision surgery of failed metal-on-metal bearings and reported samples with high wear rates had a low ALVAL score. However, tissue samples with low volumes of wear debris had a high ALVAL score and demonstrated reactions similar to hypersensitivity reactions. These authors suggested that during high wear scenarios, there is an increased risk of pseudotumours, whilst hypersensitivity will predominate during low wear. However as previously described, pseudotumours have been reported in patients where low wear rates have occurred.

Table 1.2 – Summary of cytokine release studies after exposure to cobalt chromium wear particles

Study	Cell type	Cytokine Expression	Particle size	Particle/Ion concentration	Assay
Granchi *et al*.(1999)	Mononuclear cells from patients of failed metal THRs	↑ TNF-α, but no increase in IL-6 or GM-CSF.	-	Cr ions = 5.5 ng/ml Co ions = 1 µg/ml	ELISA
Trindade *et al*.(2001)	Macrophages and lymphocytes	↑ IL-6 and TNF-α	1 – 5 µm.	Insufficient details given of particle concentration	ELISA
Masui *et al*.(2005)	Murine trabecular bone model	No effect on TNF-α No effect on RANKL/OPG ratio.	1.8 ± 0.7 µm	Approximately 1 x 10^8 particles per 25.5 gram mouse	ELISA
Papageorgiou *et al*.(2007)	Fibroblasts	No increase in TNF-α, IL-6, IL-10, TGF-β	29.5 ± 6.3 nm and 2.904 ± 0.064 µm	0.0005 – 5000 μm^3/cell	ELISA
Kaufman *et al*.(2008)	Human macrophages	↑ TNF-α, IL-6, IL-1β, IL-8.	0.48 µm	853 particles per macrophage	Protein chip analysis
Dalal *et al*.(2012)	Macrophages Fibroblasts Osteoblasts	↑ IL-6, TNF-α, IL-8, IL-1β.	1.1 µm	1:5 – 1:100 particles per cell	ELISA
Rose *et al*.(2012)	Macrophages	↑ TNF-α	0.147 ± 0.37 µm	0.001 – 1 mg/100 µl	ELISA
Posada *et al.* (2015a)	U937 histiocytes	↑ TNF-α, IL-6, IFN-γ	150 nm – 6.5 µm	156.25 $\mu g/cm^2$	ELISA

A proposal by Brown *et al.* (2013) suggested that ALVAL and pseudotumour reactions are dependent upon on CoCr particle size. Micron sized (2.9 µm ± 1.06 µm) and nanometre sized (32 nm ± 21 nm) CoCr particles were injected peri-articularly into the

right knee of 6-8 week old mice. After 40 weeks, the knee tissues from the mice exposed to the nanometre particles retained Cr but lost Co, suggesting that Co is lost through corrosion. However, the ratio of Co:Cr for the micron sized particles remained similar to the bulk metal material and loss of Co and Cr was thought to be caused by the physical removal of the particles. Mononuclear cells isolated from the treated mice also demonstrated significantly elevated expression of IL-2 and IFN-γ, but not IL-4 and IL-10 when challenged with Co and Cr ions, at four weeks. These authors proposed that the micron sized particles are physically removed, possibly by macrophages, which caused the activation of lymphocytes. It is thought that a Th1 lymphocyte response predominates as indicated by the cytokine expression profile, which was indicative of a type IV hypersensitivity reaction. This work is particularly interesting as it suggests that particle size, rather than wear volumes has a greater effect on the immune response.

1.4.3 Adverse effects of ceramic-on-ceramic bearings *in vivo*

The biocompatibility of alumina or zirconia wear particles is relatively good due to the low wear rates and inert nature of ceramics. Isolated incidences of osteolysis have been reported for ceramic-on-ceramic THRs, however this was associated with severe malpositioning, leading to high wear (D'Antonio *et al.* 2012). Nich *et al*. (2006) observed no osteolysis in 41 patients who had received ceramic-on-ceramic implants, after a 16 year follow-up study. Historically, failure of ceramic-on-ceramic THRs was often associated with catastrophic fracture of the implant. Whilst, the hardness of ceramics leads to minimal wear, their brittle nature means they are susceptible to fracture. Modern cup designs have been designed to reduce the risk of fracture, for example the use of metallic acetabular cup liners. Nevertheless, Amanatullah *et al*. (2011) reported a fracture rate of 2.6% in 125 patients, 5 years after implantation of ceramic-on-ceramic THRs. Furthermore, ceramic-on-ceramic THRs have been associated with squeaking when the patient uses the affected hip joint, although the

incidence of this is currently low with estimation ranging from 0.2 – 4.2% of ceramic-on-ceramic THRs (Jarrett *et al.* 2009; Amanatullah *et al.* 2011; Owen *et al.* 2014).

Histological analysis of the periprosthetic tissues from patients with ceramic-on-ceramic THRs revealed the presence of wear debris within the tissues (Hatton *et al.* 2002; Shishido *et al.* 2006; Esposito *et al.* 2013). However, the characteristic adverse responses of a high ALVAL score and necrosis observed in tissues surrounding metal-on-metal THRs were not apparent. Although a low level macrophage and lymphocyte infiltrate were observed in the periprosthetic tissues (Esposito *et al.* 2013). Similarly Hatton *et al.* (2002) reported the presence of necrotic tissues as well as macrophages, neutrophils and lymphocytes in periprosthetic tissues of patients who had received a Mittelmeier ceramic-on-ceramic THR. Interestingly, in comparison to periprosthetic tissue from patients undergoing revision surgery for Charnley prosthesis, significantly more neutrophils were observed. However, as previously described, ceramic-on-ceramic THRs are not as strongly associated with osteolysis as UHMWPE-on-metal THRs (D'Antonio *et al.* 2014).

1.4.3.1 Immunological responses to alumina wear particles

The effect of alumina and zirconia wear particles on cells of the immune system *in vitro* has also been investigated. Similar to the effect of CoCr wear particles, the expression of cytokines after exposure to alumina or zirconia particles varies between studies as described in Table 1.3. Indeed TNF-α expression in macrophages, osteoblasts and fibroblasts was reported to increase in the presence of alumina wear particles (Dalal *et al.* 2012). However, Granchi *et al.* (1999) reported no increase in TNF-α release in osteoblasts challenged with 1 µm sized alumina wear particles at particles doses of 0.001 to 1 $mg.ml^{-1}$. Interestingly Catelas *et al*. (1999) observed no difference in cytokine production in osteoblasts cells challenged with 4.5 µm sized alumina particles and 0.6 µm sized zirconia particles. The discrepancies between the results may be

partially explained by the use of particles and particle doses which are not clinically relevant. For instance, a number of studies have used large micron sized particles, however ceramic simulator and *ex vivo* studies have demonstrated a bimodal distribution of both nanoscale and micron sized particles (Hatton *et al.* 2002; Tipper *et al.* 2002). In addition to this, the particle volume of 500 μm^3 per cell required to induce cytokine release from macrophages is relatively high and the wear rates of ceramic-on-ceramic THRs are low, indicating that these volumes of particles are unlikely to occur *in vivo* (Hatton *et al.* 2003).

Table 1.3 – Summary of cytokine release studies after exposure to alumina or zirconia wear particles.

Study	Cell type	Particle size	Particle dose	Cytokine Expression	Assay
Catelas *et al*. (1999)	Macrophages	Alumina (up to 4.5 µm) Zirconia (up to 0.6 µm)	5 – 2500 particles per macrophage	↑ TNF-α No effect on IL-1α and IL-1β	ELISA
Hatton *et al*. (2003)	Human peripheral blood mononuclear phagocytes	Bimodal alumina particles (5 – 20 nm and 0.2 – 10 µm)	Particle volume of 1 – 500 μm^3 per cell	↑ TNF-α at high concentrations	ELISA
Granchi *et al*. (2004)	Osteoblast and osteoclast	Alumina (1.0 µm)	1, 0.1, 0.01, and 0.001 mg/ml	No effect on TNF-α, GM-CSF. ↑ IL-6	ELISA
Kaufman *et al*. (2008)	Human macrophages	Alumina 0.23µm	Average number of particles per cell: 3732	↑ TNF-α, IL-6, IL-1β, IL-8.	Protein chip analysis
Dalal *et al*. (2012)	Macrophages Fibroblasts Osteoblasts	0.5 – 0.9 µm	5:1 – 100:1 particle: cell ratio	↑ IL-6, TNF-α, IL-8, IL-1β.	ELISA

1.4.4 The effect of alumina and cobalt chromium wear particles on cell viability

In vitro studies have investigated the effect of alumina and CoCr wear particles on the cell viability of various cell types which are detailed in this section.

1.4.4.1 The effect of alumina wear particles on cell viability

A number of studies have observed limited or no reduction in cell viability upon exposure to alumina or zirconia wear particles (Catelas *et al.* 1999; Hatton *et al.* 2002; Germain *et al.* 2003; Granchi *et al.* 2004; Gutwein and Webster 2004; Dalal *et al.* 2012; Rose *et al.* 2012). Interestingly, no difference in the cytotoxic effects of alumina and zirconia particles has been reported (Catelas *et al.* 1999). However, many of these studies did not use clinically relevant particle sizes (Yoshida *et al.* 2003; Granchi *et al.* 2004; Gutwein and Webster 2004; Yamamoto *et al.* 2004). Germain *et al.* (2003) demonstrated cell specific reactions to clinically relevant ceramic wear particles, whereby no cell death was observed for a fibroblast cell line. However, in contrast, at the highest particle volume of 50 μm^3 per cell, a significant reduction in cell viability was reported for a histiocyte cell line.

Particle size has been reported to affect the cytotoxic effects of alumina wear particles. Germain *et al.* (2003) reported that clinically relevant wear particles, isolated from hip simulators, induced more cell death in comparison to micron sized particles. However, other studies reported that a reduction in particle size also led to a decrease in cell death (Gutwein and Webster 2004; Dalal *et al.* 2012; Rose *et al.* 2012). Gutwein & Webster (2004) hypothesised that the large particles used in these studies were more likely to be phagocytosed, leading to macrophage activation and subsequent cell death. As described in section 1.3.2, a bimodal particle distribution of nanoscale and micron sized alumina particles have been retrieved from microseparation hip simulator studies. Therefore the mechanism of particle uptake, which is partly dependent on

particle size, may have an effect on cell viability. However, the conclusions from these studies are limited as it is not known if interference of the particles with the assay results was taken into consideration. Particles have been previously reported to have a direct impact on biochemical assays, either by reducing or increasing assay output readings, which may have caused the differences between the studies (Monteiro-Riviere *et al.* 2009).

1.4.4.2 The effect of cobalt chromium wear particles on cell viability

Extensive necrosis in periprosthetic tissues has been reported in patients with metal-on-metal implants. Numerous *in vitro* studies have demonstrated a reduction in cell viability following exposure to CoCr wear particles as well as Co and Cr ions. Many reports demonstrated that Co and Cr ions induced cytotoxic effects in a time and dose dependent manner (Catelas *et al.* 2001c; Germain *et al.* 2003; Fleury *et al.* 2006; Papageorgiou *et al.* 2007; Andrews *et al.* 2011; Posada *et al.* 2014; Posada *et al.* 2015b). However, direct comparisons between studies is complex, particularly if different particle sizes, particle concentrations, assay choice and cell types are used. This is further compounded if details of particle sizes or the exact concentration of particles used in the published literature is unclear.

From the published literature particle size has been reported to affect CoCr wear particle cytotoxicity, with micron particles predominantly inducing a lower reduction in cell viability than nanoscale particles (Germain *et al.* 2003; Brown *et al.* 2006; Bhabra *et al.* 2009; Brown *et al.* 2013). For example, Papageorgiou *et al.* (2007) reported that nanoscale CoCr wear particles at a particle volume of 50 μm^3 per cell or greater significantly reduced cell viability after 24 hours, whilst micron sized CoCr particles only induced a significant reduction after 4 days at the particle volume of 500 μm^3per cell.

Another important parameter is the concentration of particles added to the cells in the various *in vitro* studies. The range of particle concentrations varies greatly between

studies. For instance, Yoshia *et al.* (2003) studied the effect of micron sized CoCr particles on the viability of macrophages, however it was estimated from the method details given that an approximate particle volume per cell was over a hundred times greater than the highest particle volumes used by Germain *et al.* (2003), Brown *et al.* (2006), and Papageorgiou *et al.* (2007). Considering the annual volumetric wear of a well-positioned metal-on-metal THR is approximately 1 – 3 mm^3, the particle doses used in this study were not deemed clinically relevant.

Whilst cytotoxic effects of CoCr wear particles have been studied, limited studies have investigated if CoCr wear particles Co and Cr ions can promote cell necrosis or apoptosis (Granchi *et al.* 1998; Catelas *et al.* 2001c; Posada *et al.* 2014). Catelas *et al.* (2001c) demonstrated that Co(II) and Cr(III) ions at a concentration of 10 and 500 ppm, respectively induced apoptosis in J774 murine macrophages after 24 hours. Interestingly Posada *et al.* (2014) demonstrated that nanoscale CoCr wear particles cultured with Co ions caused a significant reduction in cell viability of U937 histiocytes in comparison to Co ions alone. The authors hypothesised that in an acidic environment, such as at the site of inflammation, ion dissolution is greater and cell death could be intensified by the presence of both ions and particles.

1.4.5 Wear particles, oxidative stress and genotoxic effects

Alongside cell viability studies, the effect of alumina and CoCr wear particles on oxidative stress and genotoxicity have been reported.

1.4.5.1 Alumina wear particles, oxidative stress and genotoxic effects

Alumina particles have been reported to induce genotoxic effects *in vitro*, however to a lesser extent than CoCr particles (Parry *et al.* 2010; Tsaousi *et al.* 2010). Currently no patient studies have reported any adverse effects from the genotoxic effects of alumina

particles. Tsaousi *et al.* (2010) investigated the effects of alumina particles of different size (0.2 – 2 µm) and alumina fibres (0.9 µm by 12 µm) on primary human fibroblasts (HFBs). After 24 hours, alumina particles were reported to induce the increase of micronucleated cells, with alumina fibres having the greatest effect. No double stranded DNA breaks were detected. However, the authors used very large alumina fibres, which have not been detected in alumina wear particle retrieval studies (Hatton *et al.* 2002). Therefore the clinical relevance of these results is limited. Parry *et al.* (2010) also reported single stranded breaks in the DNA of primary HFBs cultured with alumina model particles across a placenta-like BeWo cell barrier. Furthermore, Petit *et al.* (2005) reported no protein oxidation or nitration, which is an indicator of oxidative stress of U937 histiocytes, of U937 histiocytes cultured with alumina model particles using Western blot techniques.

1.4.5.2 Cobalt chromium wear particles, oxidative stress and genotoxic effects

Epidemiology studies on the carcinogenic effect of exposure to CoCr wear particles and associated ions have been inconsistent. Gillespie *et al*. (1988) observed an elevated incidence of haemopoietic and lymphatic cancers in patients 10 years post implantation of a UHMWPE-on-metal implant. Furthermore, metal-on-metal THR patient studies have reported an increase in lethal and non-lethal aneuploidy and chromosomal translocations (Dunstan *et al.* 2008). In contrast, Visuri *et al.* (2010) reported no increase in the risk of cancer in patients with THRs, including metal-on-metal prostheses, compared to the general population 13 years using the Finnish Arthroplasty Register and Finnish Cancer Registry. Similarly Lalmohamed *et al.* (2013) studied the increased risk of cancer after implantation of a THR, including metal-on-metal THRs and hip resurfacing implants in 11,450 patients in England. Using data from the Clinical Practice Research Datalink, National Joint Registry and Hospital Episode Statistics databases, between 2003 and 2010, no association between metal-on-metal prostheses and an increased risk of cancer was reported.

Cobalt chromium wear particles have been reported to induce DNA damage, whereby nanoscale particles (30 nm) induced more DNA damage than micron sized particles (2.9 μm) in fibroblast cells (Papageorgiou *et al.* 2007). Furthermore, Parry *et al.* (2010) and Bhabra *et al*. (2009) reported nanoscale CoCr wear particles (30nm) could cause indirect DNA damage of fibroblast cells across a cellular barrier of human trophoblast choriocarcinoma cells (BeWo cells). The DNA damage consisted of DNA double stranded breaks and chromosomal aberrations. It was proposed that the CoCr particles induced damage to the BeWo cells either *via* mitochondrial damage, or hypoxia-like induced conditions. Parry *et al.* (2010) reported that the threshold of 0.00036 mg/cm^2 of CoCr nanoscale wear particles were required to caused DNA damage across a trophoblast cell barrier. The authors hypothesised that this particle dose was greater than the wear volumes generated by well-functioning THRs, but could be achieved in malpositioned, high wearing THRs and as such, DNA damage could occur upon exposure to CoCr nanoscale wear particle *in vivo*. However, the timescale used in this study in comparison to the survivorship of metal-on-metal THRs make direct comparisons complex.

In peripheral blood taken from patients with well-functioning metal-on-metal THRs, 1 – 4 ppb of Co and Cr ions have been measured. Interestingly, Parry *et al.* (2010) reported that relatively low Cr (III) and Co(II) ions of 2 and 1.3 ppm, respectively could cause single stranded, double stranded and alkaline labile sites across a trophoblast cell barrier. In addition, studies have shown that Co ions can induce chromosomal aberrations, causing single stranded breaks and crosslinking of DNA strands (Lloyd *et al.* 1998; Baldwin *et al.* 2004; Witkiewicz-Kucharczyk and Bal 2006; Figgitt *et al.* 2010). In addition to this, when Cr(VI) is reduced, Cr(III) is capable of binding to proteins, amino acids, RNA and DNA (O'Brien 2003; Tkaczyk *et al.* 2009).

A number of studies have reported an association between oxidative stress and CoCr wear particles and ions (Bagchi *et al.* 2002; Petit *et al.* 2005; Fleury *et al.* 2006; Petit *et al.* 2006; Papageorgiou *et al.* 2007). Nanoscale and micron sized CoCr wear particles

and Cr(VI) ions have been reported to induce radicals in cells, such as superoxide anion radicals and hydroxyl radicals (Bagchi *et al.* 2002; Papageorgiou *et al.* 2007). Papageorgiou *et al.* (2007) reported that micron sized CoCr particles (2.9 μm) induced more oxidative stress than the nanoscale CoCr particles (30 nm) at a particle dose of 500 μm^3 per cell after 24 hours. This suggests that CoCr particles of different sizes potentially induce different mechanisms of DNA damage. In addition to generating ROS, CoCr particles and ions can potentially cause oxidative stress by altering antioxidant enzyme activity (Fleury *et al.* 2006; Tkaczyk *et al.* 2010). Furthermore, Co(II) and Cr(III) ions can induce protein oxidation and nitration, which can cause a reduction in protein function (Petit *et al.* 2005; Fleury *et al.* 2006; Petit *et al.* 2006). For instance, Fleury *et al.* (2006) measured protein oxidation in a osteoblast cell line cultured in the presence of 2.5 ppm of Co(II) ions and 25 ppm of Cr(III) ions after 72 hours, suggesting that Co ions are able to induce protein oxidation at low ion concentrations.

1.5 The effect of wear particles from total hip replacements on the cell plasma membrane

As previously described a wide range of the patient reported responses and cell studies have demonstrated adverse effects to THR wear particles. However, the interactions of wear particles with cells, and the factors influencing these, are not fully understood (Gill *et al.* 2012). In particular interactions of wear particles with the plasma membrane and possible toxic effects on the membrane are not known. A number of reviews have called for studies into this area, as when the wear particles are released, the first barrier the particle will encounter is the plasma cell membrane (Billi and Campbell 2010; Simonsen *et al.* 2011; Gill *et al.* 2012).

1.5.1 Internalisation of cobalt chromium and alumina wear particles into cells

CoCr wear particles have been reported to be internalised within cells, including macrophages in periprosthetic tissues from patients with metal-on-metal THRs and therefore the particles must pass the plasma membrane (Willert *et al.* 1996; Davies *et al.* 2005; Willert *et al.* 2005; Langton *et al.* 2010; Underwood *et al.* 2011; Goode *et al.* 2012; Matthies *et al.* 2012) A limited number of *in vitro* studies have also reported internalisation of CoCr wear particles into fibroblasts and macrophages (Lewis *et al.* 2007; Papageorgiou *et al.* 2007; Behl *et al.* 2013). Papageorgiou *et al.* (2007) demonstrated that both nanoscale and micron sized CoCr wear particles could be internalised into primary HFBs. The nanoscale wear particles were observed within vacuoles and dispersed randomly within the cytoplasm. In contrast, the micron sized particles were located in the cytoplasm, surrounding the nucleus. Interestingly, the micron-sized particles remained within the cells 5 days after exposure, whilst the CoCr nanoparticles appeared to have been dissolved or corroded with large electron dense deposits in the cell. The loss of cobalt was also reported for mice exposed to CoCr nanoscale within the joint space after 40 weeks (Brown *et al.* 2013). Colognato *et al.* (2008) also demonstrated the uptake of nanoscale Co particles and Co(II) ions in human peripheral leukocytes. Whilst the Co nanoparticles were internalised, the authors observed no change in Co^{2+} ion uptake over the baseline levels after 24 hours. This is in contrast to reports, which suggest that Co^{2+} is more cytotoxic as it is able to pass the cell membrane (Catelas *et al.* 1999; Andrews *et al.* 2011). At present there are no reports on the internalisation of alumina wear particles from THRs into cells. Hashimoto and Imazato (2015) observed model alumina particles within macrophages using TEM techniques. However the authors failed to confirm the presence of the particles using EDX analysis and therefore it is possible that the particles were actually artefacts from the staining process used in sample preparation.

1.5.1.1 Wear particle uptake and effects on cell viability

Currently there are few reports that investigate the interaction of CoCr and alumina particles with the cell plasma membrane and the subsequent biocompatibility of the wear particles. More specifically it is not known how particles bind to and are taken up through the cell plasma membrane and how this consequently affects cell viability. Lewis *et al.* (2007) reported micron sized CoCr model particles were internalised *via* phagocytosis in fibroblast cells. However, fibroblasts are not professional phagocytes and therefore it is not clear how relevant these findings were. Furthermore, Alexander and Aaseth (1995) reported the internalisation of chromate into red blood cells and liver cells *via* anionic-exchange carriers. The authors used an irreversible anion exchange inhibitor, 4, 4'-diisothiocyanatostilbene-2, 2'-disulfonic acid to determine the uptake mechanism. Nevertheless, the use of inhibitors is not always accurate as the inhibitors can be cytotoxic and lack specificity (Soenen *et al.* 2011). Potnis *et al.* (2013) reported the internalisation of CoCr particles into macrophages *via* the TLR-4 receptor using more specific antibody inhibition and gene silencing techniques. Nonetheless the authors used model particles, with an average size of 800 nm, which is much larger than the wear particles characterised from THRs. Therefore, the effect of CoCr and alumina wear particles on the cell membrane remains an area worthy of investigation.

1.5.2 Structure of the cell plasma membrane

The lipid bilayer of the plasma membrane is comprised of phospholipids and cholesterol interspersed with membrane proteins (Voet *et al.* 2013). The lipid bilayer is primarily formed from glycerophospholipids, also referred to as phosphoglycerides, whereby the hydrophobic tails associate with each other and the polar, hydrophilic head groups are exposed to the aqueous solvent (Voet *et al.* 2013). A second major component of the plasma membrane is cholesterol, which has a fused ring structure that provides rigidity and a polar hydroxyl group to give cholesterol its amphiphilic properties. Cholesterol is a major component of the cell plasma membrane and the

structure of the plasma membrane allows it to act as a selectively permeable barrier, thus providing homeostasis within the cell. The main modes of entry of nanoparticles into the cell, across the membrane barrier, are described in Table 1.4 (Canton and Battaglia 2012).

Table 1.4 – Common modes of nanoparticle entry across the cell plasma membrane. (Canton and Battaglia 2012)

Mode of entry	Description
Phagocytosis	Receptor mediated by the use of opsinins
Macropinocytotosis	Non-specific engulfment of the extracellular fluid by wave-like sheets of the plasma membrane
Clathrin- mediated endocytosis	Pits within membrane are coated with clathrin to form clathrin coated vesicles
Caveolae- mediated endocytosis	Membrane pits are coated with caveolae
Diffusion	Passive process and cargo is not internalised by vacuoles

1.5.3 The effect of particles on the cell plasma membrane within the field of nanotoxicology

Whilst there are limited reports on the effect of wear particles from THRs on the plasma membrane, there are a number of studies using manufactured nanoparticles such as gold, silica and titanium dioxide. Therefore, studies on these can be used to help predict the interactions of THR wear particles with the plasma membrane. The area of nanotechnology is continually expanding, with applications in medicine, cosmetics, and engineering. There has been significant interest in how nanoparticles bind and pass the cell membrane, in particular within the area of drug delivery.

1.5.3.1 Factors affecting particle and membrane interactions, uptake and cell viability

Studies on manufactured nanoparticles, such as gold nanoparticles, have revealed a number of particle characteristics which can influence their effect on the cell plasma membrane (Krpetic *et al.* 2010). These factors are also likely to play a role in the effect on THR wear particle interactions with the cell plasma membrane and subsequent effects on cell viability. Whilst a number of nanotoxicology studies have investigated specific factors effecting particle: membrane interactions, most notably particle size, precise mechanisms are difficult to determine. This is due to the inconsistencies between different studies, such as cell type, cell viability assays used and particle concentration. A number of reviews on nanotoxicology have highlighted the need for the standardisation of techniques, but thus far there is still wide variation between research groups (Oberdorster *et al.* 2007; Kroll *et al.* 2009; Krug and Wick 2011). Therefore the factors outlined below give a general overview of potential factors impacting particle: membrane interactions and subsequent effects on the cell viability. Furthermore, it is likely that the particle characteristics, such as surface chemistry and particle size all contribute to particle: membrane interactions.

1.5.3.1.1 Particle size and composition

In general the particle entry pathway across the membrane is determined by the cargo size (Krug and Wick 2011). For instance, Rejman *et al.* (2004) demonstrated that latex particles, less than 200 nm in diameter, were able to enter murine melanoma cells *via* clathrin mediated endocytosis, whereas 500 nm sized particles were internalised by caveolae mediated endocytosis. In addition, phagocytosis was associated with particles greater than 1 µm. However this study failed to investigate the possible effects of the different internalisation mechanisms on cell viability. Furthermore, there is conflicting evidence on whether nanoparticles can pass the cell membrane *via* non-endocytic pathways or through diffusion and appears to be highly dependent on other

factors such as particle composition. For example Mu *et al.* (2012) observed the passive uptake of 14 nm silica particles into A549 lung epithelial cells, which induced a reduction in cell viability at particle concentrations of 1 $\mu g.ml^{-1}$ or higher.

1.5.3.1.2 Particle Morphology

Particle morphology is another parameter which can impact particle uptake and cell viability. Champion *et al.* (2007) demonstrated that polystyrene particles of different shapes, including needle-like and spherical particles, were internalised into macrophages at varying rates. The spherical particles were more likely to be internalised more than the needle-like particles. Furthermore, these authors stated that when the surface area was too large, the macrophages spread around the particles, rather than internalising them. This is similar to histological analysis of periprosthetic tissue from UHMWPE implants, which reported the presence of giant cells around needle shaped particles (Schmalzried and Callaghan 1999). Moreover, the particle aspect ratio is also a key factor in particle uptake. The rate of uptake has been reported to be reduced as the particle aspect ratio is increased (Canton and Battaglia 2012).

1.5.3.1.3 Particle Surface Chemistry

Research into the role of nanoparticle surface chemistry has reported a general trend that anionic or neutral nanoparticles are internalised less readily than cationic particles (Canton and Battaglia 2012). This is due to the cationic particles being able to bind to the negatively charged proteoglycans expressed on the cell surface (Mislick and Baldeschwieler 1996). However, this trend may be an oversimplification, as surface chemistry also determines the colloidal stability of the nanoparticles in solution and their ability to remain dispersed. This is particularly important for prevention of aggregation of particles as this is likely to change the internalisation mechanisms of particles into cells (Krug and Wick 2011).

Another consideration is the release of ions from the particle surfaces. Mu *et al.* (2014) studied the Zn(II) ion release of uncoated zinc oxide nanoparticles and aliphatic polyether-coated zinc oxide nanoparticles *in vitro*. Uncoated zinc oxide nanoparticles were reported to release more ions from the particle surface. However the coated nanoparticles were observed to interact with the cell membrane and were internalised into A549 lung epithelial cells at a faster rate. Furthermore, the coated particles were demonstrated to reduce the cell viability to a greater extent than the uncoated nanoparticles. The authors hypothesised that once internalised, the coated zinc oxide nanoparticles were able to release more Zn(II) ions within the cell, which in turn had a detrimental effect on the cell viability.

1.5.4 The effect of protein coronae on particle interactions with the cell plasma membrane

When particles are released into biological fluid, such as the synovial fluid *in vivo* and foetal bovine serum (FBS) *in vitro*, the surface of the particles is immediately covered by proteins from the surrounding biological medium (Mahmoudi *et al.* 2011). The variety proteins bound to the particle surface is dependent upon on where the particles are released within the body and what supplemented medium is used for *in vitro* experiments (Ma *et al.* 2015). The formation of a protein corona on the surface of the particles can lead to the exposure of new epitopes and altered properties of the particles. This can alter the particle: cell interactions and subsequent biocompatibility (Rauch *et al.* 2013). It is hypothesised that cellular responses, including cell viability and inflammation, reported in the literature are predominately caused by protein coronae on particles rather than the bare particle surface (Rauch *et al.* 2013).

The formation of a protein corona is a dynamic process and evolves over time. The high surface reactivity of nanoscale particles due to the large surface area: volume ratio allows the rapid binding of proteins. Over time, there is an exchange of low-

affinity, high abundant proteins with higher affinity, less abundant proteins. Eventually a protein corona consisting of a hard and soft corona is formed. The hard corona is the inner layer where a slow exchange with the proteins within the environment occurs. For the outer layer, the soft corona, there is a faster exchange of free proteins in the surrounding medium (Ma *et al.* 2015). It is thought that the hard corona determines the biological fate of nanoscale particles and the interaction with the cell membrane (Nel *et al.* 2009).

The formation of a protein corona on the particle surface is determined by a number of factors. These include the characteristics of the particles such as size, charge, shape and the biological medium that the particles are exposed to (Nel *et al.* 2009; Fleischer and Payne 2014b; Mirshafiee *et al.* 2015; Pozzi *et al.* 2015; Shang and Nienhaus 2015). Upon the formation of a protein corona, the proteins bound to the surface can denature, causing the unfolding of the structure and exposure of new epitopes, leading to new biological interactions (Yan *et al.* 2013; Ma *et al.* 2015).

1.5.4.1 The effect of protein coronae on particle biocompatibility

The protein coronae is largely responsible for cellular uptake mechanisms and subsequent cellular responses, such as cell viability (Horie *et al.* 2009; Mu *et al.* 2012; Mbeh *et al.* 2014; Cheng *et al.* 2015; Duan *et al.* 2015; Franchi *et al.* 2015; Landgraf *et al.* 2015). For example Duan *et al*. (2015) revealed reduced uptake of BSA coated graphene oxide nanoparticles, which had a limited effect on the viability of A549 lung epithelial cells in comparison to uncoated particles.

Within the area of THR wear particle toxicity, the phenomenon of protein coronae has not been adequately investigated and there are a relatively small number of reports. It is thought that the pathogenesis of delayed hypersensitivity reactions is caused by cobalt and chromium ions binding to proteins and generating metal-ion modified peptides, which can induce an immune response (Hallab *et al.* 2000; Hallab *et al.* 2004;

Davies *et al.* 2005; Willert *et al.* 2005). However, the protein corona was not characterised, and the mechanism of interaction with the membrane and how this may influence the biological fate of the wear particles is unknown. Lewis *et al*. (2007) reported micron sized CoCr particles incubated in minimum essential medium (MEM) prior to exposure to fibroblasts were less likely to be internalised than particles which had not been incubated in medium. However, the particles used were much larger than those characterised from periprosthetic tissue and therefore this study is not clinically-relevant.

The direct effect of protein coronae on nanoparticle interactions with the cell membrane has also been investigated. Churchman *et al.* (2013) reported that zinc oxide (ZnO) nanoparticles incubated with bovine serum albumin (BSA) induced more membrane activity, such as an increase in ordering of the lipid bilayer. In addition to this, Lesniak *et al.* (2012) reported that in the presence serum, silica particles bound to a model 1-palmitoyl-2-oleoyl-sn-glycero-3-phosphocholine (POPC) membrane to a lesser extent than particles in the absence of serum. These authors hypothesised that the serum bound to the membrane and subsequently reduced the number of available binding sites on the membrane surface for the particles to come into contact with. Furthermore, in the presence of serum, specific receptor binding to the cell plasma membrane has also been reported to be effected. Denatured fibrinogen coated gold nanoparticles were revealed to bind to the integrin receptor Mac-1 on macrophage cell plasma membranes, which induced the release of inflammatory mediators, including TNF-α (Deng *et al.* 2011).

Fleisher and Payne (2014a) demonstrated that particle composition can play a key role in particle interactions with the cell plasma membrane. In the presence of MEM, supplemented with 10% (v/v) FBS, uptake of cationic polystyrene nanoparticles was increased in comparison to particles incubated in the absence of serum in kidney epithelial cells *in vitro*. In contrast, under the same conditions, uptake of anionic polystyrene nanoparticles was reduced. This phenomenon was observed with

polystyrene particles of varying diameter and cell type (Fleischer and Payne 2014a; Fleischer and Payne 2014b). Using competitive assays, protein: particle complexes were incubated with free BSA and it was revealed that the anionic nanoparticles competed with the free BSA to bind to the BSA receptor. In contrast, particle uptake of cationic nanoparticles was unaffected by the presence of free BSA. Further competitive assays demonstrated that cationic nanoparticles bound to scavenger receptors on the cell plasma membrane.

1.6 The use of biomimetic systems to determine the effect of wear particles on the cell plasma membrane

The effect of nanoscale and micron sized alumina and CoCr wear particles on the plasma membrane can be investigated using biomimetic systems. These systems have recently been advocated as suitable experimental models to investigate ion transport, membrane damage, and membrane binding by manufactured nanoparticles. A wide range of biophysical methods have been reported in the literature to characterise the interaction of manufactured nanoparticles and these are summarised in Table 1.5. These techniques often use model membranes, with varying degrees of complexity, to represent the cell plasma membrane. These include the use of tethered bilayer lipid membranes (tBLMs) and solid supported bilayer lipid membranes (sBLMs). The techniques of particular interest to this current study are discussed in detail.

Table 1.5 – Commonly used techniques to investigate particle interactions with the model plasma membranes (Mahmoudi *et al.* 2011; Escorihuela *et al.* 2015).

Technique	Overview of principle
Atomic force microscopy (AFM)	Uses a highly sensitive scanning probe across the sample surface to determine mechanical and chemical properties of sample
Dual polarization interferometry (DPI)	Uses polarised light from a laser passing through various waveguides and interacts with immobilised sample (i.e. the tethered membrane model). Changes in the resulting optical interference pattern are caused by changes in the structure and mass of the immobilised molecules.
Electro-chemical impedance spectroscopy (EIS)	Measures particle or ion transport across a tethered membrane model.
Quartz crystal microbalance with dissipation (QCM-D)	Measures changes in frequency and dissipation of an oscillating quartz crystal as an indicator of particle binding.
Surface plasmon resonance	Measures changes in resonating surface plasmons on metal sensor
Vesicle leakage assays	Pore formation of membrane causes release of dye from fluorescently loaded vesicles.

1.6.1 Surface plasmon resonance

Surface plasmon resonance (SPR) can be used to measure the adsorption of substances onto the a planar gold or silver sensor by detecting changes in the refractive index of the surface layer of a solution in contact with the sensor. The change in the refractive index causes a change in the reflected intensity angle and a sensorgram can plot this angle against time (Figure 1.4). When light is emitted from a light source, at a certain incidence angle, light is adsorbed by the electrons at the surface boundary between the sensor and the contact solution. This causes the

electrons, also referred to as surface plasmons, to resonate. The resonating surface plasmons are sensitive to the environment including the refractive index and the film thickness of an adsorbed layer. These then change the intensity of the reflected light, which can be measured. The binding kinetics of a material onto the sensor can also be investigated by observing the sensorgram as a function of time (Mahmoudi *et al.* 2011).

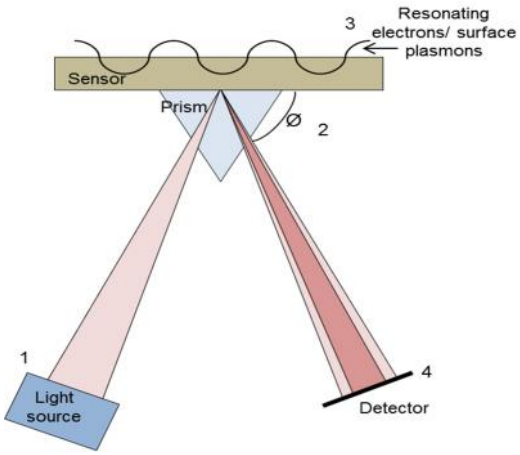

Figure 1.4 – The principle of surface plasmon resonance. 1 – Light is emitted from light source and hits the underside of the sensor chip. 2 – At a certain incidence angle (resonance angle), light is adsorbed by the electrons in the metal sensor, causing them to resonate. 3 – These resonating electrons (surface plasmons) are sensitive to the refractive index of the surrounding medium and the thickness of the sensor. 4 – The resulting electrons appear as a dark band by the detector. (Mahmoudi *et al.* 2011).

1.6.2 Vesicle leakage assays

In order to study the effect of particles on the cell membrane integrity, simple vesicle leakage assays have previously been used. Unlike techniques such as TEM analysis, vesicle leakage assays allow the quantification of the ability of particles to form membrane pores and thus damage the membrane. This method is based upon lipid vesicles being loaded with an auto-quenching fluorescent dye. Upon damage to the vesicle membrane, the dye is released, reducing auto-quenching and the increase in fluorescent intensity can be measured using a fluorometer (Naumann *et al.* 2011). Studies have revealed that silica and zinc oxide nanoparticles can induce membrane damage to model membrane vesicles in a dose dependent manner. However this was

only observed at the higher particle concentrations, which were equal or greater than 10 µg.ml^{-1} (Mu *et al.* 2012; Mu *et al.* 2014).

1.6.3 Quartz crystal microbalance with dissipation

The interactions and binding of nanoparticles or wear particles to a model membrane can also be measured using quartz crystal microbalance (QCM) systems with or without dissipation. This is a highly sensitive technique and can be modified to increase the complexity of the membrane model. Therefore the effect of specific factors on wear particle interactions with the cell plasma membrane can be investigated.

1.6.3.1 Principle of quartz crystal microbalance with dissipation

Quartz crystal microbalance measures changes in mass (Δm) per unit area by monitoring the change in frequency (Δf) of a resonating quartz crystal (Dixon 2008). The unique structure of the quartz crystal allows it to exhibit a piezoelectric effect (i.e. can produce an electrical current *via* pressure). Sandwiched between a pair of electrodes, when an alternating current is applied to a quartz crystal, it will oscillate at its resonant frequency of 4 – 6 MHz (Dixon 2008). The frequency of the oscillating crystal is dependent on the thickness of the crystal and therefore binding of materials to the sensor increases the thickness and in turn reduces the oscillating frequency. A change in the frequency of a rigid layer formed on the sensor surface directly corresponds to a change in mass as shown in the Sauerbrey equation below (Sauerbrey 1959).

$$\Delta m = -C\frac{1}{n}\Delta f$$

c = constant of quartz crystal properties (in this case 17.7 ng.cm^{-2}.s^{-1})
m = mass
n = overtone
f = frequency

Since the introduction of QCM, the applications of the technology have continued to expand such as solid supported bilayer lipid membranes (sBLMs) (Cho *et al.* 2010). For non-rigid layers, QCM can be combined to quantify the change in dissipation of the system, known as QCM with dissipation (QCM-D). The dissipation measures the loss of energy in the system from each oscillation divided by the total energy stored in the system. This can also be monitored alongside the change in frequency in real-time (Dixon 2008). When a soft layer is bound to the quartz crystal, it is deformed during oscillation and therefore a high dissipation is measured ($\Delta D > 0$). In contrast a rigid layer will mirror the crystal oscillation without being deformed ($\Delta D = 0$). During the formation of a sBLM, the lipid vesicles bind onto the surface of the crystal until saturation and burst to form a planar bilayer. Due to the hydrophobic and hydrophilic properties of phospholipids, the vesicles will arrange themselves to form a bilayer with a layer of polar head groups orientated towards the liquid interface and a second layer towards the solid surface (Kunze *et al.* 2011).

The inclusion of dissipation measurements allows structural information, binding strength and the swelling or hydration of the bound layers to be monitored in real-time. Multiple overtones (n) of the resonant frequency are also measured. Only the odd overtones (n = 3 – 13) can be excited electrically as these harmonics induce charges of the opposite sign at each end of the crystal surface (Kunze *et al.* 2011).

1.6.3.2 Nanoparticle interactions with a plasma membrane using quartz crystal microbalance with dissipation techniques

The advantage of the QCM-D is that it is high sensitivity and is able to measure changes in masses as low as 100 $pg.cm^{-2}$ of the crystal area (Dixon 2008). This method has been used successfully to measure membrane binding of synthetic nanoparticles onto a model membrane, including silica, copper, and zinc oxide nanoparticles (Mu *et al.* 2012; Karlsson *et al.* 2013; Mu *et al.* 2014). A typical example

was reported by Mu *et al.* (2012) whereby the binding of silica nanoparticles onto a sBLM, was measured using QCM–D (Figure 1.5). A reduction in the oscillating frequency was measured as the nanoparticles bound to the membrane. The change in the dissipation of oscillation was minimal, thus indicating a tight interaction between the particles and the membrane. Interestingly, it was observed that the introduction of washing steps did not alter the frequency or dissipation, thus indicating that the particles were irreversibly bound to the membrane. Furthermore, the addition of more nanoparticles did not alter the frequency, suggesting that particle binding onto the membrane had reached saturation point. Therefore this technique is highly advantageous in assessing particle and membrane interactions and could potentially be used for THR wear particles.

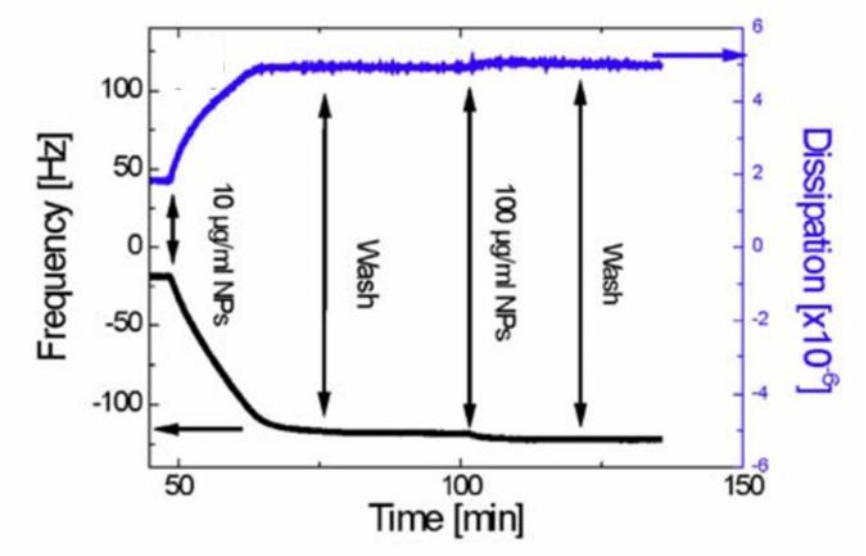

Figure 1.5 – Silica nanoparticles binding to a model membrane using quartz crystal microbalance with dissipation. An example of particle binding to a sBLM, using QCM-D, whereby a reduction in frequency (black) of approximately 90 Hz was measured upon the addition of the 10 $\mu g.ml^{-1}$ of 14nm silica nanoparticles. A small increase in dissipation (blue) of approximately 3 x 10^{-6} was also measured, indicating a tight interaction (Mu *et al.* 2012; copyright right permission granted by publisher).

Due to the sensitivity of QCM-D, factors effecting particle and model membrane interactions can be investigated, including particle morphology, size, and particle coating (Karlsson *et al.* 2013; Mu *et al.* 2014). Furthermore, the effect of protein

coronae can also be explored (Lesniak *et al.* 2012; Lesniak *et al.* 2013). Lesniak *et al.* (2013) reported that the addition of BSA to polystyrene particles reduced the binding of the particles to sBLM using QCM-D. The model membranes can also be tailored to each experiment and proteins can be incorporated into the membrane to investigate particle: protein interactions (Kunze *et al.* 2011).

The effects of albumin and endothelial cell attachment on to UHMWPE and CoCr substrates have previously been investigated by QCM-D, whereby the crystal surface was coated with the biomaterial of choice and the binding of substrate was measured (Serro *et al.* 2010; Castellanos *et al.* 2015). Castellanos *et al*. (2015) demonstrated that the addition of surface coatings on a CoCr alloy surface could improve cell binding for cardiovascular applications. However, at present the binding of wear particles from THRs to a model lipid membrane has not been investigated using QCM-D techniques.

1.7 Project aim

Currently little is known about the precise response mechanisms of cells to CoCr and, in particular, alumina particles. Specifically, how do the effects described above caused by alumina and CoCr particles manifest into the larger scale problems observed in patients? Studies published to date have failed to analyse the effects of CoCr and alumina wear particles interactions with the plasma membrane. Furthermore, it is not known if the passing of the particles through the membrane induces cytotoxic effects, or whether a reduction in the cell viability occurs once the particles are internalised. Furthermore it is not known what factors influence particle: membrane interactions and subsequent cellular responses, such as the formation of protein corona or the presence of specific membrane proteins. Large gaps in the knowledge about CoCr and alumina particles remain. Therefore, research into the fundamentals of particle: membrane interactions will provide an insight into the biocompatibility of alumina and CoCr particles.

This project aims to determine if nanoscale and micron sized alumina and CoCr particles are able to damage or passively pass the cell membrane with adverse consequences.

1.7.1 Specific objectives

The main objectives of this study are listed below and are summarised in Figure 1.6.

- To generate nanoscale CoCr particles using simple configuration wear simulator.
- To characterise nanoscale CoCr particles alongside commercially available micron sized CoCr wear particles using SEM image analysis. To characterise nanoscale and micron sized alumina particles, isolated from an alumina powder.
- To determine the effects of nanoscale and micron sized alumina and CoCr particles on primary HFBs and U937 histiocytes in terms of cell viability.
- To study the effect of nanoscale and micron sized alumina and CoCr particles on membrane integrity and binding using model membrane systems.
- To study the effect of nanoscale and micron sized alumina and CoCr particles on membrane integrity and binding using a model lipid membrane (a sBLM) with incorporated fibroblast membrane proteins.
- To study the effect of nanoscale and micron sized alumina and CoCr particles on fibroblast cell viability and particle uptake in the presence of FBS.
- To study the effect of nanoscale and micron sized alumina and CoCr particles on membrane integrity and binding using a model lipid membrane (a sBLM) in the presence of FBS.
- To study the effect of nanoscale and micron sized alumina and CoCr particles on membrane integrity and binding using a model lipid membrane (a sBLM) with incorporated fibroblast membrane proteins, in the presence of FBS.

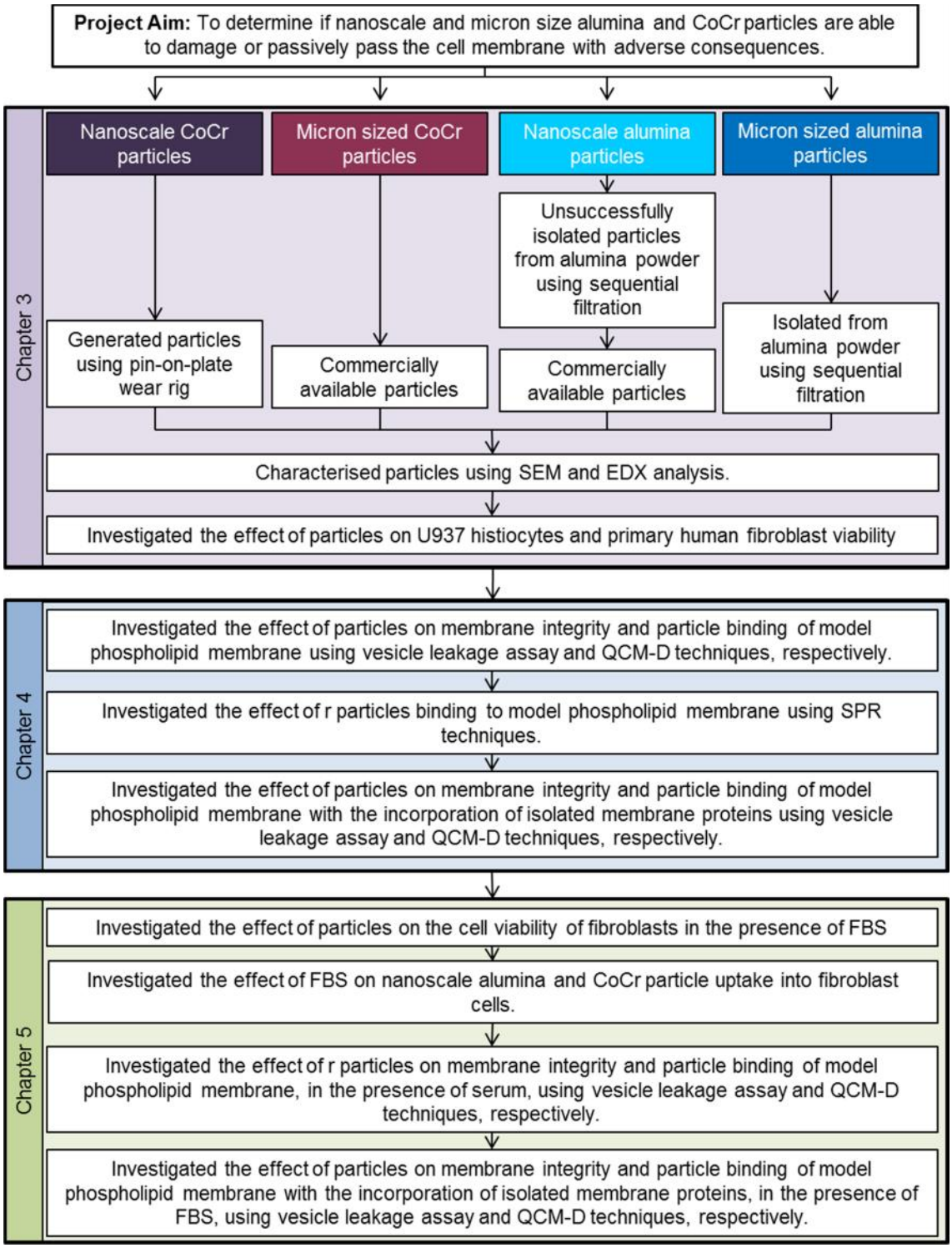

Figure 1.6 – Flow diagram of project objectives and experimental methods.

Chapter 2

Materials & Methods

2.1 Materials

2.1.1 Nanoscale and micron sized cobalt chromium and alumina particles

Commercially available particles of alumina ceramic (nanoscale and micron sized) and micron sized CoCr particles were used throughout the study (Table 2.1). Nanoscale CoCr particles were generated in house (Section 2.2.1).

Table 2.1 – Alumina and cobalt chromium particles used during the project

Particle Type	Composition	Supplier
Micron sized CoCr particles	62.2% Co 28.7% Cr 0.71% Ni	Sandvik Osprey Ltd, Neath, U.K.
Nanoscale CoCr particles	ASTM F1537	Generated in house from supplier Depuy, Leeds, U.K
Micron sized alumina particles	Zirconia toughened Al_2O_3	BIOLOX forte, manufactured by Ceramtec AG, Plochingen, Germany
Nanoscale alumina particles	Al_2O_3	PlasmaChem, Berlin, Germany

2.1.2 Cobalt chromium pins and plates

Six CoCr pins were machined from a high carbon > 0.2% (w/w) CoCrMo alloy (ASTM F1537). The pins were polished in house by Mrs. Jane Cardie (Technician, School of Mechanical Engineering) with a radius of curvature of 100° and finished

to a surface roughness (Ra) of 0.02 – 0.04 µm (Figure 2.1). Smooth CoCr plates used in the 6 station wear rig were also machined from the same high carbon CoCr alloy, with a Ra of 0.01 – 0.02 µm.

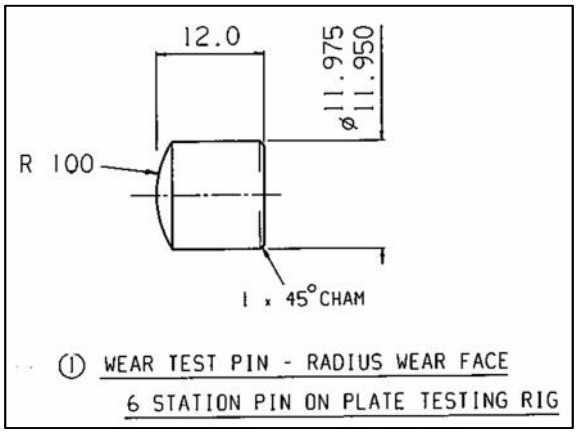

Figure 2.1 – Dimensions of machined cobalt chromium pins used in the pin-on-plate wear simulators. R – Radius of curvature. Ø – Diameter of pin.

2.1.3 Membrane lipids and cholesterol

A lipid mixture, similar to that found in fibroblast plasma membranes was prepared from extracted porcine brain lipids (Riordan 1979). The following phospholipid and cholesterol compounds were used to form the model fibroblast membranes (Table 2.2).

Table 2.2 – Phospholipid and cholesterol compounds used to form the model fibroblast membranes

Compound	Suppliers	Product Code
Cholesterol	Sigma Aldrich, UK	C8667
Porcine brain phosphatidylcholine	Avanti Polar Lipids, Alabaster, USA	840053C
Porcine brain phosphatidylserine	Avanti Polar Lipids, Alabaster, USA	840032C
Porcine brain phosphatidylethanolamine	Avanti Polar Lipids, Alabaster, USA	840022C

2.1.4 Cells

The cells used throughout this study are listed in Table 2.3.

Table 2.3 – Cells used throughout this study and suppliers

Cell line	Type	Species	Supplier
L929	Fibroblast	Murine	European Collection of Animal Cell Culture
U937	Histiocyte	Human	European Collection of Animal Cell Culture
Primary dermal fibroblasts	Fibroblast	Human	NHS Blood and Transplant

2.1.5 Chemicals

The chemicals used throughout this study are listed in Appendix A, Table 1.

2.1.6 Computer Software

The computer software used throughout this study are listed in Appendix A, Table 2.

2.1.7 Consumables

The general consumables used throughout this study are listed in Appendix A, Table 3.

2.1.8 Equipment

The equipment used throughout this study is listed in Appendix A, Table 4.

2.1.9 Glassware

The glassware used throughout this project is listed in Appendix A, Table 5.

2.1.10 Stock solutions

2.1.10.1 3-(N-morpholino)propanesulfonic acid (MOPS) buffer for membrane and particle experiments

A stock solution of 20mM 3-(N-morpholino)propanesulfonic acid (MOPS) with 30 mM sodium sulphate (Na_2SO_4) was prepared in ultrapure distilled water. Once in solution, the pH was adjusted to pH 7.4 and stored at room temperature for approximately one month.

2.1.10.2 Cell culture medium and supplements

The cell culture medium for both L929 and primary human fibroblast (HFB) cells was Dulbecco's Modified Eagles Medium (DMEM), without L-glutamine. U937 cells were cultured in Roswell Park Memorial Institute (RPMI) 1640 medium. Both types of medium were supplemented with 10% (v/v) foetal bovine serum (FBS), 2 mM L-glutamine and 100 $\mu g.ml^{-1}$ penicillin:streptomycin. Supplemented cell culture medium was stored at 4°C for a maximum of 4 weeks.

2.1.10.3 Homogenising solution for cell plasma membrane isolation

The homogenising solution was made fresh on the day of cell plasma membrane isolation and was stored on ice. Sucrose, at a concentration of 250 mM was dissolved in 10 mM Tris-HCl, pH 7.5. This was supplemented with one tablet of Roche "Complete" proteinase inhibitors (containing a broad spectrum of serine,

cysteine and metalloproteases inhibitors) per 50 ml of the homogenising solution and 1 mM dithiothreitol (DTT). A 1M solution of phenylmethanesulfonyl fluoride (PMSF) was prepared in ethanol and added to the homogenising solution at a final concentration of 0.5 mM.

2.2 Methods

2.2.1 Particle generation using six station pin-on-plate simple configuration wear simulator

Cobalt chromium particles were generated using the six station pin-on-plate wear simulator, which was designed and manufactured by the School of Mechanical Engineering, University of Leeds. Smooth, high carbon, CoCr alloy pins and plates were used as described in section 2.1.2.

2.2.1.1 Cleaning of rig components

All CoCr pins and plates were cleaned using ultrasonication whilst immersed in 70% (v/v) isopropanol for 10 minutes at room temperature. The six station rig was cleaned, whereby all the components were washed in household detergent and immersed in 1 % (v/v) Trigene for 20 minutes. All components were then rinsed in copious amounts of water, followed by a final rinse in distilled water. Finally all components were dried using disposable paper towelling before being ready for use (Figure 2.2).

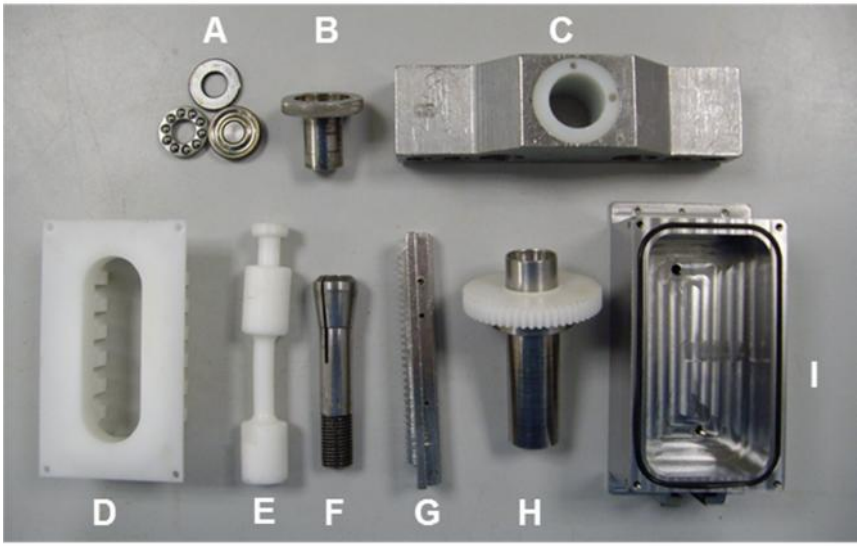

Figure 2.2 – Components of the six station pin-on-plate simple configuration wear simulator. A – Ball bearing assemblies. B – Threaded nut. C – Bridge section. D – Polymer baffle. E – Connecting rod. F – Collet. G – Toothed rack. H – Pin holder with polymer gear wheel. I – Plate bath and rubber seal.

2.2.1.2 Assembly of six station pin-on-plate simple configuration wear simulator

The pins and plates were individually numbered and the pairing of the pin and plates for each station remained constant throughout the tests. The orientation of the plate within the bath also remained the same. The components were assembled, whereby each plate was screwed into a separate bath. A rubber seal was placed in the groove of the bath and a plastic baffle was secured into position, covering the top of the bath. The toothed racks were screwed into position on the side of each bath. Each numbered bath was secured into place on the rig at the corresponding station number (Figure 2.3A). Each pin was placed in a pin collet, using metal spacers to ensure that the pin protruded approximately 5 mm from the collet (Figure 2.3B). The pin and pin collet were placed in the pin holder, which was then slotted into the corresponding bridge section of the rig (Figure 2.3C). The pin holder and bridge section were secured into position and the connection between the pin holder and toothed rack on the bath was checked (Figure 2.3D). Washers

were then placed on top of the pin holder and a small amount of Vaseline® was put on the washers to act as a lubricant. One end of the plastic connecting rod was slotted into the holder at the front of each bath and the other end of the rod was secured to the scotch yoke mechanism (Figure 2.3E).

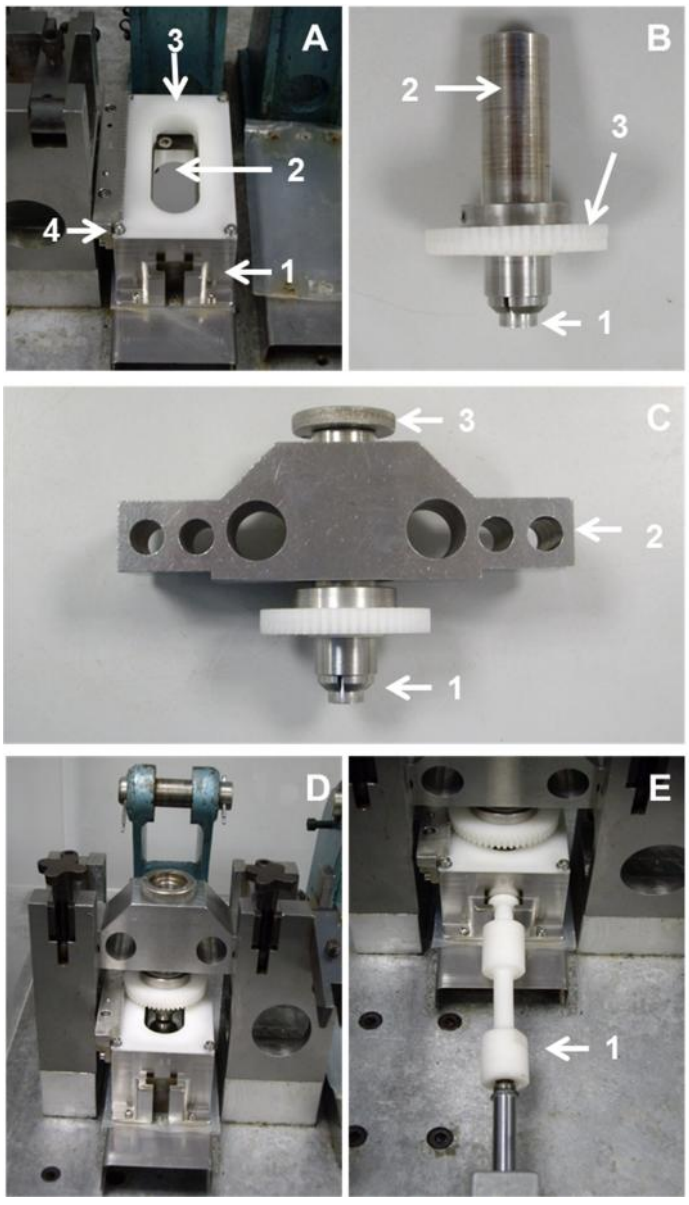

Figure 2.3 – Assembly of the six station pin-on-plate simple configuration wear simulator. A – The bath (1) containing the plate component (2) was secured into position on the rig with corresponding baffle (3) and toothed rack (4). B - The pin (1) was placed in the collet and pin holder (2) with plastic gear wheel (3) attached. C – The pin and pin holder (1) were slotted into the corresponding bridge section (2) and secured into position using a threaded nut (3). D – The bridge section and pin holder were secured into position over the bath. E – The plastic connecting rod (1) was slotted into the groove of the bath and screwed onto the scotch yoke mechanism.

2.2.1.3 Generation of cobalt chromium particles using six station pin-on-plate simple configuration wear simulator

The lubricant used was ultrapure deionised water and approximately 30 ml was added to each bath. The pin holder was lifted slightly to ensure the presence of lubricant between the pin and plate prior to commencing the operation of the wear rig. The cantilever arm was secured into position using the pivot pins. Using a spirit level and spanner, the pin on the cantilever arm was altered to ensure the arm was level.

The cycle counter on the rig was set to zero and the motor was turned on. The frequency was recorded and adjusted to 1 Hz or 60 cycles.min^{-1}, with a stroke length of 28 mm and a rotation ± 30°. A steel weight was then added to each of the cantilever arms to correspond to 80 N per station (Figure 2.4). The rig was operated for 2 weeks during the day (approximately 8 hours per day). Before switching off the rig at the end of each day, the speed was slowly reduced and the weights were removed. The lubricant was topped up each day to maintain sufficient lubrication. Upon completion of the pin-on-plate testing, the number of cycles was recorded and the rig was dismantled. The pin, CoCr plate, bath and lubricant were subjected to ultrasonication in ultrapure distilled water for short intervals (10 – 15 seconds) to dislodge any adherent particles. The lubricant containing the particle debris for each station was transferred into appropriately labelled sterile plastic pots and stored at -20°C.

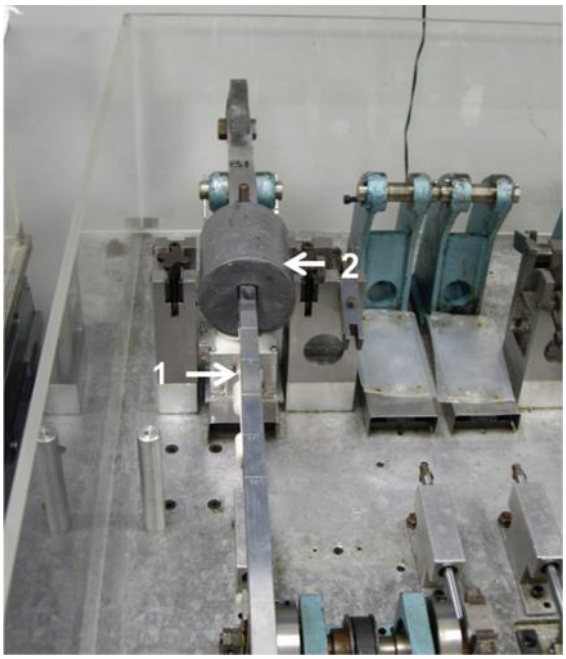

Figure 2.4 – Assembled station of the six station wear rig with cantilever arm (1) and weight (2).

2.2.1.4 Centrifuging cobalt chromium nanoscale particle stock

The CoCr nanoscale particles in distilled water generated in section 2.2.1, were defrosted and subjected to sonication for 30 minutes to disperse the particles. In order to form a more concentrated particle stock to be sterilised, the particle suspension was transferred to clean polycarbonate centrifuge tubes and placed in a SS-34 centrifuge rotor. The centrifuge tubes used were appropriate for the SS-34 centrifuge rotar. The particle suspension was centrifuged for 30 minutes at 45 000 g at 4°C. The supernatant was removed and the particle pellet was suspended in 5 ml of ultrapure distilled water. The particle suspension was subjected to sonication for 20 minutes and then transferred into a clean glass universal. The particle suspension was stored at -20°C until required.

2.2.2 Preparation of particles for cell culture studies

A small sterile glass vial was covered with foil and weighed using the AT21 balance, which is sensitive to 10^{-6} grams. A reference glass vial was weighed, followed by the glass vial and the balance was zeroed between each repeat. The mass of the reference vial and vial were measured until five repeats were within 100 µg of one another. The reference vial was used to account for the changes of the atmospheric conditions of the measuring environment before and after the adding of the particles to the glass vial. The particle suspension (section 2.2.1) was thawed and a small amount (2 – 3 ml) was pipetted into the pre-weighed vial. The particles were then placed in the oven for 4 hours at 190°C to sterilise the particles and to remove the water. The vial was weighed again until 5 repeats were within 100 µg of one another were obtained. The mass of the particles was calculated by subtracting the average weight of the vial from the average weight of the vial plus the particles. This mass was adjusted according to the changes in the weight of the reference vial before and after adding the particles to take into account the changes in the atmospheric conditions. The particles were suspended with the appropriate volume of sterile ultrapure distilled water to give a stock particle concentration of 1 $mg.ml^{-1}$, which was stored at -20ºC.

2.2.3 Cell culture

2.2.3.1 Resurrection of L929 and U937 cell lines

A cyrovial of approximately 1 x $10^6.ml^{-1}$ of cells was removed from the liquid nitrogen dewar and quickly thawed in a water bath at 37°C. Once thawed, the cells were immediately transferred to a sterile universal containing pre-warmed fresh culture medium (10ml). The cell suspension was centrifuged (150g) for 10 minutes at 20°C. For U937 cells the cell suspension was centrifuged at 200g for 10 minutes

at 20°C. The supernatant was removed and discarded and the pellet was suspended in 2ml of fresh culture medium. The cell suspension was added to a sterile culture flask (75 cm^2) containing 10 ml of fresh cell culture medium and incubated at 37^oC in 5% (v/v) CO_2 in air until approximately 80% confluent. Confluency was determined using a light microscope and adherent cells which covered at least 80% of the flask plastic within the field of view were deemed confluent. For the non-adherent U937 cells, the cells were determined to be confluent when the field of view, under the light microscope, was occupied by more than 50 – 60% cells. The cell culture medium was changed every 2-3 days for the L929 cells until confluent. For the U937 cells, 3 ml of fresh cell culture medium was added to each flask every 2 days until the cells were confluent. The U937 cells were incubated in cell culture flasks at a 45° angle at 37^oC in 5% (v/v) CO_2 in air.

2.2.3.2 Resurrection of human fibroblast cells

A cyrovial of cells was removed from the liquid nitrogen dewar and quickly thawed in a water bath at 37°C. Once thawed the cell suspension was added to 10 ml of pre-warmed cell culture medium in a 75 cm^2 culture flask. The cells were incubated at 37°C in 5% (v/v) CO_2 in air for 18 hours to allow the cells to adhere to the tissue culture plastic. Once adhered, the cell culture medium was replaced with 10 ml of fresh medium. The cell culture medium was changed every 2 – 3 days until the cells were 80% confluent.

2.2.3.3 Cell culture maintenance of U937 histiocytes and L929 and human fibroblast cells

Once the cells had achieved 80% confluency the cell culture medium was removed from the flask and the cells were gently washed twice with 10ml of sterile

Dulbecco's phosphate buffer saline (DPBS) (without calcium and magnesium). The cells were treated with trypsin-ethylenediaminetetraacetic acid (EDTA) (1 ml) for 5 – 10 minutes in 5% (v/v) CO_2 in air at 37°C to detach the cells from the flask. The side of the culture flask was firmly tapped to dislodge the cells from the tissue plastic and the trypsin-EDTA was inhibited by the addition of fresh cell culture medium containing 10% (v/v) FBS. The cell suspension was transferred into a sterile universal and centrifuged (150g) for 10 minutes. The U937 cells are a suspension cell line and therefore once confluent, the cell suspension was also centrifuged (150g) for 10 minutes. The following steps of cell maintenance were used for all cells types. The supernatant was carefully aspirated from the pellet and suspended in 5 ml of DMEM culture medium. A trypan blue exclusion assay was performed (section 2.2.3.4) and the cells were seeded into a fresh cell culture flask (75 cm^2 or 175 cm^2) at a seeding density of (1 x 10^4 cells per cm^2) with either 10 ml or 20 ml of fresh DMEM cell culture medium, respectively. The cells were incubated in 5% (v/v) CO_2 in air at 37°C and the cell culture medium was replaced every 2 – 3 days until confluent. Cells were maintained for up to 12 passages before being discarded.

Cells were stored in long term storage by passaging the cells as described above. The cells were suspended at a density of 1 x 10^6 cells.ml^{-1} in DMEM supplemented with 20 % (v/v) FBS and 10 % (v/v) filter sterilised dimethyl sulphoxide (DMSO). A volume of 1.5 ml of the cell suspension was transferred into each labelled, sterile cryovial and placed in a freezing pot containing isopropanol. The cyrovials were placed at -80^{o}C for 4 hours before being transferred into liquid nitrogen for long-term storage.

2.2.3.4 Trypan blue exclusion assay

Cell viability was determined by diluting a small aliquot (20 µl) of the suspended cell pellet with 20 µl of trypan blue. Using a Neubauer haemocytometer and light

microscope, the total number of cells was counted from a 10 µl aliquot of the trypan blue: cell suspension mixture. A minimum of 100 cells and a maximum of 300 cells were counted within the 25 counting squares of the haemocytometer. The number of non-viable cells was subtracted from the total cell count to give the number of viable cells. Non-viable cells appeared blue, whereas viable cells were transparent in appearance. The number of viable cells per ml was calculated using the following formula:

$$\text{Number of cells. ml}^{-1} = (\text{number of viable cells}) \times 2 \times 10^4$$

2 = dilution factor of the cell suspension within the trypan blue

10^4 = dilution factor to account for volume of haemocytometer

2.2.4 Culturing cells in the presence of nanoscale and micron sized alumina and cobalt chromium particles

The effect of nanoscale and micron sized alumina and CoCr particles on the cell viability of L929, primary HFB and U937 cells was determined using the ATP-lite and MTT cell viability assays. A flask of L929 and primary HFB cells, which were greater than 80% confluent, was treated with trypsin-EDTA and a cell count was performed (section 2.2.3.3 and 2.2.3.4). An appropriate volume of cell culture medium was added to the cell suspension to give a final cell density of $1x10^5.ml^{-1}$. For the U937 cells, the cells were not treated with trypsin, but the cell suspension was centrifuged at 200g for 10 minutes and a cell count was performed (section 2.2.3.4). The volume of the U937 cell suspension was altered to give a final cell density of $2x10^5.ml^{-1}$. For each well, 100 µl of the cell suspension was added to a sterile, clear, flat-bottomed 96 well plate and incubated in 5% (v/v) CO_2 in air at 37^{o}C. In the case of U937 cells U-shaped 96 well plates were used. A separate plate was prepared for each time point and each cell viability assay to be

performed. The cells were incubated for 18 hours to allow the cells to adhere or form a cell spheroid for non-adherent cells.

The cells were cultured with nanoscale CoCr particles (section 2.2.1) or commercially available micron sized CoCr particles (section 2.1.1) at particle volumes per cell of 50 μm^3, 5 μm^3, 0.5 μm^3, 0.05 μm^3, 0.005 μm^3 and 0.0005 μm^3 using the calculation in Appendix B. For the alumina particles, the cells were cultured with nanoscale or micron sized particles at particle volumes per cell of 500 μm^3, 50 μm^3, 5 μm^3, 0.5 μm^3, 0.05 μm^3, 0.005 μm^3 and 0.0005μm^3 using the calculation in Appendix B. Particle volume to cell number ratios were used in the cell viability experiments to allow an accurate comparison between experiments using different particle sizes (Matthews *et al*. 2000). Matthews *et al*. (2000) reported histological analysis of wear debris to be at a particle volume of approximately 60 μm^3 per macrophage. Previous studies have reported alumina and CoCr nanoscale particles to significantly affect cell viability at particle volumes of at least 5 μm^3 and 50 μm^3, respectively. Therefore, whilst the range of particle volumes used were greater than what would be expected from the wear volumes produced *in vivo,* the main aim of this study was to compare the cell viability results against the published literature. Hence, the particle volumes used reflected previously published literature (Germain *et al.* 2003; Papageorgiou *et al.* 2007). Each particle suspension was sonicated for 5 minutes before 100 µl of each particle suspension was added to the cells. The negative control was cells in 200µl of medium and the positive control was camptothecin at a final concentration of 2 $\mu g.ml^{-1}$. A particle only control was included which was the highest particle dose in medium in the absence of cells. A blank was also included which was 200 µl of medium only. Each treatment was repeated six times and the cells were cultured with the particles in 5% (v/v) CO_2 in air at 37^oC. The cell viability was assessed over 5 days at specific time points of day 0, 1, 3 and 5. Each experiment was repeated at least twice.

2.2.5 Determination of cell viability

Cell viability was determined using two different assays, the ATP-lite and MTT assay. Nanoscale particles have been reported to directly interfere with a number of cell viability assays and generate misleading results (Monteiro-Riviere *et al.* 2009). Therefore the combination of using two assays was used to provide a better understanding of how the particles affect cell viability. The ATP-lite assay is highly sensitive and can measure ATP levels in as few as ten cells. Upon cell death, a reduction in cellular ATP will occur, and can be used as an indicator of cytotoxicity (Crouch *et al.* 1993). The MTT assay measured the reduction of a yellow tetrazole to a purple formazan by dehydrogenase activity of viable, metabolising cells. Consequently this assay measures the effect of cell metabolism (Stockert *et al.* 2012).

2.2.5.1 Determination of the cell viability using the ATP-lite assay

The ATP detection kit assay (ATP-lite™ assay), which measures the levels of ATP present within the cells by the reaction of ATP with D-luciferin and is outlined in the following reaction (Crouch *et al.* 1993). Based on this reaction, the amount of ATP present can be determined by measuring the emission of light from the sample.

ATP + D-Luciferin + oxygen → Oxyluciferin + adenosine monophosphate + inorganic pyrophosphate + CO_2 + Light

The culture medium was removed from each well of the 96-well plate and replaced with 100 µl of fresh cell culture medium before commencing the assay. For U937 cells, the plate were centrifuged at 200g for 1 minute at 20°C prior to 100 µl of medium being removed from each well. Mammalian cell lysis solution was added to

each well (50 µl) and the plate was shaken (80g) for 5 minutes. Reconstituted lyophilised substrate was then added at a volume of 50 µl per well and again the plate was shaken (80g) for 5 minutes. The cell suspension in each well was transferred to the corresponding well of a 96-well Optiplate® and an adhesive clear film lid was placed over the plate to prevent contamination. The plate was read using a luminescence reader, which dark-adapted the plate for 10 minutes and measured the luminescence of each well for 10 seconds using MikroWin 2000 software. The output was presented as counts per second (CPS) and was exported to the Excel computer software (2010 version). The average of the blank readout was subtracted from all the results except for the cells which were cultured with the highest particle volume, whereby the particle only control was subtracted instead. This was to ensure that the particles did not directly interfere with the assay and produce “false positive” or “false negative” results.

2.2.5.2 Determining cell metabolism using the 3-(4,5-dimethylthiazol-2-yl)-2,5-diphenyltetrazolium bromide (MTT) assay

Cell metabolism was also determined using the 3-(4,5-dimethylthiazol-2-yl)-2,5-diphenyltetrazolium bromide (MTT) assay, which is a yellow tetrazole and is reduced to a purple formazan by viable, metabolising cells (Figure 2.5) (Stockert *et al.* 2012). The absorbance reading of the formazan can be measured as an indicator of cell metabolism. The formazan is water insoluble and must be liberated from the cells using acidified sodium dodecyl sulphate (SDS-HCl) to lyse the cells.

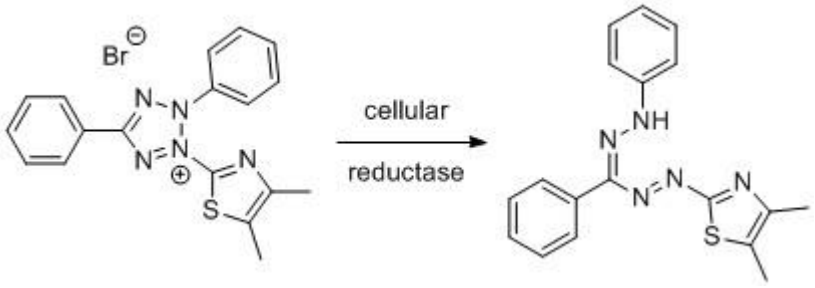

Figure 2.5 – Reduction of 3-(4, 5-dimethylthiazol-2-yl)-2, 5-diphenyltetrazolium bromide, (MTT) to a purple formazan.

For L929 and primary HFB cells, 200 µl of the culture medium was removed from each well of the 96-well plate before commencing the assay and replaced with 100 µl of fresh medium. For U937 cells, the plates were centrifuged at 200g for 1 minute at 20°C prior to 100 µl of medium being removed from each well. The MTT solution (5 $mg.ml^{-1}$ diluted in PBS) was added to each well (20 µl) for 4 hours. The MTT product was released from the cells using SDS-HCl, whereby 10 g of SDS was dissolved in 100 ml of distilled water. Once dissolved, 1 ml of 1M of HCl was added. The solution was filter sterilised using a 0.2 µm pore size filter and 100 µl of SDS-HCl was added to each well and incubated in 5% (v/v) CO_2 in air at 37^{o}C for 18 hours. The absorbance was read at 570 nm using the MultiScan plate reader and ScanIt MSS software (version 2). The average absorbance measurements for the blank were subtracted from all the absorbance values of the treatment groups. However, for the cells cultured in the presence of the highest particle volume, the average absorbance for the particle only control was subtracted instead.

2.2.6 Determination of the effects of nanoscale and micron sized alumina and cobalt chromium particles on model membranes

In order to determine the effect of nanoscale and micron sized alumina and cobalt chromium particles on the cell plasma membrane, a series of experiments using a

model membrane have been used. This model membrane mimics the composition of the plasma membrane of human fibroblast cells. The model membrane has various degrees of complexity, with some experiments including the addition of isolated membrane proteins into the model membrane. Furthermore this series of model membrane experiments used vesicle leakage assays and QCM-D techniques. Vesicle leakage assays involved the formation of lipid vesicles loaded with an auto-quenching fluorescent dye. When incubated with particles, if the particles induced membrane damage, the fluorescent dye was released from the vesicles and the fluorescence of the released dye was measured using a fluorescent spectrometer. Particle binding to the model membrane was also determined using the QCM-D technique, whereby a planar bilayer of the lipids was formed on an oscillating quartz crystal. Upon the binding of the particles to the membrane, a change in the frequency and dissipation of the crystal and surrounding environment could be measured in real-time. These parameters were analysed to determine if binding had occurred.

2.2.6.1 Formation of phospholipid: cholesterol membrane mixture

A lipid mixture, similar to the composition of the plasma membrane of human fibroblast cells was prepared from extracted porcine lipids (Riordan 1979). Cholesterol, phosphatidylcholine, phosphatidylserine, and phosphatidylethanolamine were combined at a weight ratio of 5:10:2:3, respectively (section 2.1.3). The lipid mixture was dissolved in chloroform: methanol (1:1) and 5 mg aliquots of the lipid mixture were transferred into sterile 1.5 ml glass vials. The chloroform: methanol solution was removed by drying the glass vial aliquots in a desiccator, under vacuum, for at least 2 hours. The lid of each vial was slightly loosened and stored in a round bottom, short neck flask with stopcock adaptor under nitrogen, at -20°C until required.

2.2.6.2 Formation of lipid vesicles for vesicle leakage and quartz crystal microbalance with dissipation experiments

Lipid vesicles were formed by suspending a 5 mg vial of the lipid mixture prepared in section 2.2.6.1 in 1 ml of 20 mM MOPS with 30 mM sodium sulphate, pH 7.4. The lipids were dispersed in the solution by vortexing at 30 second intervals until the lipid mixture was cloudy and no precipitate on the bottom of the vial was observed. In order to form the vesicles the lipid mixture was passed through a track-etched polycarbonate filter with a pore size of 100nm, using an extruder (Figure 2.6).

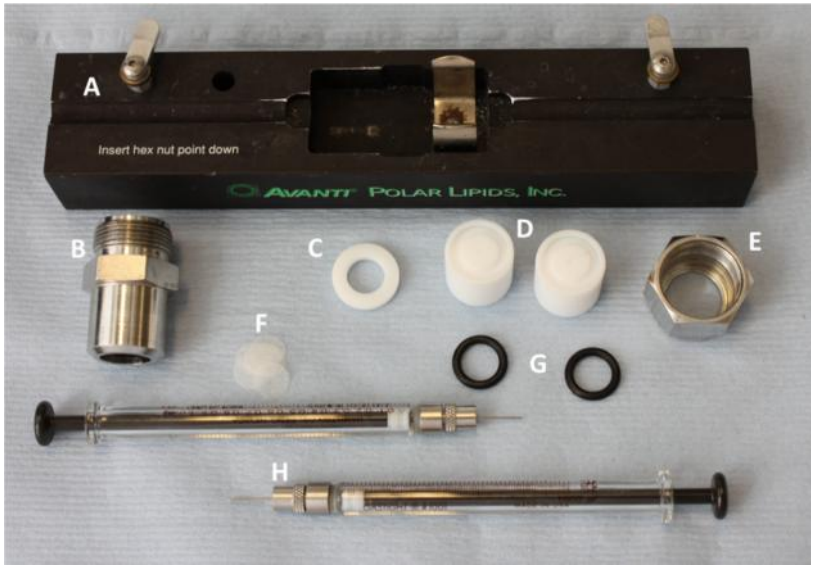

Figure 2.6 – Components of the vesicle extruder. A – Extruder holder. B – Large extruder outer casing. C – Teflon bearing. D – Internal membrane supports. E – Small extruder outer casing. F – Filter supports. G – O-rings. H – Glass syringes.

The extruder was assembled by placing each O-ring onto the two internal membrane supports. Two pre-wetted filter supports were placed on to each internal membrane support with the O-rings facing up (Figure 2.7A). The Teflon bearing was placed into the smaller extruder casing component, followed by one of the internal membrane supports (Figure 2.7B). Using tweezers a track-etched

polycarbonate filter with a pore size of 100nm was placed over the filter support of the internal membrane support. The second plastic holder (O-ring facing down) was placed on top of the filter and the second larger extruder outer casing was placed over the internal membrane supports and screwed tight to secure the components into position (Figure 2.7C & D).

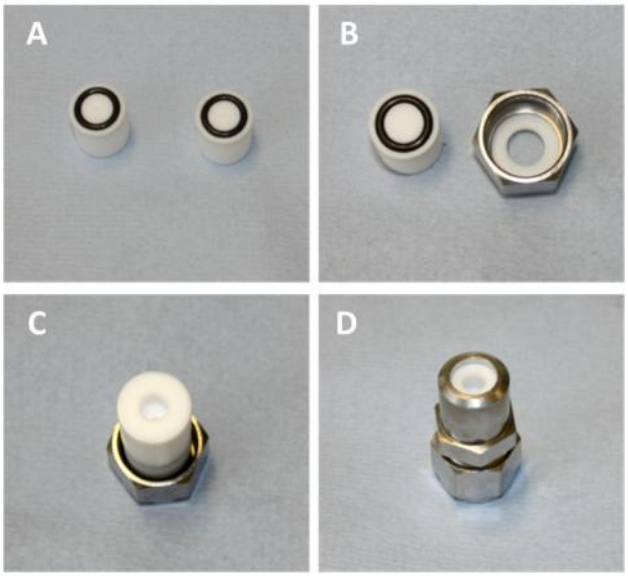

Figure 2.7 – Assembling vesicle extruder. A – The internal membrane supports with O rings and filter supports. B – Teflon bearing is placed in the smaller extruder casing, followed by one of the internal membrane supports. C – The polycarbonate filter is placed on top of one of the internal membrane supports. The second internal membrane support is placed face down on top on the membrane. D – The larger outer extruder casing is screwed into position to secure the components together.

To ensure there were no leakages, 1 ml of 20 mM MOPS with 30 mM sodium sulphate, pH 7.4 was passed through the extruder using the glass syringes (Figure 2.8). The solution was removed into a waste pot and replace with the lipid mixture. The lipid mixture was passed through the membrane at least 11 times to ensure sufficient vesicle formation. The vesicle mixture was then transferred into a 1.5 ml Eppendorf and stored at 4°C until required. The vesicle mixture was stored for a maximum of 3 days before being discarded.

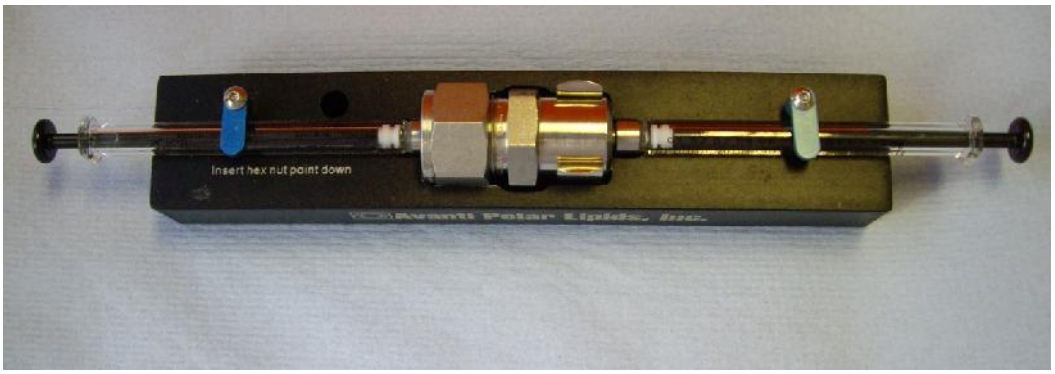

Figure 2.8 – Assembled extruder with syringes.

2.2.6.3 Determination of vesicle leakage in the presence of nanoscale and micron sized alumina and cobalt chromium particles

To measure the potential the of nanoscale and micron sized alumina and CoCr particles to damage the lipid membrane, a simple vesicle leakage assay was used.

2.2.6.3.1 Preparation of carboxylfluorescein loaded lipid vesicles

Carboxylfluorescein (CF) loaded lipid vesicles were formed by suspending a 5 mg vial of lipids (section 2.2.6.1) with 1 ml of 50 mM carboxylfluorescein (CF) dye (pH 7.4). After vortexing, the lipid suspension was passed through a track-etched polycarbonate filter with a pore size of 400nm using an extruder as described in section 2.2.6.2. The vesicles encapsulated with the dye were separated from the remaining CF dye using a size exclusion chromatography G-25 column (Nap-5, GE Healthcare Sciences). The column was placed in a clamp and stand and rinsed three times with approximately 3 ml of DMEM medium (without phenol red or any L-glutamine and antibiotic supplements). The vesicle mixture (0.5 ml) was then added to the column and the vesicles were eluted from the column by adding 1 ml of DMEM medium (without phenol red) (Figure 2.9). The eluted vesicles were

collected in a Eppendorf and stored at 4°C until required for a maximum of 3 days before being discarded.

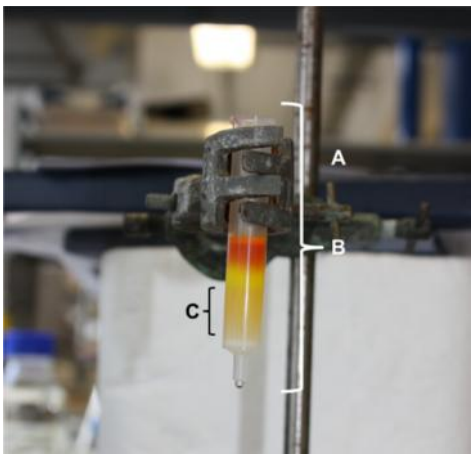

Figure 2.9 – Separation of fluorescently loaded lipid vesicles from the fluorescent dye. A – Stand and clamp. B – Size exclusion chromatography G-25 column. C – Band of vesicles isolated from fluorescent dye.

2.2.6.3.2 Measuring vesicle leakage in the presence of alumina and cobalt chromium particles using a fluorescence spectrometer

The leakage of fluorescent dye from the vesicles incubated in the presence of nanoscale and micron sized alumina and CoCr particles was monitored using a fluorescence spectrometer (LS 55, Perkin-Elmer) and the FL Win Lab computer software (version 4) in real time. The excitation wavelength of the CF dye was 492 nm with an emission wavelength of 517 nm. A 1:100 dilution of the CF loaded vesicles in DMEM medium (without phenol red) was placed on ice. A quartz cuvette was inserted into the cuvette holder of the fluorescence spectrometer and the diluted CF loaded vesicles were further diluted in 1:100 DMEM medium (without phenol red) within the cuvette. The fluorescence was monitored for at least 200 seconds prior to the addition of particles. The particles (nanoscale and micron sized alumina or CoCr particles) were added to the cuvette at incremental concentrations of 1, 10 and 100 $\mu g.ml^{-1}$ for at least 200 seconds for each particle concentration. Following this, to ensure the vesicles had completely lysed and released any

encapsulated dye, 6 µl of 10% (w/v) Triton X-100 was added to the sample. An average fluorescence reading of at least 200 seconds for each particle concentration and Triton-X 100 was recorded and the values were presented as a percentage of the Triton X-100 measurements. Each vesicle leakage experiment was repeated three times. A paired t-test was performed on the measurements recorded for each particle concentration to determine statistical significance. The data was found to be normally distributed and 95% confidence limits and statistical data were performed on the raw data.

2.2.6.3.3 Investigation into the quenching effect of particles on the vesicle leakage assay

The vesicle leakage assays were performed as described in section 2.2.6.3.2. However, once the fluorescence of the diluted vesicles had been monitored for at least 200 seconds, 6 µl of 10% (w/v) Triton X-100 was added prior to the addition of the particles to the cuvette. This was to ensure that the fluorescent dye had been completely released from the vesicles in order to determine the effect of the particles on the absorbance reading of the dye. After at least 200 seconds, the particles (nanoscale and micron sized alumina or CoCr particles) were added to the cuvette at incremental final concentrations of 1, 10 and 100 $\mu g.ml^{-1}$. An average fluorescence reading for at least 200 seconds for each particle concentration and the Triton-X 100 treatment was measured and the values were presented as a percentage of Triton X-100. Each vesicle leakage experiment was repeated three times. A paired t-test was performed on the results between each treatment group to determine statistical significance.

2.2.6.4 Determining particle binding to a model lipid membrane using quartz crystal microbalance with dissipation

Particle binding on a planar lipid bilayer was monitored using quartz crystal microbalance with dissipation. Lipid vesicles were formed from a 5 mg vial suspended in 20 mM MOPS with 30 mM sodium sulphate, pH 7.4 and kept on ice until required as previously described in section 2.2.6.1. All solutions used in these experiments, including; 20 mM MOPS with 30 mM sodium sulphate, pH 7.4, DMEM cell culture medium, and ultrapure distilled water were degassed using sonication, whilst under vacuum, for approximately 15 minutes.

2.2.6.4.1 Cleaning of quartz sensors

Silicon dioxide coated quartz sensors were cleaned thoroughly prior to commencing the experiments. The sensors were placed in a Teflon instrument chamber and bath-sonicated in 2% (w/v) SDS dissolved in ultrapure distilled water for 10 minutes at room temperature (Figure 2.10A). The sensors within the Teflon instrument chamber were then rinsed at least six times in ultrapure distilled water and dried under a flow of nitrogen gas. The sensors were then transferred, face up, onto a piece of aluminium foil (approximately 20 cm by 20 cm) and cleaned by placing the sensors in a UV-Ozone cleaner for 20 minutes (Figure 2.10B). Using a pair of flat edged tweezers, the sensors were then placed in each of the chambers of the Q sense machine, sensor face down and in the correct orientation as shown in Figure 2.10C. The chamber lids were placed on top of the chambers and screwed into position. Each chamber was turned over and locked into position in the machine by sliding the metal bar at the front of each chamber (Figure 2.10D). The QCM-D machine and peristaltic pump are shown in Figure 2.10E.

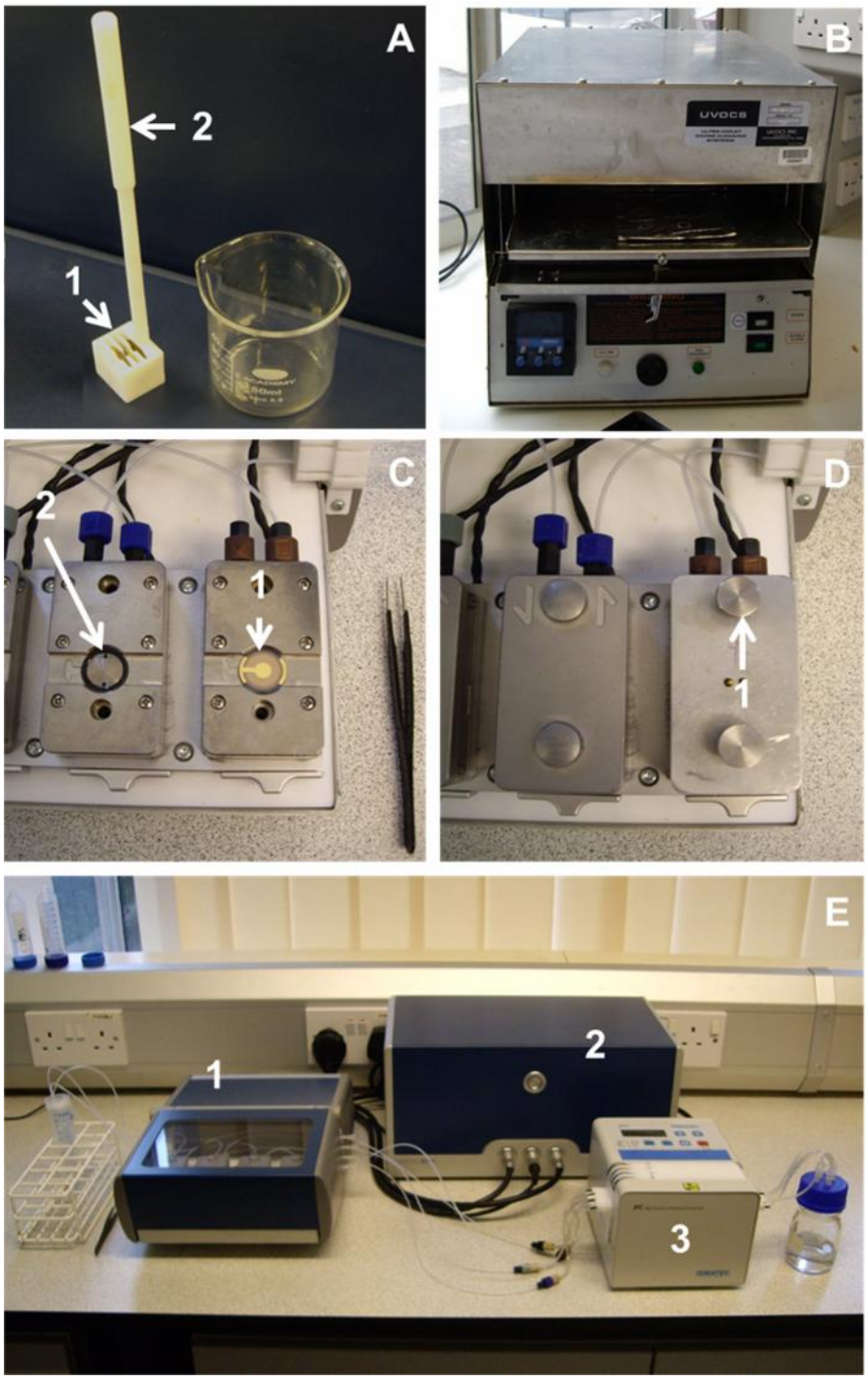

Figure 2.10 – Cleaning of the sensors and assembly of quartz crystal microbalance with dissipation machine. A – Silicon dioxide coated quartz sensors (1) were placed in a Teflon instrument holder (2) and immersed in 2% (v/v) SDS, followed by washing with ultrapure distilled water. B – Sensors were cleaned in a UV-Ozone cleaner. C – Sensors (1) were placed, faced down into each of the chambers (2). D – The chamber lids were screwed into position (1) and the chambers were secured in place. E – QCM-D machine consisting of four chambers (1), a detector (2) and peristaltic pump (3).

2.2.6.4.2 Quartz crystal microbalance with dissipation machine set up

Using the QSoft programme (version 4.1), the frequency and dissipation of the sensors in air was measured to check sensor integrity. The starting solution of DMEM was flowed through the chambers at an initial flow rate of 0.5 ml per minute using a peristaltic pump for approximately 5 minutes. The flow rate was then reduced to 70 µl per minute and remained constant throughout the experiment. The frequency and dissipation of the sensors was measured in DMEM to check sensor integrity. Using the QSoft programme, the experiment was then started and the change in frequency and dissipation were monitored over time until the measurements stabilised. This was dependent on the presence of air bubbles in the solution or the sensor age. Once the frequency and dissipation had settled, the monitoring was restarted and the frequency and dissipation in the starting solution was automatically set at zero by the software. Changes in the dissipation, ΔD, and normalised changes in the frequency, Δf ($f = f_n/n$, where n is the number of the overtone, n = 3 – 13), were monitored in real time. The QCM-D was then ready for the formation of the lipid bilayer and subsequent exposure to the particles.

2.2.6.4.3 Lipid bilayer formation

Once the starting solution had flowed through the sensor chambers for at least 15 minutes, the solution was changed to 20mM MOPS with 30 mM Na_2SO_4, pH7.4. The lipid vesicles (section 2.2.6.1) were diluted in 20mM MOPS with 30 mM Na_2SO_4, pH7.4, at a final concentration of 0.5 $mg.ml^{-1}$ with 10 mM $CaCl_2$. After 10 minutes, the 20mM MOPS with 30 mM Na_2SO_4, pH7.4 was exchanged for the diluted lipid vesicles and flowed through the chambers for a minimum of 20 minutes. After 20 minutes, to remove loosely bound vesicles and Ca(II), 1 mM of EDTA dissolved in ultrapure distilled water was flowed through the chambers for 15 minutes. The solution was then exchanged with DMEM. The formation of a planar

lipid bilayer on the silicon oxidase surface was confirmed by a change in frequency of -27 to -30 Hz and a dissipation 0 to 0.5 $x10^6$ (Mu *et al.* 2012).

2.2.6.4.4 Addition of particles to membrane bilayer

Once the lipid bilayer had formed, the particles of choice were added to the chambers. Particle concentrations of 1 $\mu g.ml^{-1}$, 10 $\mu g.ml^{-1}$ and 100 $\mu g.ml^{-1}$ diluted in DMEM were flowed through the chambers in succession for at least 25 minutes. DMEM was flowed through the chambers for at least 25 minutes between the addition of each particle concentration to remove any unbound particles. Due to the sensitivity of the QCM-D equipment, each experiment was repeated twice using a different reconstituted lipid vesicle vial. For clarity, only the overtone 9 (n = 9) of the normalised frequency and dissipation is reported in the results.

2.2.6.5 Isolation of plasma membrane proteins from fibroblasts and histiocytes

The presence of membrane proteins within the model lipid membrane and the subsequent effect on the interactions of alumina and CoCr particles was determined. In order to perform these experiments, the membrane proteins from L929, primary HFB and U937 cells were isolated and incorporated into the lipid vesicles, which were used for the vesicle leakage assays and QCM-D experiments.

2.2.6.5.1 Harvesting adherent L929 cells and primary human fibroblasts

At least 20 confluent T175 cm^2 flasks of cells were harvested for each plasma membrane isolation experiment. Under aseptic conditions, the medium was

aspirated and discarded from each of the flasks. A volume of 10 ml of sterile filtered, ice cold DPBS containing 1mM EDTA (DPBS:EDTA solution) was added to each flask and incubated at room temperature for 10 minutes. The cells were then detached from the flasks using a cell scraper. The cell suspension was transferred into a sterile universal and centrifuged at 1000 g for 20 minutes at 4°C. The supernatant was removed and the cell pellet was suspended in 10 ml of ice cold DPBS:EDTA solution. The cell suspension was centrifuged again at 1000 g for 20 minutes at 4°C. The supernatant was removed and suspended with the DPBS:EDTA solution and centrifuged again as previously described. The pellet was suspended with the DPBS:EDTA solution to give a total volume of 2 ml, also known as the packed cell volume (PCV).

A cell count was performed on the PCV as described in section 2.2.3.4. At least 1 x 10^8 cells were required for the subsequent isolation protocol. The PCV was separated into two labelled cryovials and snap frozen in liquid nitrogen. The vials were then stored at -80°C until required.

2.2.6.5.2 Harvesting suspension U937 histiocytes

At least 20 confluent T175 flasks of cells (approximately 1 x 10^8 cells) were required for each plasma membrane isolation experiment. The cells were removed from each flask into a sterile universal and centrifuged at 1000 g for 20 minutes at 4°C. The cell pellet was suspended with 10 ml of DPBS:EDTA and centrifuged at 1000 g for 20 minutes at 4°C. This centrifugation step was repeated once more and the pellets were pooled to give a total volume of 2 ml. A cell count was performed (section 2.2.3.4) and the cells were snap frozen as described in section 2.2.6.5.1.

2.2.6.5.3 Cell disruption using a ball-bearing homogeniser

All solutions and tubing were placed on ice prior to commencing the procedure. The PCV was thawed rapidly in a 30°C water bath and transferred into a universal. The PCV was suspended in 2 ml of homogenising solution (section 2.1.10.3) and placed immediately on ice. The ball-bearing homogeniser was then used to break the cells. The ball-bearing homogeniser was assembled by placing the ball bearing into the central compartment of the homogeniser. The end plates were screwed into position to secure the ball bearing within the homogeniser. A long metal syringe needle was attached to a disposable 2.5 ml syringe and 1 ml of the PCV was transferred into the syringe. The metal needle was removed and the syringe was connected to the inlet of the homogeniser. A second disposable 2.5 ml syringe was connected to the outlet of the homogeniser (Figure 2.11). The PCV was then syringed into the homogeniser and collected in the second syringe. To ensure complete cell disruption of the PCV, the cell suspension was passed through the homogeniser ten times. The process was repeated for the entire volume of the PCV.

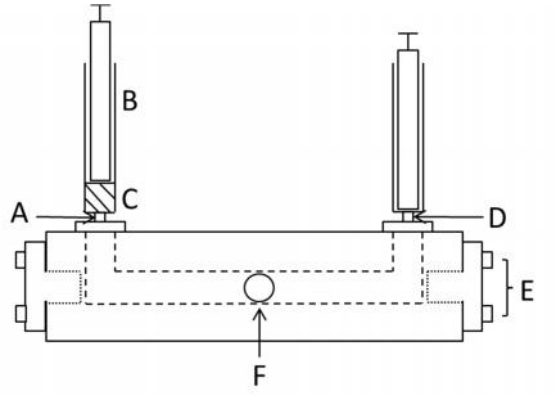

Figure 2.11 – Diagram of assembled ball-bearing homogeniser. A – Inlet of homogeniser. B – 2.5 ml syringe. C – Packed cell volume. D – Outlet of homogeniser. E – End plate screwed into position. F – Ball bearing in bore of homogeniser.

The homogenate was transferred to a 15 ml Falcon tube and homogenising solution (section 2.1.10.3) was added to give a final volume of 10 ml. The suspension was

then centrifuged at 800 g for 10 minutes at 4°C. The supernatant was collected in a 50 ml Falcon tube and homogenising solution was added to give a final volume of 20 ml. The suspension was centrifuged at 6000 g for 10 minutes at 4°C. The supernatant was then transferred into 14 ml thin walled ultracentrifugation tubes and using the SW-40 Beckmann rotor, the samples were centrifuged at 100,000 g for 30 minutes at 4°C. The supernatant was discarded and the pellets were resuspended and pooled in 500 µl of 10mM Tris-HCl, pH 7.5. To ensure complete resuspension of the pellets, a long, 1 mm gauge, metal needle attached to a 5 ml syringe was used to disrupt the pellet.

2.2.6.5.4 Membrane fractionation using a sucrose density gradient

The suspended pellet from section 2.2.6.5.3 was transferred into a 14 ml thin walled ultracentrifugation tube. A volume of 1.34 ml of 70% (w/v) sucrose diluted in 10 mM Tris-HCl, pH 7.5 was mixed with the pellet. Using a glass Pasteur pipette, the following sucrose solutions (dissolved in 10 mM Tris-HCl, pH 7.5) were carefully added to the sample, layer by layer; 3ml of 44% (w/v) sucrose, 3 ml of 31% sucrose and 2 ml of 9% (w/v) sucrose. The sucrose gradient was then centrifuged in a Beckmann SW-40 rotor at 100,000 g, for 90 minutes at 4°C without the brake applied.

The bands at the interfaces of the 9/31% (w/v) sucrose and the 31/45% (w/v) sucrose were pooled and collected into a clean 14 ml thin walled ultracentrifugation tube using a glass Pasteur pipette.

The collected bands were diluted at least 3 fold with 10 mM Tris-HCl, pH 7.5 and then centrifuged in a Beckmann SW-40 rotor at 100,000 g, for 30 minutes at 4°C. The pellet was resuspended in 200 µl of 20 mM MOPS with 30 mM sodium sulphate, pH 7.4 and a 30 µl aliquot was placed in an Eppendorf to perform a bicinchoninic acid (BCA) assay to determine the concentration of protein recovered

(section 2.2.6.5.5). The remaining isolated membrane sample were transferred to a labelled cyrovial and snap frozen in liquid nitrogen before being stored at -80°C.

2.2.6.5.5 Determining the concentration of isolated membrane protein using the bicinchoninic acid assay

An Eppendorf containing a 30 µl aliquot of the isolated membrane protein sample isolated in section 2.2.6.5.4 was defrosted in a 30°C water bath. The sample was separated into three wells of a Nunc® flat-bottom 96 well plate at a volume of 10 µl per well. A volume of 15 µl of ultrapure distilled water was added to each well to give a total sample volume of 25 µl per well. A bovine serum albumin (BSA) standard curve was established using a stock solution of 0.4 $mg.ml^{-1}$ BSA dissolved in ultrapure distilled water. A volume of 25 µl of each of the following standard curve concentrations (0, 2, 4, 6, 8 and 10 µg of BSA per well) was added in triplicate to the 96 well plate.

The BCA working solution was prepared by diluting one part of 4% (w/v) copper (II) sulphate pentahydrate solution with 49 parts of the BCA solution A (Pierce®, Thermo Fisher Scientific), which contains bicinchonia acid, $NaCO_3$, sodium tartrate, sodium bicarbonate in 0.1M NaOH, pH 11.5. A volume of 200 µl of the BCA working solution was added to each well of the sample and the BSA standards. The 96 well plate was then covered with a lid and incubated in a 37°C incubator for 30 minutes. After the incubation period, the absorbance of the standards and samples was read at 562 nm using the MultiScan plate reader and ScanIt MSS software (version 2). A calibration curve of the BSA concentration (in micrograms) against the absorbance of the standards was plotted with a linear trend-line. Using the linear equation of the standard curve, the amount of protein in micrograms for each sample was calculated. Taking into account the dilution factor, the concentration of the protein of each sample was calculated in $mg.ml^{-1}$.

2.2.6.6 Optimising the concentration of isolated fibroblast plasma membranes for quartz crystal microbalance with dissipation

The isolation of cell plasma membranes from fibroblasts and macrophages is detailed in section 2.2.6.5. In order to form a solid supported planar membrane for QCM-D analysis, the optimal protein concentration of the isolated membranes was investigated. The isolated plasma cell membranes of L929 fibroblast were used to optimise the concentration of protein required to form a solid supported planar membrane. A 5 mg vial of lipids (section 2.2.6.1) was reconstituted in 1 ml of 20 mM MOPS with 30 mM sodium sulphate, pH 7.4. The concentration of the isolated L929 fibroblast proteins was determined using the BCA assay (section 2.2.6.5.5). A range of 0.5 $mg.ml^{-1}$ protein: lipid mixtures, diluted in 20 mM MOPS with 30 mM sodium sulphate, pH 7.4 were prepared containing different amounts of protein from the membrane extraction at 0.1, 0.2 and 0.3 mg ml^{-1}, to give a ratio of 20%, 40% and 60% (w/w) of protein to lipid. To form the vesicles, each solution was extruded first through a track-etched polycarbonate filter with a pore size of 200nm followed by a 100 pore size track-etched polycarbonate filter as described in section 2.2.6.2. The vesicle solutions were kept on ice until required and any remaining vesicles were discarded after 24 hours.

The QCM-D analysis was performed at described in section 2.2.6.4, whereby each sensor corresponded to a different concentration of the isolated protein: lipid solution. In brief, the protein: lipid vesicle solutions were flowed through each chamber for 10 minutes at a flow rate of 70 µl per minute. This was followed by a 20 minute ultrapure distilled water plus 1 mM EDTA wash. The solution was changed to DMEM and once the frequency and dissipation had stabilised the experiment was terminated. The results of the change in frequency and dissipation

were compared for each protein: lipid solution to establish which concentration generated the most stable solid supported planar membrane.

2.2.6.7 Formation of protein: lipid vesicles for quartz crystal microbalance with dissipation and vesicle leakage analysis.

A protein: lipid solution diluted in 20 mM MOPS with 30 mM sodium sulphate, pH 7.4 was prepared, consisting of 0.1 mg ml^{-1} protein and 0.4 mg ml^{-1} lipid (20% (w/w) protein to lipid ratio) (see section 2.2.6.6 for optimisation of protein concentration). To form the vesicles, the solution was extruded first through a 200 nm pore size filter followed by a 100 pore size filter as described in section 2.2.6.2. The vesicle solutions were kept on ice until required. The vesicle leakage and QCM-D experiments were performed as described in section 2.2.6.3 and 2.2.6.4, respectively.

2.2.6.8 Modelling quartz crystal microbalance with dissipation data

The computer software, QTools (version 3.1) was used to model the QCM-D data, using the Voight viscoelastic model. The first layer of the model was established to represent the sBLM. The outputs for layer one were then used to model the second layer, which represented the bound particles. The outputs of the second layer were the viscosity, shear modulus and thickness of the particle layer. These outputs indicated if particle binding occurred and the effect on the viscoelastic sBLM. The fixed parameters for the densities of each layer are listed in Table 2.4, which were used for the Voight model.

Table 2.4 – Fixed parameters used for modelling quartz crystal microbalance with dissipation Density of alumina from manufacturer's specifications as described in section 2.1.1 (PlasmaChem, Berlin, Germany). (Behl *et al*. 2013; Jing *et al.* 2014; Malmström *et al.* 2007).

Fixed Parameter	Density (kg/m^3)
Lipid bilayer	1000
Alumina particles	3900
CoCr particles	7700

2.2.7 Statistical analysis

2.2.7.1 Confidence Levels

Data was analysed using Microsoft Excel (version 2010) and the mean and 95% confidence levels (CL) were calculated. The 95% confidence levels (α = 0.05) were calculated using the descriptive statistics of Microsoft Excel.

$$\text{mean} = \frac{\sum x}{n}$$

$$\text{Standard deviation} = \sqrt{\frac{\sum x^2}{n\text{-}1}}$$

$$\text{Standard error (SE) of the mean} = \frac{\text{Standard deviation}}{\sqrt{n}}$$

$$95\%\ \text{CL} = \text{mean} \pm t \times \text{SE}$$

X = Individual value

n = Sample number

2.2.7.2 Statistical analysis

Data was analysed by one way analysis of variance (ANOVA) and individual differences between group means were determined using the Tukey-method to calculate the minimum significant difference (MSD) (p=0.05). The MSD was calculated using the following equation:

$$\mathrm{MSD} = Q\ (\alpha[k,v])\ \mathrm{X}\ \mathrm{SE}$$

Q = Critical value

α = p = 0.05

k = number of groups

v = degree of freedom (n-1)

For the vesicle leakage assays, the group means were analysed using a paired t-test and results with a $p < 0.05$ were significantly different.

Chapter 3

Generation, characterisation and biocompatibility of cobalt chromium alloy and alumina ceramic particles

3.1 Introduction

Total hip replacements have been hugely successful in treating end stage osteoarthritis of the hip joint, leading to over 83,000 primary hip replacement operations being performed, in the UK, in 2014 (NJR 2015). However, THRs consisting of a traditional UHMWPE acetabular cup component were historically associated with high wear rates and promoting osteolysis, eventually leading to late stage aseptic loosening (Ingham and Fisher 2000; Caton and Prudhon 2011). In the 1980s, there was a rise in the popularity of CoCr alloy metal-on-metal THRs, which was shortly followed by alumina-based ceramic prostheses. These bearing materials were perceived as an attractive alternative for younger and more active patients (Bessette *et al.* 2003). This was partly due to the low wear rates of the THRs and therefore was thought to promote implant survivability, which would delay or prevent the need for revision surgery (Smith *et al.* 2001; Dowson *et al.* 2004a; Dowson *et al.* 2004b; Dowson and Jin 2006). However, more recently CoCr alloy metal-on-metal prostheses and the wear particles produced have been associated with adverse responses in patients including pseudotumours, causing a rise in revision surgeries. At present it is unclear on the mechanism of these adverse responses. In addition to this, the popularity of ceramic-on-ceramic THRs has continued to rise in the UK, although this is not the case in the USA (Berry & Lieberman 2012). Nevertheless, there are limited relevant cell studies on the particles generated from these implants.

3.1.1 Cobalt chromium total hip replacements and resurfacing implants

The wear of retrieved, second generation CoCr metal-on-metal THRs has been reported to be 5 µm per year, when the femoral head component is positioned central to the acetabular cup following the initial running in phase (Sieber *et al.* 1999). Simulator studies of optimally positioned metal-on-metal implants have reported wear rates less than 1 mm^3 per million cycles (Clarke *et al.* 2000; Smith *et al.* 2001; Dowson *et al.* 2004a; Dowson *et al.* 2004b; Vassiliou *et al.* 2007).

Cobalt chromium wear particles, generated by metal-on-metal prostheses, have been observed to be predominately nanoscale in size from both retrieval and simulator studies (Doorn *et al.* 1998; Firkins *et al.* 2001b; Brown *et al.* 2007; Goode *et al.* 2012). Doorn *et al.* (1998) reported that CoCr wear particles isolated from periprosthetic tissues of patients undergoing revision surgery had a mean diameter of 81 nm. The morphology of the particles was also observed to be round in morphology, with some shard-like particles using TEM. Simulator studies of metal-on-metal THRs have reported CoCr wear particles to be slightly smaller, with a mean size of 30 – 40 nm (Firkins *et al.* 2001b; Williams *et al.* 2003; Brown *et al.* 2007; Papageorgiou *et al.* 2007).

Until recently large diameter THRs and hip resurfacing implants were increasing in popularity, especially with active patients due to a perceived increased range of motion and low wear (Dowson and Jin 2006; Underwood *et al.* 2011). However as described in Chapter one, the wear particles and ion release from these implants have been associated with adverse reactions in patients including type IV delayed hypersensitivity reactions and pseudotumours (Pandit *et al.* 2008; Hart *et al.* 2009; Gill *et al.* 2012). Retrieval studies have reported incidences of high wear rates of 22 mm^3 per year of large diameter hip resurfacing implants (Langton *et al.* 2010; Joyce *et al.* 2011; Lord *et al.* 2011). Furthermore, these implants have been associated

with elevated corrosive wear at the taper junction due to the combination of a large femoral head on a small femoral neck component, causing an increased frictional torque (Langton *et al.* 2011). Simulator studies have demonstrated that non-optimum positioning of the implant, such as the introduction of translational or rotational malpositioning can increase the wear rates in comparison to well positioned implants (Brown *et al.* 2007; Williams *et al.* 2008; Leslie *et al.* 2009; Fisher 2011; Leslie *et al.* 2013; Williams *et al.* 2013).

3.1.2 Alumina ceramic total hip replacements

The low wear rates of alumina based ceramic-on-ceramic THRs have led to difficulties in the estimation of the wear rates. Patient retrieval studies have predicted the wear rates to be less than 0.5 mm^3 per year (Esposito *et al.* 2012). Simulator studies have also reported wear rates of 0.22 mm^3 per million cycles or less, even under adverse conditions (Nevelos *et al.* 2001; Stewart *et al.* 2003; Al-Hajjar *et al.* 2010; Al-Hajjar *et al.* 2013).

Alumina ceramic wear particles from ceramic-on-ceramic THR simulator studies and retrieval studies were reported to have a wide size distribution with a bimodal size distribution observed (Hatton *et al.* 2002; Tipper *et al.* 2002). Using TEM, a size range of 5 – 90 nm was reported, whereas when SEM analysis was used a size distribution of 0.05 – 3.2 µm was observed. It is thought that the wide range of particle sizes was caused by the introduction of translational malpositioning (Tipper *et al.* 2002). Fluoroscopy studies predicted that translational malpositioning occurred in approximately half of polyethylene-on-metal THRs and the introduction of these conditions for ceramic-on-ceramic THRs generates a characteristic wear stripe on the femoral head and cup edge (Lombardi *et al.* 2000; Stewart *et al.* 2003). Nevertheless, the introduction of translational malposition has been reported to not extensively elevate the wear rates of ceramic-on-ceramic THRs, even when

the acetabular cup in positioned at a high abduction angle (Al-Hajjar *et al.* 2010; Al-Hajjar *et al.* 2013).

3.1.3 Biocompatibility of wear particles from total hip replacements

3.1.3.1 Particle sources

To determine the biocompatibility of CoCr and alumina particles *in vitro*, a variety of particle sources have been used in the reported literature. These include the use of commercially available particles and particles isolated from joint simulators, excised tissue or simple pin-on-plate wear simulators. One of the main advantages of using wear particles from joint and pin-on-plate wear simulators or excised tissue is being able to use clinically relevant wear particles (Jin *et al.* 2000; Brown *et al.* 2007). However, if proteins are present in the samples, such as in the simulator lubricant, it is technically difficult to isolate the particles in order to visualise the particles and determine size distribution accurately. This is especially problematic for CoCr wear particles, which are susceptible to extremes of pH and high temperatures, which lead to aggregation, changes in particle size or loss of particles (Catelas *et al.* 2001a; Catelas *et al.* 2001b). Isolating CoCr and alumina wear particles from serum is particularly challenging due to their small particle size and the low wear rates experienced under standard gait conditions (Brown *et al.* 2007; Billi *et al.* 2012b). Moreover, alkaline digestion methods have been reported to alter the morphology, shape, and composition of CoCr wear particles (Catelas *et al.* 2001a; Catelas *et al.* 2001b). Particle preparation can also have an effect on particle characterisation, for example the resin embedding and sample preparation for TEM analysis has been shown to cause aggregation, thus potentially causing particle size inaccuracies (Doorn *et al.* 1998).

Simple configuration pin-on-plate wear simulators mimic the wear mechanisms and kinematics of the THRs during the normal gait cycle (Jin *et al.* 2000; Jin *et al.* 2006). The advantage of using pin-on-plate simulators is that they have been demonstrated to generate clinically relevant CoCr wear particles using water as a lubricant (Jin *et al.* 2000). This is particularly advantageous as it eliminates the need for any digestion protocol to isolate the particles, and particles can be recovered by filtration or centrifugation.

Another factor affecting the use of particles from tissue or joint simulators, which utilise lubricants containing serum, is the low wear rates. This is particularly problematic for alumina wear particles as the wear rates of ceramic-on-ceramic THR are very low (Al-Hajjar *et al.* 2010; Affatato *et al.* 2012; Esposito *et al.* 2012). At present the isolation methods developed and detailed in the ISO standard 17583 do not allow sufficient volumes of particles to be isolated. Therefore a number of studies have used commercially available particles, such as particles of alumina powders used in orthopaedic device manufacturing.

3.1.3.2 Cell studies on wear particles

Hard-on-hard bearings became more popular due to the low wear rates and the generation of predominately nanoscale wear particles (Dowson and Jin 2006). It was thought that this would reduce the incidence of osteolysis and aseptic loosening often associated with higher wearing traditional UHMWPE THRs (Ingham and Fisher 2000; Brown *et al.* 2006). However, as previously described, adverse tissue reactions, associated with CoCr wear particles, have been extensively reported by patients with metal-on-metal THRs or resurfacing implants, which has led to the continued monitoring of patients with such devices (Davies *et al.* 2005; Pandit *et al.* 2008; Natu *et al.* 2012; MHRA 2015). In contrast, alumina wear particles have only been associated with isolated incidences of tissue necrosis *in*

vivo (Niche *et al.* 2006; Affatato *et al.* 2012). This lack of obvious adverse responses to alumina wear particles is partly due to the low wear rates of ceramic-on-ceramic THRs with *in vitro* studies only reporting adverse effects at high particle doses, which would not be observed clinically (Germain *et al.* 2003; Rose *et al.* 2012).

A number of *in vitro* studies have examined the effect of CoCr and alumina wear particles on a variety of cell types as described in detail in Chapter one. As well as causing genotoxicity, inflammation and oxidative stress, CoCr wear particles have been reported to be cytotoxic in a dose- and time-dependent manner (Hatton *et al.* 2003; Brown *et al.* 2006; Posada *et al.* 2014). In contrast alumina nanoscale and micron sized wear particles have been reported to be cytotoxic only at very high particle concentrations (Germain *et al.* 2003; Papageorgiou *et al.* 2007; Rose *et al.* 2012). However, limited conclusions can be made as numerous studies do not use clinically relevant particles (Hallab *et al.* 2000; Tsaousi *et al.* 2010; Dalal *et al.* 2012; Caicedo *et al.* 2013). Alongside particle dose and exposure time, wear particle composition, size and shape are of particular importance in terms of the cellular response to particles (Yoshida *et al.* 2003; Kwon *et al.* 2009; Dalal *et al.* 2012). The effect of particle size on cell viability has been widely studied and in general CoCr micron sized particles are less cytotoxic in comparison to nanoscale CoCr particles (Germain *et al.* 2003; Papageorgiou *et al.* 2007). Although it must be noted that this does not necessarily mean the micron sized particles do not induce other cell responses, such as inflammation (Brown *et al.* 2013). The relationship between particle size and cell responses is less clear for alumina wear particles with some studies reporting smaller particles induced a greater effect on cell viability and vice versa (Catelas *et al.* 1999; Germain *et al.* 2003; Gutwein and Webster 2004). Particle shape has been reported to affect cell viability with a larger aspect ratio of alumina model particles were associated with a greater effect on cell mortality (Yoshida *et al.* 2003). Therefore in order to determine the precise mechanism of

particle toxicity, particles which are similar in terms of size, composition and shape to the published literature should be used for cell studies and to produce more meaningful conclusions.

3.2 Aims and objectives

The aim of the first part of this chapter was to generate and isolate nanoscale and micron sized alumina ceramic and CoCr particles. Nanoscale CoCr particles were generated using a six station pin-on-plate wear simulator employing the same alloy used in the manufacture of metal-on-metal THRs. The lubricant chosen was water, which removed the need for lubricant digestion. To study the effect of particle size, CoCr micron sized particles were also used. These were sourced from a commercially available CoCr powder, which has a similar composition to the CoCr alloy used for metal-on-metal THRs. For the alumina particles, a powder of alumina, which is used to manufacture ceramic hip components, was used. By means of sequential filtration techniques, attempts were made to isolate the nanoscale and micron particle size fractions. All particle types were characterised in terms of size, morphology, composition using SEM, EDX analysis and image analysis software (Image Pro Plus).

The second half of this chapter was concerned with determining if the isolated particles were comparable to the published literature in terms of their effect on the cell viability of primary HFBs and a U937 histiocyte cell line. Whilst a number of studies previously outlined in Chapter one have studied the effect of particles on a range of cell responses, the most common and simplest method was to investigate the effect on cell viability. This was determined using two cell viability assays to ascertain the cytotoxic potential of the isolated particles. After characterisation, the particle stocks could be used for further cell studies including cell membrane studies to determine how and if the particle interact and disrupt the cell membrane.

3.2.1 Objectives

The objectives of this part of the thesis are outlined in Figure 3.1 and included:

- To generate CoCr alloy particles using a six station pin-on-plate simulator
- To sequentially filter an alumina powder to isolate the micron sized alumina particles
- To optimise the sequential filtration method to isolate the nanoscale alumina particles from an orthopaedic alumina powder
- To characterise nanoscale and micron sized alumina and CoCr particles using SEM, EDX analysis and image analysis software, Image Pro Plus
- To investigate the effect of nanoscale and micron sized alumina ceramic and CoCr particles on the cell viability of primary HFBs and a U937 histiocyte cell line using the ATPlite and MTT assays

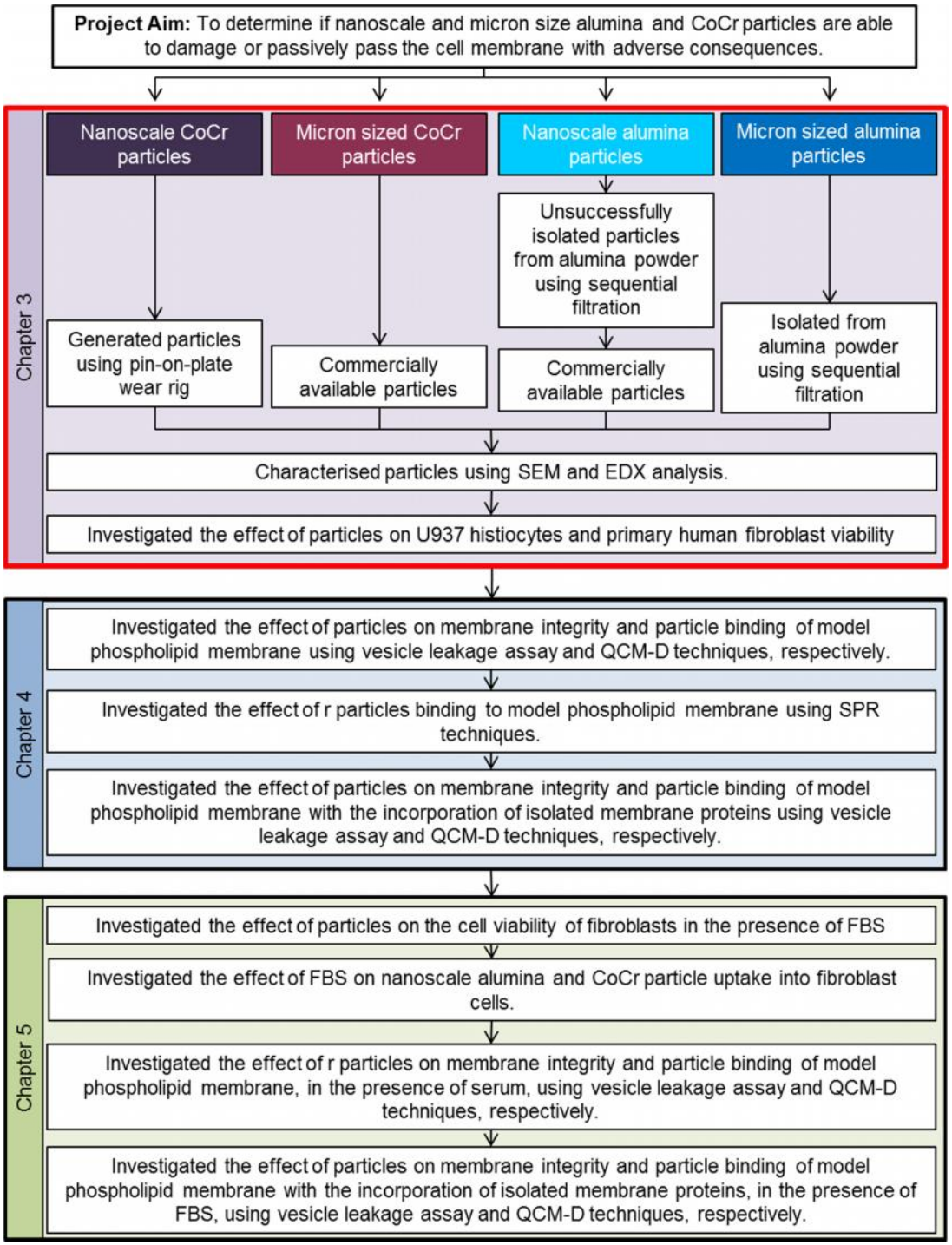

Figure 3.1 – Outline of thesis and Chapter three methods

3.3 Materials and methods

3.3.1 Materials

3.3.1.1 Cobalt chromium and alumina particles

Nanoscale and micron sized alumina and CoCr particles are detailed in section 2.1.1.

3.3.2 Methods

3.3.2.1 Sequential filtration of alumina powder to isolate the nanoscale and micron sized particle fraction for subsequent particle studies

In order to isolate nanoscale alumina particles, an alumina powder (section 2.1.1) was sequentially filtered to isolate the micron sized and nanoscale particles.

3.3.2.1.1 Pre-weighing of filter membranes to calculate recovery rates of nanoscale and micron sized particle fractions from an alumina orthopaedic powder

Before commencing, 5 ml of 70% (v/v) ethanol in water was filtered through a 0.015 µm pore size polycarbonate filter and the filter was dried under an infrared light for at least 4 hours in a laminar flow hood. The filter was stored in a temperature and moisture controlled environment of the measurement laboratory (School of Mechanical Engineering, Faculty of Engineering) for 48 hours before being weighed using an AT21 microbalance. An average of 5 measurements were recorded, which were within 10 µg of one another. The mean weight of the filter was recorded.

3.3.2.1.2 Preparation of filtration equipment

The filtration glassware was washed and scrubbed using household detergent and a bottle brush and rinsed at least three times with distilled water, followed by a final rinse in ultrapure distilled water. The glassware was wrapped in foil and sterilised in the oven at 190°C for 4 hours. The polymer part of the filtration unit was washed and scrubbed using household detergent and rinsed with copious amounts of distilled water and rinsed three times with distilled water, followed by a final rinse with ultrapure distilled water. All filtration was performed in a class I laminar flow hood and all equipment was sterilised in a hot air oven at 190°C for 4 hours. The sterile glass filtration unit was assembled as described in Figure 3.2.

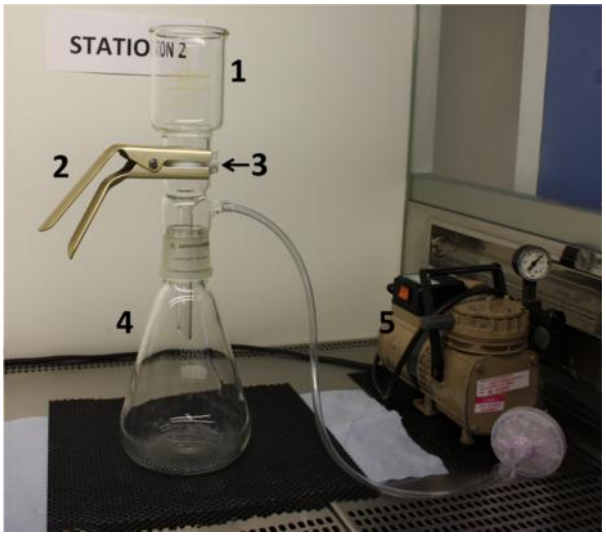

Figure 3.2 - Assembled filtration unit for isolating nanoscale and micron sized fraction of orthopaedic powder. 1 – Glass reservoir. 2 – Clamp. 3 – Filter membrane and polymer filter support. 4 – Collection flask. 5 – Vacuum pump.

3.3.2.1.3 Filtration of powder to isolate the nanoscale particle fraction

A small mass of alumina particles (0.1 grams), weighed into a clean 500 ml Duran glass bottle, was subjected to sonication in 500 ml of 70% (v/v) ethanol for 30 minutes immediately prior to filtration. The particle suspension was subsequently filtered through varying series of filters with pore sizes ranging from 10 µm to

0.015 µm in an attempt to isolate a large mass of nanoscale particles (Table 3.1). Each filter was flushed with at least 20 ml of distilled water to remove any trapped particles prior to removing the filter from the filtration unit. The filter membrane was removed and placed in a 250 ml sterile plastic pot with a small amount of ultrapure water (20 – 30 ml). The filter membrane was then sonicated to remove the collected particles, which were stored at -20°C. The remaining filtrate was sonicated for 30 minutes and then filtered through the filter with the next smallest pore size. Finally the filtrate was filtered the through a pre-weighed 0.015 µm filter. The 0.015 µm filter was dried under an infrared lamp for at least 4 hours and weighed as described in section 3.3.2.1.1. The recovered particle mass was determined by subtracting the original mass of the filter.

Table 3.1 – Sequence of filtration steps used to isolate the nanoscale particle fraction from an alumina powder. The alumina powder of a specified weight was filtered through a series of filter membranes with different pore sizes.

Method	Sequence of filter membrane pore sizes used (µm)
A	10 → 1 → 0.1 → 0.015
B	1 → 0.1 → 0.015
C	10 → 1 → 0.8 → 0.015
D	10 → 0.8 → 0.015
E	10 → 0.4 → 0.015

3.3.2.1.4 Filtration of the alumina powder to isolate the micron sized particle fraction

A small mass of alumina particles (0.1 grams) in a clean 500 ml Duran glass bottle was subjected to sonication in approximately 500 ml of 70% (v/v) ethanol for 30 minutes immediately prior to filtration. The particle suspension was subsequently filtered through a filter membrane with a pore size of 10 µm. The filter was flushed with at least 20 ml of distilled water to remove any trapped particles, prior to

removing the filter from the filtration unit. The remaining filtrate was sonicated and then filtered through a 0.1 µm filter membrane. Again this filter was flushed with at least 20 ml of distilled water to remove any trapped particles prior to removing the filter from the filtration unit. The 0.1 µm filter membrane was removed and placed in a 250 ml sterile plastic pot with a small amount of water (20 – 30 ml). The filter membrane was sonicated to remove the collected particles. A small aliquot (1 ml) of this particle suspension was filtered through the pre-weighed 0.015 µm filter in order to determine the mass of particles recovered. The filter was dried under an infrared lamp for at least 4 hours and weighed as described in section 3.3.2.1.1. The recovered particle mass was determined by subtracting the original mass of the filter. The remaining particle suspension was stored at -20°C for long term storage.

3.3.2.2 Characterisation of nanoscale and micron sized alumina and cobalt chromium particles

The size, composition and morphology of the particles were determined and analysed using SEM and EDX analysis

3.3.2.2.1 Preparation of particles for scanning electron microscope analysis

Approximately 5 ml of 70% (v/v) ethanol was filtered through a 0.015 µm pore size filter membrane. A small volume (100 µl) of one of the nanoscale and micron sized CoCr and alumina particle stocks, described in section 2.1.1 and 3.3.2.1.4 were diluted 1:10 with 70% (v/v) ethanol. The diluted particle stock was sonicated for 30 minutes before being filtered through a pre-weighed 0.015 µm pore size filter membrane. The filter was dried under an infrared lamp for 4 hours. A small section of the dried filter membrane was mounted on to a 2.5 cm aluminium short stub using an adhesive carbon tab and the edges of the filter were coated with carbon paste. The CoCr nanoscale, alumina nanoscale and alumina micron sized particle

samples were sputter coated with a platinum and palladium composite to a thickness of 3 – 10 nm. The CoCr micron sized particles were coated with a carbon film at a thickness of 3 – 10 nm.

3.3.2.2.2 Imaging and characterisation of particles

The CoCr nanoscale, alumina nanoscale and alumina micron size particles were visualised using the Leo 1530 FEGSEM at a working distance of 3 – 4 mm and an acceleration of 3 kV. Images were taken at magnifications of x 60 K, x 90 K, x 150 K and x 300 K. The micron size CoCr particles were visualised using the Hitachi SU8230 SEM at a working distance of 3 mm and at 1 kV and imaged by Mr Imran Asif (Faculty of Engineering, University of Leeds). Due to the large size of the particles, images were taken at lower magnifications of x 1.5 K and x 5 K, The SEM images were analysed using the image analysis software, Image Pro Plus (version 6.1) to measure the maximum length and area of the particles. Approximately 150 particles were characterised in total and only particles where the entire circumference could be observed were measured. The results were expressed as percentage particle size and percentage particle area distribution graphs.

3.3.2.2.3 Energy dispersive x-ray spectroscopy analysis of particles

Pin point EDX analysis of nanoscale and micron sized alumina and CoCr particles was performed using the Gemini EDX analyser at a working distance of 8.5 mm, 10 kV and a magnification of x 10 - 20 K. The EDX spectra were acquired using AZtec software (version 2). For EDX analysis of alumina nanoscale particles, the sample was coated with 3 – 10 nm of a palladium: iridium mixture rather than a platinum:palladium composite, which was used for the SEM images

3.4 Results

3.4.1 Sequential filtration of alumina orthopaedic powder to isolate the nanoscale particle fraction for subsequent particle studies

Initially it was intended for the nanoscale alumina debris to be isolated from an alumina powder using sequential filtration. However, as shown in Table 3.2 the recovery of nanoscale debris was relatively low, with method A and B only recovering 15 – 16 µg of nanoscale particles from a starting weight of 0.1 g of powder. Optimisation of the filtration process included suspending the particles in 70% (v/v) ethanol instead of water and increasing the particle dilution, however, these changes did not improve the recovery rates of nanoscale particles. Therefore, the 0.1 µm filter membrane was omitted and replaced with a 0.8 µm filter membrane (method C & D) or a 0.4 µm filter membrane (method E). However, none of the optimisation steps attempted allowed recovery of a sufficient mass for future cell culture experiments as tens of milligrams was required in total. Therefore, a commercially available nanoscale alumina powder was purchased and was used in the cell viability assays and membrane toxicity experiments.

Table 3.2 – Optimisation methods and recovery of isolating alumina nanoscale particles from an alumina powder. The alumina powder of a specified weight was filtered through a series of filter membranes with different pore sizes. The recovery weight of the nanoscale alumina particles is recorded for each method.

Method	Sequence of filter membrane pore sizes used (µm)	Starting Weight (g)	Recovery (µg)
A	10 → 1 → 0.1 → 0.015	0.101	15
B	1 → 0.1 → 0.015	0.1	16
C	10 → 1 → 0.8 → 0.015	0.102	13.2
D	10 → 0.8 → 0.015	0.1	94.9
E	10 → 0.4 → 0.015	0.5	167.2

3.4.2 Characterisation of commercially available nanoscale alumina particles

The aim of this series of experiments was to characterise commercially available nanoscale alumina particles which could be used in subsequent cell culture response assays. A small mass (0.01 g) of alumina particle suspension was suspended in 70% (v/v) ethanol and subjected to sonication for 30 minutes. The particle suspension was immediately filtered on to a 0.015 µm filter membrane and analysed using FEGSEM as described in section 3.3.2.2. The alumina nanoscale particles formed large aggregates, making characterisation of individual particles difficult. However, the smaller particles were mostly oval in morphology, whereas the larger nanoscale particles were observed to be more polygonal in shape as shown in Figure 3.3.

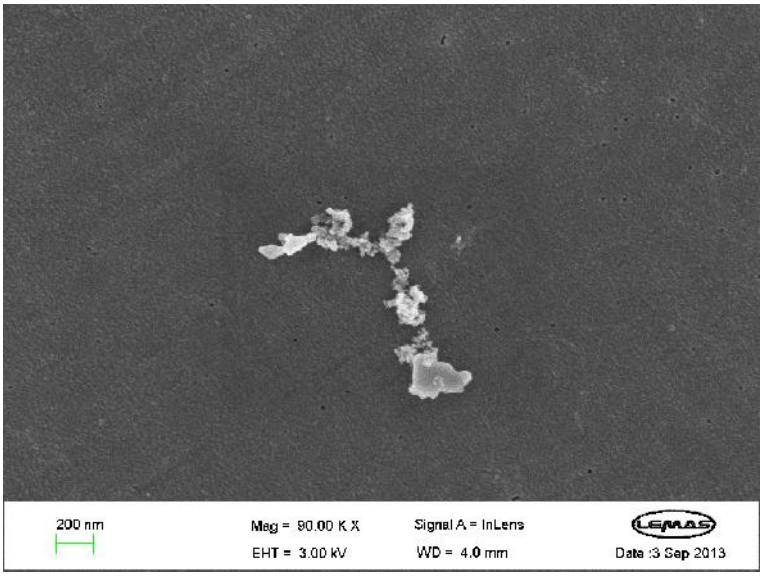

Figure 3.3 – Scanning electron microscopy image of nanoscale alumina particles. Particles were isolated from a commercially available alumina powder and filtered onto a 0.15 µm pore filter membrane. Particles in this image were observed at 90 K magnification, 3 kV, and working distance of 4 mm.

EDX analysis was performed on the nanoscale alumina particles and an example EDX spectrum is shown in Figure 3.4. The main peaks detected were aluminium and oxygen. The iridium peaks within the spectrum were attributed to the coating of the particle samples.

The nanoscale alumina particles were characterised using the SEM images and the image analysis software, Image Pro Plus (section 3.3.2.2.2). Particles ranging from 10 – 265 nm were measured. The mode size of the particles was measured at 30 – 39 nm, with a mean particle size of 39.5 nm (± 26.5 nm SD, as shown in Figure 3.5A). The majority of the particles were less than 40nm in size, accounting for 88% of the total sample. Particles sized 30 – 39 nm had the largest particle area, accounting for 36 % of the particles measured (Figure 3.5B).

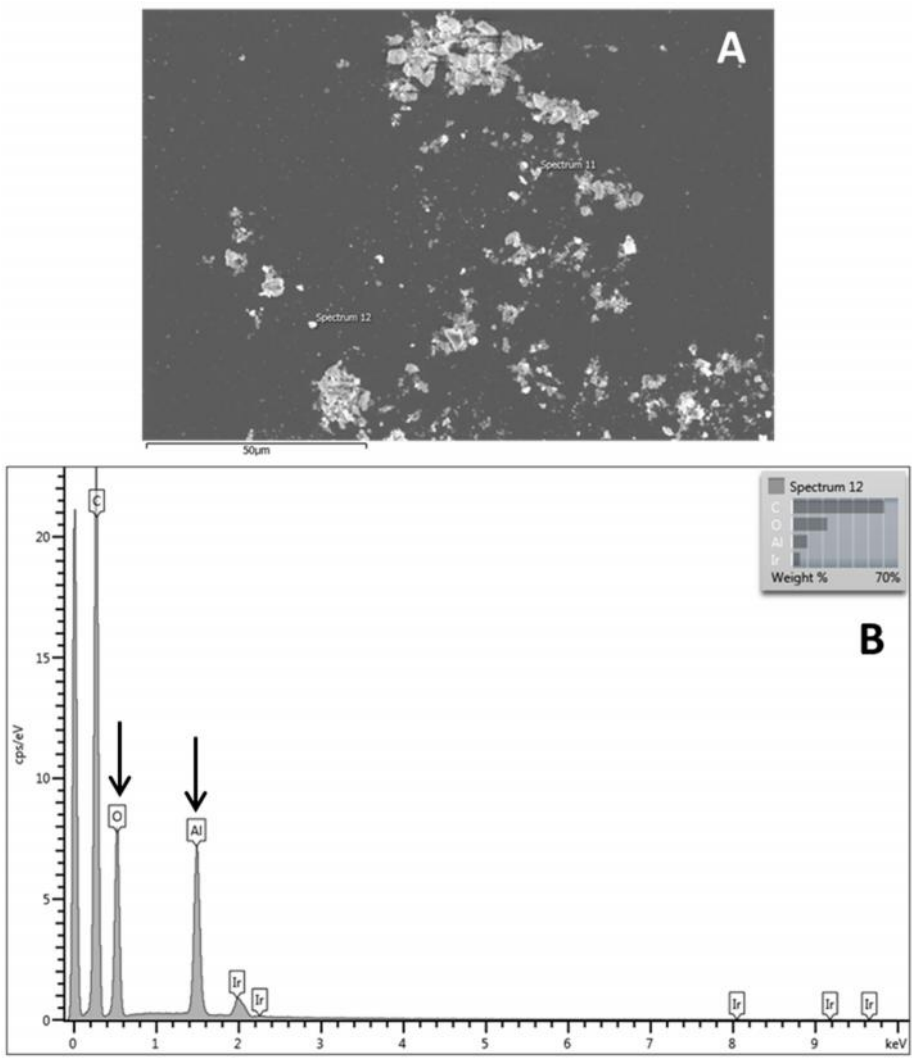

Figure 3.4 – Pin point energy-dispersive X-ray spectroscopy of nanoscale alumina particles. Nanoscale alumina particles were filtered onto a 0.015 µm pore sized filter membrane and placed on an aluminium stub. The sample was coated with a palladium: iridium composite at a thickness of 3 – 10 nm. Pin point EDX analysis was performed at a working distance of 8.5 mm, 10 kV and a magnification of 20 K. (A) Image of analysed alumina particles. (B) Example EDX spectrum. Arrows indicate characteristic elements of particles.

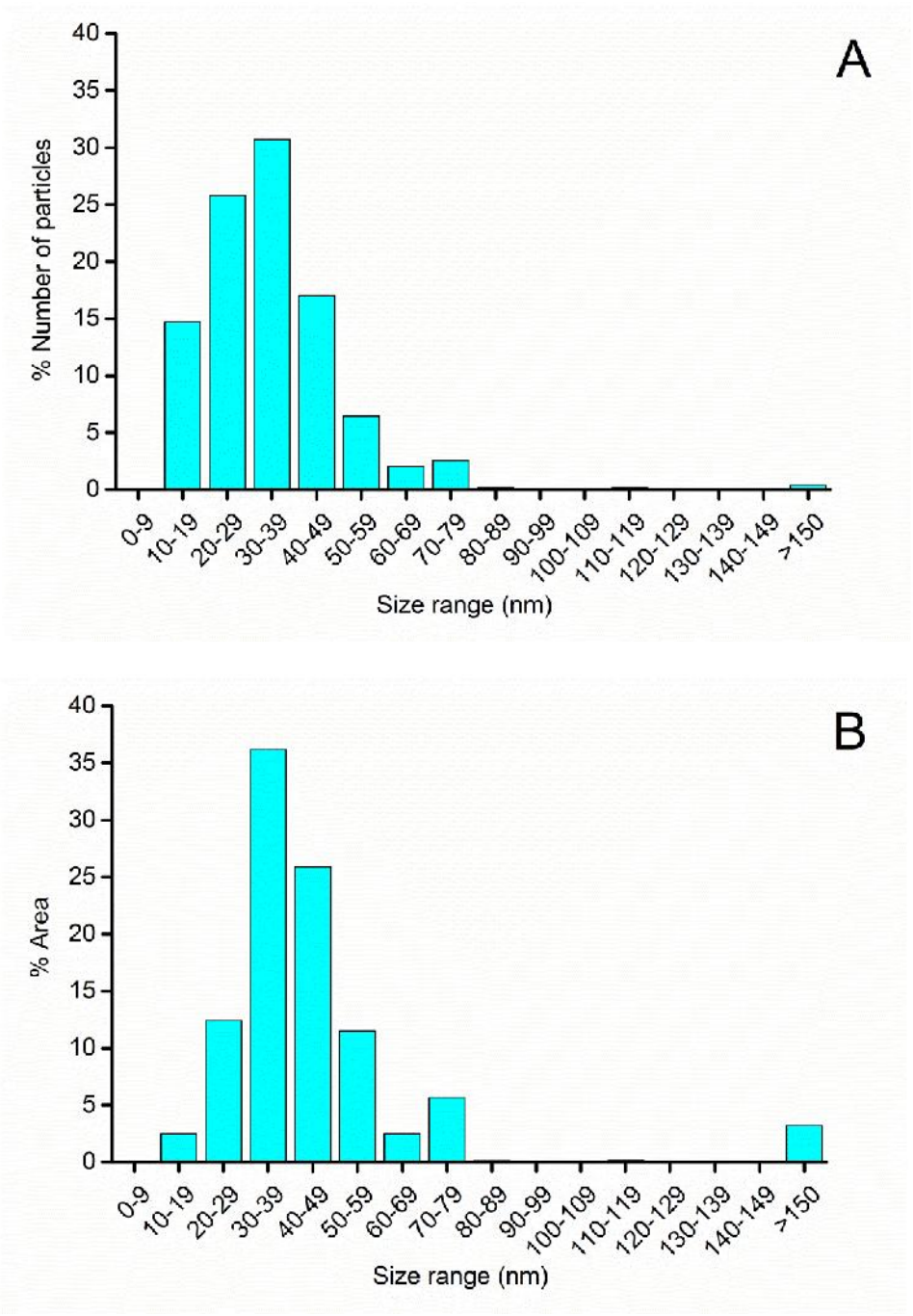

Figure 3.5 – Percentage size (A) and area (B) distribution of nanoscale alumina particles. Nanoscale alumina particles were suspended in 70% (v/v) ethanol and collected onto a 0.015 µm pore size filter. The dried filter was placed on an aluminium platform stub and coated with platinum. Particles were imaged using FEGSEM analysis and the percentage distribution of the maximum length and area of the particles was determined using Image Pro-Plus 6.1 software. At least 150 particles were characterised in total from approximately 10 images.

3.4.3 Characterisation of micron sized alumina particles

Alumina micron sized particles were isolated from an alumina powder as described in section 3.3.2.1. The particles were isolated from the powder by filtering the powder through a 10 µm filter membrane and subsequently collected on to a 0.1 µm filter membrane. An aliquot of the particle suspension was analysed on a 0.015 µm filter membrane and visualised using FEGSEM (section 3.3.2.2). A representative image of the alumina micron size particles is shown in Figure 3.6.

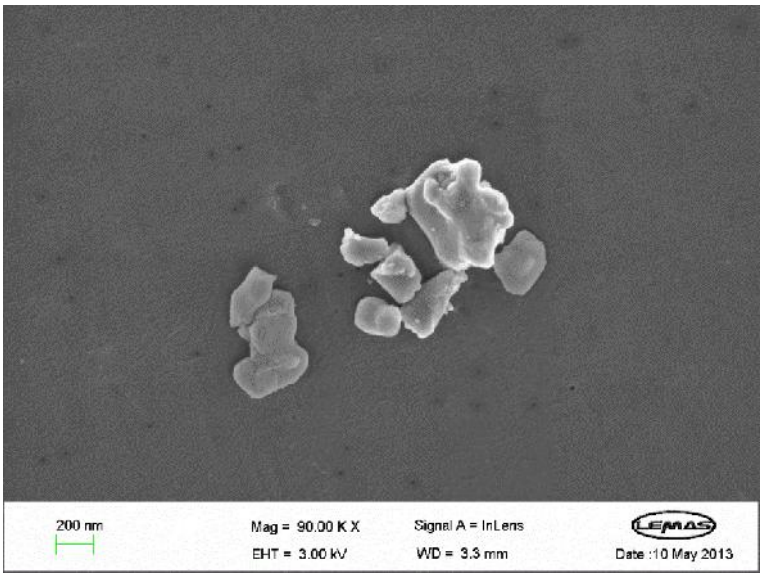

Figure 3.6 – Scanning electron microscopy image of isolated micron sized alumina particles. Particles were isolated from an aluminium oxide orthopaedic powder and filtered through a 10 µm and 1 µm pore filter. Particles in this image were observed at 60 K magnification, 3 kV, and at a working distance of 3.3 mm.

The micron sized alumina particles had a polygonal shard-like morphology and similar to the nanoscale alumina particles, the particles had a tendency to aggregate. EDX analysis was performed on the isolated particles and an example EDX spectrum is shown in Figure 3.7. The main peaks detected were aluminium and oxygen. The platinum and palladium peaks within the spectrum are attributed to the coating of the particle samples. Furthermore, the large peak close to 0 KeV was a characteristic carbon peak

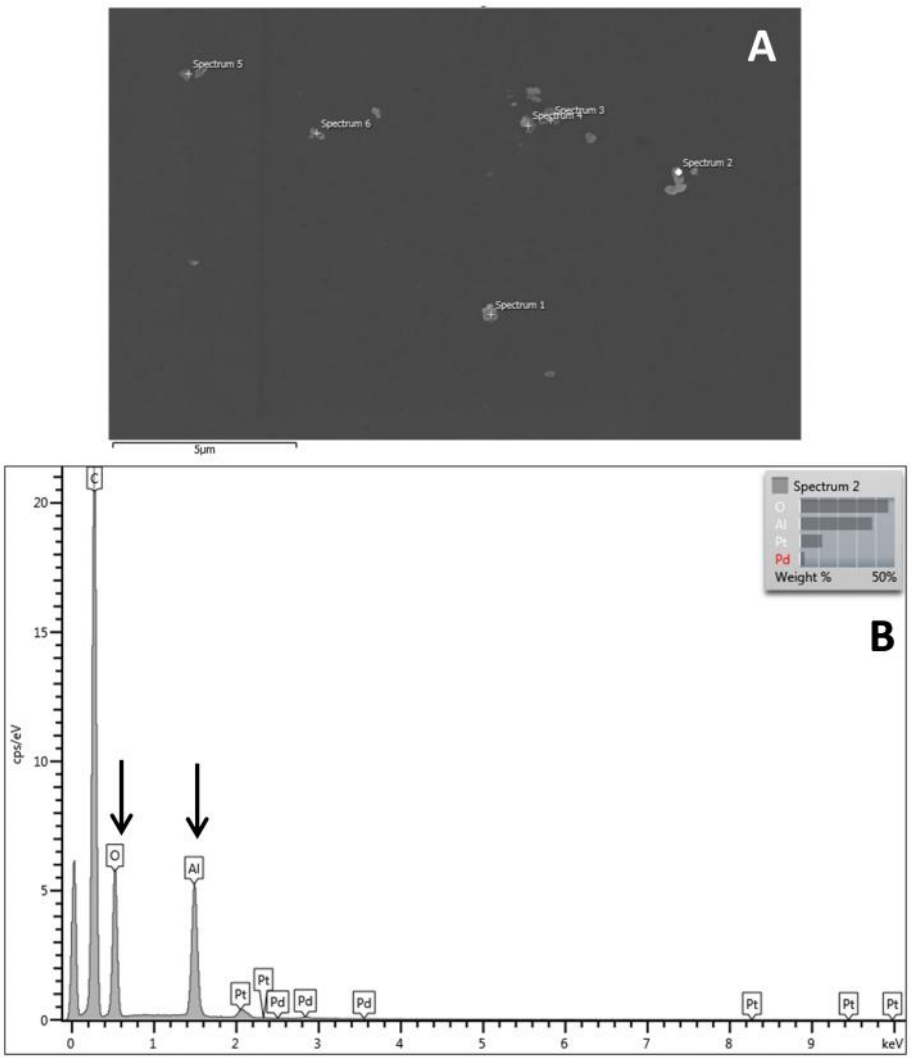

Figure 3.7 – Pin point energy-dispersive X-ray spectroscopy of micron sized alumina particles. Micron sized alumina particles were filtered onto a 0.015 µm pore sized filter membrane and placed on an aluminium stub. The sample was coated with a platinum: palladium composite at a thickness of 3 – 10 nm. Pin point EDX analysis was performed at a working distance of 8.5 mm, 10 kV and a magnification of 20K. (A) Image of analysed micron sized alumina particles. (B) Example EDX spectrum of micron sized alumina particles. Arrows indicate characteristic elements of particles.

Characterisation of the imaged particles using Image Pro Plus revealed a wide distribution of particles sizes from 17 nm to 1464 nm in diameter. The mode particle size was 400 – 449 nm, making up 19 % of the particle size distribution (Figure 3.8A). Similarly, the particle area distribution also had a wide distribution, with particles sized 250 – 549 nm making up the majority of the particle area (89% of the

particle area). The mode of the particle area distribution was also 400 – 449 nm, comprising of 20 % of the total percentage area distribution (Figure 3.8B).

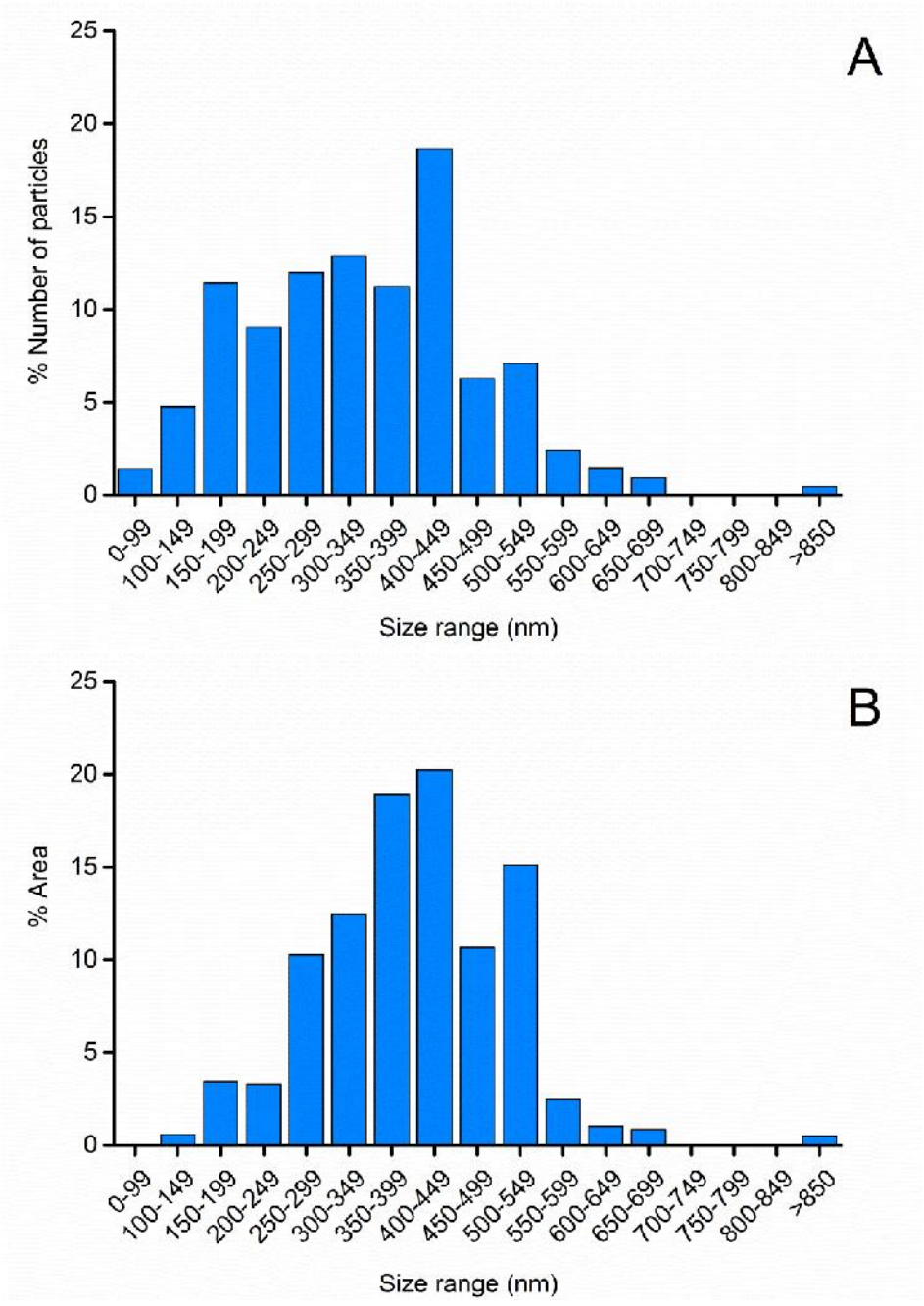

Figure 3.8 – Percentage size (A) and area (B) distributions of micron sized alumina particles. Using sequential filtration, micron sized alumina particles were isolated from a powder. Collected particles were imaged using FEGSEM analysis and the percentage distribution of the maximum length and area of the particles was determined using Image Pro-Plus 6.1 software. At least 150 particles were characterised in total.

3.4.4 Characterisation of cobalt chromium particles generated using a pin-on-plate simulator

The CoCr particles were generated using a six station pin-on-plate rig, (section 2.2.1). An aliquot of the CoCr particle suspension was subjected to sonication, filtered on to a 0.015 µm filter membrane and analysed using FEGSEM, as described in section 3.3.2.2. A representative FEGSEM image is shown in Figure 3.9. The CoCr nanoscale particles generated were mostly round to oval in morphology and occasionally shard-like particles were detected.

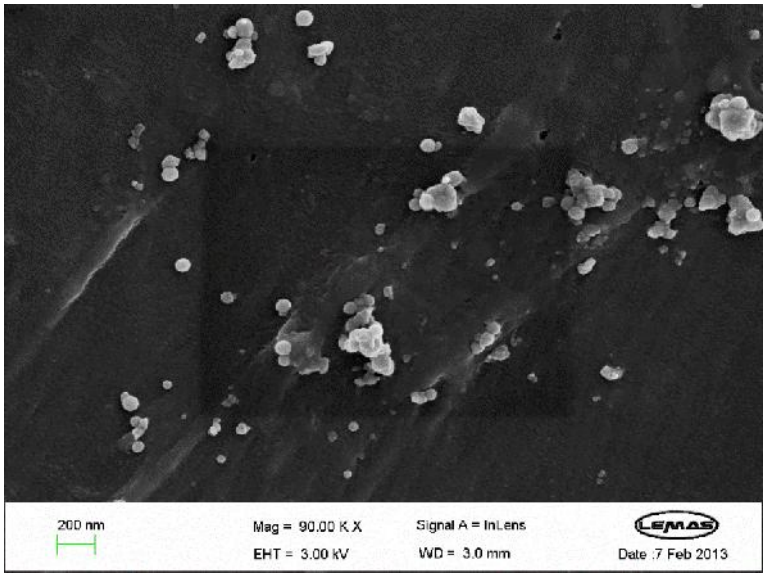

Figure 3.9 – Representative scanning electron microscopy image of isolated cobalt chromium particles. Particles were generated using a six station pin-on-plate wear rig and isolated by filtration onto a 0.015 µm pore size polycarbonate membrane. Particles in this image were observed at 90 K magnification, 3 kV, and working distance of 3.0 mm.

Pin point EDX analysis was performed to confirm the composition of the CoCr particles and an example EDX analysis spectrum and corresponding image is shown in Figure 3.10. The EDX analysis confirmed that the particles imaged were indeed CoCr particles, which consisted of cobalt and chromium. Molybdenum was not detected in any of the EDX spectrums.

The CoCr nanoscale particles were characterised using the FEGSEM images and the image analysis software, Image Pro Plus (section 3.3.2.2.2). The mode size of

the particles was measured at 40 – 49 nm; however particles up to 236 nm were measured (Figure 3.11A). Whilst the majority of the particles were 40 – 49 nm in size, the particles sized 70 – 79 nm had the largest particle area, making up 18 % of the particles measured (Figure 3.11B). However, the majority of the particle area distribution comprised of particles sized 40 – 89 nm (77% of the total particle area).

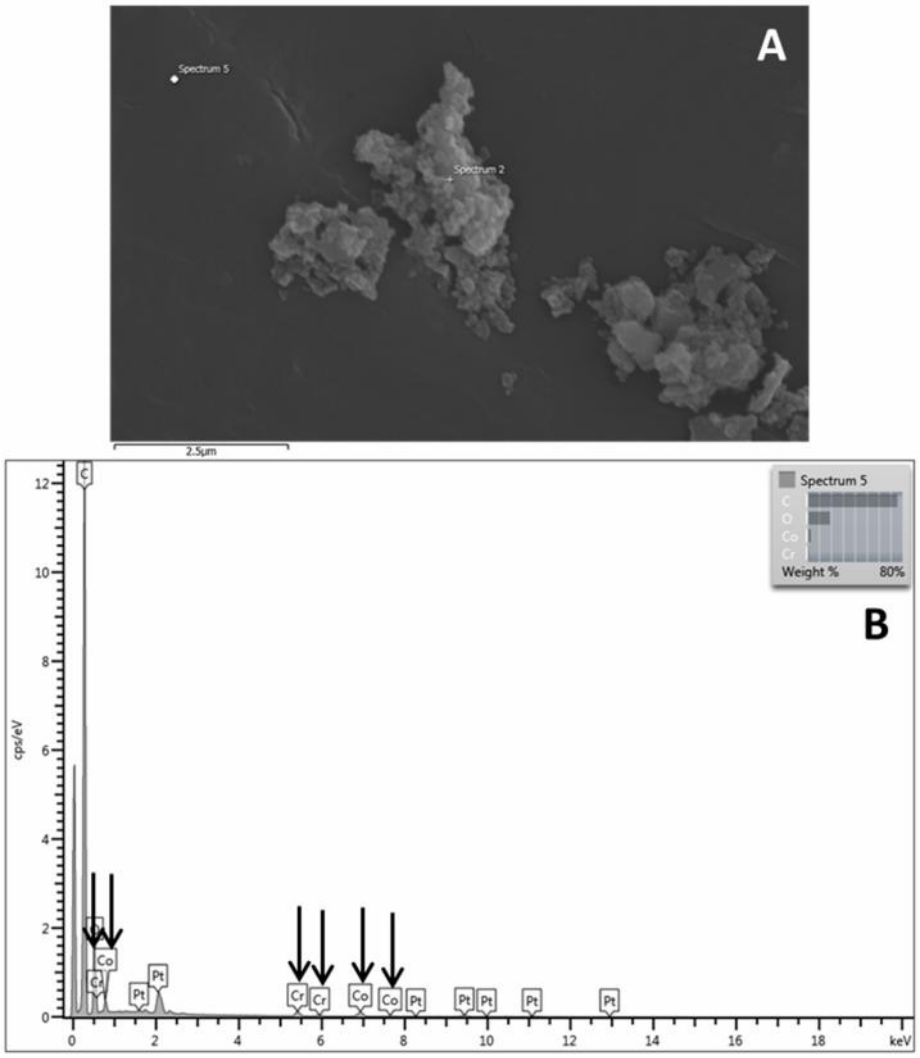

Figure 3.10 – Pin point energy-dispersive X-ray spectroscopy of nanoscale cobalt chromium particles. Nanoscale CoCr particles were filtered onto a 0.015 µm pore sized filter membrane and placed on an aluminium stub. The sample was coated with a platinum:palladium composite at a thickness of 3 – 10 nm. Pin point EDX analysis was performed at a working distance of 8.5 mm, 10 kV and a magnification of 20K. (A) Image of analysed nanoscale CoCr particles. (B) Example EDX spectrum of nanoscale CoCr particles. Arrows indicate characteristic elements of particles.

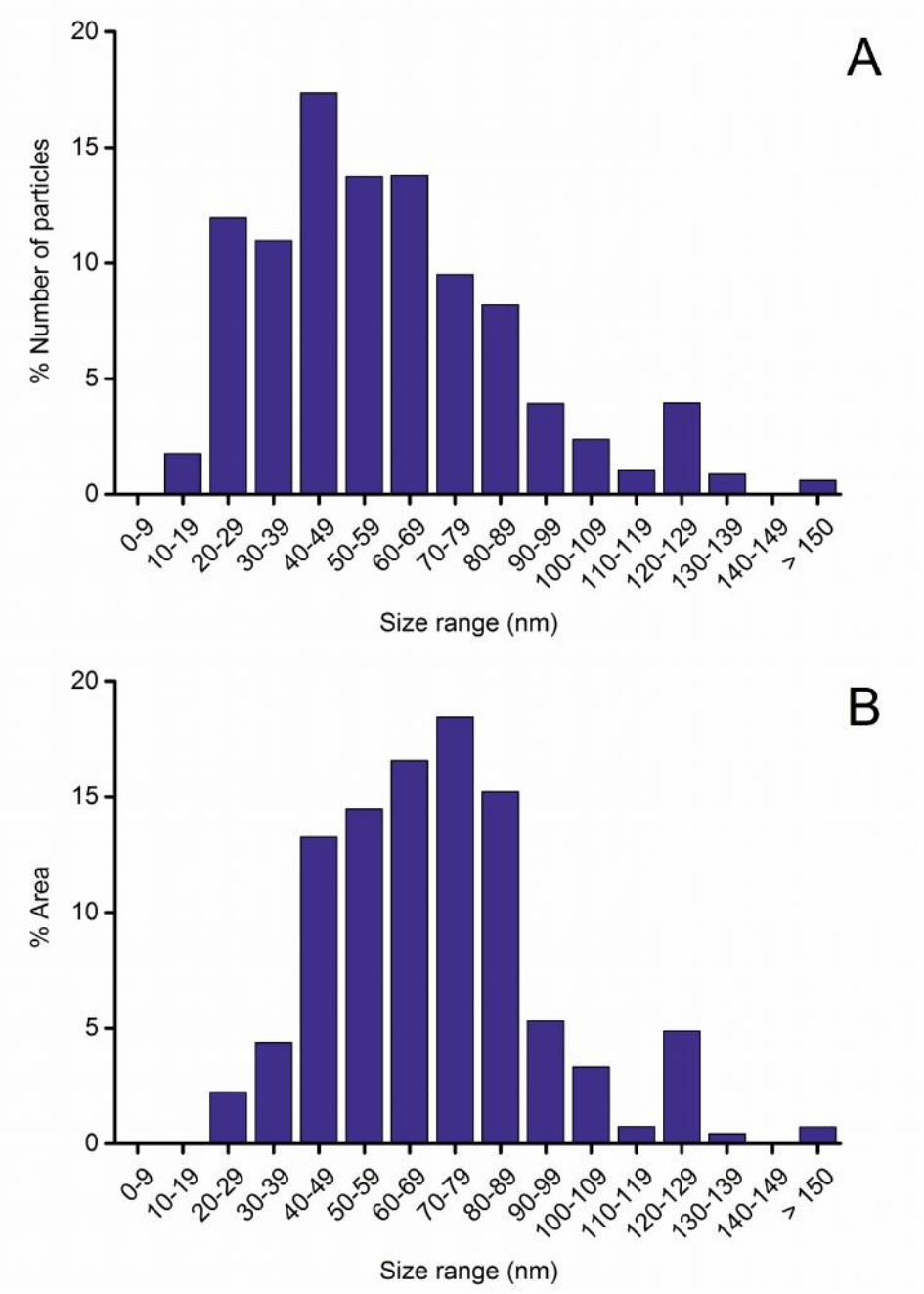

Figure 3.11 – Percentage size (A) and area distribution (B) of nanoscale cobalt chromium particles. Particles were generated using a six station pin-on-plate wear simulator. Particles were imaged using FEGSEM analysis and the percentage distribution of the maximum length and area of the particles was determined using Image Pro-Plus 6.1 software. At least 150 particles were characterised in total.

3.4.5 Characterisation of commercially available micron sized cobalt chromium particles

An aliquot of the commercially available micron sized CoCr particle suspension in 70% (v/v) ethanol was subjected to sonication, filtered through a 0.015 µm filter membrane and analysed using SEM as described in section 3.3.2.2. A representative FEGSEM image is shown in Figure 3.12. The CoCr micron size particles were observed to be round in morphology with the occasional oval shaped particles detected. Whilst some aggregates were observed, this was with much less frequency than for the nanoscale alumina and CoCr particles.

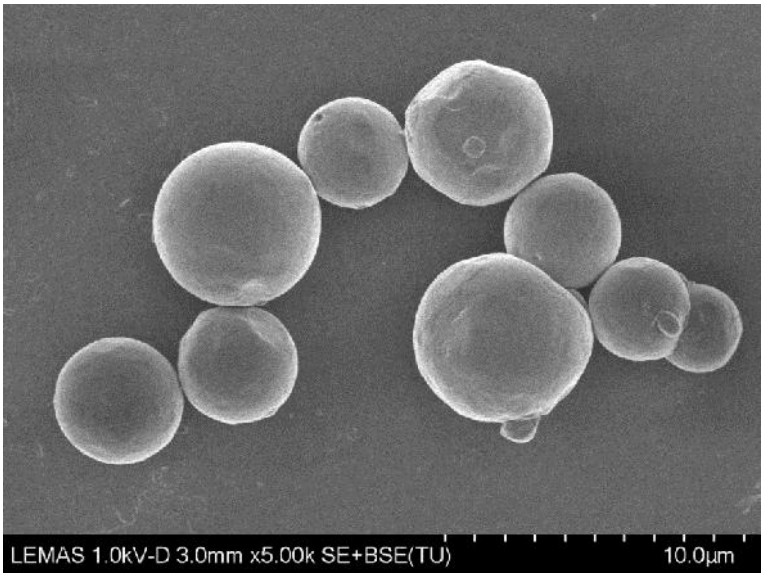

Figure 3.12 – Representative scanning electron microscopy image of commercially available micron sized cobalt chromium particles. Particles were isolated from a CoCr powder and filtered onto a 0.015 µm pore size polycarbonate membrane. Particles in this image were taken at x5 K magnification, 1 kV, and working distance of 3.0 mm.

EDX analysis was performed to confirm the composition of the CoCr micron size particles and an example of an EDX analysis spectrum and corresponding image is shown in Figure 3.13. The EDX analysis confirmed that the particles imaged were comprised of cobalt and chromium. Pin point EDX analysis also revealed that the majority of the CoCr particles consisted of cobalt. The CoCr alloy also contained

molybdenum, which unlike the CoCr nanoscale particle samples was detected in some of the EDX spectra.

The CoCr micron particles were characterised using the FEGSEM images and the image analysis software, Image Pro Plus (section 3.3.2.2.2). A wide distribution of particle sizes were measured, with particles ranging from 150 nm to 6.95 µm. The mode size of the particles was measured at 2 – 3 µm with a mean particle size of 3.26 µm (SD ± 1.30 µm) as shown in Figure 3.14A. Whilst the majority of the particles were 2 – 3 µm in size, the particles sized between 3 – 4 µm had the largest particle area, contributing up 38 % of the particles measured (Figure 3.14B).

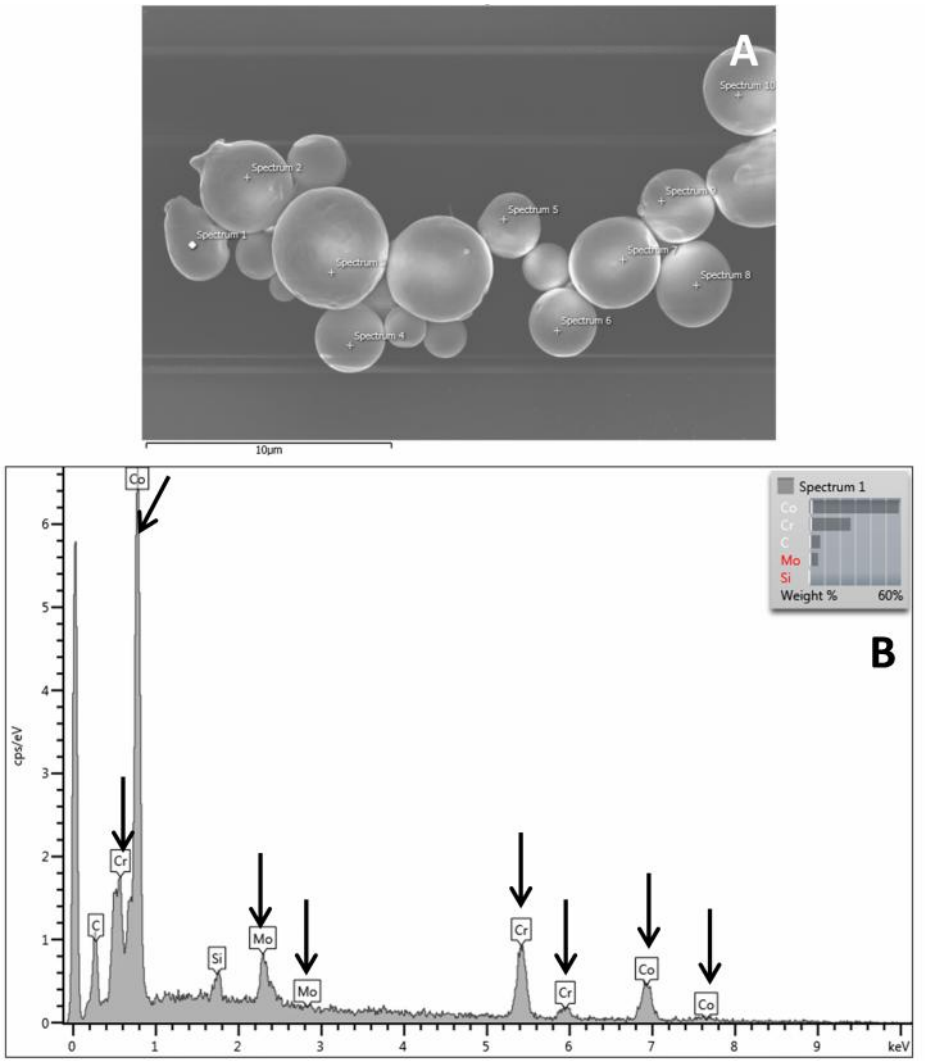

Figure 3.13 – Pin point energy-dispersive X-ray spectroscopy of micron sized cobalt chromium particles. Micron sized CoCr particles were filtered onto a 0.015 µm pore sized filter membrane and placed on an aluminium stub. The sample was coated with a carbon composite at a thickness of 3 – 10 nm. Pin point EDX analysis was performed at a working distance of 8.5 mm, 10 kV and a magnification of 10K. (A) Image of analysed of micron sized CoCr particles. (B) Example EDX spectrum of micron sized CoCr particles. Arrows indicate characteristic elements of particles.

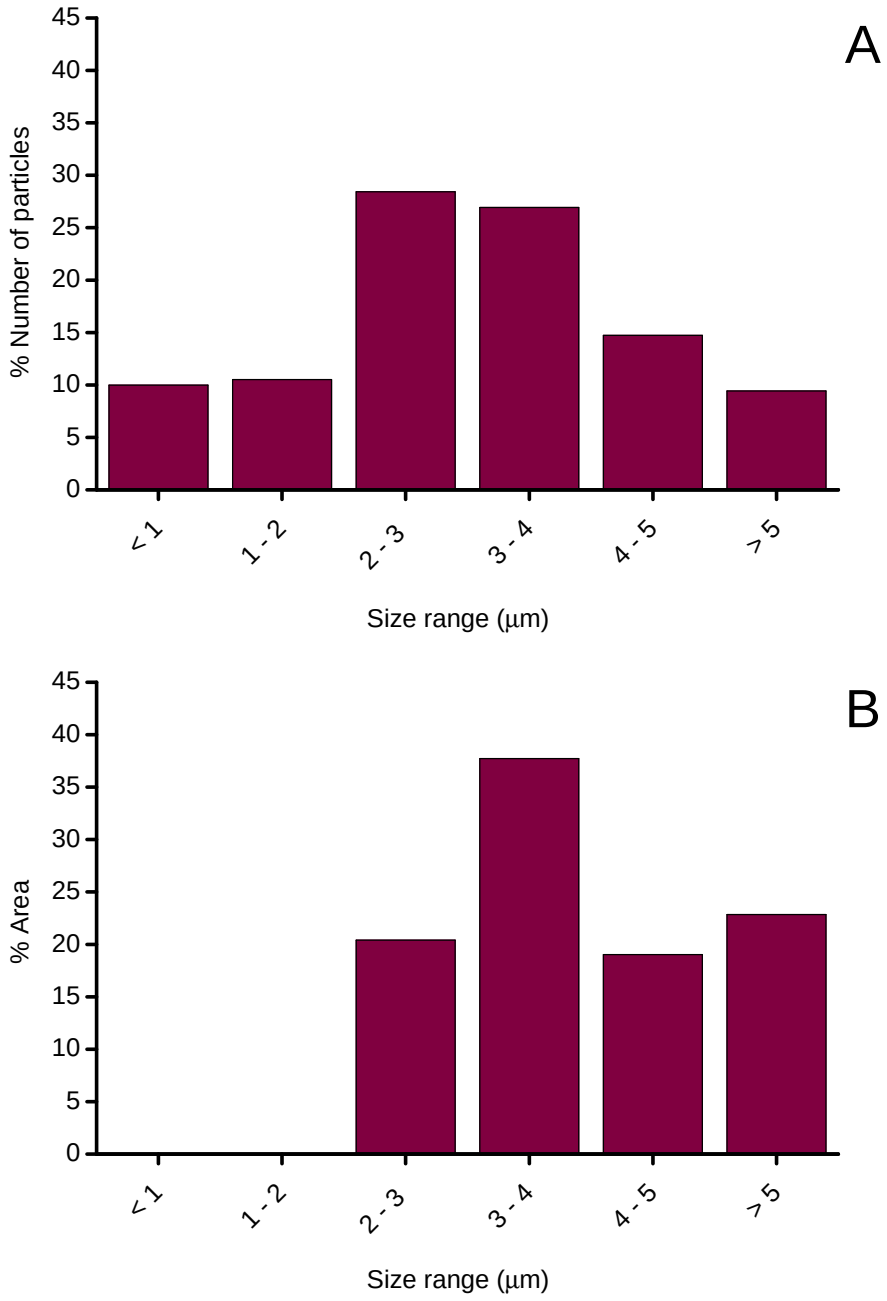

Figure 3.14 – Percentage size (A) and area (B) distribution of micron sized cobalt chromium particles. Micron sized CoCr particles were suspended in 70% (v/v) ethanol and collected onto a 0.015 µm pore size filter. The dried filter was placed on an aluminium platform stub and coated with carbon. Particles were imaged using FEGSEM analysis and the percentage distribution of the maximum length and area of the particles was determined using Image Pro-Plus 6.1 software. At least 150 particles were characterised in total.

3.4.6 The effect of nanoscale and micron sized alumina and cobalt chromium particles on the cell viability of U937 histiocytes and primary human fibroblasts

The aim of this part of the study was to compare the effect of nanoscale and micron sized alumina and CoCr particles on cell viability with other relevant *in vitro* studies within the published literature. The simplest method was to investigate the effect of the particles on the cell viability on U937 histiocytes and primary HFBs. These cell types have been previously cultured in the presence of CoCr and alumina particles in the published literature and therefore the results from this study could be compared (Matthews *et al.* 2000; Germain *et al.* 2003; Brown *et al.* 2006; Papageorgiou *et al.* 2007; Brown *et al.* 2013). In brief, the U937 histiocytes were seeded into a 96 well plate at a density of 2 x 10^5.ml^{-1}. For the primary HFBs, the cells were seeded at a density of 1 x 10^5.ml^{-1}.The cell density of the U937 histiocytes and primary HFBs for the cell viability ATPlite and MTT assays were previously described by Germain *et al.* (2003) and Papageorgiou *et al.* (2007), respectively. Cells were cultured in the presence of nanoscale or micron sized alumina particles at particle volumes per cell of 0.0005 to 500 μm^3 per cell (n = 6). For the CoCr nanoscale and micron sized particles, the cells were cultured with the particles at volumes of 0.0005 to 50 μm^3 per cell (n = 6).

3.4.6.1 The effect of nanoscale and micron sized alumina and cobalt chromium particles on the viability of U937 histiocytes

The effect of the nanoscale and micron sized alumina and CoCr particles on the viability of U937 histiocytes was assessed using the ATPlite and MTT assay. These results were then compared against the published literature to determine if the particles induced a similar response.

3.4.6.1.1 The effect of nanoscale and micron sized alumina particles on histiocyte cell viability using the ATPlite and MTT assay.

U937 histiocytes were cultured in the presence of nanoscale or micron sized alumina particles at particle volumes of 0.0005 to 500 μm^3 per cell. Cell viability was measured at 0, 1, 3, 5 days after incubation using the ATPlite and MTT assays (section 2.2.5). The results were expressed as a percentage of the cell only control. Raw data were analysed using one way ANOVA and individual differences between the means were determined using the Tukey method to calculate the MSD. Significant ($p < 0.05$) adverse effects on cell viability in comparison to the cell only control are indicated by an asterisk (*) in the subsequent graphs.

The ATPlite assay revealed no significant reduction in the cell viability for all particle doses in comparison to the cell only negative control for both the nanoscale and micron sized alumina particles (Figure 3.15A & 3.15B, respectively). Indeed on occasion, the cell viability in the presence of the nanoscale or micron size particles was higher than the cell only negative control. However, this difference was not significant. A significant reduction in cell viability was measured for the positive control of 2 $\mu g.ml^{-1}$ camptothecin. After 24 hours of culture with the positive control, there was an approximate 90% reduction in cell viability in comparison to the cell only negative control for both the nanoscale and micron sized particles.

The MTT assay results were comparable to the ATPlite assay results (Figure 3.16). Again the positive control (2 $\mu g.ml^{-1}$ camptothecin) caused a significant reduction in cell proliferation after 24 hours in comparison to the cell only negative control in all experiments (Figure 3.16A and 3.16B, respectively). The main difference between the ATPlite and MTT assays was observed for the nanoscale alumina particles at a particle volume of 500 μm^3 per cell at day 3 and 5. This particle volume had a significant effect on the cell viability, and at day 3 there was an approximate 50% reduction in cell viability, however, at day 5 this is reduced slightly to a 45%

reduction for the MTT assay. Nevertheless this was still a significant reduction in cell proliferation in comparison to the cell only control.

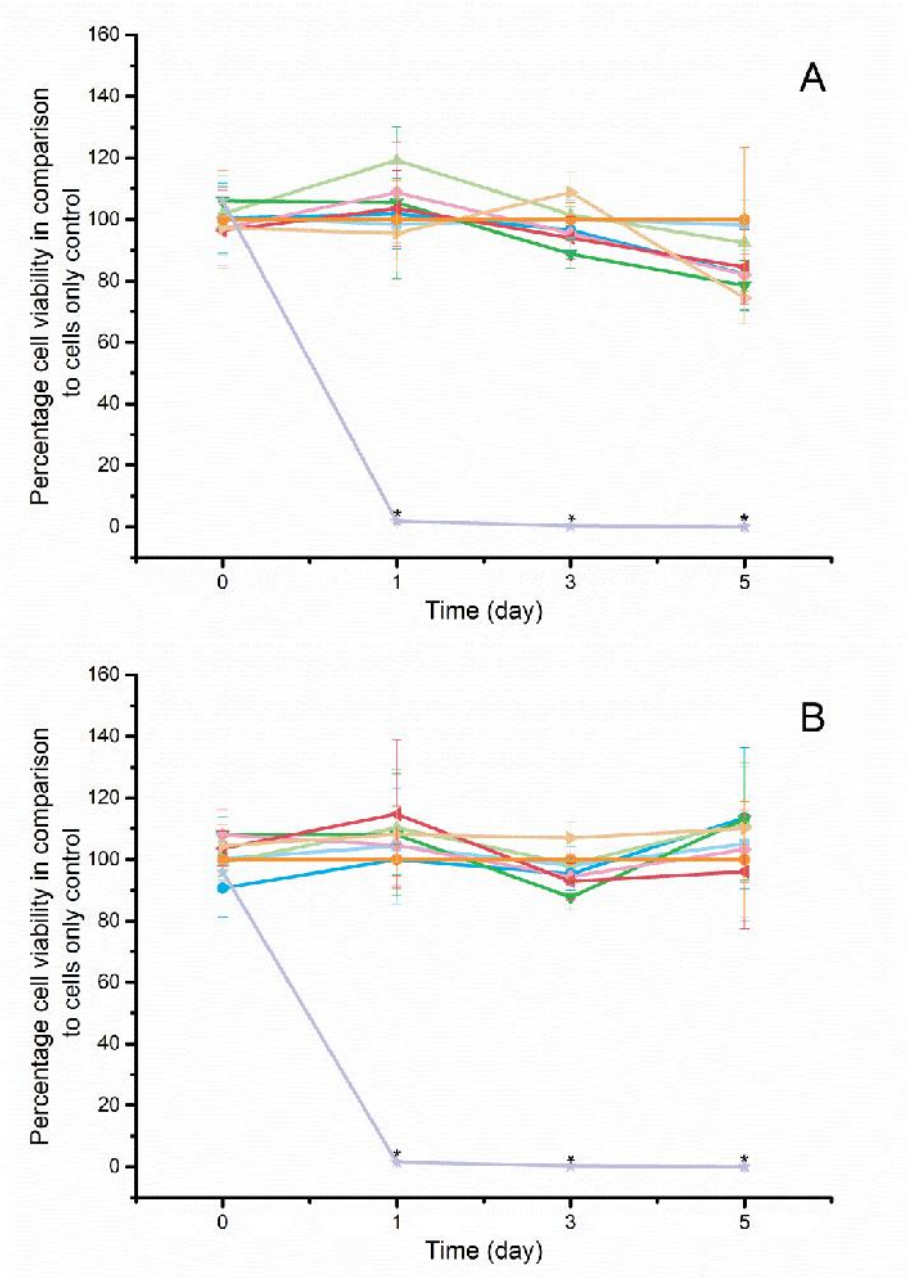

Figure 3.15 – The effect of nanoscale alumina particles (A) and micron sized alumina particles (B) on U937 cell viability using the ATPlite assay. U937 histiocytes were cultured with nanoscale and micron sized alumina particles for 5 days. Cell viability was determined using the ATPlite assay and presented as a percentage viability compared to the cell only negative control. Data was analysed using one-way analysis of variance (ANOVA) and the MSD was calculated using the Tukey method. A statistically significant reduction ($p<0.05$) in the cell viability in comparison to the cell only control, are indicated by an asterisk (*). Error bars represented ± 95% CI levels, n = 6 (■: 500 μm^3 per cell; ●: 50 μm^3 per cell; ▲: 5 μm^3 per cell; ▼: 0.5 μm^3 per cell; ♦: 0.05 μm^3 per cell; ◄: 0.005 μm^3 per cell; ►: 0.0005 μm^3 per cell; ●: cell only control; ★: 2 $\mu g.ml^{-1}$ camptothecin).

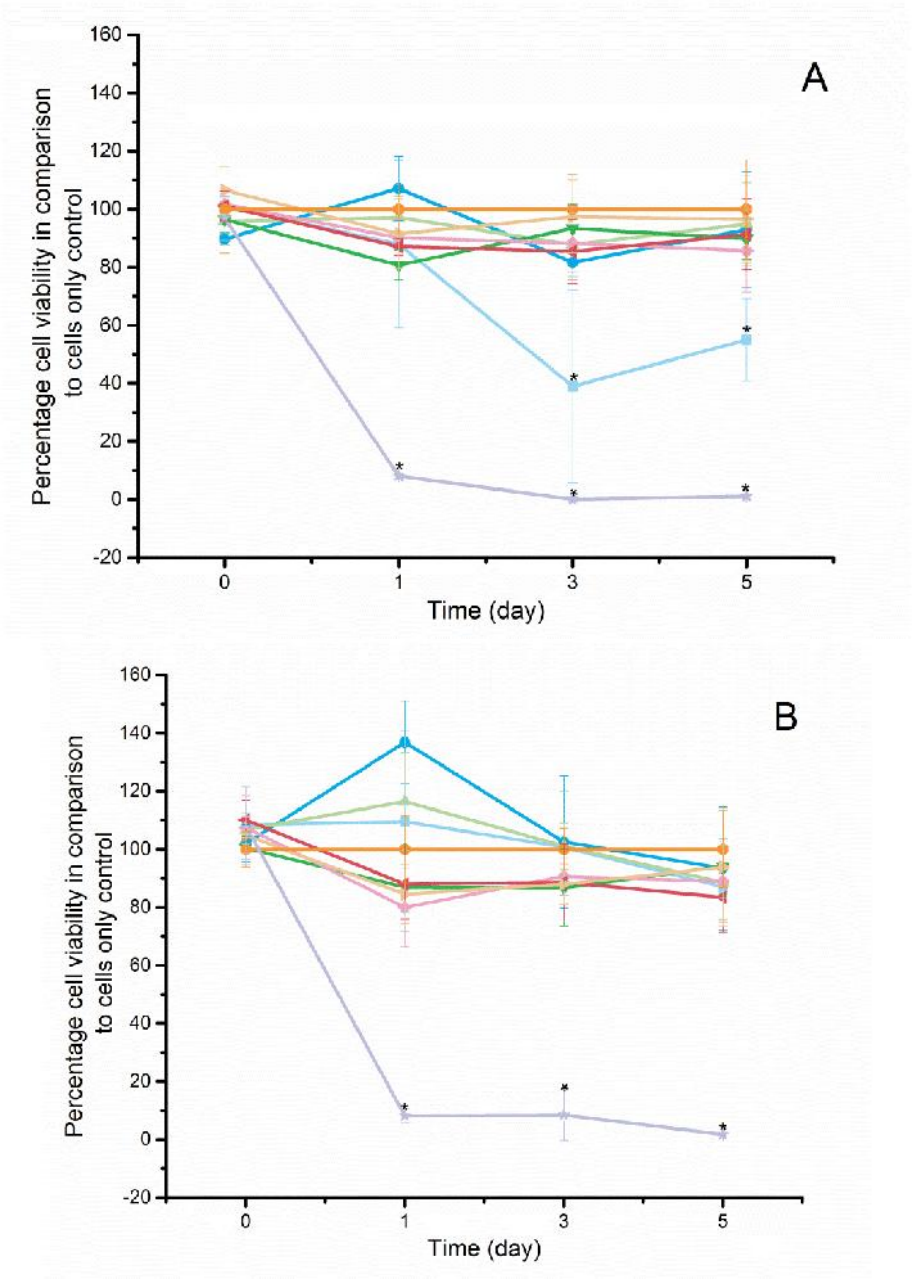

Figure 3.16 – Effect of nanoscale (A) and micron sized (B) alumina particles on U937 cell viability using the MTT assay. U937 histiocytes were cultured with nanoscale and micron sized alumina particles for 5 days. Cell viability was determined using the MTT assay and presented as a percentage viability compared to the cell only negative control. Data was analysed using one-way analysis of variance (ANOVA) and the MSD was calculated using the Tukey method. A statistically significant reduction ($p<0.05$) in the cell viability in comparison to the cell only control, are indicated by an asterisk (*). Error bars represented ± 95% CI levels, n = 6 (■: 500 μm^3 per cell; ●: 50 μm^3 per cell; ▲: 5 μm^3 per cell; ▼: 0.5 μm^3 per cell; ♦: 0.05 μm^3 per cell; ◄: 0.005 μm^3 per cell; ►: 0.0005 μm^3 per cell; ●: cell only control; ★: 2 $\mu g.ml^{-1}$ camptothecin).

3.4.6.1.2 The effect of nanoscale and micron sized cobalt chromium particles on U937 histiocyte cell viability using the ATPlite and MTT assay.

U937 histiocytes were cultured in the presence of nanoscale or micron sized CoCr particles at particle volumes per cell of 0.0005 to 50 μm^3 per cell. Cell viability was measured at 0, 1, 3, 5 days after incubation using the ATPlite and MTT assays (section 2.2.4). The results were expressed as a percentage of the cell only control.

For the ATPlite assay, both the nanoparticle and micron sized CoCr particle studies, the positive control (2 $\mu g.ml^{-1}$ camptothecin), caused a significant reduction in cell viability in comparison to the cell only negative control (Figure 3.17A & 3.17B, respectively). The majority of the particle volumes of micron sized CoCr particles had no significant effect on U937 viability over the five days of culture. The exception was that after five days an approximate 40% drop in cell viability was measured for the highest particle volume of 50 μm^3 per cell in comparison to the cell only negative control. In contrast the nanoscale CoCr particles had a greater detrimental impact on the cell viability. For the ATPlite assay, after one day of culture, the highest particle volume of 50 μm^3 per cell had a significant effect on the cell viability with a 30% reduction in viability. After five days of culture, this had increased to at least a 98% drop in viability. Furthermore, particle volumes of 5 μm^3 per cell of nanoscale CoCr significantly reduced cell viability in comparison to the cell only negative control after 3 and 5 days of culture.

Similar results were obtained using the MTT assay to assess cell viability. The positive control, 2 $\mu g.ml^{-1}$ camptothecin, significantly reduced cell viability after one day of culture (Figure 3.18A and 3.18B, respectively). In contrast to the ATPlite assay results (Figure 3.17B), no significant drop in cell viability was measured for any of the particle volumes over the five days of culture with the micron sized CoCr particles. The nanoscale CoCr particles were also observed to have less of an effect on the cell viability in comparison to the results obtained with the ATPlite

assay. Only the highest particle volume of 50 μm^3 per cell of nanoscale CoCr particles produced a reduction in cell viability from day one onwards. However, a much larger decrease in the cell viability was measured in comparison to the ATPlite assay results. Cell viability was reduced almost to zero after one day with 50 μm^3 per cell of nanoscale CoCr particles, which was greater than the positive control.

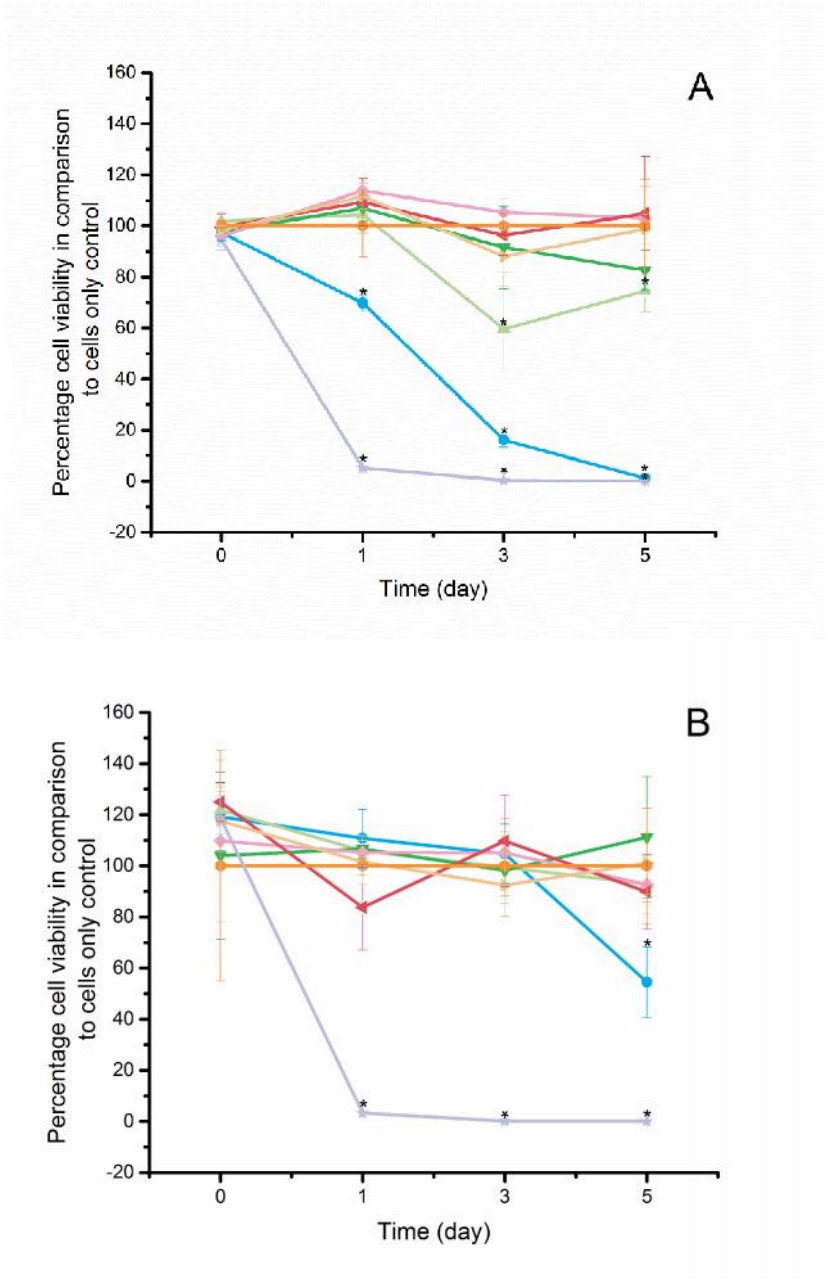

Figure 3.17 – Effect of nanoscale (A) and micron sized (B) cobalt chromium particles on U937 cell viability using the ATPlite assay. U937 histiocytes were cultured with nanoscale and micron sized CoCr particles for 5 days. Cell viability was determined using the ATPlite assay and presented as a percentage viability compared to the cell only control. Data was analysed using one-way analysis of variance (ANOVA and the MSD was calculated using the Tukey method. A statistically significant reduction ($p<0.05$) in the cell viability in comparison to the cell only control, are indicated by an asterisk (*). Error bars represented ± 95% CI levels, n = 6. (●: 50 μm^3 per cell; ▲: 5 μm^3 per cell; ▼: 0.5 μm^3 per cell; ♦: 0.05 μm^3 per cell; ◄: 0.005 μm^3 per cell; ►: 0.0005 μm^3 per cell; ●: cell only control; ★: 2 $\mu g.ml^{-1}$ camptothecin).

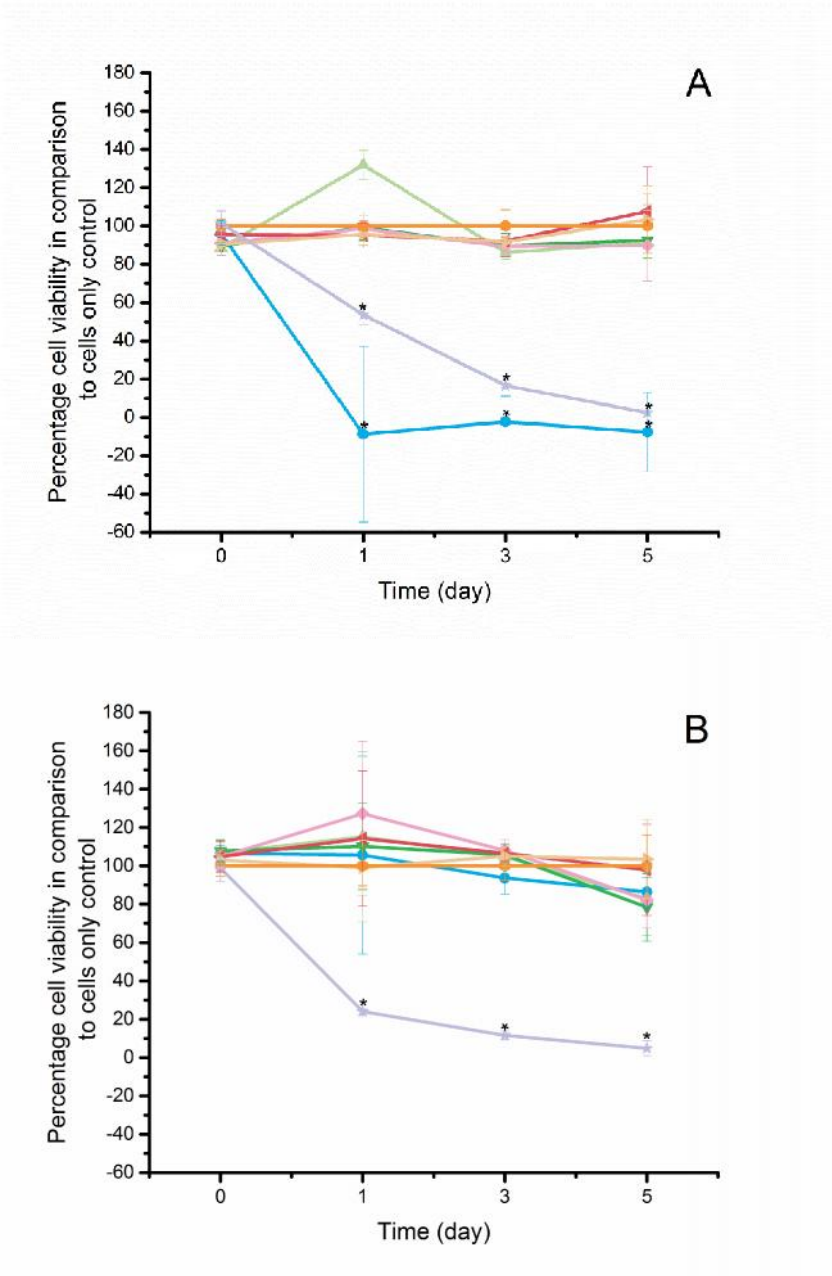

Figure 3.18 – Effect of nanoscale (A) and micron sized (B) cobalt chromium particles on U937 cell viability using the MTT assay. U937 histiocytes were cultured with nanoscale and micron sized CoCr particles for 5 days. Cell viability was determined using the MTT assay and presented as a percentage viability compared to the cell only control. Data was analysed using one-way analysis of variance (ANOVA) and the MSD was calculated using the Tukey method. A statistically significant reduction ($p<0.05$) in the cell viability in comparison to the cell only control, are indicated by an asterisk (*). Error bars represented ± 95% CI levels, n = 6. (●: 50 μm^3 per cell; ▲: 5 μm^3 per cell; ▼: 0.5 μm^3 per cell; ♦: 0.05 μm^3 per cell; ◄: 0.005 μm^3 per cell; ►: 0.0005 μm^3 per cell; ●: cell only control; ★: 2 $\mu g.ml^{-1}$ camptothecin).

3.4.6.2 The effect of alumina and cobalt chromium nanoscale and micron size particles on the cell viability on primary human fibroblast cells

The effect of the previously characterised nanoscale and micron sized alumina and CoCr particles on the viability of HFBs were assessed using the ATPlite and MTT assay. These results were then compared against the published literature to determine if a similar response occurred in the presence of the particles.

3.4.6.2.1 The effect of nanoscale and micron sized alumina particles on primary human fibroblast cell viability using the ATPlite and MTT assays

Primary HFBs were cultured in the presence of nanoscale or micron sized alumina particles at particle volumes per cell of 0.0005 to 500 μm^3 per cell. Cell viability was measured at 0, 1, 3, 5 days after incubation using the ATPlite and MTT assays (section 2.2.4). The results were expressed as a percentage of the cell only control.

The nanoscale alumina particles had no effect on cell viability for all the particle volumes over the five days of culture as determined by the ATPlite assay (Figure 3.19A). The positive control, (2 $\mu g.ml^{-1}$ camptothecin) caused a significant reduction in cell viability, resulting in an approximate 90% reduction after 5 days of culture. None of the particle volumes of the micron sized alumina particles had any significant effect on HFB cell viability in comparison to the cell only control. Only the positive control, (2 $\mu g.ml^{-1}$ camptothecin) had a significant effect on viability after one day of culture (Figure 3.19B).

Similar results were obtained with the MTT assay. Primary HFBs were cultured with particle volumes per cell of 0.0005 to 500 μm^3 per cell of nanoscale alumina particles over 5 days. The only significant effect on the cell viability was observed for the positive control (Figure 3.20A). In contrast the micron sized alumina

particles, at high particle volumes, had a significant effect on fibroblast proliferation in comparison to the cell only control. The highest particle volume of 500 μm^3 per cell caused a 52% reduction in cell viability after one day of culture, although this reduced to 29% after 5 days. A 19% reduction in cell viability was also measured with the micron sized alumina particle volume of 50 μm^3 per cell after one day of culture (Figure 3.20B).

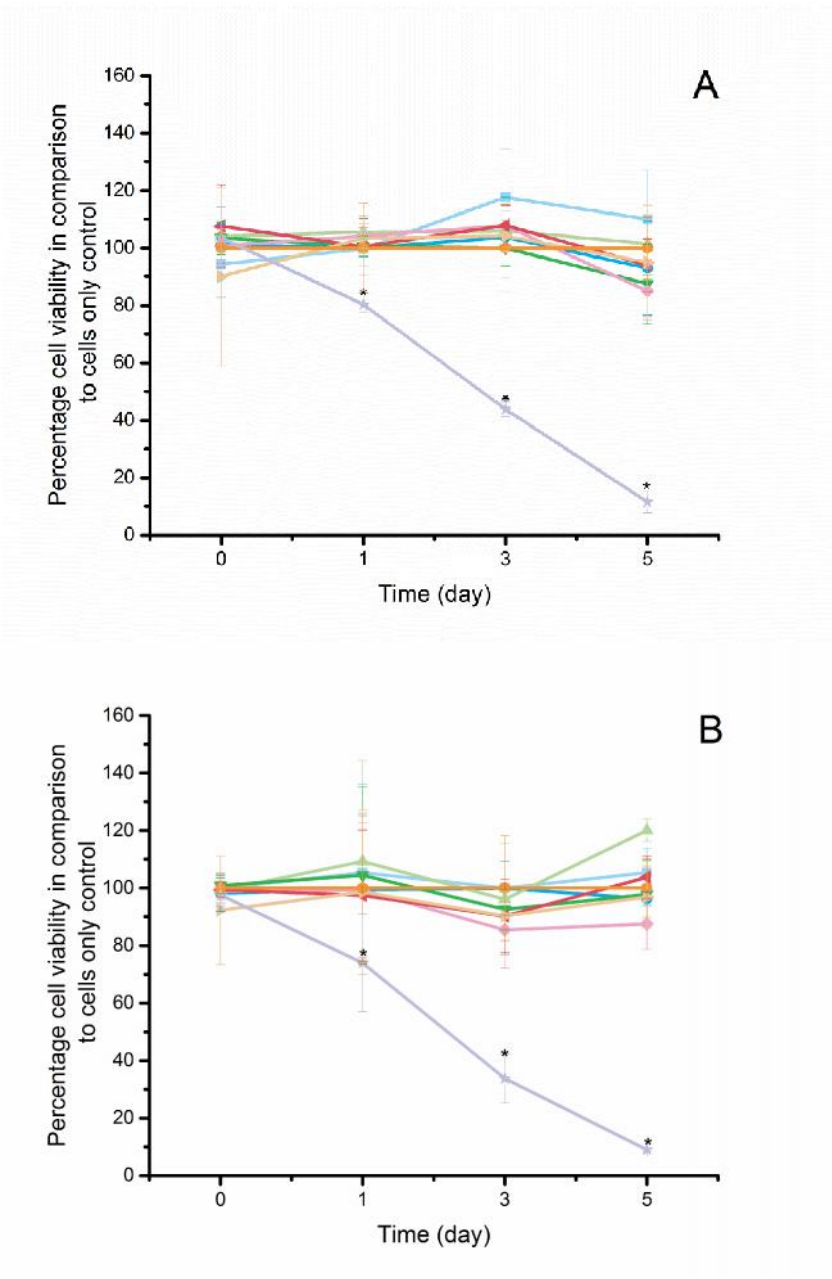

Figure 3.19 – Effect of nanoscale (A) and micron sized (B) alumina particles on primary human fibroblast viability using the ATPlite assay. Primary HFBs were cultured with nanoscale and micron sized alumina particles for 5 days. Cell viability was determined using the ATPlite assay and presented as percentage viability compared to the cell only control. Data was analysed using one-way analysis of variance (ANOVA) and the MSD was calculated using the Tukey method. A statistically significant reduction ($p<0.05$) in the cell viability in comparison to the cell only control, are indicated by an asterisk (*). Error bars represented ± 95% CI levels, n = 6. (■: 500 μm^3 per cell; ●: 50 μm^3 per cell; ▲: 5 μm^3 per cell; ▼: 0.5 μm^3 per cell; ♦: 0.05 μm^3 per cell; ◄: 0.005 μm^3 per cell; ►: 0.0005 μm^3 per cell; ●: cell only control; ★: 2 $\mu g.ml^{-1}$ camptothecin).

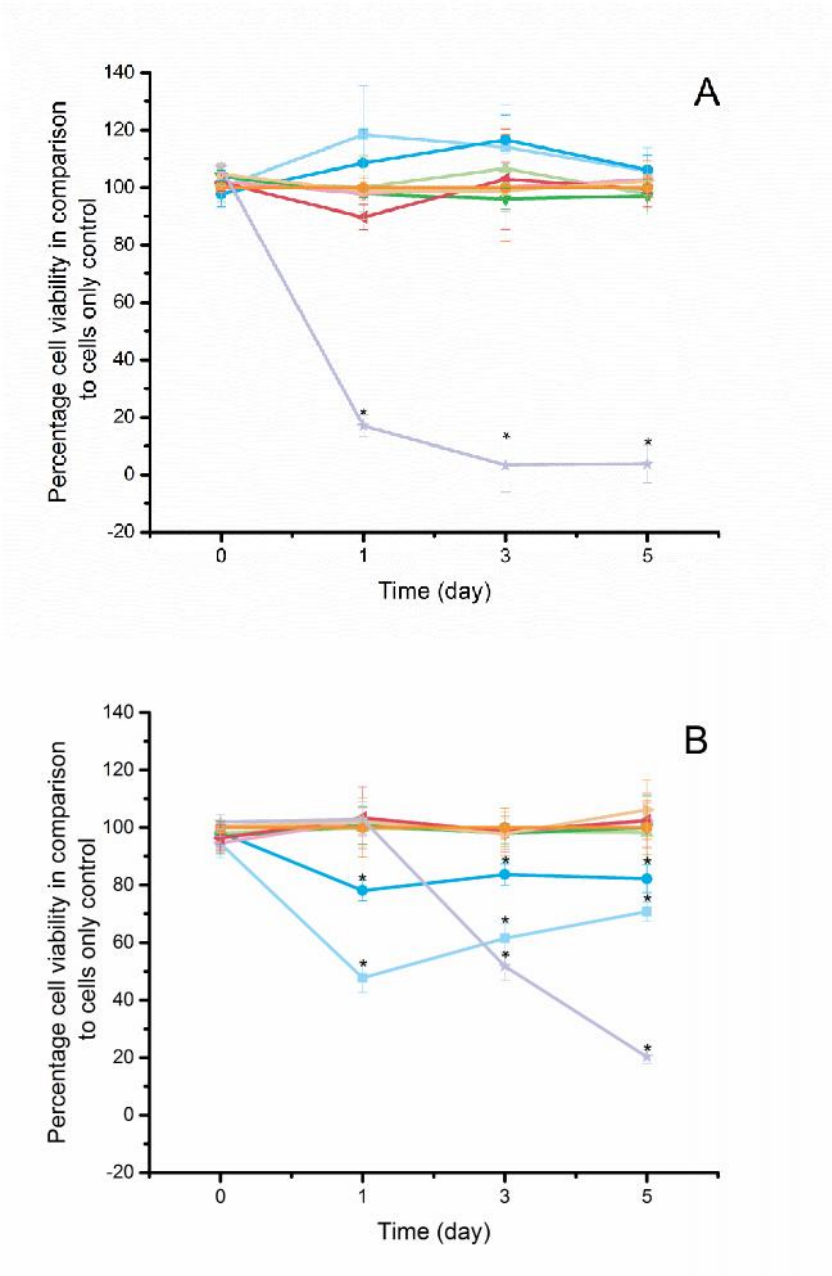

Figure 3.20 – Effect of nanoscale (A) and micron sized (B) alumina particles on primary human fibroblast viability using the MTT assay. Primary HFBs were cultured with nanoscale and micron sized alumina particles for 5 days. Cell viability was determined using the MTT assay and presented as percentage viability compared to the cell only control. Data was analysed using one-way analysis of variance (ANOVA) and the MSD was calculated using the Tukey method. A statistically significant reduction ($p<0.05$) in the cell viability in comparison to the cell only control, are indicated by an asterisk (*). Error bars represented ± 95% CI levels, n = 6. (■: 500 μm^3 per cell; ●: 50 μm^3 per cell; ▲: 5 μm^3 per cell; ▼: 0.5 μm^3 per cell; ♦: 0.05 μm^3 per cell; ◄: 0.005 μm^3 per cell; ►: 0.0005 μm^3 per cell; ●: cell only control; ★: 2 $\mu g.ml^{-1}$ camptothecin).

3.4.6.2.2 The effect of nanoscale and micron sized cobalt chromium particles on human fibroblast cell viability using the ATPlite and MTT assay

Primary HFBs were cultured in the presence of nanoscale or micron sized CoCr particles at particle volumes per cell of 0.0005 to 50 μm^3 per cell. Cell viability was measured at 0, 1, 3, 5 days after incubation using the ATPlite and MTT assays (section 2.2.4). The results were expressed as a percentage of the cell only control.

A dose- and time-dependent effect of nanoscale CoCr particles on the human fibroblast viability was observed using the ATPlite assay (Figure 3.21A). After one day of culture, the particle volume of 50 μm^3 per cell, caused a 37% decrease in the cell viability in comparison to the cell only control. This was further reduced to a 65% drop in cell viability by day 5. At the time points of day 3 and 5, the particle volume of 5 μm^3 per cell also induced a significant reduction in cell viability in comparison to the cell only control. In contrast, the only significant reduction in the cell viability for the primary HFBs cultured with micron sized CoCr particles was measured for the positive control, (2 $\mu g.ml^{-1}$ camptothecin, Figure 3.21B).

Large reductions in cell viability in comparison to the cell only control for the highest nanoscale CoCr particle volume of 50 μm^3 per cell was measured using the MTT assay (Figure 3.22A). Furthermore particle volumes of 5 μm^3 per cell also had a significant effect on cell viability after one day of culture, with an average 13% drop in viability over day 1, 3 and 5 of culture. After 3 and 5 days of culture, the particle volume of 0.5 μm^3 per cell also reached significance. However, the majority of the particle volumes of the micron sized CoCr particles had no effect on the cell viability using the MTT assay (Figure 3.22B). The only exception was the highest particle volume of 50 μm^3 per cell, which had a significant detrimental effect on the cell viability from one day of culture.

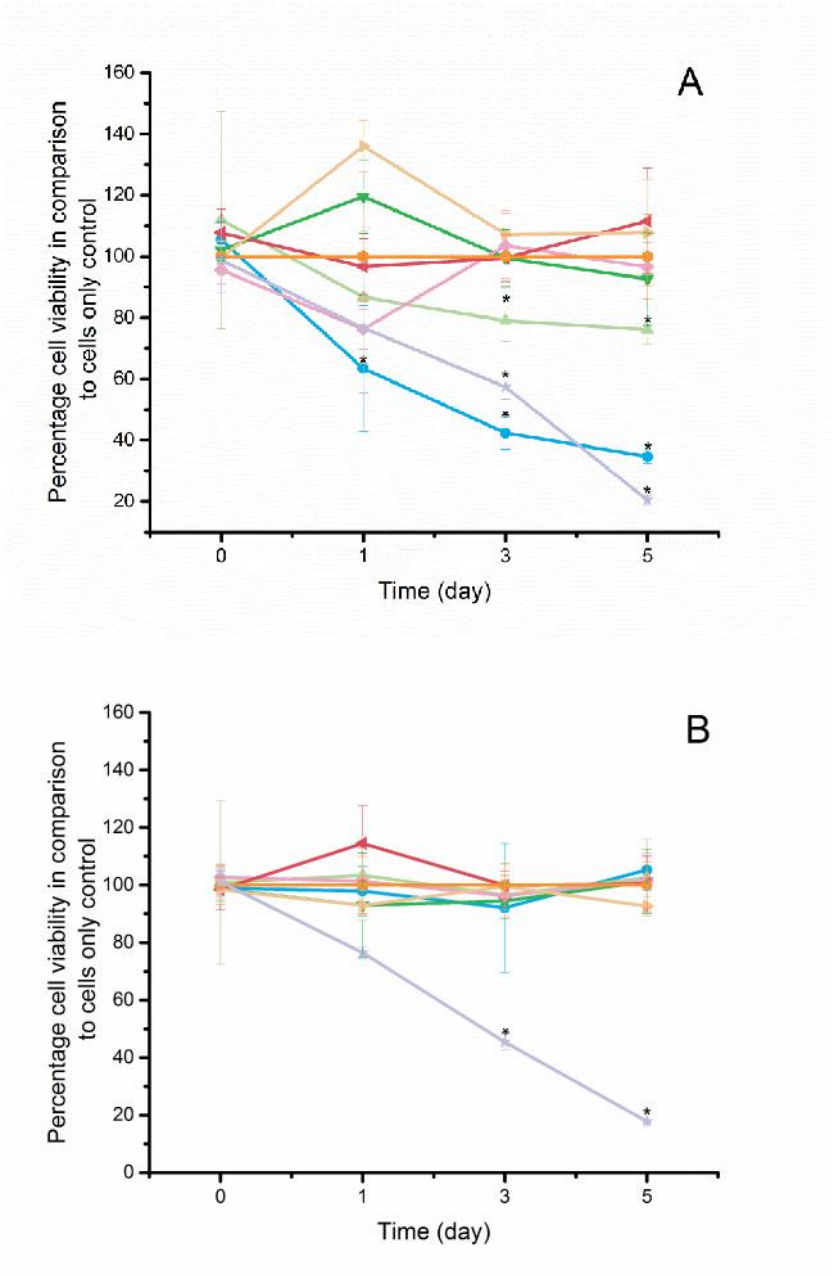

Figure 3.21 – Effect of nanoscale (A) and micron sized (B) cobalt chromium particles on primary human fibroblast viability using the ATPlite assay. Primary HFBs were cultured with nanoscale and micron sized CoCr particles for 5 days. Cell viability was determined using the ATPlite assay and presented as percentage viability compared to the cell only control. Data was analysed using one-way analysis of variance (ANOVA) and the MSD was calculated using the Tukey method. A statistically significant reduction ($p<0.05$) in the cell viability in comparison to the cell only control, are indicated by an asterisk (*). Error bars represented ± 95% CI levels, n = 6. (●: 50 μm^3 per cell; ▲: 5 μm^3 per cell; ▼: 0.5 μm^3 per cell; ♦: 0.05 μm^3 per cell; ◄: 0.005 μm^3 per cell; ►: 0.0005 μm^3 per cell; ●: cell only control; ★: 2 $\mu g.ml^{-1}$ camptothecin).

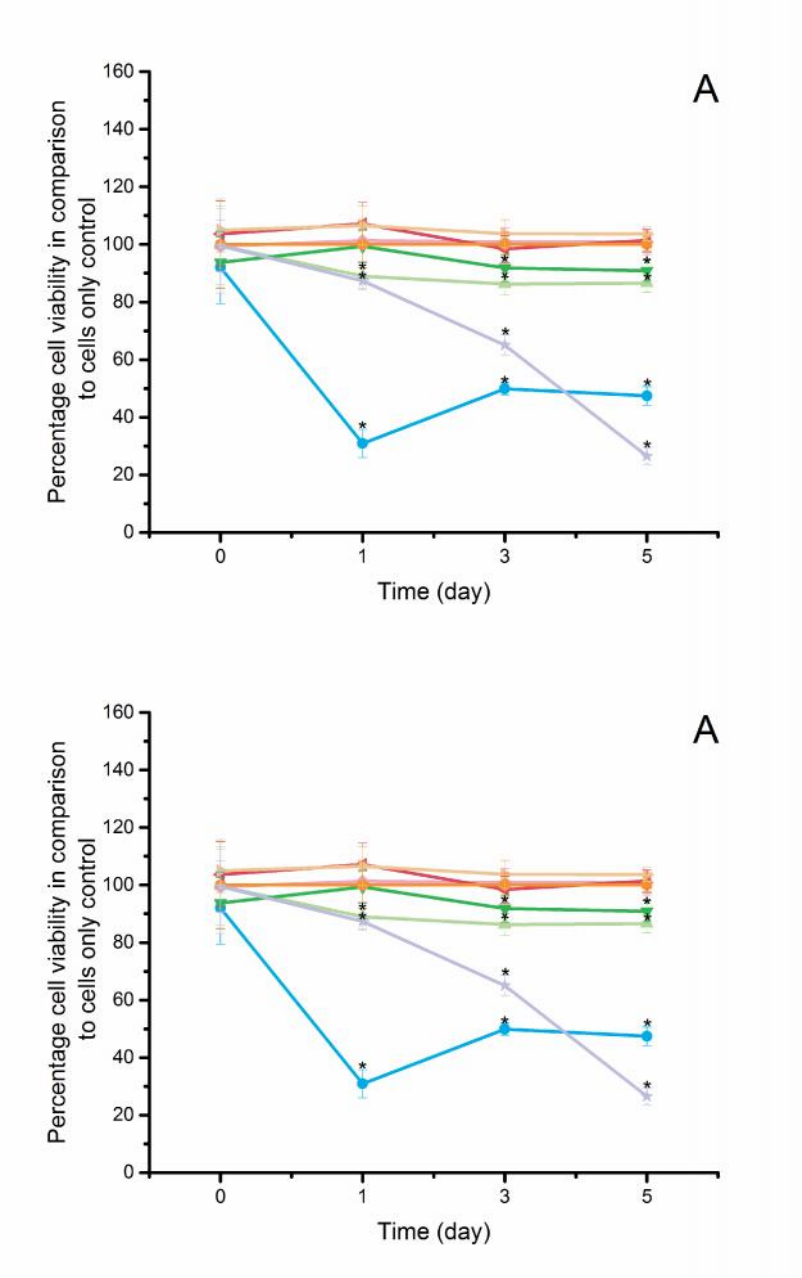

Figure 3.22 – Effect of nanoscale (A) and micron sized (B) cobalt chromium particles on primary human fibroblast viability using the MTT assay. Primary HFBs were cultured with nanoscale and micron sized CoCr particles for 5 days. Cell viability was determined using the MTT assay and presented as percentage viability compared to the cell only control. Data was analysed using one-way analysis of variance (ANOVA) and the MSD was calculated using the Tukey method. A statistically significant reduction ($p<0.05$) in the cell viability in comparison to the cell only control, are indicated by an asterisk (*). Error bars represented ± 95% CI levels, n = 6. (●: 50 μm^3 per cell; ▲: 5 μm^3 per cell; ▼: 0.5 μm^3 per cell; ♦: 0.05 μm^3 per cell; ◄: 0.005 μm^3 per cell; ►: 0.0005 μm^3 per cell; ●: cell only control; ★: 2 $\mu g.ml^{-1}$ camptothecin).

3.5 Discussion

The aim of this part of the study was to generate, isolate and characterise nanoscale and micron sized alumina and CoCr particles. The particles were characterised in terms of size, morphology, composition and effect on cell viability in comparison to the published literature on particles prior to them being used for cell membrane toxicity studies.

3.5.1 Isolation and characterisation of nanoscale and micron sized alumina particles

The micron sized alumina powder were characterised *via* SEM and were revealed to have a wide distribution of particle sizes, ranging from less than 20 nm up to 1464 nm. As the particle size distribution included micron sized particles and to differentiate from the nanoscale alumina particles, which had a mode particle size tenfold lower than this particle stock, this particle type was referred to as the micron sized alumina particles. The morphology of the particles was observed to be polygonal in shape. This orthopaedic powder has previously been used in the reported literature to determine the effect of the viability of fibroblasts and histiocytes and a comparable mode particle size of 0.5 µm, with polygonal shard-like morphology was previously reported. Furthermore, Hatton *et al.* (2003) reported similar findings for micron sized alumina particles isolated from the orthopaedic powder and particles isolated from joint simulator lubricant in terms of TNF-α production from PBMNCs. Therefore this particle source was deemed appropriate for further cell-based experiments.

Alumina particles isolated from periprosthetic tissue during revision surgery have a wide size distribution, ranging from a few nanometres to less than 5 µm in diameter (Hatton *et al.* 2002; Tipper *et al.* 2002). The large size range is thought to be

caused by the introduction of translational malpositioning, causing stripe wear and a bimodal particle size distribution. Indeed, Tipper *et al.* (2002) observed wear particles generated under standard gait conditions, to be 2 – 27.5 nm in diameter when visualised by TEM. However, when microseparation conditions were introduced, the particle diameter increased to 0.02 – 1 µm. Translational malpositioning has been reported to occur in all bearing types *in vivo* and is characterised by an elliptical stripe on the femoral head and on the rim of the acetabular cup of ceramic-on-ceramic THRs (Nevelos *et al.* 1999; Lombardi *et al.* 2000; Stewart *et al.* 2003; Glaser *et al.* 2008). Therefore a wide particle size distribution and in particular a bimodal particle size distribution is clinically relevant. Hence the effect of nanoscale alumina particles was also included in this investigation.

The wear rates of ceramic-on-ceramic THRs have been reported to be as low as 0.1 mm^3 per million cycles, with some simulator studies reporting no measurable wear (Nevelos *et al.* 2001; Stewart *et al.* 2003; Vassiliou *et al.* 2007; Al-Hajjar *et al.* 2010; Al-Hajjar *et al.* 2013). Due to the low wear rates and the small size of the alumina wear particles, methods to isolate ceramic particles from tissues or from serum lubricants have not been reliably successful for isolating the very small volumes of particles generated and it was not practical to attempt to recover particles from serum lubricants from hip simulator studies to use in the cell studies reported here (Hatton *et al.* 2002; Tipper *et al.* 2002). Therefore, an alternative approach was taken to sequentially filter an alumina powder used in the manufacture of ceramic THR components and supplied by the manufacturer, Ceramtec to allow the desired particle size range to be isolated. Nevertheless, the retrieval of sufficient nanoscale particles was technically very challenging, even with modifications and optimisation of the filtration method. This included using different suspension media and using filters of various pore sizes in order to capture as many nanoscale particles as possible. A large enough volume of particle could not

be isolated to complete all cell studies using this technique and instead a commercially available alumina powder was purchased and used for all subsequent experiments.

The nanoscale alumina particles from this current study were observed to have formed large aggregates with a mostly oval morphology. The mode size of the particles was measured at 30 – 39 nm; however particles up to 265 nm were measured. The majority of the particles were less than 40nm in size, representing 88% of the particles measured. As previously stated, alumina wear particles isolated from periprosthetic tissues or from simulator studies of hip prostheses have a bimodal size distribution. The nanoscale fraction of this bimodal size distribution have been reported to be less than 20 nm (Hatton *et al.* 2002; Tipper *et al.* 2002; Germain *et al.* 2003). The nanoscale alumina particles used in this study were larger at 30 – 39 nm, with a mean of 39.5 nm (± SD 26.5 nm), which did not reflect the published literature. However, the effect of the nanoscale alumina particles can be compared against the micron sized alumina particles to determine the effect of particle size on the subsequent membrane studies.

3.5.2 Generation and characterisation of nanoscale and micron sized cobalt chromium particles

Cobalt chromium nanoscale particles were generated using a six station pin-on-plate wear simulator as these conditions have been used previously in the literature for simple pin-on-plate wear studies and represent the loading and kinematic conditions of a standard gait cycle in the hip (Jin *et al.* 2000). Clinically relevant particles have also been generated from hip simulator studies, using 25% (v/v) bovine serum as the lubricant (Brown *et al.* 2007). However, the recovery of metal wear debris from serum has been reported to be difficult, as lubricant proteins and

other contaminants are challenging to remove and particle loss remains an issue (Brown *et al.* 2007; Billi *et al.* 2012a; Billi *et al.* 2012b). Furthermore, alkaline digestion methods have been reported to alter the morphology, shape, and composition of CoCr wear particles (Catelas *et al.* 2001a; Catelas *et al.* 2001b). A number of isolation methods have been developed, including by Brown *et al*. (2007) who developed a multiple step enzymatic digestion protocol. However, enzymatic digestion has been reported to affect particle size and induce aggregation (Catelas *et al.* 2001a; Lu *et al.* 2012). In addition, Billi *et al*. (2012b) developed an isolation method, which deposits the particles onto a silicon wafer using ultracentrifugation methods. However, the removal of the wear particles from the wafer remains problematic. Therefore, the use of a simplified pin-on-plate wear simulator was chosen, as sufficient wear volumes of clinically relevant CoCr debris can be produced within a short timeframe. Furthermore, water was used as the lubricant, which can be removed by evaporation (190°C for 4 hours), leaving behind sterile and endotoxin-free particles (Germain *et al.* 2003; Brown *et al.* 2006; Papageorgiou *et al.* 2007; Brown *et al.* 2013).

The CoCr particles were observed to have a mode size of 40 – 49 nm. The particles were round in morphology with occasional shard-like particles. The particle mode size was similar to the reported literature for CoCr wear particles isolated from periprosthetic tissues. Doorn *et al*. (1998) isolated CoCr wear particles from periprosthetic tissues of 13 patients undergoing revision surgery of Morris hip prostheses. The median of the particle sizes from each of the samples ranged from 51 to 116 nm, with an average of 81 nm. The particles were also observed to be round in morphology, with some shard-like particles. Simulator studies have reported CoCr wear particles to be slightly smaller, with a mean size of less than 40 nm, with no shard-like particles detected (Firkins *et al.* 2001b; Brown *et al.* 2007; Papageorgiou *et al.* 2007). One possible explanation for this is the use of wrought or cast CoCr components in the wear studies, which have been demonstrated to

have varying wear rates (Dowson *et al.* 2004a). Whilst no shard-like particles were detected in these studies, they have been detected in *ex vivo* tissue studies from hip resurfacing implants (Xia *et al.* 2011; Goode *et al.* 2012).

The composition of CoCr particles was confirmed using pin-point EDX analysis, and cobalt and chromium was detected in the spectrum of the nanoscale CoCr particles. Wear particles generated from well positioned metal-on-metal THRs have been reported to be comprised of oxidised chromium with little or no cobalt detected (Madl *et al.* 2015). Under normal physiological conditions a passive layer of oxidised chromium is formed. In stimulator studies, using serum lubricant, this passive layer is 85 nm thick, whereas using water as the lubricant, the passive layer is 3 – 3.5 nm thick (Madl *et al.* 2015). Therefore, *in vivo* and under optimal conditions, the wear particles generated are from the passive layer and it is the oxidised chromium which will interact with the cells. Whilst the passive layer is not as thick in simulator studies using water as the lubricant, the wear particles still consist of oxidised chromium, but to a lesser extent (Madl *et al.* 2015). It is assumed that the nanoscale CoCr particles generated in this current study consisted of oxidised chromium. However, further investigation would be required to confirm this.

Molybdenum makes up 5 – 7% of the overall composition of the bulk alloy, however, it was rarely detected in any of the samples in this study. Molybdenum was only detected the EDX spectra of the micron sized CoCr particles. Goode *et al.* (2012) also failed to detect molybdenum in CoCr particles isolated from periprosthetic tissues. The detection of low concentrations of elements *via* EDX analysis can cause small peaks within the spectrum to be masked by background emissions, thus reducing the level of detection (Bell and Garratt-Reed, 2003). Two different EDX analysers were used to detect the nanoscale and micron sized CoCr

particles and therefore this may have been a cause for the differences in the spectra.

The mode particle size of the micron sized CoCr particles was measured at 2 – 3 µm, with a mean particle size of 3.26 µm (± SD 1.30 µm). The particles were round in shape and had a composition similar to the nanoscale CoCr particles generated by the wear simulator, with the majority of the particle consisting of cobalt. This particle stock has been previously characterised in the literature and have been reported to have a mean particle size of 2.97 µm with a round morphology (Papageorgiou *et al.* 2007).

3.5.3 Effect on cell viability of nanoscale and micron sized alumina and CoCr particles on primary human fibroblasts and histiocytes

The cell viability of primary HFBs and a U937 human histiocyte cell line in the presence of nanoscale and micron sized alumina and CoCr particles was investigated using the MTT and ATPlite assay. The ATPlite assay is highly sensitive and can measure ATP levels in as few as ten cells. Upon cell death, a reduction in cellular ATP occurs, and this can be used as an indicator of cytotoxicity (Crouch *et al.* 1993). The MTT assay measures the reduction of a yellow tetrazole to a purple formazan by NAD(P)H-dependent oxidoreductase enzymes and can be used as an indicator of cell metabolism. Cells which are viable will reduce the tetrazole substrate more rapidly than cells with reduced metabolism or non-viable cells. However, the reduction of the tetrazole substrate can be affected if the cells are subjected to oxidative stress (Stockert *et al.* 2012). The effect of the particles on the cell viability was compared against the relevant published literature.

3.5.3.1 Assay choice and particle interference

An additional control was also included in both assays for all particle types, which measured the potential interference of the particles with the results. Previous studies have revealed that the highly reactive surface of nanoparticles can interfere with biochemical assays and induce false negative or false positive results. Therefore, it is now common practice within the field of nanotoxicology to use to different cell assays in order to determine a greater understanding of the particles on the cells (Monteiro-Riviere *et al.* 2009). To investigate the potential effect of alumina and CoCr particles on the ATPlite and MTT assay, the highest particle volume (500 μm^3 per cell and 50 μm^3 per cell, respectively) were incubated in cell culture medium in the absence of cells. The readouts were subtracted from the absorbance or luminescence readings for the cells cultured in the presence of the corresponding highest particle volume.

During this study it was noted that the nanoscale and micron sized alumina particles, at the highest particle volumes, had a positive effect on the absorbance readings of the MTT assay. However not all of the reported literature has taken the impact of particle interference with cell viability assays into consideration. Indeed, Roualdes *et al.* (2010) and Dalal *et al.* (2012) both stated that alumina particles tested had a significantly positive effect on the cell viability at high particle concentrations. However, these findings are likely to be caused by the particles inducing a higher than expected assay readout rather than the particles effecting cell viability. An extreme example was noted by Granchi *et al.* (2004) whereby the alumina particles interfered with the alamar blue assay performed and the results for highest particle concentrations of 0.1 and 1 $mg.ml^{-1}$ had to be disregarded.

Unlike the nanoparticles and micron sized alumina particles, no detrimental effect was observed for the CoCr particle only control for both assays. However, Dalal *et al.* (2012) and Papageorgiou *et al.* (2007) noted that CoCr wear particles

significantly increased cell viability using an LDH assay at high particle concentrations. Nevertheless, it was not apparent whether particle only controls was used and whether these results reflected the actual effects of the particle on the cells. Therefore the approach of this study was to use two assays in conjunction with two different cell types in order to gain a better understanding on the effects of the particles.

3.5.3.2 The effect of nanoscale and micron sized alumina particles on U937 histiocytes and human fibroblasts using the ATPlite and MTT assay

The results from this study demonstrated that nanoscale and micron sized alumina particles had a limited effect on the cell viability for both U937 histiocytes and primary HFBs. No significant effects were observed for the nanoscale and micron sized alumina particles on the U937 histiocytes and primary HFBs using both the ATPlite and MTT assay. Only the nanoscale alumina particles had a statistically significant effect on the U937 histiocyte viability at the highest particle volume of 500 μm^3 per cell after 3 days of culture when assessed using the MTT assay. In contrast, significant effects of micron sized alumina particles on viability were observed for the primary HFBs at particle volumes of 50 and 500 μm^3 per cell, after one day of culture, when assessed using the MTT assay. The ATPlite assay measure ATP levels in cells, whereby viable cells will have a greater ATP concentration. The MTT assay is a measure of cell metabolism and detects the reduction of MTT by NAD(P)H-dependent oxidoreductase enzymes. As previously described, the reduction of the tetrazole substrate is greater in viable, metabolising cells in comparison to cells with a reduced metabolism. Hence, the decrease in formazan formation can be caused by a reduction in cell metabolism rather than cell number and is why the MTT assay is not a direct measure of cell proliferation. In addition to this, a reduction in the tetrazole substrate can occur when the cells are

subjected to oxidative stress. Therefore the differences in the ATPlite and MTT assay results may be caused other factors rather than just a reduction in cell number. Without further investigation it is difficult to ascertain the exact cause, however the results highlight the need to use more than one assay to gain a better understanding of particle toxicity.

At present there is limited published literature on the cytotoxic effects of clinically relevant alumina wear particles. From the data available, a number of these studies did not use clinically relevant particles, making direct comparisons to the literature difficult (Yoshida *et al.* 2003; Granchi *et al.* 2004; Gutwein and Webster 2004; Yamamoto *et al.* 2004). However, Germain *et al.* (2003) and Hatton *et al.* (2003) used alumina wear particles from ceramic-on-ceramic hip joint simulators, and compared the effects with particles isolated from the same orthopaedic powder used in this current study. Hatton *et al.* (2003) reported that both particle sources had no significant effect on the cell viability of PBMNCs after 24 hours using the MTT assay. Germain *et al.* (2003) also reported a limited effect of the alumina particles on U937 histiocytes and L929 murine fibroblasts over 5 days using the ATPlite assay. The only significant reduction in the cell viability was observed for the predominately nanoscale (5 – 30 nm) alumina particles isolated from the hip joint simulator after three days of culture with U937 histiocytes at a particle volume of 50 μm^3 per cell. However, the current study did not observe any significant effect on cell viability of U937 histiocytes incubated with the alumina nanoscale particles at the same particle volumes. This small discrepancy between the current study and results from Germain *et al.* (2003) could be caused by the differences in the particle source, leading to small differences in the particles size and composition. Interestingly Germain *et al.* (2003) also observed that differences in the effect of alumina particles were dependent on the cell type as no significant reduction in cell viability was observed for the L929 fibroblasts cultured in the presence of alumina wear particles.

Studies using commercially available alumina particles have also reported the effect of alumina particles on the viability of a number of cell types, with most studies only reporting cytotoxic effects at high particle concentrations (Catelas *et al.* 1999; Germain *et al.* 2003; Hatton *et al.* 2003; Granchi *et al.* 2004; Gutwein and Webster 2004; Dalal *et al.* 2012). However, there are inconsistencies in the literature with respect to the effect of alumina particle size on cell viability. The present study revealed that minor differences between the cytotoxicity of the nanoscale and micron sized alumina particles was dependent on cell type and assay choice. Germain *et al*. (2003) also noted a moderate difference between nanoscale and micron sized alumina particles with an 18% reduction in U937 histiocyte viability after 3 days. In contrast, Catelas *et al.* (1999) and Gutwein & Webster (2004) reported an increase in cell death with increasing particle size. This could be caused by different cell types used or alternatively the methods employed. The interference of the particles with the assays used or the presence of endotoxins could have impacted the results. Unfortunately neither Catelas *et al.* (1999) and Gutwein & Webster (2004) state if appropriate particle controls nor methods to remove endotoxins from the particles were used and therefore it is not known if these affected the outcomes of the studies.

Overall the results from this present study suggest that the nanoscale and micron sized alumina particles are significantly cytotoxic at high particle doses. However, as previously described the low wear rates of ceramic-on-ceramic THRs mean that the likelihood of cells in periprosthetic tissues encountering these particle doses is rare. Indeed the incidences of any biological adverse tissue reactions, such as osteolysis have only been described in extreme cases (Morlock *et al.* 2001; Jarrett *et al.* 2009; D'Antonio *et al.* 2012). These incidences were attributed to severe malpositioning of the implant or mismatching of the femoral head and acetabular cup component. Therefore it can be concluded that alumina based ceramic particles are relatively bioinert.

3.5.3.3 The effect of nanoscale and micron sized cobalt chromium particles on U937 histiocytes and human fibroblasts using the ATPlite and MTT assay

The results from this study revealed that nanoscale and micron sized CoCr particles induced a significant reduction in U937 histiocytes and human fibroblast viability in a time- and dose-dependent manner. The nanoscale CoCr particles significantly reduced the viability at the particle volumes of 50 μm^3 per cell or greater for both U937 histiocytes and primary HFBs using the ATPlite assay. The highest particle volume of 500 μm^3 per cell had a significant effect on the viability of U937 histiocytes after one day when assessed using the MTT assay. The greatest effect on cell viability was measured for the primary HFBs cultured with the nanoscale CoCr particles. A significant reduction in the cell viability was measured, using the MTT assay, for particle volumes of 0.5, 5 and 50 μm^3 per cell after three days in culture. Whilst the general trend between the two assays was similar, small differences between the assays and cell types were observed, suggesting CoCr cytotoxicity is sensitive to the assay and cell type used. In particular differences in the response of cell lines in comparison to primary cells have been reported (Geraghty *et al.* 2014). For instance immortalised endothelial cell lines have been demonstrated to express different cell markers and receptors in comparison to primary cells (Unger *et al.* 2002). Immortalised cell lines have been reported to lose the characteristics of the original tissue they were isolated from and to be susceptible to genetic drift and contamination as they divide (Geraghty *et al.* 2014). Therefore the greater responses of the HFBs in comparison to the U937 cell line, in the presence of alumina and CoCr particles, may be caused by this.

Studies using the same pin-on-plate simulator method to generate CoCr particles reported very similar results to this current study (Germain *et al.* 2003; Brown *et al.* 2006; Papageorgiou *et al.* 2007; Bhabra *et al.* 2009; Papageorgiou *et al.* 2014). Indeed some of these studies have used cell types also employed in this present

study. Papageorgiou *et al.* (2007) observed a significant reduction in human fibroblast viability after 1 day using the MTT assay. Furthermore, Germain *et al.* (2003) reported that nanoscale CoCr wear particles at a particle volume of 50 μm^3 per cell reduced U937 histiocyte and L929 fibroblast cell viability in comparison to the cell only control after 5 days. This was also observed in this current study at the equivalent particle volumes after 5 days of culture with U937 histiocytes using both the MTT and ATPlite assay.

Particle size was observed to affect cell viability of U937 histiocytes and primary HFBs. The micron sized CoCr particles had no effect on the viability of U937 histiocytes and primary HFBs when assessed using the ATPlite assay. In contrast, the MTT assay revealed that the highest particle volume dose of 50 μm^3 per cell reduced the viability of primary HFBs in comparison to the cell only control after 1 day. Similarly, a significant effect on the viability was measured for U937 histiocytes cultured with micron sized CoCr particles at a particle volume of 50 μm^3 per cell after five days using the MTT assay. Germain *et al*. (2003) also reported micron sized CoCr wear particles (9.87 µm) were observed not to be cytotoxic to U937 histiocytes and L929 fibroblasts. Papageorgiou *et al.* (2007) reported that micron sized CoCr particles, also sourced from the same manufacturer as the particles used in the present study, were less cytotoxic than nanoscale CoCr wear particles (29.5 ± 6.3 nm) in primary HFBs. A significant reduction in the cell viability was only observed after 4 days of culture.

A limitation of the cell viability assays is that the effect of Co and Cr ions was not separately investigated. Ions are known to be released from the bearing surface and have been reported to be cytotoxic, even at physiologically relevant levels (Andrews *et al.* 2011; Posada *et al.* 2014). However the current study only investigated CoCr particles and the subsequent release of the ions over the time the particles are cultured with the cells. Therefore it cannot be determined if the

reduction in cell viability was caused by the particles, the release of ions into the surrounding culture medium, or a combination of both.

3.6 Conclusion

This part of the study aimed to generate, isolate and characterise alumina and nanoscale and micron sized CoCr particles. The nanoscale CoCr particles were revealed to be comparable to particles isolated from hip simulator studies and periprosthetic tissues from around hip prostheses in terms of size, morphology and composition. Furthermore the micron sized CoCr particles, used to investigate the role of particle size, were demonstrated to have a similar composition to the CoCr alloy used in THR manufacture. Alumina particles from THRs have been reported to have a bimodal size distribution and therefore nanoscale and micron sized alumina particles were obtained for the present study. Unfortunately the nanoscale particle fraction could not be successfully isolated from an alumina powder and a commercially available nanoscale alumina powder was used instead. The commercially available nanoscale alumina particles were larger in size in comparison to the published literature on wear particles. Nevertheless, the effect of particle size on the cell membrane can still be determined in the following chapters, which is an important factor in particle toxicity (as described in section 1.5.3.1.1).

The biocompatibility of the particles was determined by investigating the effect of the particles on the viability of U937 histiocytes and primary HFBs. The particles were revealed to have a similar effect to previous reports in the literature with nanoscale CoCr particles reducing the cell viability to a greater extent than the micron sized CoCr particles. Furthermore, the nanoscale and micron sized alumina particles only induced a statistically significant reduction in the viability of primary HFB and U937 histiocytes at very high particle doses, which was dependent on cell

type and viability assay used. Interestingly, due to the low wear rates of ceramic-on-ceramic THRs, this is unlikely to occur in a clinical situation.

The nanoscale and micron sized alumina and CoCr particles have been characterised in terms of particle size, morphology and cytotoxicity and with the exception of the nanoscale alumina particles, are comparable with results from the literature. All four particle types were deemed suitable for use in the cell membrane toxicity experiments in the subsequent sections of this study.

Chapter 4

The effect of nanoscale and micron sized alumina and cobalt chromium particles on the cell plasma membrane

4.1 Introduction

A variety of techniques have been used to investigate the role of particles on the cell plasma membrane within the field of nanotoxicology. These include the use of SPR, vesicle leakage studies and QCM-D (Green *et al.* 2000; Mu *et al.* 2012b; Karlsson *et al.* 2013). As described in Chapter one, the sensitivity of QCM-D allows potential factors affecting particle and model membrane interactions to be investigated, including particle morphology, size and composition (Mu *et al.* 2012a; Mu *et al.* 2014). The model membrane can also be tailored to each experiment and proteins can be incorporated into the membrane to investigate particle: protein interactions (Lesniak *et al.* 2013). QCM-D can be used to investigate the effect of nanoscale and micron sized alumina and CoCr particles with model membranes and to provide an insight into cellular uptake mechanisms of the particles, such as whether the particles bind non-specifically to the membrane or are receptor mediated.

4.1.1 Aims and objectives

This part of the study aimed to investigate the effect of nanoscale and micron sized alumina and CoCr particles on a model lipid membrane using vesicle leakage, QCM-D and SPR techniques. Furthermore, the effect of size and composition of the particles were investigated by comparing the outcomes for nanoscale and micron sized alumina and CoCr particles (previously characterised in Chapter three). In this first instance, a simple model membrane consisting of extracted phosphocholine, phosphoserine, and phosphoethanolamine, with cholesterol has been used, which

is similar to the lipid composition of plasma membranes of human fibroblast cells. Finally the incorporation of membrane proteins from primary HFBs into the model lipid membrane was also implemented. This was to determine more accurately the factors involved in particle: membrane interactions.

4.1.1.1 Objectives

The specific objectives of this part of the study were as follows and outlined in Figure 4.1:

- To assess the effect of nanoscale and micron sized alumina and CoCr particles on simple model membranes using vesicle leakage assays
- To investigate the binding of nanoscale and micron sized alumina and CoCr particles to a simple sBLM using QCM-D
- To model QCM-D data to ascertain if nanoscale and micron sized alumina and CoCr particles bind to a sBLM using the Voight model
- To investigate the binding of nanoscale and micron sized alumina and CoCr particles to a model membrane using surface plasmon resonance techniques
- To explore the effect of incorporating fibroblast and histiocyte membrane proteins into the sBLM on nanoscale and micron sized alumina and CoCr particle induced membrane damage
- To study the effect of incorporating of fibroblast membrane proteins into the sBLM on nanoscale and micron sized alumina and CoCr particle binding to the model membrane

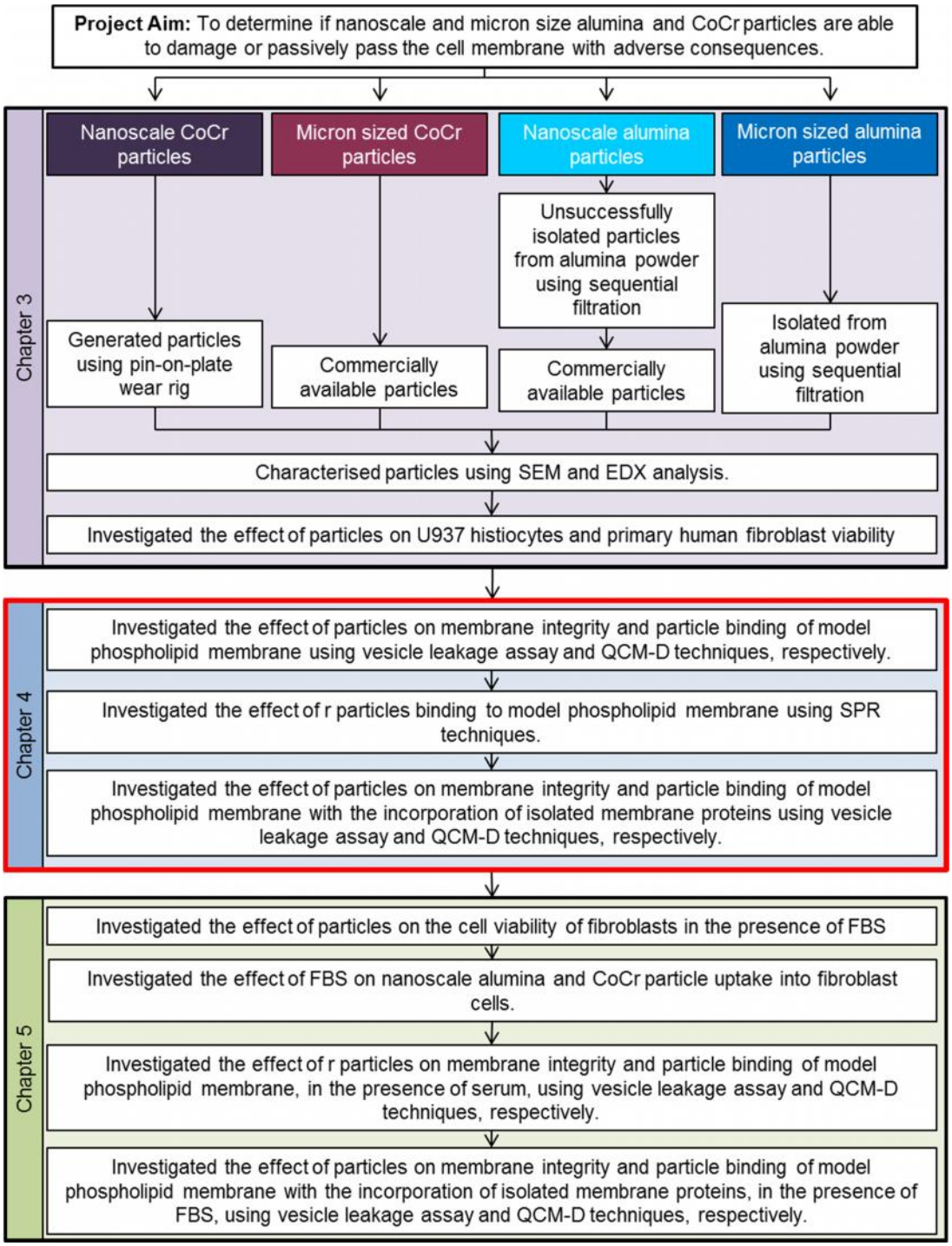

Figure 4.1 – Overall project aim and experimental work. Chapter four aims are outlined in red.

4.2 Material and methods

4.2.1 Materials

4.2.1.1 Surface plasmon resonance analysis

The materials used for the SPR analysis are listed in Table 4.1.

Table 4.1 – Materials used for surface plasmon resonance analysis

Material	Model	Supplier
Biacore® SPR machine	2000	GE Healthcare Life Sciences, Buckinghamshire, U.K.
BIAdesorb solution 1 (0.5% w/v SDS)	193606	GE Healthcare Life Sciences, Buckinghamshire, U.K.
BIAdesorb solution 2 (50 mM glycine, pH 9.5)	193607	GE Healthcare Life Sciences, Buckinghamshire, U.K.
BIAdisinfectant solution (sodium hypochlorite)	BR100666	GE Healthcare Life Sciences, Buckinghamshire, U.K.
BIAevaluation computer software	Version 3.1	GE Healthcare Life Sciences, Buckinghamshire, U.K.
HPA sensor chip consisting of alkane thiol molecules attached to a gold film.	BR100406	GE Healthcare Life Sciences, Buckinghamshire, U.K.
Octeyl glucoside	29836-26-8	Melford Laboratories Ltd., Ipswich, U.K.

4.2.2 Methods

4.2.2.1 Investigation into the effect of particles in membrane integrity using a simple vesicle leakage assay

The materials and methods for the simple vesicle leakage assay are outlined in section 2.2.6.3.

4.2.2.2 Investigation into the binding of particles using quartz crystal microbalance with dissipation

The method for using QCM-D is outlined in section 2.2.6.4.

4.2.2.3 Surface plasmon resonance analysis of nanoscale cobalt chromium particles binding to a model lipid membrane

Using the nanoscale CoCr particles as an example, the binding of the particles to a monolayer of the model lipid membrane was investigated.

4.2.2.3.1 Desorbing and sanitising the surface plasmon resonance machine

The Biacore® 2000 SPR machine was kept on standby and the machine tubing was cleaned thoroughly prior to testing. All reagents were degassed under vacuum and filtered through a 0.22 µm pore size filter. The running buffer of the machine was replaced with degassed ultrapure distilled water. Using the BIAevaluation (version 3.1) computer programme, the machine command “desorb” was selected and the chip in the machine was removed and replaced with a standard sensor chip, whilst the tubing was cleaned. Once docked, the chip and tubing was primed using degassed ultrapure distilled water. A volume of 3 ml of each of the BIAdesorb solutions 1 (0.5% w/v SDS) and 2 (50 mM glycine, pH 9.5) were placed

in glass vials and placed on the sample rack of the SPR machine. The position of the samples was entered into the computer programme and the desorb process was initiated, whereby solutions 1 and 2 were flowed through the machine tubing. Once the desorb process was completed, the Biacore machine went into standby mode. Approximately 10 ml of the BIAdisinfectant solution (sodium hypochlorite) was placed in a measuring cylinder and placed onto the sample rack of the SPR machine. The sanitise function was selected on the computer programme which flowed the disinfectant solution though the tubing of the machine. Once completed the resting buffer was changed to ultrapure distilled water and placed on standby for approximately 18 hours.

4.2.2.3.2 The formation of a monolayer of a model lipid membrane onto the sensor chip

The sensor chip within the machine was replaced with the test HPA chip (Table 4.1), which was docked into the machine and primed using the running solution (20 mM MOPS with 30 mM Na_2SO_4, pH 7.4). Once primed, the sensorgram, which measured resonance units (RU), was run until the readout had settled (approximately 1 hour). A 5 minute injection of 40 mM octyl glucoside in ultrapure distilled water was used to wash the surface of the chip, followed by rinsing with the running solution of 20 mM MOPS with 30 mM Na_2SO_4, pH 7.4. The lipid vesicles (prepared as described in section 2.2.6.2) at a final concentration of 0.5 mM in 20 mM MOPS with 30 mM Na_2SO_4 and 10 mM $CaCl_2$, pH7.4 were injected across the sensors of the chip at a rate of 5 µl per minute for at least 3 hours or until the readout had stabilised. The monolayer of the model lipid membrane was washed with three 5 minute injections of ultrapure distilled water with 1 mM EDTA to remove any unbound vesicles.

4.2.2.3.3 The addition of nanoscale cobalt chromium particles to the model lipid membrane

The running solution of 20 mM MOPS with 30 mM Na_2SO_4, pH 7.4 was changed to DMEM without any supplements. Once the readout had settled, a blank control of the equivalent volume of ultrapure water in DMEM of the highest particle concentration was injected across the sensor chip at a flow rate of 5 µl per minute for 30 minutes. DMEM were then flowed across the chip for another 30 minutes at a flow rate of 5 µl per minute. Nanoscale CoCr particles, at a concentration of 100 $\mu g.ml^{-1}$ in DMEM was flowed across the chip for 30 minutes at a flow rate of 5 µl per minute. DMEM was then flowed across the chip for 30 minutes at a flow rate of 5 µl per minute. Once completed, the chip was either placed on standby or cleaned according to section 4.2.2.3.1. The experiment was repeated twice.

4.3 Results

4.3.1 The effect of nanoscale and micron sized alumina and cobalt chromium particles on the integrity of a model lipid membrane using a simple vesicle leakage assay

In order to assess the effects of nanoscale and micron sized alumina and CoCr particles on plasma membrane integrity, a simple vesicle leakage assay was used as described in section 2.2.6.2 and 2.2.6.3.

4.3.1.1 The effect of nanoscale and micron sized alumina particles on the integrity of a model lipid membrane

Nanoscale and micron sized alumina particles induced vesicle leakage in a dose dependent manner as presented in Figure 4.2A and 4.2B, respectively. However, at the particle concentration of 1 $\mu g.ml^{-1}$, the mean vesicle leakage was barely above the baseline for both nanoscale and micron sized alumina particles. At the highest particle concentration of 100 $\mu g.ml^{-1}$, the nanoscale alumina particles caused an average 16% increase in vesicle leakage, which was statistically significant in comparison to the particle concentration of 1 $\mu g.ml^{-1}$. The nanoscale alumina particles, at a particle concentration of 10 $\mu g.ml^{-1}$ also induced statistically significant vesicle leakage in comparison to the lowest particle concentration of 1 $\mu g.ml^{-1}$. Significant increases of 3% and 20% in vesicle leakage were observed for micron sized alumina particles compared to the baseline at particle concentrations of 10 and 100 $\mu g.ml^{-1}$, respectively. These results were statistically significant in comparison to the lowest particle concentration of 1 $\mu g.ml^{-1}$.

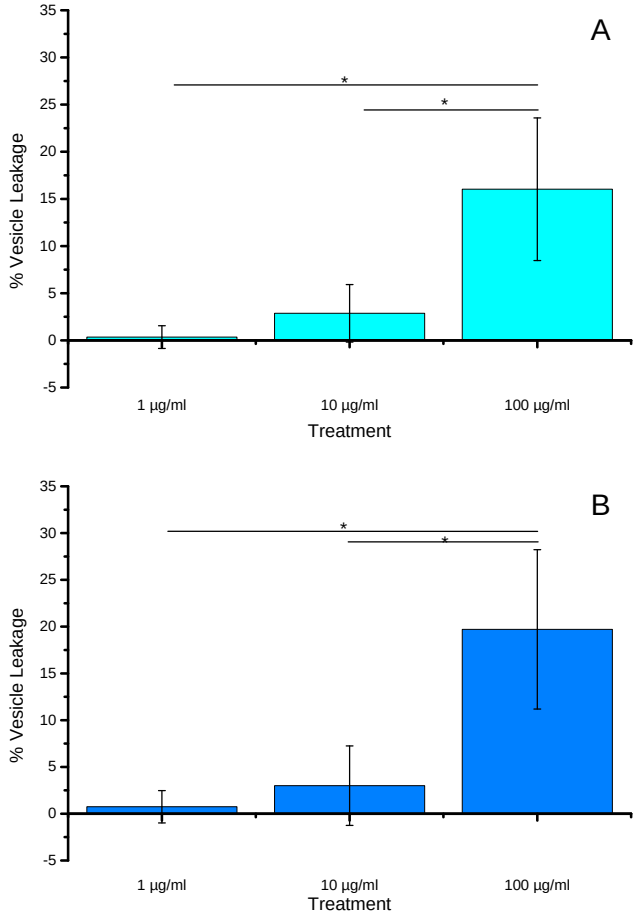

Figure 4.2 – The effect of nanoscale (A) and micron sized (B) alumina particles on the vesicle leakage of a model lipid membrane. Vesicles loaded with an autoquenching fluorescent dye were formed from lipid membranes and exposed to increasing concentrations (1 – 100 µg.ml^{-1}) of nanoscale or micron sized alumina particles. The release of fluorescent dye was measured, in real-time, using a fluorometer. Afterwards, Triton-X 100 (0.1% v/v) was added to samples to ensure complete vesicle lysis. Vesicle leakage was expressed as a percentage of the absorbance reading for the detergent Triton-X 100 sample. Raw data were analysed using paired t-test and statistically significant results ($p < 0.05$) are indicated by an asterisk (*). Error bars represented 95% confidence levels (n = 3).

4.3.1.2 The effect of nanoscale and micron sized cobalt chromium particles on the integrity of a model lipid membrane

The effect of nanoscale and micron sized CoCr particles on the fluorescent dye encapsulated vesicles was also investigated as described in section 2.2.6.3. Both nanoscale and micron sized CoCr particles also induced a dose dependent

increase in vesicle leakage. However the percentage leakage was much less than the results measured for the nanoscale and micron sized alumina particles. Even at the highest particle concentration of 100 $\mu g.ml^{-1}$, the nanoscale CoCr particles only marginally induced vesicle leakage of 4%, in comparison to the baseline levels (Figure 4.3A). Nevertheless this result was statistically significant in comparison to the lowest particle concentration of 1 $\mu g.ml^{-1}$, which only induced a 0.3% increase in the vesicle leakage. Similarly, the micron sized CoCr particles only induced 3% vesicle leakage at the highest particle concentration of 100 $\mu g.ml^{-1}$, however due to increased sample variability, this was not statistically significant in comparison to the lowest particle concentration (Figure 4.3B).

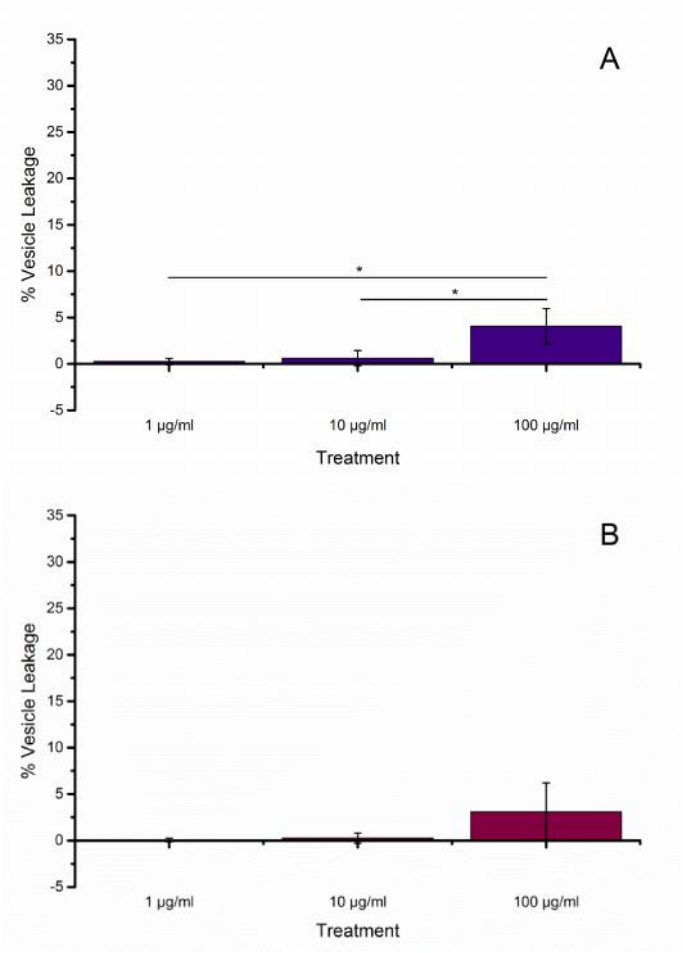

Figure 4.3 – The effect of nanoscale (A) and micron sized (B) cobalt chromium particles on the vesicle leakage of a model lipid membrane. Vesicles loaded with an autoquenching fluorescent dye were formed from lipid membranes and exposed to increasing concentrations (1 – 100 µg.ml^{-1}) of nanoscale or micron sized CoCr particles. The release of fluorescent dye was measured, in real-time, using a fluorometer. Afterwards, Triton-X 100 (0.1% v/v) was added to samples to ensure complete vesicle lysis. Vesicle leakage was expressed as a percentage of the absorbance reading for the Triton-X 100 sample. Raw data were analysed using paired t-test and statistically significant results ($p < 0.05$) are indicated by an asterisk (*). Error bars represented 95% confidence levels (n = 3).

4.3.1.3 Investigation into the potential quenching effects of nanoscale and micron sized alumina and cobalt chromium particles on the vesicle leakage assay

The potential for nanoparticles to quench light emitting assays has been extensively reported (Raikar *et al.* 2011). This may have an effect on the results obtained for

the vesicle leakage assays and must be investigated. To assess whether the nanoscale and micron sized alumina and CoCr particles could quench the excitation wavelength from the fluorescent dye, the vesicles, which encapsulated an autoquenching fluorescent dye, were formed as stated in section 2.2.6.3.3.

4.3.1.3.1 Quenching effects of nanoscale and micron sized alumina particles on the vesicle leakage assay

No overall quenching of the fluorescent dye was observed for the vesicles incubated with nanoscale alumina particles as shown in Figure 4.4A. Indeed a marginally positive effect (106% leakage) was observed, in comparison to the Triton-X 100 control for the highest particle concentration of 100 $\mu g.ml^{-1}$. This result was considered statistically significant in comparison to the lowest particle concentration of 1 $\mu g.ml^{-1}$. Again no overall quenching of the fluorescence dye was observed for the vesicles incubated with micron sized alumina particles (Figure 4.4B). At all the particle concentrations tested, the mean vesicle leakage was close to 100%.

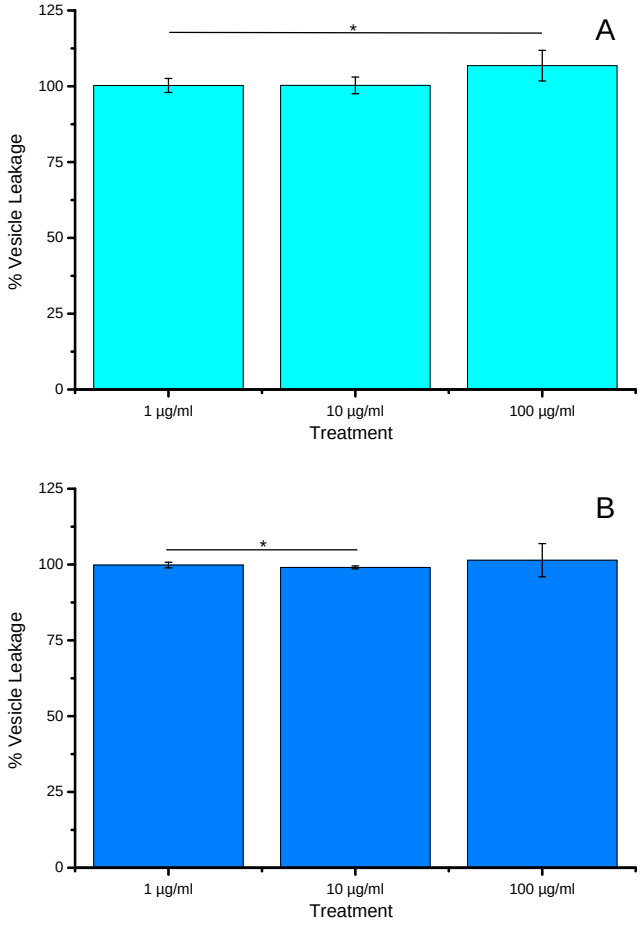

Figure 4.4 – The effect of nanoscale (A) and micron size (B) alumina particles on the quenching of the fluorescent dye. Vesicles loaded with an autoquenching fluorescent dye were formed from lipid membranes. The vesicles were then lysed with Triton-X 100 followed by the addition of increasing alumina particle concentrations (1 – 100 µg.ml^{-1}). The release of fluorescent dye was measured in real-time, using a fluorometer and vesicle leakage was expressed as a percentage of the detergent Triton-X 100. Raw data were analysed using paired t-test and statistically significant results ($p < 0.05$) are indicated by an asterisk (*). Error bars represented 95% confidence levels (n = 3).

4.3.1.3.2 Quenching effects of nanoscale and micron sized cobalt chromium particles on the vesicle leakage assay

The nanoscale CoCr particles induced a quenching effect on the fluorescent dye. The highest particle concentration of 100 µg.ml^{-1} induced a 17% reduction in the absorbance readings. This was significantly larger than the quenching effects of the particle concentrations of 1 and 10 µg.ml^{-1} (Figure 4.5A). No quenching effect was

observed for the micron sized CoCr particles at all the particle concentrations tested (Figure 4.5B). The highest particle concentration of 100 µg.ml^{-1}, with a mean vesicle leakage of 104% was significantly higher than the lowest particle concentration of 1 µg.ml^{-1} with a mean vesicle leakage of 100%.

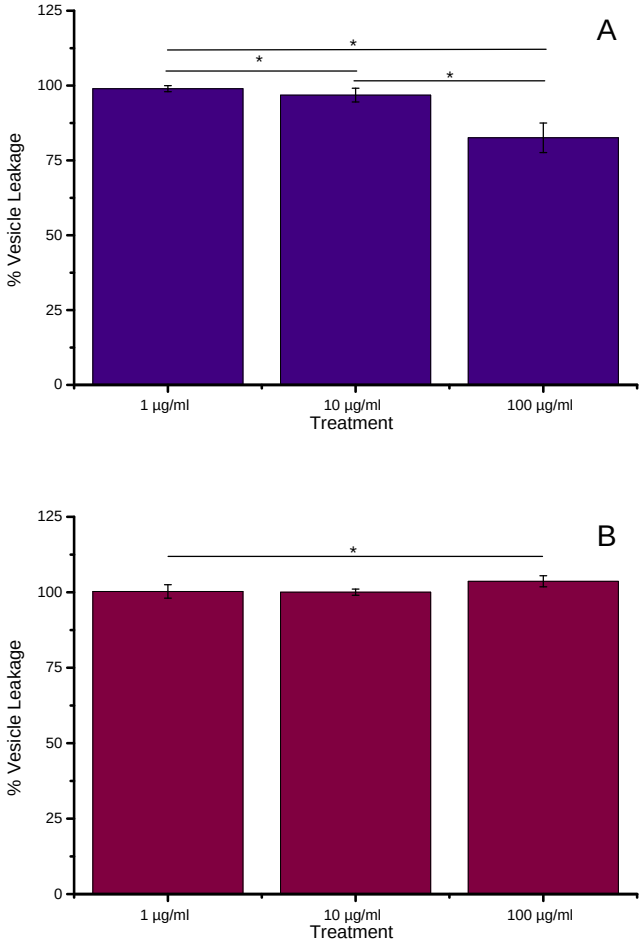

Figure 4.5 – The effect of nanoscale (A) and micron sized (B) cobalt chromium particles on the quenching of the fluorescent dye. Vesicles loaded with an autoquenching fluorescent dye were formed from lipid membranes. The vesicles were then lysed with Triton-X 100 followed by the addition of increasing CoCr particle concentrations (1 – 100 µg.ml^{-1}). The release of fluorescent dye was measured in real-time, using a fluorometer and vesicle leakage was expressed as a percentage of the detergent Triton-X 100. Raw data were analysed using paired t-test and statistically significant results ($p < 0.05$) are indicated by an asterisk (*). Error bars represented 95% confidence levels (n = 3).

4.3.2 Investigation into the binding of nanoscale and micron sized alumina and cobalt chromium particles to a model lipid membrane using quartz crystal microbalance with dissipation

In order to investigate the mechanism of particle internalisation, the ability of the nanoscale and micron sized alumina and CoCr particles to bind to the cell plasma membrane was assessed. In this series of experiments, the model lipid membrane described in section 2.2.6.1 was used, which mimics the lipid and cholesterol composition of a typical human fibroblast plasma membrane. To measure particle binding, the technique QCM-D was used.

4.3.2.1 The interaction of nanoscale and micron sized alumina particles on a model lipid membrane

A planar sBLM was established on the surface of the oscillating quartz crystal for both the nanoscale and micron sized alumina particles as observed in Figures 4.6A and 4.6B, respectively. No change in the frequency and dissipation was observed when the nanoscale alumina particles were flowed across the membrane at particle concentrations of 1 and 10 $\mu g.ml^{-1}$. However, at the highest particle concentration of 100 $\mu g.ml^{-1}$ there was a slight increase in the frequency. Most notable was the change in dissipation at the highest particle concentration of 100 $\mu g.ml^{-1}$. This effect stabilised when the membrane was washed with DMEM, although the change in dissipation was not reversed.

The micron sized alumina particles had an effect on both the frequency and dissipation change. The lowest particle concentration of 1 $\mu g.ml^{-1}$ had no effect on the frequency or dissipation, but when the next highest concentration of 10 $\mu g.ml^{-1}$ was added, a minor decrease in the frequency change of 1 Hz was observed.

Alongside this, the dissipation also increased from 0 to 1.5 x 10^{-6}. At the highest particle concentration, a minor change in the frequency was observed with a decrease of 3 Hz. Again, the largest effect was measured for the dissipation with an increase to approximately 8 x 10^{-6} at the highest particle concentration. The particle induced effects on both the frequency and dissipation stabilised upon the addition of the DMEM washes.

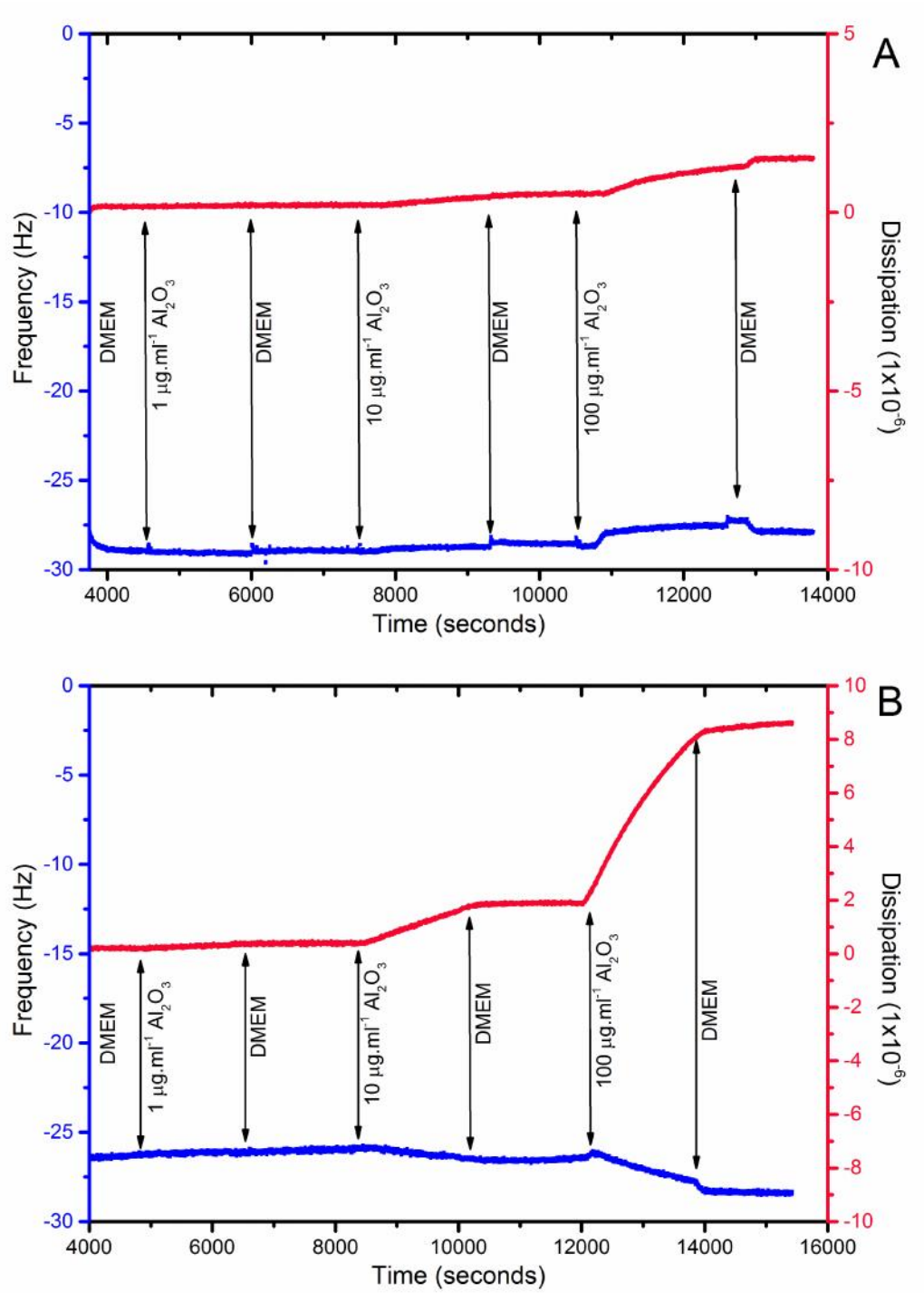

Figure 4.6 – Quartz crystal microbalance with dissipation plot of a solid supported bilayer lipid membrane in the presence of nanoscale (A) and micron sized (B) alumina particles. A sBLM formed from model lipid vesicles was generated onto an oscillating quartz crystal (not shown), resulting in a Δf of -27Hz and a Δd of < 0.5 x 10^{-6}. Commencing in DMEM, incremental concentrations (1 – 100 µg.ml^{-1}) of alumina particles followed by DMEM washes were added at times indicated by the arrows. Changes in the frequency (blue) and dissipation (red) were measured (the ninth overtone is displayed). Each experiment was repeated twice.

4.3.2.2 The interaction of nanoscale and micron sized cobalt chromium particles on a model lipid membrane

The ability of nanoscale and micron sized CoCr particles to bind to a model lipid membrane was assessed using QCM-D techniques (Figures 4.7A and 4.7B, respectively). For both series of experiments, a planar sBLM was formed on the surface of the oscillating quartz crystal with the characteristic frequency change of -27 Hz and a dissipation of approximately 0.

The nanoscale CoCr particles did not have an effect on the change in frequency and dissipation until the highest particle concentration of 100 $\mu g.ml^{-1}$ was added. Upon the addition of 100 $\mu g.ml^{-1}$ of CoCr particles a small change in the frequency was observed from -27 Hz to -26 Hz. The greatest effect was observed for the dissipation with a change from 0 to 2 $x10^{-6}$, which stabilised upon the addition of DMEM. These results were similar to the results for the nanoscale alumina particles.

The smallest effect on the frequency and dissipation change of the all the particle types tested (including the nanoscale and micron sized alumina particles) was observed for the CoCr micron sized particles. A small change in the frequency of 1 Hz was measured and an increase in the dissipation from 0 to 1.0 $x10^{-6}$ was measured. However, this change was only observed at the highest particle concentration of 100 $\mu g.ml^{-1}$. As observed with all the other particle types, this effect stabilised on the addition of DMEM.

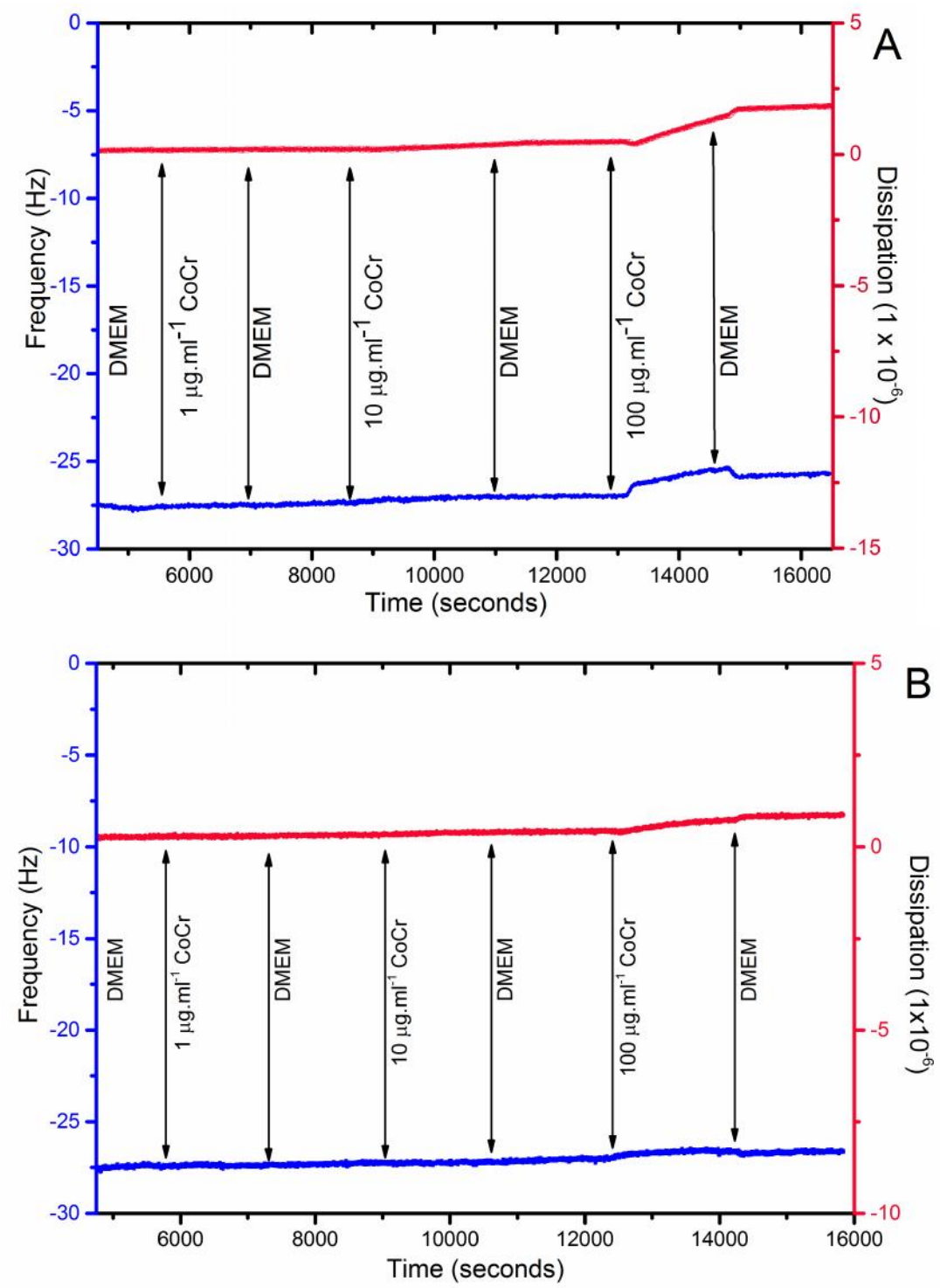

Figure 4.7 – Quartz crystal microbalance with dissipation plot of a solid supported bilayer lipid membrane in the presence of nanoscale (A) and micron sized (B) CoCr particles. A sBLM formed from model lipid vesicles was generated onto an oscillating quartz crystal (not shown). Commencing in DMEM, incremental concentrations (1 – 100 µg.ml^{-1}) of CoCr particles followed by DMEM washes were added at times indicated by the arrows. Changes in the frequency (blue) and dissipation (red) were measured (the ninth overtone is displayed). Each experiment was repeated twice.

4.3.2.3 Modelling quartz microbalance with dissipation data to determine particle binding using the Voight model

The frequency and dissipation data from the QCM-D experiments can be modelled to establish if particle binding has occurred and what effect this had on the sBLM. The results observed were greater for the dissipation compared to the frequency and it was unclear from the measured data if particle binding had occurred. Therefore, modelling method of the Voight model, described in Chapter one was used. The computer software, QTools was implemented to model the data, using the Voight viscoelastic model. This model allows the bound layers on the quartz crystal to be represented as a viscous dashpot and elastic spring connected in parallel, which is more suited for viscoelastic soft layers such as the formation of sBLM and particle binding.

The first layer of the model was established to represent the sBLM. The sBLM was modelled using the data before the addition of the particles. The parameters for layer one (shear modulus, viscosity and thickness) were then fixed and the second layer was modelled, which represents the bound particles to the sBLM. The outputs of the second layer were the layer viscosity, shear modulus and thickness. These outputs indicate if binding occurred (i.e. high shear modulus, low viscosity). However, it is noted that this model assumes that the sBLM itself is unperturbed by the addition of particles.

4.3.2.3.1 Modelling of nanoscale and micron sized alumina particles

The fixed parameters for the densities of each layer are listed in Table 4.2, which were used for the Voight model. For the nanoscale alumina particles, the fitted parameters (viscosity, shear modulus, and layer thickness) of layer one are detailed in Table 4.3 and were fixed when modelling layer two. The output of the fitted parameters for layer two indicated that the shear modulus and the viscosity were

small. The thickness of layer two was only 7.76 nm which is much smaller than the average diameter of the nanoscale alumina particles (40 nm). Therefore the outputs of layer 2 did not reflect the expected properties of nanoscale alumina particles of a high viscosity, high shear modulus and a representative thickness equal or greater to the mean particle diameter and thus indicate interactions between layer one and two was very weak.

A similar result was also observed for the modelling of the QCM-D data of the micron sized alumina particles and the model lipid membrane. The properties of layer one (the sBLM) were used to subsequently model the second layer of the micron sized alumina particles as detailed in Table 4.4. Again, the results were not characteristic of a layer of micron sized alumina particles, with small values for the viscosity. Furthermore the thickness of layer two in the model was only 4.6 nm, which was almost 100 times smaller than the mode size of the micron sized alumina particles (450 nm).

Table 4.2 – Fixed parameters used for the Voight model for nanoscale and micron sized alumina particles. The densities of layer one (sBLM) and layer two (the bound particle layer) are listed, which were used to calculate the fitted parameters of the Voight model (Jing *et al.* 2014; Malmström *et al.* 2007). Density of alumina from manufacturer's specifications as described in section 2.1.1 (PlasmaChem, Berlin, Germany)

Fixed Parameter	Density (kg/m^3)
Layer 1 (sBLM)	1000
Layer 2 (particles)	3900

Table 4.3 – Fitted parameter outputs using the Voight model for nanoscale alumina particles. Using the fixed parameters outlined in Table 4.2, Voight analysis was performed using multiple harmonics (n = 3 - 13). The shear modulus, viscosity, and thickness of layer one (sBLM) was first modelled and these fitted parameters were used to model layer two (particle layer).

Fitted Parameter	Shear Modulus (Pa)	Viscosity (kg/ms)	Thickness (nm)
Layer 1 (sBLM)	5.05×10^{5}	0.013	5.12
Layer 2 (particles)	2.12×10^{3}	2.6×10^{-4}	7.76

Table 4.4 – Fitted parameter outputs using the Voight model for micron sized alumina particles. Using the fixed parameters outlined in Table 4.2, Voight analysis was performed using multiple harmonics (n = 3 - 13). The shear modulus, viscosity, and thickness of layer one (sBLM) was first modelled and these fitted parameters were used to model layer two (particle layer).

Fitted Parameter	Shear Modulus (Pa)	Viscosity (kg/ms)	Thickness (nm)
Layer 1 (sBLM)	3.42×10^{4}	5.0×10^{-3}	5.70
Layer 2 (particles)	1.58×10^{4}	2.7×10^{-4}	4.60

4.3.2.3.2 Modelling of nanoscale and micron sized cobalt chromium particles

The effect of nanoscale and micron sized CoCr particles on the model lipid membrane were also modelled using the Voight model. The densities used to model both layer one and two are described in Table 4.5. The outputs of the model for the nanoscale and micron sized CoCr particles are detailed in Table 4.6 and 4.7, respectively. The model outputs for the nanoscale CoCr particles revealed that the shear modulus was low and had a layer thickness of 0.65 nm. This indicated that CoCr particles did not bind to the sBLM and only weakly interacted. Similarly, the model predicted that the micron sized CoCr particles had a low shear modulus.

Furthermore, the thickness of layer two, 0.01 nm, was much smaller than the mean particle size of approximately 3.26 µm. Again, the model outputs suggested extremely weak interactions between the sBLM and the CoCr particles.

Table 4.5 – Fixed parameters used for the Voight model for nanoscale and micron sized cobalt chromium particles. The fixed parameters of layer one (sBLM) and layer two (the bound particle layer) are listed, which were used to calculate the fitted parameters of the Voight model (Behl *et al*. 2013; Jing *et al.* 2014).

Fixed Parameter	Density (kg/m^3)
Layer 1 (sBLM)	1000
Layer 2 (particles)	7700

Table 4.6 – Fitted parameter outputs using Voight model for nanoscale cobalt chromium particles. Using the fixed parameters outlined in Table 4.5, Voight analysis was performed using multiple harmonics (n = 3 - 13). The shear modulus, viscosity, and thickness of layer one (sBLM) was first modelled and these fitted parameters were used to model layer two (particle layer).

Fitted Parameter	Shear Modulus (Pa)	Viscosity (kg/ms)	Thickness (nm)
Layer 1 (sBLM)	1.03×10^{7}	4.29×10^{-3}	4.53
Layer 2 (particles)	985.33	1.30×10^{-4}	0.65

Table 4.7 – Fitted parameter outputs using Voight model for micron sized cobalt chromium particles. Using the fixed parameters outlined in Table 4.5, Voight analysis was performed using multiple harmonics (n = 3 - 13). The shear modulus, viscosity, and thickness of layer one (sBLM) was first modelled and these fitted parameters were used to model layer two (particle layer).

Fitted Parameter	Shear Modulus (Pa)	Viscosity (kg/ms)	Thickness (nm)
Layer 1 (sBLM)	1.06×10^{7}	6.41×10^{-3}	4.51
Layer 2 (particles)	8581.5	1.94×10^{-4}	0.01

4.3.2.3.3 Summary of quartz crystal microbalance with dissipation results for nanoscale and micron sized alumina and cobalt chromium particles

The data from the QCM-D results were modelled using the Voight model and the results from section 4.3.2.2 suggested that overall no particle binding occurred for all particle types tested. This was based upon the predicted thickness of the particle layer being too small alongside the low shear moduli and viscosity, which did not correspond to particles being tightly bound to the sBLM.

4.3.3 Investigation into the binding of particles to a model lipid membrane using surface plasmon resonance techniques

The QCM-D data from section 4.3.2 described a large change in the dissipation in the absence of any large changes in the frequency. This phenomenon is uncommon in QCM-D and further to this, the model used assumed that the particles had not perturbed the sBLM. Therefore this part of the study aimed to confirm if particle binding occurred using the alternative technique of SPR analysis. This technique measures changes in the angle of incidence of surface plasmon electrons at the surface of a metal sensor. These surface plasmons are sensitive to changes in the refractive index and film thickness and therefore can be used to ascertain if particle binding had occurred. For this part of the study, nanoscale CoCr particles were used as an example. The sensor consisted of long-chain alkane thiol molecules bound to a gold film. A planar monolayer of the model lipid membrane was formed across the sensor in 20 mM MOPS with 30 mM Na_2SO_4, pH 7.4, which together with the alkane thiol layer on the sensor chip, forms a hybrid bilayer. The membrane was subsequently washed three times with ultrapure distilled water to remove any unbound lipids (section 4.2.2.1.2). Using DMEM, without any supplements, as the running solution, the blank was flowed across the membrane

at a rate of 40 µl per minute. The blank was then exchanged to DMEM and once the readout had stabilised, 100 µg.ml^{-1} of CoCr particles were flowed across the membrane and the association kinetics were measured as described in section 4.2.2.1.3.

The resonance units (RU) were plotted against time to ascertain the association kinetics of the CoCr particles with the membrane monolayer, as shown in Figure 4.8. A sharp reduction of approximately 250 RU was observed immediately after the blank sample was injected into the sensor cell. However, upon the addition of the DMEM running buffer, the RU baseline immediately returned to the pre-blank level. This phenomenon was also observed when the sample of 100 µg.ml^{-1} nanoscale CoCr particles was injected into the sensor cell and thus clearly reflects the change in the refractive index of the solution. Despite the initial drop of the RU baseline, no association kinetics of the CoCr particles interacting with the membrane was measured with the data being comparable to the blank sample.

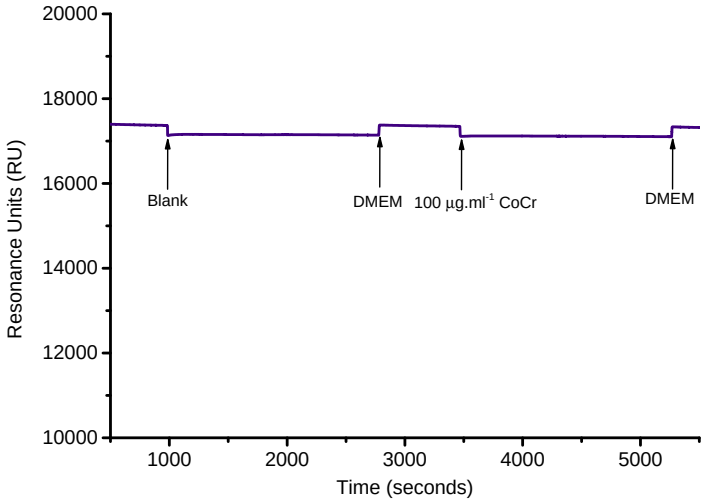

Figure 4.8 – Surface plasmon resonance analysis of nanoscale cobalt chromium particles bound to model lipid membrane. A planar, monolayer of the model lipid membrane was formed on a gold sensor coated with long-chain alkane thiol molecules (not shown). Using DMEM as the running buffer the blank of DMEM plus 10% (v/v) of ultrapure distilled water was added. After the DMEM wash, 100 µg.ml^{-1} of CoCr particles were added to the membrane and the association curve was measured. The experiment was repeated twice.

4.3.4 The incorporation of plasma membrane proteins into the model lipid membrane

In order to explore the interaction of nanoscale and micron sized alumina and CoCr particles with the cell plasma membrane, the complexity of the model lipid membrane was further increased to promote the clinical relevance of the model. Therefore the effect of the presence of plasma membrane proteins isolated from primary HFBs on particle interactions with the model lipid membrane was investigated. The membrane proteins from U937 histiocytes were also isolated as described in section 2.2.6.5. Due to sample shortage, these samples were only used in vesicle leakage assays.

4.3.4.1 Optimisation of isolated membrane protein concentration for the formation of a solid supported bilayer lipid membrane

In order to form a stable sBLM, for the QCM-D studies, the concentration of the isolated protein within the membrane was optimised, as high concentrations can inhibit planar bilayer formation (Dodd *et al.* 2008). For continuity this concentration would also be used for the vesicle leakage assays. For the optimisation studies, the membrane proteins isolated from L929 fibroblasts were used as a large amount of isolated proteins were required for the optimisation studies. As described in Chapter two, approximately 1 x 10^8 cells were required to isolate sufficient amounts of isolated membrane proteins. Therefore plasma membrane isolated from L929 fibroblasts were used as these cells are more readily available and large cell stocks can be acquired quickly. The membrane proteins were incorporated with the phospholipid:cholesterol mixture previously used in this chapter for the model lipid membrane. Lipid vesicles with 20%, 40% or 60% (w/w) of isolated membrane proteins to lipid were investigated. Mixing plasma membranes with lipids and sBLM formation are described in section 2.2.6.6, whereby the vesicles (0.5 $mg.ml^{-1}$) were

formed in 20 mM MOPS with 30 mM Na_2SO_4, pH 7.4 and flowed across the surface of the quartz crystal. The bursting of the vesicles to form a bilayer was induced by the addition of ultrapure distilled water, followed by the addition of the starting solution DMEM.

The changes in frequency and dissipation over time for the different protein concentrations are shown in Figure 4.9A and 4.9B, respectively. Upon the addition of the vesicles, for all three protein concentrations, there was a sharp decrease in the frequency, indicating rapid binding of the vesicles to the silicon dioxide coated QCM-D crystal surface. However, the vesicles formed with 20% (w/w) isolated membrane protein, burst spontaneously and formed a planar sBLM just before the ultrapure distilled water wash. Nevertheless the frequency was lower and the dissipation was higher than expected for a completely planar plasma membrane and therefore suggested that some of the adsorbed vesicles remained intact. For the vesicles with 40% (w/w) and 60% (w/w) isolated membrane proteins, the frequency continued to fall and did not recover significantly after the addition of the ultrapure distilled water and DMEM wash. This indicated that the vesicles continued to bind to the surface of the crystal, forming a layer of vesicles, rather than bursting to form a stable sBLM. This was also reflected in the dissipation results (Figure 4.9B), whereby a large reduction in the dissipation was observed for the sBLM formed from 20% (w/w) isolated membrane proteins just before the ultrapure distilled water wash was added. In contrast, the dissipation values for the sBLMs formed with 40% (w/w) and 60% (w/w) isolated membrane proteins were much higher. This suggested that a more planar sBLM was formed from vesicles containing 20% (w/w) isolated membrane proteins. Planar sBLMs are characterised by dissipation values of less than 2×10^{-6} (Richter *et al.* 2006). Therefore, all future QCM-D and vesicle leakage experiments would incorporate 20% (w/w) of the isolated membrane proteins into the lipid membrane.

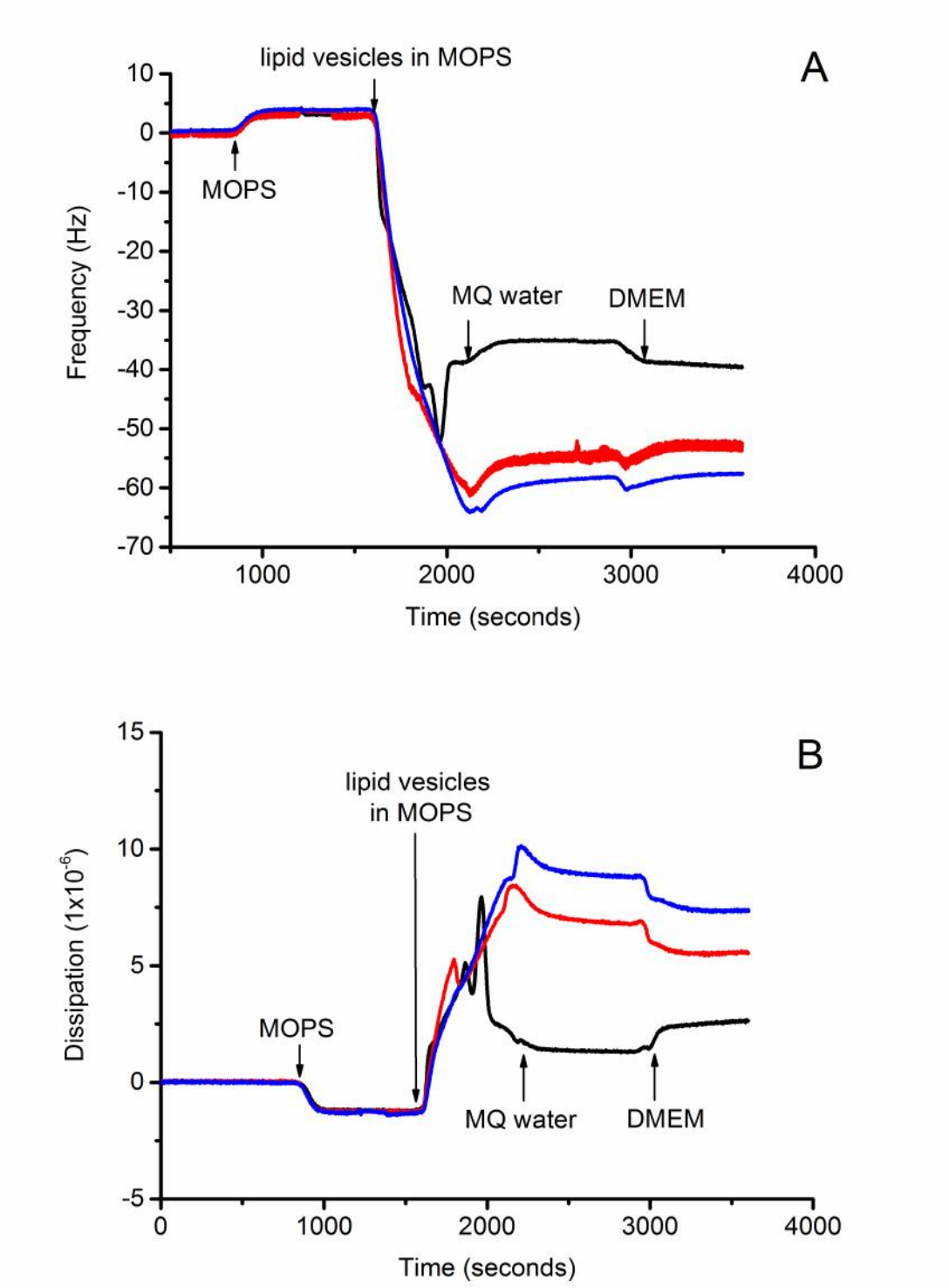

Figure 4.9 – Optimisation of isolated membrane protein concentration for the formation of a stable solid supported bilayer lipid membrane. Model lipid vesicles with 20%, 40% or 60% (w/w) proteins isolated from L929 fibroblasts were formed in MOPS. The vesicles were added to SiO_2-coated crystals and the frequency (A) and dissipation (B) were measured in real time. The ninth overtone is displayed. Key – 20% protein; – 40% protein; – 60% protein.

4.3.5 The effect of the incorporation of fibroblast and histiocyte membrane proteins into the model lipid membrane on membrane integrity in the presence of nanoscale and micron sized alumina and cobalt chromium particles

The effect of incorporating membrane proteins isolated from primary HFBs and U937 histiocytes on the membrane integrity in the presence of nanoscale and micron sized alumina and CoCr particles was investigated. The vesicle leakage studies were performed as described in section 2.2.6.3, however the major difference was the incorporation of 20% (w/w) isolated membrane proteins from primary HFBs or U937 histiocytes into the model lipid vesicles (previously optimised in section 4.3.4.1).

4.3.5.1 The effect of the incorporation of fibroblast and histiocyte membrane proteins into the model lipid membrane on membrane integrity in the presence of nanoscale and micron sized alumina particles

In the presence of nanoscale alumina particles, no release of the fluorescent dye from the vesicles containing isolated human fibroblast proteins was observed at the particle concentrations of 1 and 10 $\mu g.ml^{-1}$ (Figure 4.10A). At the highest particle concentration of 100 $\mu g.ml^{-1}$, a small increase of 3% in the vesicle leakage was measured, which was significantly greater than the vesicle leakage at the lower particle concentrations. Similar results were also measured for vesicles containing U937 histiocyte proteins in the presence of nanoscale alumina particles. Only a small vesicle leakage of 6% was observed at the particle concentration of 100 $\mu g.ml^{-1}$ (Figure 4.10B).

A dose dependent increase in the vesicle leakage was measured for the vesicles containing human fibroblast isolated proteins in the presence of micron sized alumina particles (Figure 4.10C). No vesicle leakage was observed at the lowest particle concentration of 1 $\mu g.ml^{-1}$. However at the highest particle concentration of 100 $\mu g.ml^{-1}$ the mean vesicle leakage had increased to 15%, which was statistically significant in comparison to the vesicle leakage at 1 and 10 $\mu g.ml^{-1}$. In the presence of micron sized alumina particles, a dose dependent increase in the vesicle leakage was observed for the vesicles containing U937 isolated proteins. Nevertheless the amount of released fluorescent dye was less than observed for the vesicles containing isolated primary HFBs proteins, with the highest particle concentration of 100 $\mu g.ml^{-1}$ only inducing a 8% vesicle leakage (Figure 4.10D). This result was significantly higher than the lower particle concentrations of 1 and 10 $\mu g.ml^{-1}$.

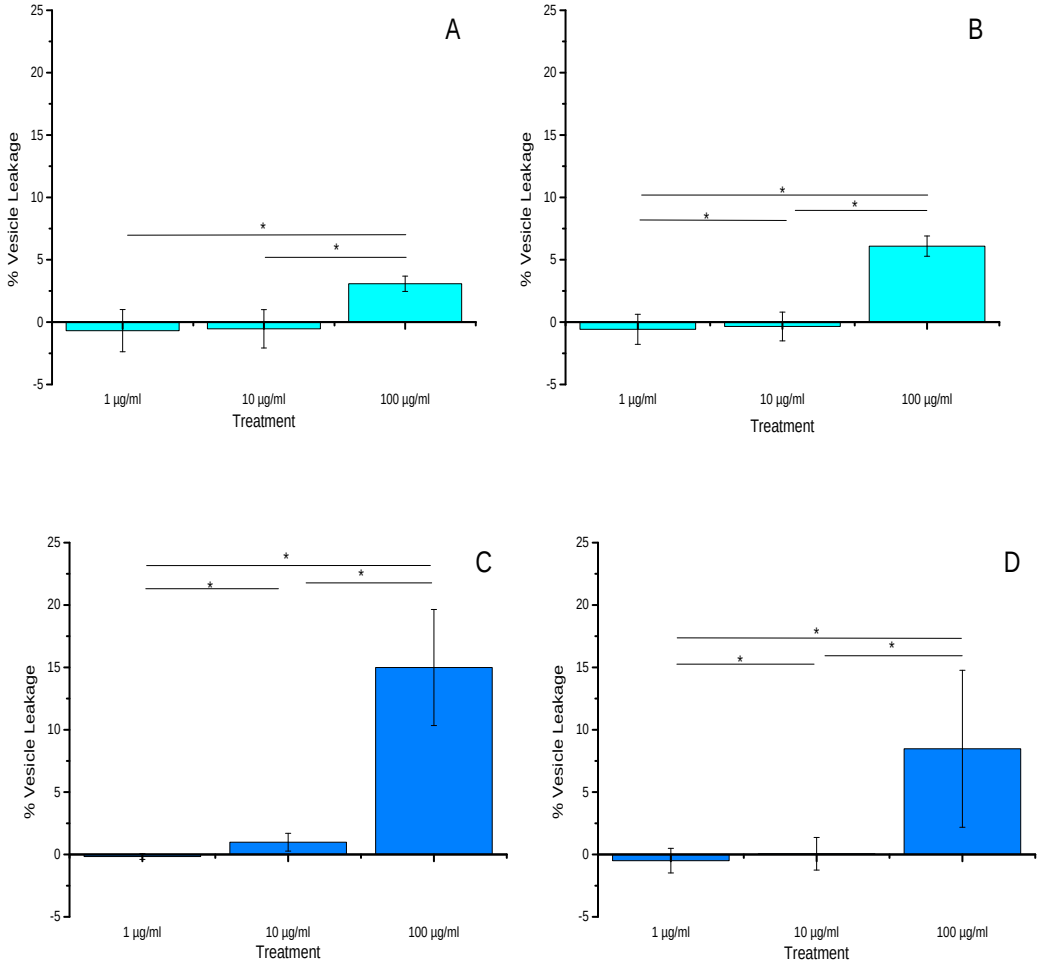

Figure 4.10 – The effect of nanoscale and micron sized alumina particles on vesicle leakage of a lipid membrane with isolated membrane proteins from human fibroblasts and U937 histiocytes. Nanoscale alumina particles were incubated with lipid vesicles consisting of 20% (w/w) isolated proteins from human fibroblast membranes (A) or isolated U937 histiocytes (B). Micron sized alumina particles were incubated with lipid vesicles consisting of 20% (w/w) isolated human fibroblast membrane proteins (C) or isolated U937 histiocytes (D). Data (n=3) is expressed as a percentage vesicle leakage of the detergent Triton-X 100. Vesicle leakage of fluorescent dye encapsulated vesicles was measured in real time and subsequent increasing particle concentrations (1, 10 and 100 µg.ml^{-1}). A paired t-test was performed in comparison to FBS only control and statistically significant results ($p < 0.05$) are indicated by an asterisk. Error bars represent 95% confidence levels.

4.3.5.2 The effect of the incorporation of fibroblast and histiocyte membrane proteins into the model lipid membrane on membrane integrity in the presence of nanoscale and micron sized cobalt chromium particles

In the presence of nanoscale CoCr particles, no vesicle leakage was observed for vesicles containing isolated primary HFBs proteins at the particle concentrations of 1 and 10 $\mu g.ml^{-1}$. Only at the highest particle concentration of 100 $\mu g.ml^{-1}$, a mean of 3% vesicle leakage was observed (Figure 4.11A). No vesicle leakage was observed for the vesicle containing isolated U937 proteins incubated with nanoscale CoCr particles, whereby the vesicle leakage was less than the baseline for all particle concentrations (Figure 4.11B). This suggested that the CoCr particles induced a quenching effect.

In the presence of micron sized CoCr particles, a small amount of vesicle leakage of 6% was observed at the particle concentration of 100 $\mu g.ml^{-1}$ for vesicles containing isolated primary HFBs proteins (Figure 4.11C). Similarly, at the highest particle concentration of 100 $\mu g.ml^{-1}$, the micron sized CoCr particles only induced a mean 8% vesicle leakage when incubated with vesicles containing U937 isolated proteins (Figure 4.11D).

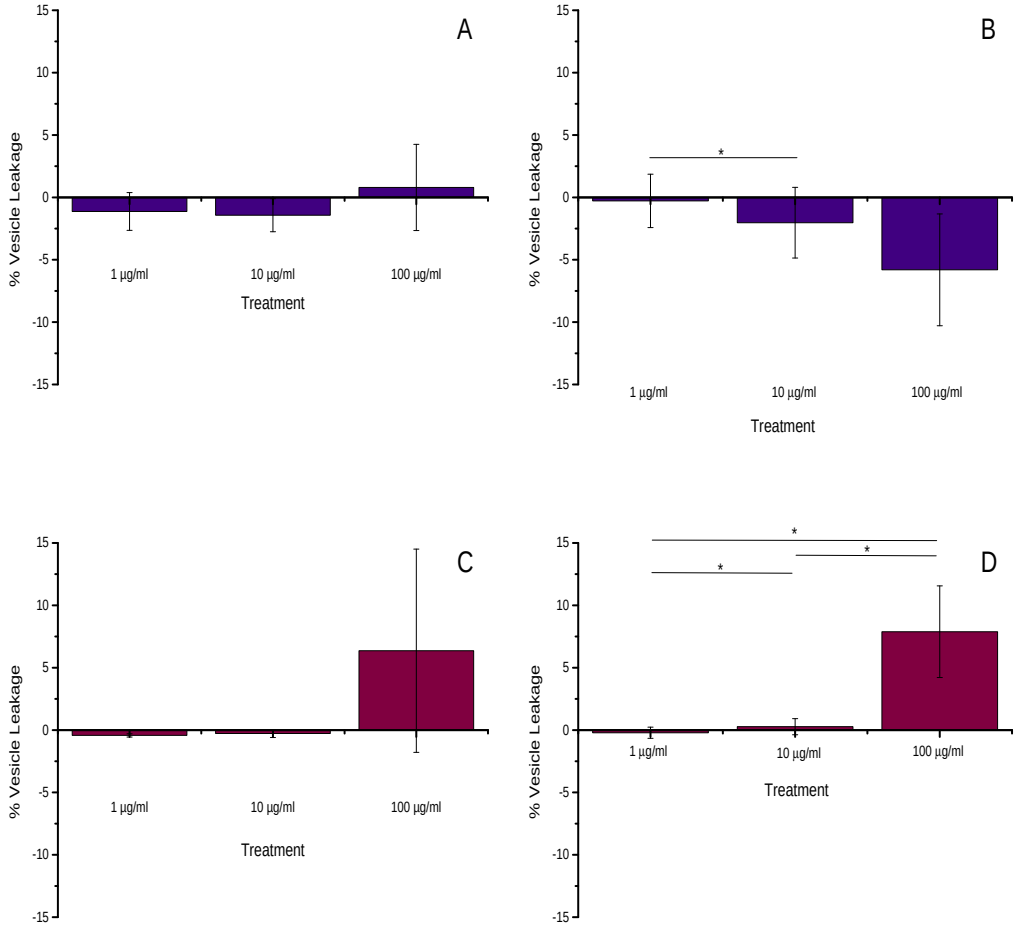

Figure 4.11 – The effect of nanoscale and micron sized cobalt chromium particles on vesicle leakage of a lipid membrane with isolated membrane proteins from human fibroblasts and U937 histiocytes. Nanoscale CoCr particles were incubated with lipid vesicles consisting of 20% (w/w) isolated proteins from human fibroblast membrane (A) or isolated U937 histiocytes (B). Micron sized CoCr particles were incubated with lipid vesicles consisting of 20% (w/w) isolated human fibroblast membrane proteins (C) or isolated U937 histiocytes (D). Data (n=3) is expressed as a percentage vesicle leakage of the detergent Triton-X 100. Vesicle leakage of fluorescent dye encapsulated around vesicles was measured in real time and subsequent increasing particle concentrations (1, 10 and 100 $\mu g.ml^{-1}$). A paired t-test was performed in comparison to FBS only control and statistically significant results ($p < 0.05$) is indicated by an asterisk (*). Error bars represented 95% confidence levels (n = 3).

4.3.6 The effect of the incorporation of fibroblast membrane proteins into the model lipid membrane on the binding of particles

The effect of incorporating membrane proteins isolated from primary HFBs on the interactions of particles was investigated using QCM-D. The QCM-D studies were performed as described in section 2.2.6.4, however the major difference was the incorporation of 20% (w/w) isolated membrane proteins from primary HFBs into the sBLM (previously optimised in section 4.3.4.1). Upon the formation of a stable sBLM, nanoscale and micron sized alumina or CoCr particles, diluted in DMEM at concentrations of 1, 10 and 100 $\mu g.ml^{-1}$, were flowed across the sBLM at a flow rate of 70 µl per minute for 30 minutes. The change in frequency and dissipation over time were monitored and for clarity, the ninth overtone is only shown for the QCM-D plots.

4.3.6.1 The effect of the incorporation of fibroblast membrane proteins into the model lipid membrane on the binding of nanoscale and micron sized alumina particles

The change in frequency and dissipation over time at the ninth overtone for the alumina nanoscale and micron sized particle QCM-D experiments are shown in Figure 4.12A and Figure 4.12B, respectively. A stable sBLM consisting of 20% (w/w) isolated membrane proteins from primary HFBs was formed for both the nanoscale and micron sized alumina particle QCM-D studies. No overall effect on the frequency was observed upon the addition of nanoscale alumina particles to the sBLM at particle concentrations equal to or less than 100 $\mu g.ml^{-1}$. No change in the frequency was observed for all the concentrations of micron sized alumina particles tested. For both the nanoscale and micron sized alumina particle experiments, the greatest change was observed for the dissipation at particle concentrations of 10

$\mu g.ml^{-1}$ or higher. For example, upon the addition of 100 $\mu g.ml^{-1}$ of nanoscale alumina particles, the dissipation increased to 8×10^{-6}. This change in dissipation stabilised upon the addition of DMEM.

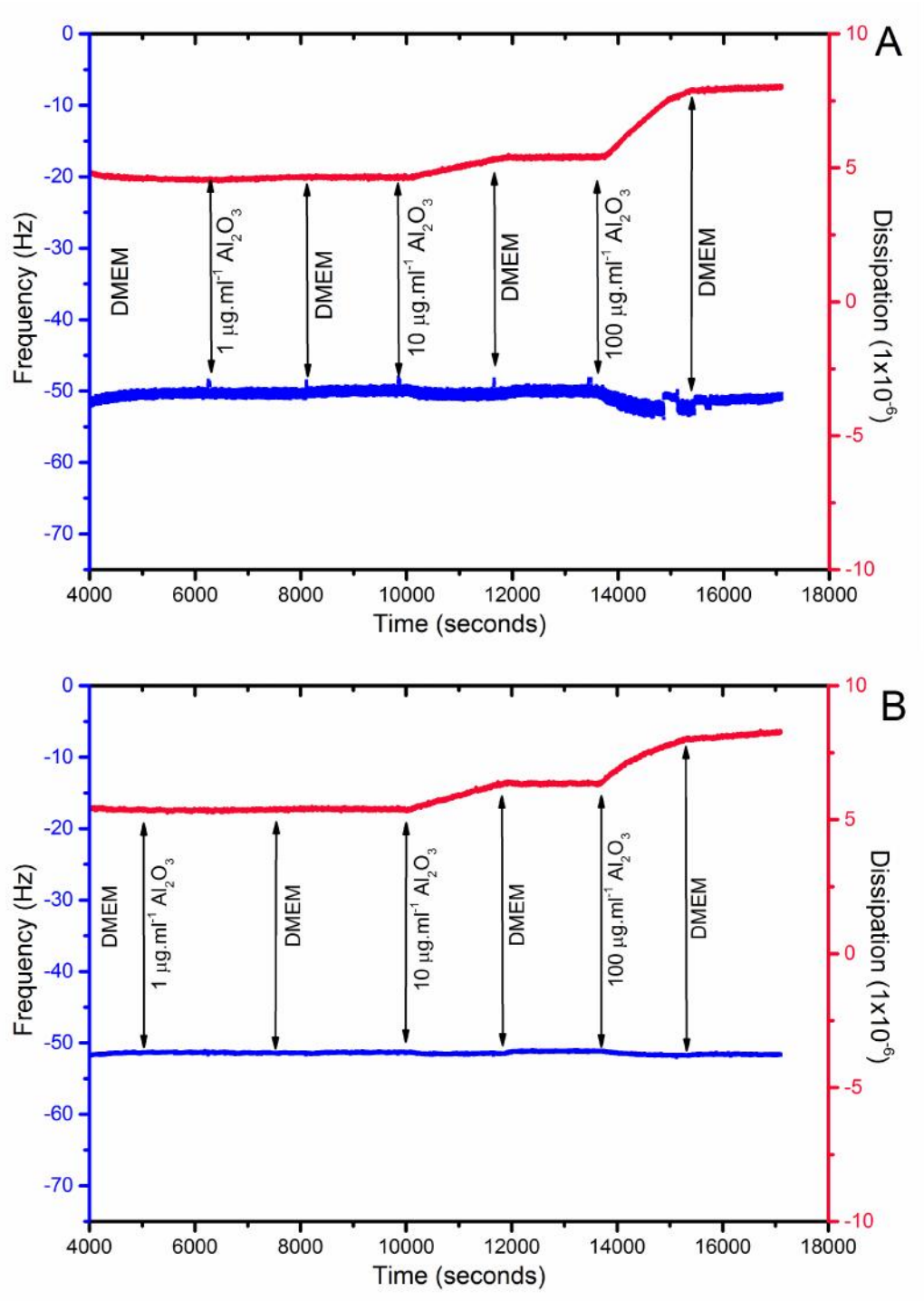

Figure 4.12 – QCM-D plot of a solid supported bilayer lipid membrane containing 20% isolated human fibroblast plasma membrane in the presence of nanoscale alumina (A) and micron sized (B) particles. A sBLM of the mixed lipid vesicles was formed onto an oscillating quartz crystal (not shown). Commencing in DMEM, incremental concentrations (1 – 100 µg.ml^{-1}) of nanoscale or micron sized alumina particles followed by DMEM washes were added at times indicated by the arrows. Changes in the frequency (blue) and dissipation (red) were measured (the ninth overtone is displayed).

4.3.6.2 The effect of the incorporation of fibroblast membrane proteins into the model lipid membrane on the binding of nanoscale and micron sized cobalt chromium particles

A stable sBLM, consisting of 20% (w/w) isolated proteins from primary HFBs, was formed for both the nanoscale and micron sized CoCr particle QCM-D studies (Figure 4.13A and 4.13B, respectively). For both the nanoscale and micron sized CoCr particle experiments, no change in the frequency was observed for all particle concentrations, which remained constant throughout the testing. A minor increase in the dissipation from 5×10^{-6} to 6.5×10^{-6} was measured when 100 $\mu g.ml^{-1}$ of CoCr nanoscale particles were flowed across the sBLM. However, this increase was less than the dissipation change observed in the alumina nanoscale and micron sized particle experiments. No change in the dissipation was measured upon the addition of micron sized CoCr particles at all the particle concentrations tested.

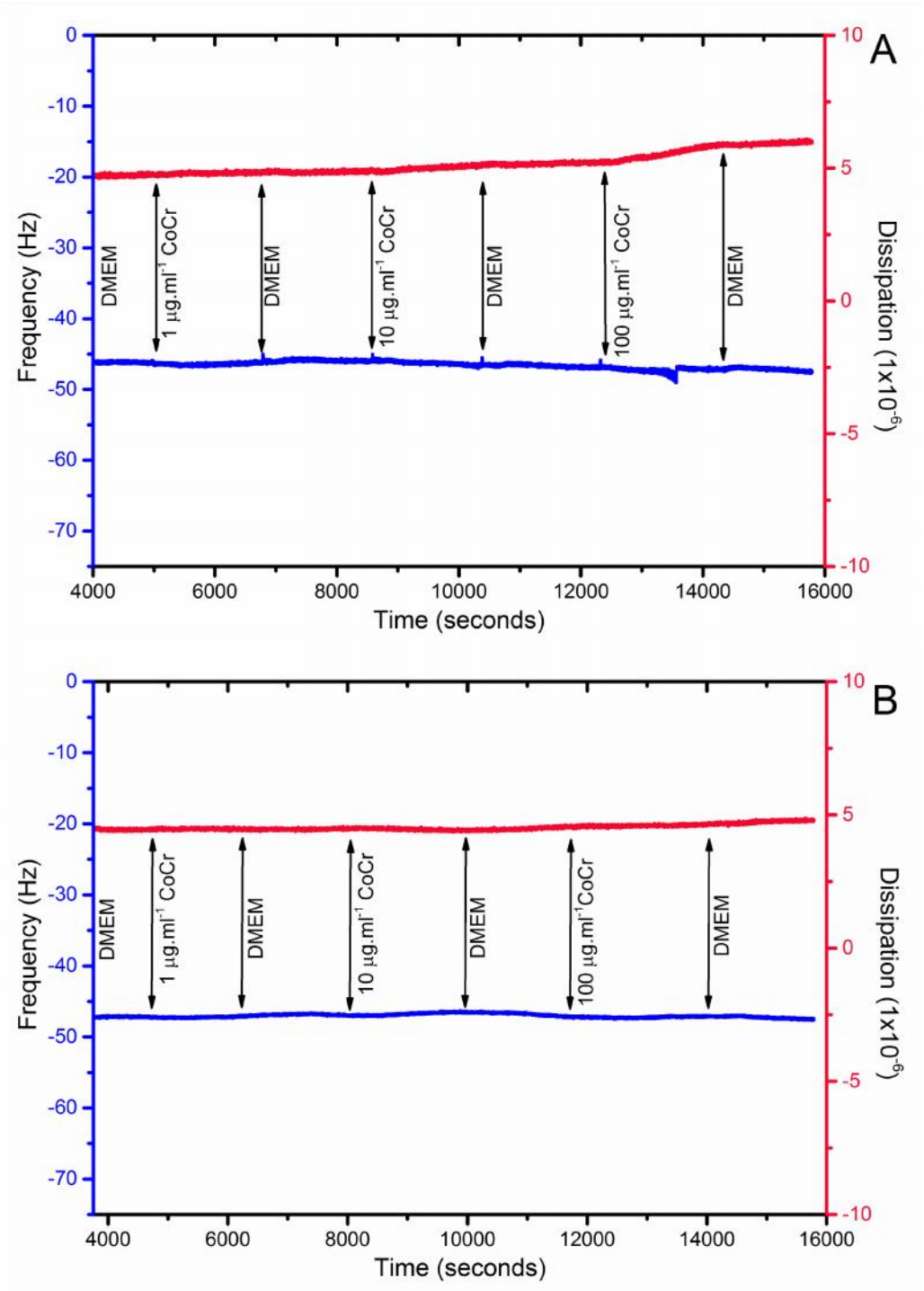

Figure 4.13 – QCM-D plot of a solid supported bilayer lipid membrane containing 20% isolated human fibroblast plasma membrane in the presence of nanoscale CoCr (A) and micron sized (B) particles. A sBLM of the mixed lipid vesicles was formed onto an oscillating quartz crystal (not shown). Commencing in DMEM, incremental concentrations (1 – 100 µg.ml^{-1}) of nanoscale or micron sized CoCr particles followed by DMEM washes were added at times indicated by the arrows. Changes in the frequency (blue) and dissipation (red) were measured (The ninth overtone is displayed).

4.4 Discussion

The aim of this part of the study was to investigate the effect of nanoscale and micron sized alumina and CoCr particles on the cell plasma membrane. Whilst a number of *in vitro* studies have explored the effect of alumina and CoCr particles on a variety of cell types, currently there are limited studies exploring the effect of these particles on the cell plasma membrane (Lewis *et al.* 2007; Goode *et al.* 2012). The plasma membrane is important for overall cell function by providing a selectively permeable barrier and structural support for the cell (Voet *et al.* 2013). Therefore the effect of particles on the cell plasma membrane integrity, binding and subsequent uptake may influence the cellular responses to the particles (Canton and Battaglia 2012). This study focused on the effect of nanoscale and micron sized alumina and CoCr particles on the cell plasma membrane and the potential impact on the cell viability.

Studies which have explored the effect of particles on the cell plasma membrane lack specificity (Lewis *et al.* 2007; Goode *et al.* 2012). These studies tend to only report particle uptake and localisation within the cells. However, these studies do not determine the factors affecting particle interactions with the cell membrane or the possible damage caused by the particles. Furthermore a large proportion of *in vitro* studies on the effect of alumina and CoCr particles on the cell viability have used model particles which are not clinically relevant in terms of particle size (Yoshida *et al.* 2003; Hallab *et al.* 2010; Dalal *et al.* 2012). As previously described in Chapter 1, particle size, composition and morphology can have an influencing effect on particle: membrane interactions and on the cell viability (Canton and Battaglia 2012). Therefore this part of the study aimed to use nanoscale and micron sized alumina and CoCr particles described in Chapter three.

In order to investigate the effect of nanoscale and micron sized alumina and CoCr particles on the cell plasma membrane, recently developed methods within the field

of nanotoxicology were implemented. These included the use of simple vesicle leakage assays, QCM-D and SPR techniques (Green *et al.* 2000; Cho *et al.* 2010; Mu *et al.* 2014). The advantage of using these techniques allows the environment in which particle: membrane interactions occur to be highly controlled. Furthermore, influencing factors, such as the presence of serum or membrane proteins can be investigated (Cho *et al.* 2010). Moreover, a number of studies investigating the effect of nanoparticles on the cell plasma membrane have used simplified model membranes, often only consisting of one type of phospholipid (Lesniak *et al.* 2012; Lesniak *et al.* 2013). However the cell plasma membrane comprises of multiple phospholipids and cholesterol (Voet *et al.* 2013). Therefore to make the model membrane more clinically relevant, the composition of the model lipid membrane employed in this study consisted of a phospholipid: cholesterol mixture similar to the composition of primary HFBs (Schroeder *et al.* 1984; Mahadik *et al.* 1994). At present this is the first instance where a model fibroblast membrane has been used to investigate particle: membrane interactions.

4.4.1 The effect of nanoscale and micron sized alumina and cobalt chromium particles on the integrity of a model lipid cell plasma membrane

The effect of nanoscale and micron sized alumina and CoCr particles on membrane integrity and the ability to damage the membrane was investigated, initially using a simple vesicle leakage assay. This vesicle leakage assay has previously been used in the published literature with alternative nanoparticles. Similar results have also been reported for silica nanoparticles whereby the particles only induced a moderate increase of up to 20% vesicle leakage, even at high particle concentrations of 100 $\mu g.ml^{-1}$ (Mu *et al.* 2012a).

The results revealed that both the nanoscale and micron sized alumina and CoCr particles induced vesicle leakage of the model lipid membrane in a dose dependent response. Surprisingly the nanoscale and micron sized alumina particles induced a larger vesicle leakage than the nanoscale and micron sized CoCr particles. Indeed at the highest particle concentration of 100 $\mu g.ml^{-1}$, the nanoscale alumina particles caused a 16% increase in vesicle leakage, whereas the nanoscale CoCr particles only induced 4% vesicle leakage at the equivalent particle concentration. Nanoscale CoCr particles were revealed to have a quenching effect on the florescent dye released from the vesicles. Nanoparticles have previously been reported to have a quenching effect on colorimetric assays and therefore this must be considered (Raikar *et al.* 2011).

Whilst the results from the chapter demonstrated that the vesicle leakage in the presence of particles was statistically significant, particularly with membrane proteins incorporated into the vesicles, this does not necessarily correlate with biological significance. Membrane pores caused by silica nanoparticles have been demonstrated to form transient pores in the membrane which may have limited effect on viability of a cell (Mu *et al.* 2012; Zhang *et al.* 2012). Furthermore the particle concentrations used in the vesicle leakage assays (up to and including 100 $\mu g.ml^{-1}$) were much higher than the concentrations used in the cell viability assays described in Chapter three and would not be observed within a clinical scenario. Therefore it is unlikely that the main mode of toxicity for nanoscale and micron sized alumina and CoCr particles is direct damage to the plasma membrane.

4.4.2 Binding of nanoscale and micron sized alumina and cobalt chromium particles to a model lipid membrane

The binding of nanoscale and micron sized alumina and CoCr particles to a model lipid membrane were also investigated using QCM-D. As outlined previously, QCM-D has been used to explore the effect of a variety nanoparticles on a sBLM, including silica and copper particles (Karlsson *et al.* 2013; Lesniak *et al.* 2013). The advantage of using QCM-D is that it is highly sensitive and can measure changes in mass as low as 100 $pg.cm^{-2}$ over the crystal area. Furthermore, due to its sensitivity this technique provides an opportunity to isolate and examine which factors are critical for particle binding to a model lipid membrane such as the presence of membrane proteins (Cho *et al.* 2010). A stable sBLM was formed using the optimised methods described by Mu *et al.*(2012; 2104). Upon the formation of the sBLM, nanoscale and micron sized alumina and CoCr particles were flowed across the membrane and the frequency and dissipation were measured. A decrease in the frequency indicated particle binding and the dissipation also provided information on the viscoelasticity of the nanoparticle layer. Due to the nature of the QCM-D method, a positive control of membrane binding was not used with each experiment in this current study. However, an example of silica nanoparticle binding to a sBLM from the literature is shown in Figure 1.5 and was used as a point of reference. Furthermore, Appendix C reveals that 10% (v/v) FBS was able to bind to the sBLM used in this current study, thus demonstrating the potential for binding to the model membrane to occur.

The results for the QCM-D experiments from this part of the study revealed that none of the nanoscale and micron sized alumina and CoCr particles caused a significant reduction in the frequency at any particle concentration tested. Indeed a minor increase in the frequency was observed for the nanoscale alumina and CoCr particles and micron sized CoCr particles. A small reduction in the frequency was

measured in the presence of the micron sized alumina particles; however this decrease of 3 Hz was very minor and did not indicate significant particle binding. Moreover, for all particle types, a rise in the dissipation was observed with increasing particle concentration. These results were unexpected. However, the changes in dissipation were measured consistently across the different types of particles and between repeats, suggesting that a degree of precision of the QCM-D method. As previously mentioned nanoparticle binding to sBLMs have be reported in the literature using QCM-D. However Mu *et al.* (2012) measured approximately a 90 Hz reduction in the frequency upon the addition of 10 $\mu g.ml^{-1}$ of 14 nm silica nanoparticles to the sBLM. Similarly Lesniak *et al.* (2013) reported a strong interaction with the model membrane with a reduction in the frequency of approximately 60 Hz after the addition of 100 nm polystyrene nanoparticles to a POPC sBLM. Mu *et al.* (2014) also reported an increase in the dissipation (7×10^{-6}) as well as a reduction in the frequency (less than 10 Hz) after the addition of polymer coated zinc oxide nanoparticles to a sBLM, suggesting a weaker interaction with the membrane.

Interestingly, Karlsson *et al.* (2013) also reported copper nanoparticles in the presence of a sBLM induced a large increase in the dissipation alongside a small increase in the frequency. Nevertheless the authors failed to explain why this occurred. Olsson *et al.* (2012) hypothesised that the increase in frequency can be caused by the particles binding to the sBLM *via* small contact points and oscillating at their own resonant frequency. The authors hypothesised a coupled resonance model whereby the particle formed resonators themselves which was dependent on the overtone number. However, the data from the present study did not fit this model and therefore this theory was unlikely to explain the results obtained in this present study.

To quantify the binding of the nanoscale and micron sized alumina and CoCr particles to the sBLM, the frequency and dissipation data at all overtones was modelled using the Voight model. The Voight model is commonly used for QCM-D studies which implement non-rigid structures on the surface of the quartz crystal. This model is able to model non-rigid layers unlike the traditionally used Saurbrey equation, which assumes a rigid layer has been formed on the surface of the crystal (Voinova *et al.* 1999). The Saurbrey equation does not take into account the dissipation and therefore can underestimate the mass bound to the quartz crystal. Instead the Voight model represents the sBLM and the layer of bound particles as a viscous dashpot and elastic spring connected in parallel. It can be used to determine the viscosity, shear modulus and thickness of each layer formed on the crystal surface (Voinova *et al.* 1999).

The modelling outputs for the nanoscale and micron sized alumina and CoCr particles revealed that stable sBLMs had been formed. However the second layer of the model was not characteristic of either alumina or CoCr particles. Therefore it was hypothesised that the increase in dissipation may have been caused by an intermediate layer being formed between the sBLM and the particles, known as a slippage layer (Daikhin *et al.* 2000). The presence of the slippage layer would have caused no overall change in the frequency but may have increased the dissipation outputs. Nevertheless, it was not possible to model this as the Voight model assumes that only two layers can be modelled, rather than three. Therefore, an alternative binding technique of SPR was used to confirm whether or not particles bound to the model lipid membrane.

4.4.3 Binding of particles to a model lipid membrane using surface plasmon resonance techniques

Surface plasmon resonance was used in conjunction with the QCM-D results to determine if particle binding to the model lipid model had occurred. This technique measures the adsorption of substances onto a planar gold or silver sensor by detecting changes in the film thickness of the sensor (Green *et al.* 2000). The binding of nanoscale CoCr particles was used as an example particle for the SPR experiments. The SPR results revealed that no binding was observed upon the addition of nanoscale CoCr particles to the model lipid membrane. Therefore it was concluded that no or very little particle binding had occurred for the QCM-D experiments. These results highlight the sensitivity of the QCM-D technique and suggest that the change in dissipation may have been caused by very weak interactions between particles and sBLM or, alternatively, a minor disrupting effect on the sBLM without permanent adherence of the particles.

4.4.4 The incorporation of fibroblast membrane proteins into the model lipid membrane on the binding of particles

To further increase the complexity and clinical relevance of the model lipid membrane, nanoscale and micron sized alumina and CoCr particles interactions to membrane proteins was also investigated. The presence of membrane proteins may also be an essential part of particle recognition and cellular internalisation. Following the optimisation studies, proteins were isolated from the plasma membranes of U937 histiocytes and primary HFBs using a sucrose gradient. This method was optimised in order to only isolate the proteins of the plasma membrane and structurally similar endosomal vesicles of the cytoplasm. This method removed the membranes of other organelles, such as mitochondria, which were considered structurally very different and may have influenced the results.

In order to form a stable sBLM for the QCM-D studies, the concentration of membrane proteins incorporated within the model lipid membrane was optimised. This is because high concentrations of proteins can inhibit bursting of the membrane vesicles once bound to the quartz crystal to form a sBLM. The formation of a sBLM was measured using 20% (w/w), 40% (w/w) and 60% (w/w) proteins isolated from L929 fibroblasts. This cell type was used as a large number of cells were required to isolate sufficient concentration of membrane proteins for the optimisation experiments. L929 cells were more readily available than the primary HFBs and U937 histiocytes and hence were used for this experiment. The results demonstrated that the optimal protein concentration was 20% to form a solid supported planar membrane. This finding was in good agreement with the results published by Dodd *et al.* (2008), where the inner membrane was isolated from *E. coli* and incorporated into a phosphatidylcholine sBLM. Using QCM-D techniques, Dodd *et al.* (2008) revealed that a protein concentration of 20% (w/w) formed a stable sBLM. Therefore a protein concentration of 20% (w/w) was incorporated into the model lipid membrane for all future experiments investigating effect of the presence of membrane proteins. The more complex model membrane has not been used in literature and was considered a novel, clinically relevant model.

The effect of nanoscale and micron sized alumina and CoCr particles on membrane integrity in the presence of membrane proteins was investigated using the vesicle leakage assay. The membrane proteins isolated from U937 histiocytes and primary HFBs were used in these experiments. For both types of isolated proteins, no extensive vesicle leakage was observed for the nanoscale and micron sized alumina and CoCr particles. However the vesicle leakage for the alumina particles was less than results for the vesicles without membrane proteins incorporated into them. For instance, 100 $\mu g.ml^{-1}$ of micron sized alumina particles induced 20% leakage for the vesicles without any membrane protein incorporated into them. When the membrane proteins were incorporated into the vesicles, the vesicle

leakage reduced to 7.5%. This difference may be caused by the presence of the proteins within the vesicles reducing the number of particle: membrane interactions to occur and thus fewer pores within the membrane were formed. Alternatively, the presence of proteins in the vesicles may alter the vesicle stability, making them less susceptible to pore formation. Nevertheless, these results suggest that pore formation within the cell membrane is not the main mode of particle toxicity.

Nanoscale and micron sized alumina and CoCr particle interactions with the sBLM containing 20% (w/w) isolated membrane proteins was also explored. Due to low recovery rates from U937 histiocytes, only the proteins isolated from primary HFBs were tested. Again the results for the nanoscale and micron sized alumina and CoCr particles demonstrated no overall decrease in the frequency. Instead an increase in the dissipation was observed. As described above, these results were considered negative, with no or weak particle binding occurring in the presence of membrane proteins. The binding of particles, from THRs or commercially available nanoparticles, to a model membrane containing isolated primary HFBs has not been investigated in the literature, making comparisons difficult. As previously described, this phenomenon of an increase of dissipation observed in this current study has been reported by Karlsson *et al.* (2013). Using QCM-D, copper nanoparticles were washed across a simple lipid membrane, in the absence of membrane proteins, which caused an increase in dissipation. The authors did not explain why this occurred, but as described in this present study, concluded that particle binding had not occurred. Therefore other factors must be considered to determine the effect of alumina and CoCr particles on the cell plasma membrane.

4.4.5 Conclusion

This part of the study aimed to investigate the effect of nanoscale and micron sized alumina and CoCr particles on the cell plasma membrane. *In vitro* studies on the

effect of CoCr and alumina particles have failed to investigate the potential effects on the cell plasma membrane. This is particularly important as the interactions with the plasma membrane can determine downstream effects such as cell viability. Using a novel model lipid membrane, which was similar in composition to primary HFBs, it was revealed that the nanoscale and micron sized alumina and CoCr particles did not directly damage the model membrane, even in the presence of isolated membrane proteins from U937 histiocytes and primary HFBs. Furthermore, using the highly sensitivity technique of QCM-D, the nanoscale and micron sized alumina and CoCr particles induced an increase in the dissipation. Modelling of the frequency and dissipation using the Voight model did not reveal characteristic results for particles bound to the sBLM. These results were confirmed by SPR and the increases in dissipation for the QCM-D experiments were likely to be non-specific artefacts due to the sensitivity of QCM-D or minor alterations of the sBLM layer. Moreover, the incorporation of membrane proteins from primary HFBs into the model membrane also demonstrated that no particle binding occurred. Therefore this series of experiments have revealed that the particles did not bind to the sBLM or induce membrane damage detectable by these methods under the conditions used.

Chapter 5

The effect of serum proteins on the interaction of nanoscale and micron sized alumina and cobalt chromium particles with a model lipid membrane

5.1 Introduction

This part of the present study focused on the effect of serum proteins on particle interactions with a model lipid membrane. The results from the previous chapter demonstrated no or a weak interaction of the particles to a sBLM, even in the presence of isolated membrane proteins from primary HFBs or U937 histiocytes. To investigate further the effects of nanoscale and micron sized alumina and CoCr particles on the cell plasma membrane, other factors need to be considered. One such factor is the formation of a protein corona on the surface of the particles and its influence on particle toxicity. A protein corona is formed when proteins from the surrounding biological medium adhere to the particles (Rauch *et al.* 2013). The particles can potentially interact with a diverse range of biological molecules including proteins, receptors and glycoproteins. The bound proteins on the particle surface change the surface characteristics and in turn can alter the cellular response to the particles, such as cell viability, oxidative stress and genotoxic effects (Rauch *et al.* 2013).

The formation of a protein corona is likely to happen immediately after the release of the wear particles from the bearing surface and into the joint capsule (Catalani *et al.* 2011). Catalani *et al.* (2011) confirmed that chromium ions bind to human serum albumin (HSA) from patients with CoCr alloy THRs. Chromium (Cr^{3+}) and aluminium ions (Al^{3+}) have also been demonstrated to bind to transferrin (Vincent and Love 2012). Hence investigation into the effect of protein coronae on particle toxicity is

particularly relevant and further provides a greater understanding of *in vitro* cell viability studies on wear particles.

As yet, very few studies have investigated the role of proteins adsorbed on the surface of alumina and CoCr particles on the cell membrane and subsequent particle biocompatibility (Hallab *et al.* 2000; Lewis *et al.* 2007; Potnis *et al.* 2013). Lewis *et al.* (2007) compared the uptake of model CoCr particles into fibroblasts which had either been pre-incubated with HSA for 5 days or were pre-incubated for 1 hour in MEM only. After 48 hours, the particles incubated in MEM, prior to exposure to fibroblasts, were more likely to be internalised and induce single stranded DNA breaks. Hallab *et al.* (2000) demonstrated *in vitro* that CoCr model particles bound to high molecular weight proteins within human serum were more likely to induce lymphocyte proliferation in comparison to cells exposed to CoCr particles in the absence of serum. However, both these studies used micron sized model particles and therefore it is not known if this would occur for more clinically relevant nanoscale CoCr wear particles.

The occurrence of protein coronae is an area of interest within the field of nanotechnology (Dai *et al.* 2015). In order to improve the therapeutic effects of nanoparticles, particularly those used in medical applications, a number of studies have reported the role of protein coronae on particle toxicity which can reduce or increase potential particle toxicity. In addition these types of studies can provide useful indications on the potential cellular effects of protein coronae formed on the surface of the particles (Dai *et al.* 2015; Mirshafiee *et al.* 2015; Shang and Nienhaus 2015).

The formation of a protein corona on the particle surface is determined by a number of factors. These include the characteristics of the particles such as size, charge, shape and the proteins within the biological medium that the particles are exposed

to (Hu *et al.* 2014; Pozzi *et al.* 2015). Albumin is the most abundant protein in serum (55%) and *in vitro* cell studies on particle toxicity often use medium supplemented with 10% (v/v) FBS. Bovine serum albumin (BSA) has been reported to bind to model CoCr particles (Smith *et al.* 2004; Lewis *et al.* 2007; Vidal and Muñoz 2011). Alongside albumin, less abundant proteins such as immunoglobulins and growth factors are present within the serum (Rauch *et al.* 2013). Therefore, unless a free serum environment is specifically used for cell studies, it is presumed that the particles cultured with cells are coated with proteins. However this process is often not considered when determining mechanisms of particle toxicity on cells.

In vitro studies on the formation of a protein corona, using manufactured nanoparticles, have demonstrated a diverse range of cell responses (Deng *et al.* 2011; Fleischer and Payne 2014b; Hu *et al.* 2014; Borgognoni *et al.* 2015; Cheng *et al.* 2015; Duan *et al.* 2015; Landgraf *et al.* 2015; Mirshafiee *et al.* 2015). Indeed, the protein corona can influence particle uptake, for example the binding of BSA to graphene oxide nanoparticles has been reported to reduce the physical interaction and entry into A549 lung epithelial cells (Duan *et al.* 2015). However, the coating of serum albumin onto carbon nanoribbons was demonstrated to increase particle uptake into A549 lung epithelial cells (Mbeh *et al.* 2014). Other studies have demonstrated that protein coronae on titanium dioxide and gold nanoparticles can induce a greater detrimental effect on cell viability (Borgognoni *et al.* 2015; Cheng *et al.* 2015). In contrast, other studies have reported a reduced effect on cell viability of a variety of cell types cultured with metal nanoclusters, graphene oxide and iron oxide nanoparticles with bound proteins on the particle surface (Duan *et al.* 2015; Landgraf *et al.* 2015; Shang and Nienhaus 2015).

More specifically, studies investigating the effect of protein coronae on particle: membrane binding have reported conflicting results (Nel *et al.* 2009; Deng *et al.* 2011; Vincent and Love 2012; Lesniak *et al.* 2013; Fleischer and Payne 2014b; Hu

et al. 2014; Cheng *et al.* 2015; Duan *et al.* 2015; Mirshafiee *et al.* 2015). For example Lesniak *et al.* (2013) reported reduced binding of carboxylated polystyrene nanoparticles to a POPC sBLM in the presence of serum, using QCM-D techniques. The authors proposed that the formation of a protein corona shielded the binding sites in the membrane, thus reducing membrane: particle interactions. In contrast, fibrinogen coated gold nanoparticles were reported to increase the binding of particles to the integrin receptor Mac-1 in human promyelocytic leukaemia (HL-60), embryonic kidney (HEK293) and monocyte (THP-1) cell lines. It was suggested that the fibrinogen denatured onto the particle surface and increased the binding affinity to the Mac-1 receptor in the cell membrane (Deng *et al.* 2011).

The discrepancies between these studies mean forming conclusions about the influencing factors of particle binding and subsequent effects on cells is difficult. Especially as there is no standardisation of methods and it is unknown how much of an influence the use of different cell types and the formation of different protein coronae can have on particle interactions with the membrane and particle biocompatibility (Horie *et al.* 2009). Within the field of wear particle toxicity, the lack of evidence means that the effect of different joint replacement materials is unclear. Furthermore, current published literature on particle binding to the cell membrane using QCM-D techniques have used simple phospholipid membrane model (Lesniak *et al.* 2013). These membranes often only contain one type of phospholipid (usually POPC), which does not reflect the composition of a typical human cell plasma membrane. As previously described a plasma membrane contains multiple types of phospholipids and cholesterol as well as integrated membrane proteins (Voet *et al.* 2013). Therefore this part of the study aimed to use a model lipid membrane, also used in chapter four, to closely represent the structure of human fibroblast membranes (Schroeder *et al.* 1984; Mahadik *et al.* 1994). Furthermore, the integration of membrane plasma proteins isolated from primary HFBs would allow

the investigation into the role of membrane proteins on particle binding in the presence of FBS.

5.1.1 Aims and Objectives

The aim of this part of the study was to investigate if the addition of FBS with the nanoscale and micron sized alumina and cobalt chromium particles influences particle cytotoxicity and membrane interactions. In the first instance the effect of the presence or absence of 10% (v/v) FBS in the cell culture medium on L929 fibroblast viability was explored. Further the internalisation and localisation of alumina and CoCr in the presence or absence of FBS was investigated using TEM techniques. These experiments aimed to determine if the particles were internalised and if the particles are actively taken up within vesicles or distributed throughout the cytoplasm. More specifically the effect of the formation of a protein corona on particle interactions with a lipid model membrane, also used in Chapter four, was investigated. The effects of membrane proteins and protein corona formation on particle membrane binding were also explored. These experiments were designed to provide an insight into the factors influencing particle binding and uptake into cells, specifically fibroblasts, using a model of a human fibroblast cell.

5.1.2 Objectives

The specific objectives of this part of the study were as follows and are outlined in Figure 5.1:

- To investigate the effect of 10% (v/v) FBS on L929 fibroblast cell viability in the presence of nanoscale and micron sized alumina and CoCr particles

- To explore nanoscale alumina and CoCr particle uptake into L929 fibroblasts in the presence or absence of 10% (v/v) FBS using TEM techniques
- To assess the effects of nanoscale and micron sized alumina and CoCr particles on membrane integrity in the presence of 10% (v/v) FBS.
- To investigate the binding of nanoscale and micron sized alumina and CoCr particles to a model plasma membrane, in the presence of FBS, using QCM-D
- To explore the effect of incorporating of isolated membrane proteins into the model membrane on membrane damage caused by nanoscale and micron sized alumina and CoCr particles using vesicle leakage assays in the presence of 10% (v/v) FBS
- To explore the effect of incorporating isolated membrane proteins of primary HFBs into model membranes on nanoscale and micron sized alumina and CoCr particle binding using QCM-D in the presence of FBS

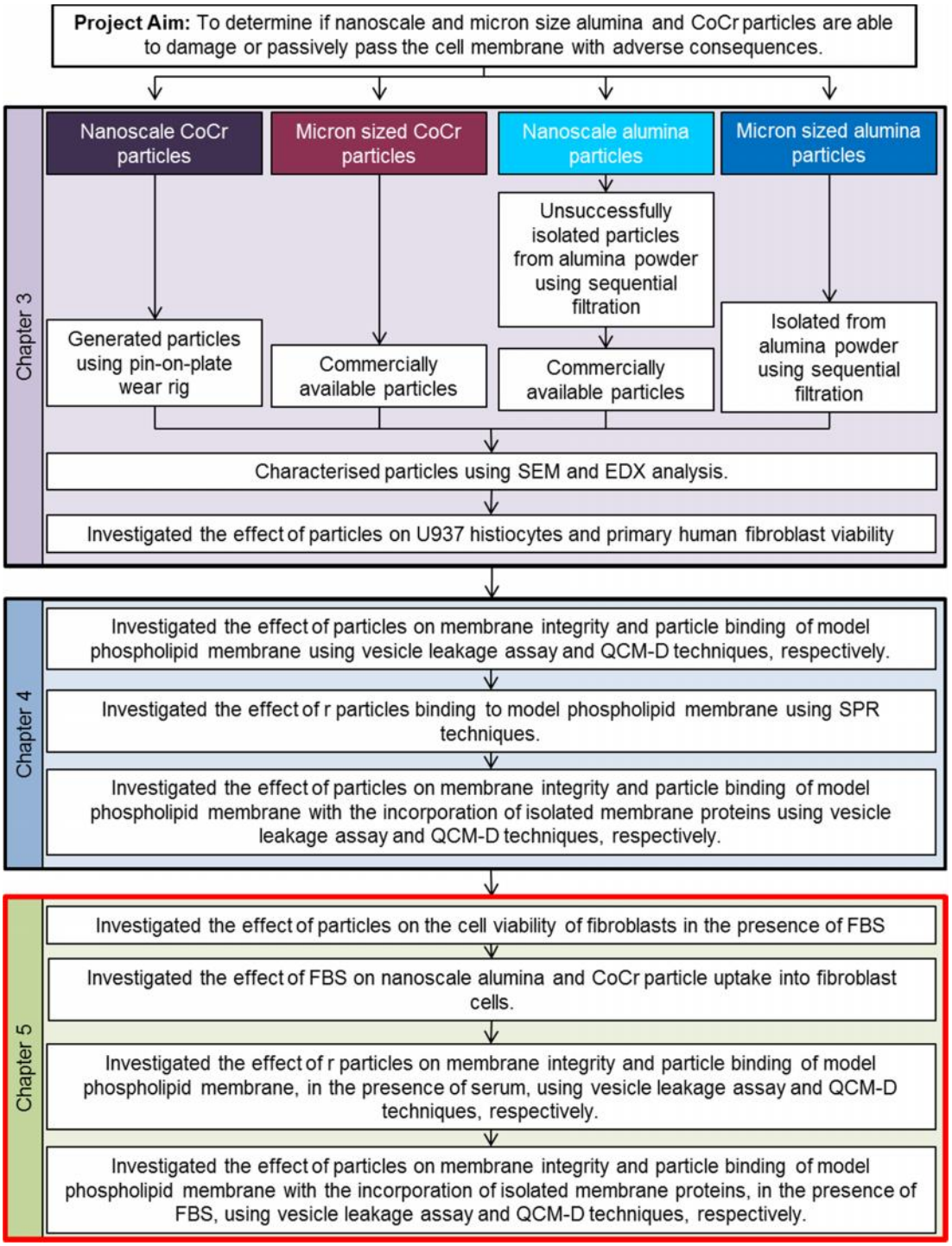

Figure 5.1 – Overview of project and outline of chapter five methods

5.2 Material and methods

5.2.1 Materials

Materials and equipment required for sample preparation for TEM analysis are listed in Table 5.1.

Table 5.1 – Materials and equipment used to prepare cell samples for transmission electron microscopy analysis

Chemical/ Material	Supplier
2, 4, 6-Tris (dimethylaminomethyl) phenol (DMP30) (R1065)	Agar Scientific, Stansted, U.K.
24 well flat cell culture plate (142475)	Thermofisher Scientific, Langenselbold, Germany.
Araldite resin (R1042)	Agar Scientific, Stansted, U.K.
Copper grids (200 nm grids) (AGG2710C)	Agar Scientific, Stansted, U.K.
Dental wax strips (AGG381)	Agar Scientific, Stansted, U.K.
Diamond blade (DiATOME 45° AGG339-8)	Agar Scientific, Stansted, U.K.
Dodecenylsuccinic anhydride (DDSA) (R1053)	Agar Scientific, Stansted, U.K.
EDX analysis system and software (Inca version 4.1)	Oxford Instruments, Abington, U.K.
Eppendorf centrifuge (5415R)	Eppendorf, Stevenage, U.K.
Ethanol (absolute) (64-17-5)	Sigma-Aldrich, Irvine, U.K.
Filter paper (1001090)	Whatman, Maidstone, U.K.
Glutaraldehyde (AGR1009)	Agar Scientific, Stansted, U.K.
Osmium tetraoxide (AGR1015)	Agar Scientific, Stansted, U.K.
Plate heater (AGG3328)	Agar Scientific, Stansted, U.K.

Chemical/ Material	Supplier
Polypropene oxide (R1080)	Sigma-Aldrich, Irvine, U.K.
Reynold's lead citrate (AGR1210)	Agar Scientific, Stansted, U.K.
Sodium hydroxide 1M (S/4920/60)	Fisher Scientific, Loughborough, U.K.
TEM (JEOL 1400)	Jeol, Peabody, U.S.A.
TEM for EDX analysis (Tecnai F20 TEM)	FEI, Hillsboro, USA.
Trichloroethylene (GPR 30497)	VWR Chemicals, Lutterworth, U.K.
Ultramicrotome (Reicher-Jung Microtome Ultracut E)	Leica Microsystems, Milton Keynes, U.K.
Ultramicrotome glass (for glass blades) (B329)	Agar Scientific, Stansted, U.K.
Uranyl acetate (AGR1260A)	Agar Scientific, Stansted, U.K.

5.2.1.1 Araldite resin for embedding of cell samples for transmission electron microscopy imaging

A volume of 27 ml of Araldite was added to 23 ml of dodecenylsuccinic anhydride (DDSA) in a clean 150 plastic pot and stirred carefully with a glass stirrer to avoid bubble formation. Once mixed, 1 ml of 2, 4, 6-Tris (dimethylaminomethyl) phenol (DMP30) was added and the resin was mixed thoroughly using a glass stirrer. The resin was placed into 20 ml glass vials and stored at 4°C for a maximum of 24 hours.

5.2.2 Methods

5.2.2.1 The effect of particles on L929 fibroblast cell viability in the absence or presence of 10% (v/v) foetal bovine serum

L929 fibroblasts were passaged and seeded into flat bottomed 96 well plates at a cell density of $1x10^5.ml^{-1}$ as described in section 2.2.4. After 16 hours, the cell culture medium was replaced with either DMEM with 10% (v/v) FBS or DMEM

without FBS. Two sets of each particle volume were made up in either DMEM with 10% (v/v) FBS or DMEM without FBS. The cells, with six replicates, were cultured with nanoscale or micron sized CoCr particles at particle volumes per cell of 50 μm^3, 5 μm^3, 0.5 μm^3, 0.05 μm^3 and 0.005 μm^3. For the nanoscale and micron sized alumina particles, the cells were cultured with particles at a particle volume per cell of 500 μm^3 50 μm^3, 5 μm^3, 0.5 μm^3 and 0.05 μm^3. Each particle suspension was sonicated immediately before 100 µl of the particle suspension was added to the cells. The negative control was cells in 200µl of the corresponding medium (DMEM with or without 10% (v/v) FBS) and the positive control was camptothecin at a final concentration of 2 $\mu g.ml^{-1}$. A particle only control was included which was the highest particle dose in the corresponding medium (DMEM with or without 10% (v/v) FBS) in the absence of cells. A blank was also included which was 200 µl of corresponding medium only (DMEM with or without 10% (v/v) FBS). Each treatment was repeated six times and the cells were cultured with the particles in 5% (v/v) CO_2 in air at 37^oC. The cell viability was assessed over 5 days at specific time points of day 0, 1, 2, 3 and 5. The cell viability was assessed using the MTT assay (section 2.2.5) and the experiment was repeated twice, with 6 replicates, to ensure repeatability.

5.2.2.2 Transmission electron microscopy analysis of L929 fibroblasts cultured with nanoscale alumina and cobalt chromium particles in the absence or presence of 10% (v/v) foetal bovine serum

The internalisation of nanoscale alumina and CoCr particles into L929 fibroblast cells was analysed using TEM techniques.

5.2.2.2.1 Culturing L929 fibroblasts with nanoscale alumina and CoCr particles in the absence or presence of 10% (v/v) foetal bovine serum

L929 fibroblasts were treated with trypsin and seeded onto a 24 well culture plate at a density of 2 x 10^4 cells.ml^{-1} as described in section 2.2.4. For each well, 500 µl of the cell suspension was added and were incubated at 37°C, 5% (v/v) CO_2 for 16 hours to allow the cells to adhere. The medium was then replaced with fresh DMEM medium either with or without 10% (v/v) FBS. Two sets of each particle volume were diluted in either DMEM supplemented with 10% (v/v) FBS or DMEM without FBS. The cells were cultured with nanoscale CoCr particles at a particle volume per cell of 50 μm^3, 5 μm^3 and 0.5 μm^3. For the nanoscale alumina particles, the cells were cultured with particles at a particle volume per cell of 50 μm^3 and 5 μm^3. Each particle suspension was sonicated immediately before 500 µl of the appropriate particle suspension was added to the corresponding wells.

Based upon the cell viability results, after 48 hours, the cells cultured with nanoscale CoCr particles were treated with trypsin. After 5 days, cells cultured with nanoscale alumina particles were treated with trypsin to remove the cells from the cell culture plate. The medium from all wells were removed and discarded and the cells were washed twice with 500 µl of DPBS before being incubated with 250 µl of trypsin. The plates were incubated at 5% (v/v) CO_2 in air at 37^{o}C for ten minutes. DMEM was then added to each well (750 µl) and the cell suspension of each well was transferred to separately labelled, sterile 1.5 ml Eppendorfs and centrifuged at 200 g for 10 minutes at room temperature. A volume of 500 µl of DPBS was carefully added to each Eppendorf in order to not disturb the pellet prior to fixation.

5.2.2.2.2 Fixation of L929 fibroblasts cultured with nanoscale alumina and cobalt chromium particles

The samples from section 5.2.2.2.1 were fixed with 2.5% (v/v) glutaraldehyde in 0.1M phosphate buffer for 2.5 hours at room temperature. Using a glass pipette, the glutaraldehyde was removed and discarded and the pellets were incubated with 0.1M phosphate buffer for 30 minutes. The pellets were then centrifuged at 200 g for 2 minutes before 0.5 ml of 1% osmium tetraoxide in 0.1M phosphate buffer was added to each sample (made in house by Mr. M. Fuller, Faculty of Biological Sciences). After 1 hour, the cells were centrifuged at 200 g for 2 minutes and the osmium tetraoxide solution was replaced with 0.5 ml of 0.1M phosphate buffer. After 20 minutes, the phosphate buffer was removed and discarded and the samples were dehydrated by incubating the samples with 0.5 ml of increasing concentrations of ethanol; 20%, 40%, 60%, 80% and 100% (v/v) for 20 minutes each. The 100% (v/v) ethanol wash was repeated to ensure complete sample dehydration.

The samples were then embedded in an Araldite resin (section 5.2.1.1). Each sample was incubated with 0.5 ml of 50:50 Araldite: propylene oxide mixture and incubated for 16 hours at room temperature. The 50:50 resin was then removed, using a glass Pasteur pipette and replaced with 0.5 ml of 75:25 Araldite: propylene oxide solution for 3 hours. The 75:25 Araldite: propylene oxide solution was carefully removed by pouring off the excess and replaced with approximately 1 ml of neat Araldite resin. Leaving the lids of the Eppendorfs open, the samples were incubated for 3 hours at room temperature. The excess resin was poured off each sample and replaced with fresh Araldite resin. The samples were placed in a 60°C oven for 16 hours to fix the samples.

5.2.2.2.3 Sectioning of fixed L929 fibroblasts cultured with nanoscale alumina and cobalt chromium particles

The resin embedded samples (section 5.2.2.2.2) were then sectioned and placed onto copper grids for TEM analysis. The samples were prepared using a saw and filed to fit into the nuck of the microtome and were secured into position using a screw (Figure 5.2). A glass blade with a 45° angle blade (made in house by Mr. M. Fuller, Faculty of Biological Sciences) was secured into position in the blade holder of the microtome and thin sections, 0.5 µm thick, were cut until the sample within the resin was exposed (Figure 5.3A). Using a glass blade, with an attached boat to collect the sections, the sample was aligned with the blade and the boat was filled level with distilled water (Figure 5.3B).

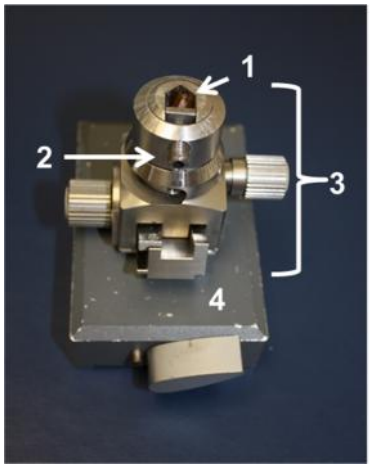

Figure 5.2 – Resin embedded sample secured into the nuck of microtome for sectioning. 1 – Resin embedded sample. 2 – Screw to secure sample to nuck. 3 – Nuck of the microtome. 4 – Nuck holder.

The automatic sectioning dial was selected and approximately 15 sections, 90 nm thick were cut. To reduce wrinkling of the sections a wooden dowel rod was soaked in trichloroethylene and the dowel rod was gently wafted over the samples in the boat. Using a pair of tweezers, a 5 mm round copper grid (200 nm grid size) was placed on to the surface of the water in the boat and the sections transferred from

the water to the grid. The grid was then placed sample side up onto a piece of filter paper. The samples were stored in a sample holder, at room temperature until required

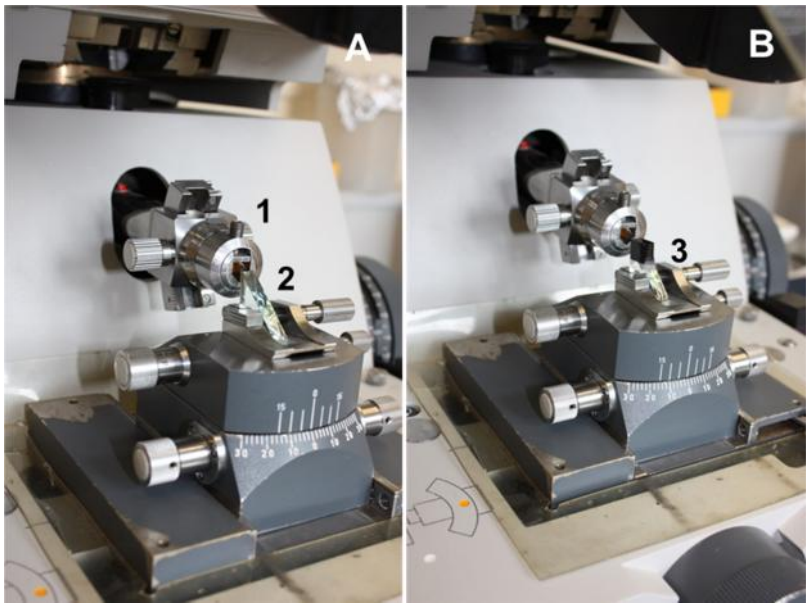

Figure 5.3 – Resin embedded sample in microtome with glass blade (A) and glass blade with attached boat (B). 1 – Secured sample in nuck of microtome. 2 – Glass blade in knife holder. 3 – Glass blade with boat to collect samples.

5.2.2.2.4 Contrast staining of transmission electron microscopy samples

To prepare the samples for TEM analysis, the sample grids were contrast stained with uranyl acetate and lead citrate. On the designated radiation bench, a drop of saturated uranyl acetate (made in house by Mr. M. Fuller, Faculty of Biological Sciences) per sample grid was placed onto a piece of dental wax strip. Using tweezers, each sample grid was placed on the uranyl acetate drop with the sample side in contact with the drop. After 2 hours, the grids were gently rinsed in distilled water and placed face down, on a drop of Reynold's lead citrate on a piece of wax in a glass petri dish (made in house by Mr. M. Fuller, Faculty of Biological Sciences). To reduce the lead citrate deposits, a small volume of 1M NaOH was added to the petri dish to surround the piece of wax. After 20 minutes, the sample grids were rinsed with 0.2M NaOH, followed by a final rinse in distilled water. The excess water

was blotted onto a small piece of filter paper and the samples were stored in a sample holder until required.

5.2.2.2.5 Transmission electron microscopy imaging and energy-dispersive X-ray spectroscopy analysis of L929 fibroblasts cultured with nanoscale alumina and cobalt chromium particles

The samples were visualised using a JEOL 1400 TEM at 120 kV at magnifications ranging from 1K to 5.5K. To differentiate between staining artefacts and particles, pin point EDX analysis was performed using a Tecnai F20 TEM and Oxford Instrument EDX system with the sample grid placed at a 15° tilt. The TEM images were used to size the particle agglomerates within the cells. The computer software, Image Pro Plus (version 6.1) was used. The means of the particle agglomerate at different concentrations, in the presence or absence of 10% (v/v) FBS were analysed using a one-tailed student's t-test.

5.2.2.3 The effect of particles on the vesicle leakage of a model lipid plasma membrane in the presence of 10% (v/v) foetal bovine serum

Vesicle leakage assays in the presence of 10% (v/v) FBS were performed. The 400 nm carboxylfluorescein loaded lipid vesicles were prepared as described in chapter 2, section 2.2.6.3. The leakage of the vesicles over time was monitored using a fluorometer as described in section 2.2.6.3 except that prior to the addition of the particles, 10% (v/v) FBS was added to the cuvette and the fluorescence was measured. Each vesicle leakage experiment was repeated three times. A paired t-test was performed on the results between each treatment group and 10% (v/v) FBS only to determine statistical significance ($p<0.05$).

5.2.2.4 The effect of particles on the vesicle leakage of a model lipid plasma membrane containing isolated plasma membrane proteins in the presence of 10% (v/v) foetal bovine serum

Plasma membrane proteins from primary HFBs and U937 histiocytes were isolated as described in section 2.2.6.5. Optimisation experiments from section 4.3.4.1 determined that a concentration of 20% (w/w) protein within the lipid membrane formed a stable bilayer for QCM-D experiments and was used for all subsequent studies, including the vesicle leakage assays performed here. The vesicle leakage assays were performed as described in section 5.2.2.3; however the vesicles consisted of phospholipids, cholesterol and 20% (w/w) of the isolated membrane proteins as described in section 2.2.6.2.

5.2.2.5 Quenching effect of particles on the vesicle leakage assay in the presence of 10% (v/v) serum

The vesicle leakage assays were performed as described in section 2.2.6.3. However, once the fluorescence of the diluted vesicles had been monitored for at least 200 seconds, 10% (v/v) of FBS diluted in DMEM without phenol red was added and the fluorescence was measured. An average absorbance reading over at least 200 seconds for each particle concentration was calculated and presented as a percentage of the reading for the Triton X-100.

5.2.2.6 Investigation into the binding of particles to a solid supported bilayer lipid membrane using quartz crystal microbalance with dissipation in the presence of foetal bovine serum

The binding of nanoscale and micron sized alumina and CoCr particles to a lipid membrane (used in Chapter four) in the presence of FBS was measured using

QCM-D. Foetal bovine serum was demonstrated to have a high binding affinity to the sBLM. Therefore, in order to measure any small interactions of the particles to the sBLM, the concentration of FBS diluted in DMEM was optimised.

5.2.2.7 Optimising the concentration of foetal bovine serum for quartz crystal microbalance with dissipation

The vesicles and QCM-D crystals were prepared as described in section 2.2.6.3 and 2.2.6.4, respectively. Upon the formation of a sBLM, as described in section 2.2.6.4, the starting solution of DMEM was replaced with DMEM supplemented with 0.1% (v/v) or 10% (v/v) FBS. The change in the frequency and dissipation were measured to determine if the measurements stabilised.

5.2.2.8 The binding of particles to a solid supported bilayer lipid membrane in the presence of 0.1% (v/v) foetal bovine serum

Prior to the QCM-D experiment the particles of choice were incubated with DMEM supplemented with 0.1% (v/v) FBS at particle concentrations of 1 $\mu g.ml^{-1}$, 10 $\mu g.ml^{-1}$ and 100 $\mu g.ml^{-1}$. These solutions were then incubated at 37°C for 16 hours. The sBLM was formed for the QCM-D experiment as described in section 2.2.6.4. Once the bilayer had been formed, the starting solution of DMEM was replaced with DMEM supplemented with 0.1% (v/v) FBS. Once the readout had stabilised, the particles were added. The particle concentrations of 1, 10 and 100 $\mu g.ml^{-1}$ diluted in DMEM supplemented with 0.1% (v/v) FBS was flowed across the sBLM for at least 25 minutes. Following this, DMEM supplemented with 0.1% (v/v) FBS was flowed across the sBLM for at least 25 minutes to wash away any unbound particles.

5.2.2.9 The binding of particles to a solid supported bilayer lipid membrane containing isolated plasma membrane proteins in the presence of 0.1% (v/v) foetal bovine serum

Plasma membrane proteins from primary HFBs were isolated as described in section 2.2.6.5. Optimisation experiments from section 4.3.4.1 determined that a concentration of 20% (w/w) of the protein within the lipid membrane formed a stable bilayer for QCM-D and was used for all studies. The QCM-D experiments were performed as described in section 2.2.6.4; however the vesicles, which formed the sBLM, consisted of lipids, cholesterol and 20% (w/w) of the isolated membrane proteins as described in section 2.2.6.7.

5.3 Results

5.3.1 The effect of the presence of foetal bovine serum on particle cell viability

The aim of this part of the study was to investigate the role of proteins within FBS on the effect of nanoscale and micron sized alumina and CoCr particles on the cell viability of L929 fibroblasts. This work followed on from an undergraduate student final year project (Moisley 2014).

.

5.3.1.1 The effect of nanoscale and micron sized alumina particles on L929 fibroblast cell viability in the absence or presence of foetal bovine serum

In the presence of 10% (v/v) FBS, only the nanoscale alumina particles at a particle volume of 500 μm^3 per cell caused a significant reduction in the cell viability at day 2 and 5 in the presence of FBS in comparison to the cell only control (Figure 5.4A). No other particle volume induced a significant effect on cell viability. In contrast, in the absence of 10% (v/v) FBS, by day 5 of culture, the nanoscale alumina particles induced a significant decrease in cell viability at the highest particle volumes of 500 and 50 μm^3 per cell in comparison to the cell only control (Figure 5.4B). Comparisons of the cell viability results in the absence or presence of 10% (v/v) FBS was performed (Table 5.2). The analysis revealed that in the absence of 10% (v/v) FBS the particle volumes of 500 and 50 μm^3 per cell significantly reduced the cell viability in comparison to cells cultured in the presence of FBS at equivalent particle doses after 3 days of culture. A statistically significant difference was measured for the particle volume of 500 μm^3 per cell after 2 days of culture.

After 5 days of culture, the micron sized alumina particles significantly reduced cell viability, in the presence of 10% (v/v) FBS at particle volumes of 500 and 50 μm^3 per cell in comparison to the cell only control (Figure 5.5A). A 15% and 18% loss in cell viability in comparison to the cell only control was measured at day 5 for the particle volumes of 500 and 50 μm^3 per cell, respectively. In the absence of 10% (v/v) FBS, the micron sized alumina particles had a larger effect on the cell viability in comparison to the cell only control. At the particle volumes of 500 and 50 μm^3 per cell, a 42% and 35% reduction in cell viability was observed after day 1, respectively (Figure 5.5B). The cell viability results in the presence or absence of 10% (v/v) FBS were compared (Table 5.3). After 1 day of culture the particle volumes of 500 and 50 μm^3 per cell significantly reduced the cell viability in the absence of FBS in comparison to cells cultured in the presence of FBS with the corresponding particle doses. This significant difference was observed over the 5 days of culture.

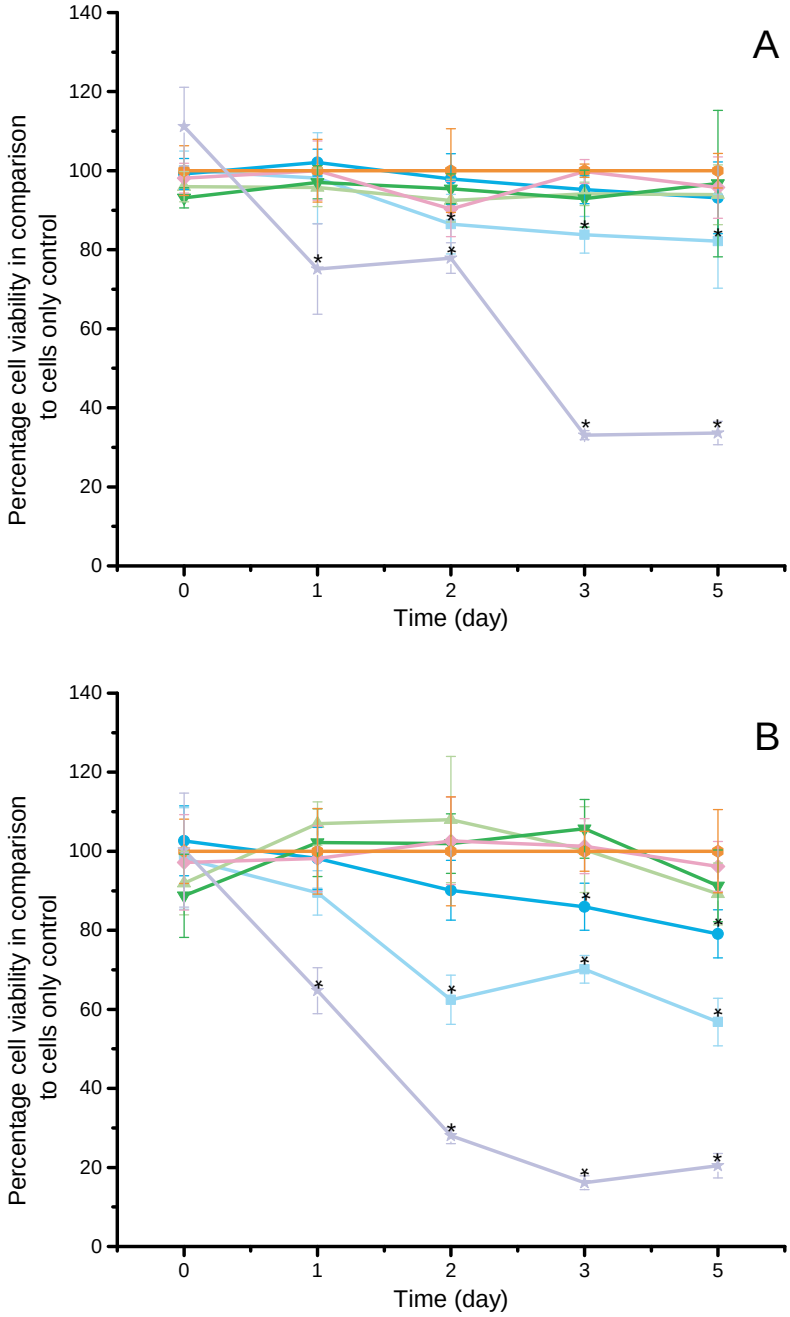

Figure 5.4 - The effect of nanoscale alumina particles on L929 cell viability in the presence (A) or absence (B) of 10% (v/v) foetal bovine serum using the MTT assay. Cell viability is presented as percentage viability in comparison to the cell only control. One-way ANOVA tests were performed and the MSD was calculated using the Tukey method. The mean (+/- 95% CL) was plotted (n=6) and statistically significant results ($p<0.05$) are indicated by an asterisk (*). (■: 500 μm^3 per cell; ●: 50 μm^3 per cell; ▲: 5 μm^3 per cell; ▼: 0.5 μm^3 per cell; ♦: 0.05 μm^3 per cell; ●: cell only control; ★: 2 $\mu g.ml^{-1}$ camptothecin).

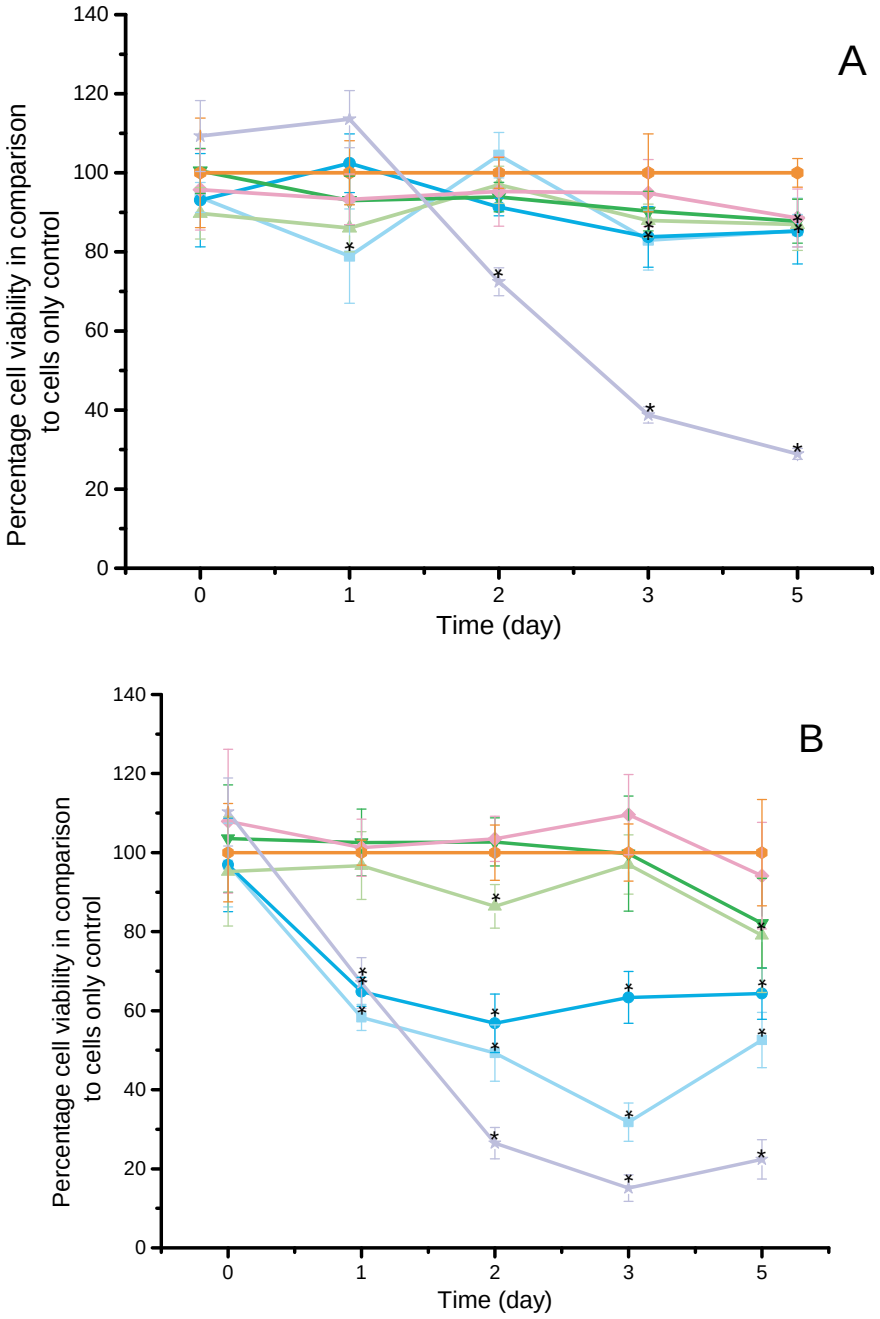

Figure 5.5 - The effect of micron sized alumina particles on L929 cell viability in the presence (A) or absence (B) of 10% (v/v) foetal bovine serum using the MTT assay. Cell viability is presented as percentage viability in comparison to the cell only control. One-way ANOVA tests were performed and the MSD was calculated using the Tukey method. The mean (+/- 95% CL) was plotted (n=6) and statistically significant results ($p<0.05$) are indicated by an asterisk (*). (■: 500 μm^3 per cell; ●: 50 μm^3 per cell; ▲: 5 μm^3 per cell; ▼: 0.5 μm^3 per cell; ♦: 0.05 μm^3 per cell; ●: cell only control; ★: 2 $\mu g.ml^{-1}$ camptothecin).

	Particle volume (μm^3 per cell)				
Time (day)	**500**	**50**	**5**	**0.5**	**0.05**
0	-	-	-	-	-
1	-	-	-	-	-
2	+	-	-	-	-
3	+	+	-	-	-
5	+	+	-	-	-

Table 5.2 – Statistical analysis on the effect of nanoscale alumina particles on L929 cell viability in the presence or absence of 10% (v/v) foetal bovine serum. A two way ANOVA were performed and the MSD was calculated using the Tukey method. Statistically significant results ($p<0.05$) are indicated by a plus sign (+). A red plus sign (+) indicated that the results in the presence of 10% (v/v) FBS induced a statistically significant reduction in the cell viability in comparison to the cells in the absence of FBS. A green plus sign (+) indicated that the results in the absence of 10% (v/v) FBS induced a statistically significant reduction in the cell viability in comparison to the cells in the presence of FBS.

	Particle volume (μm^3 per cell)				
Time (day)	**500**	**50**	**5**	**0.5**	**0.05**
0	-	-	-	-	-
1	+	+	-	-	-
2	+	+	-	-	-
3	+	+	-	-	-
5	+	+	-	-	-

Table 5.3 – Statistical analysis on the effect of micron size alumina particles on L929 cell viability in the presence or absence of 10% (v/v) foetal bovine serum. A two way ANOVA were performed and the MSD was calculated using the Tukey method. Statistically significant results ($p<0.05$) are indicated by a plus sign (+). A red plus sign (+) indicated that the results in the presence of 10% (v/v) FBS induced a statistically significant reduction in the cell viability in comparison to the cells in the absence of FBS. A green plus sign (+) indicated that the results in the absence of 10% (v/v) FBS induced a statistically significant reduction in the cell viability in comparison to the cells in the presence of FBS.

5.3.1.2 The effect of nanoscale and micron sized cobalt chromium particles on L929 fibroblast cell viability in the absence or presence of foetal bovine serum

In the presence of 10% (v/v) FBS, the nanoscale CoCr particle volumes of 50, 5 and 0.5 μm^3 per cell had a significant effect on the cell viability after 2 days of culture in

comparison to the cell only control (Figure 5.6A). After 5 days of culture only the highest particle volume of 50 μm^3 per cell induced a statistically significant reduction in the cell viability in comparison to the cell only control. In the absence of 10% (v/v) FBS, only the particle volume of 50 μm^3 per cell caused a significant reduction in the cell viability in comparison to the cell only control, with an average 25% loss in cell viability over the 5 days of culture (Figure 5.6B). A statistically significant difference between cells cultured with nanoscale CoCr particles in the presence of 10% (v/v) FBS in comparison to cells cultured with the CoCr particles in the absence of FBS was measured. After 1 day of culture the particle volume of 5 μm^3 per cell, in the presence of FBS induced a significant reduction in cell viability in comparison to cells cultured in the absence of FBS. After 2 days of culture the particle volume of 50 μm^3 per cell significantly reduced the cell viability in the presence of FBS in comparison to cells cultured in the absence of FBS at the corresponding particle doses. The difference between the cell viability results in the presence or absence of 10% (v/v) FBS was not statistically significant after 2 days of culture (Table 5.4).

There was minimal difference in the results for L929 fibroblasts cultured with CoCr micron sized particles in the presence or absence of 10% (v/v) FBS. In the presence of 10% (v/v) FBS, only the highest particle volume of 50 μm^3 per cell induced a 35% reduction in the cell viability after 2 days in comparison to the cell only control (Figure 5.7A). However by day 3, no significant difference was measured. Similarly, in the absence of 10% (v/v) FBS the only particle volume of 50 μm^3 per cell caused a 40% loss in the cell viability by day 2. Again, by day 3 this particle volume had no significant effect on the cell viability (Figure 5.7B). No statistical difference between cells cultured with the micron CoCr particles in the presence or absence of 10% (v/v) FBS was observed at any time point (Table 5.5).

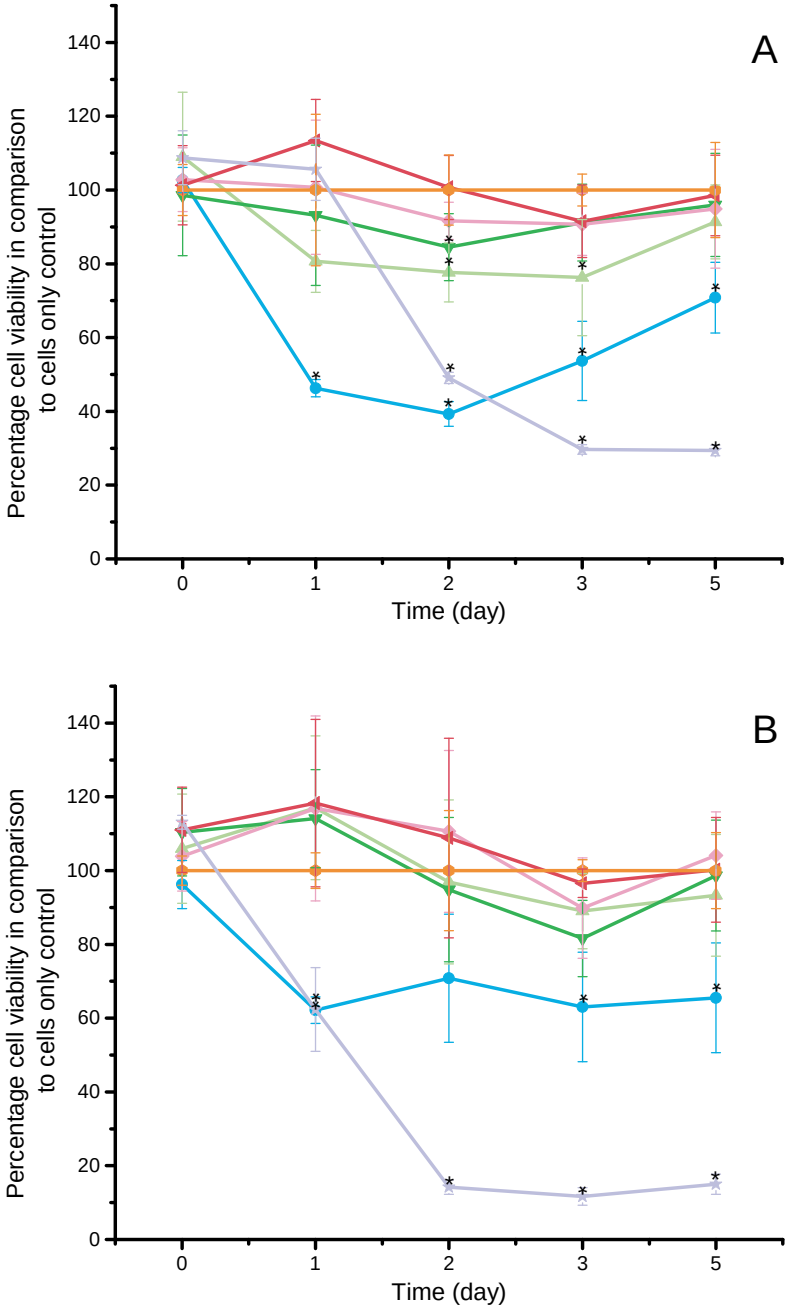

Figure 5.6 - The effect of nanoscale CoCr particles on L929 cell viability in the presence (A) or absence (B) of 10% (v/v) foetal bovine serum using the MTT assay. Cell viability is presented as percentage viability in comparison to the cell only control. One-way ANOVA tests were performed and the MSD was calculated using the Tukey method. The mean (+/- 95% CL) was plotted (n=6) and statistically significant results ($p<0.05$) are indicated by an asterisk (*). (●: 50 μm^3 per cell; ▲: 5 μm^3 per cell; ▼: 0.5 μm^3 per cell; ♦: 0.05 μm^3 per cell; ◄: 0.005 μm^3 per cell; ●: cell only control; ★: 2 $\mu g.ml^{-1}$ camptothecin).

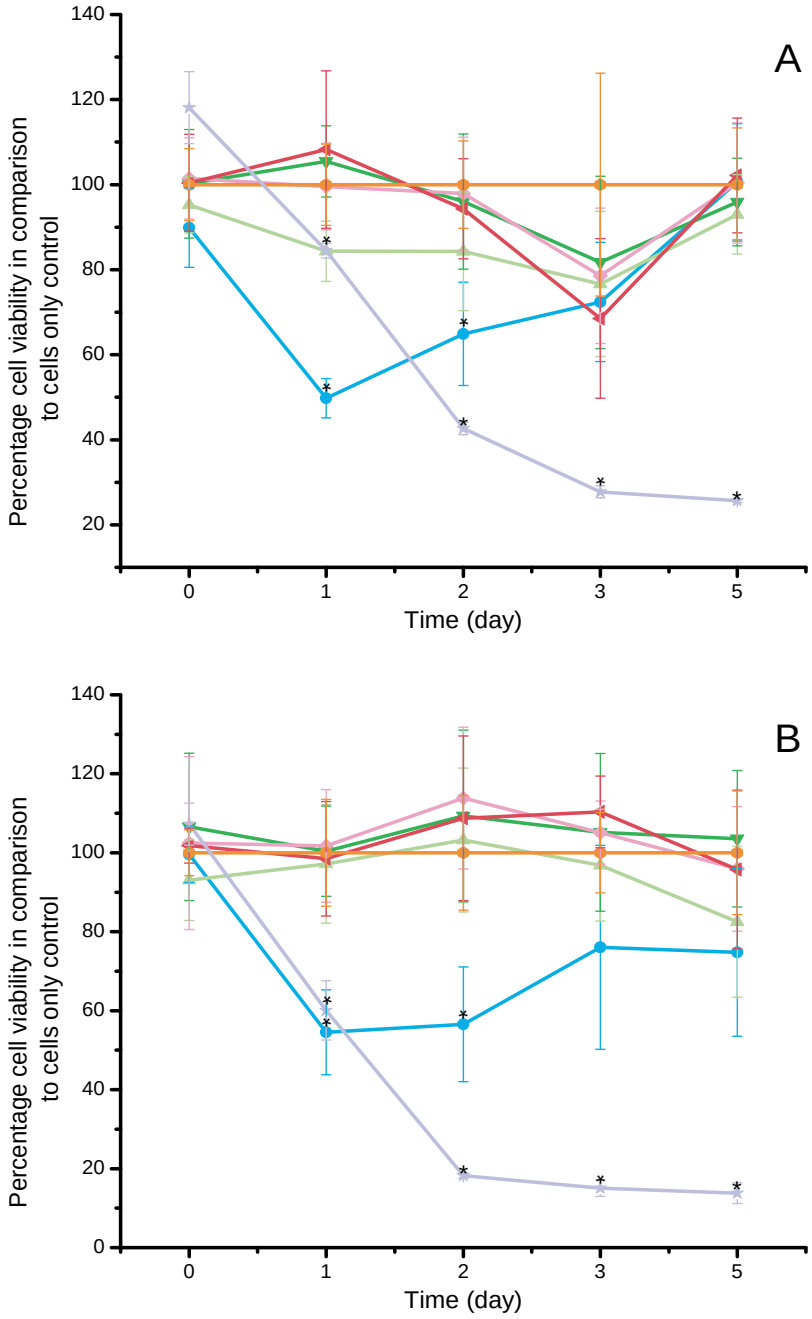

Figure 5.7 - The effect of micron sized CoCr particles on L929 cell viability in the presence (A) or absence (B) of 10% (v/v) foetal bovine serum using the MTT assay. Cell viability is presented as percentage viability in comparison to the cell only control. One-way ANOVA tests were performed and the MSD was calculated using the Tukey method. The mean (+/- 95% CL) was plotted (n=6) and statistically significant results ($p<0.05$) are indicated by an asterisk (*). (●: 50 μm^3 per cell; ▲: 5 μm^3 per cell; ▼: 0.5 μm^3 per cell; ♦: 0.05 μm^3 per cell; ◄: 0.005 μm^3 per cell; ●: cell only control; ★: 2 $\mu g.ml^{-1}$ camptothecin).

	Particle volume (μm^3 per cell)				
Time (day)	**50**	**5**	**0.5**	**0.05**	**0.005**
0	**-**	**-**	**-**	**-**	**-**
1	**-**	**+**	**-**	**-**	**-**
2	**+**	**-**	**-**	**-**	**-**
3	**-**	**-**	**-**	**-**	**-**
5	**-**	**-**	**-**	**-**	**-**

Table 5.4 – Statistical analysis on the effect of nanoscale cobalt chromium particles on L929 cell viability in the presence or absence of 10% (v/v) foetal bovine serum. A two way ANOVA were performed and the MSD was calculated using the Tukey method. Statistically significant results ($p<0.05$) are indicated by a plus sign (+). A red plus sign (+) indicated that the results in the presence of 10% (v/v) FBS induced a statistically significant reduction in the cell viability in comparison to the cells in the absence of FBS. A green plus sign (+) indicated that the results in the absence of 10% (v/v) FBS induced a statistically significant reduction in the cell viability in comparison to the cells in the presence of FBS.

	Particle volume (μm^3 per cell)				
Time (day)	**50**	**5**	**0.5**	**0.05**	**0.005**
0	**-**	**-**	**-**	**-**	**-**
1	**-**	**-**	**-**	**-**	**-**
2	**-**	**-**	**-**	**-**	**-**
3	**-**	**-**	**-**	**-**	**-**
5	**-**	**-**	**-**	**-**	**-**

Table 5.5 – Statistical analysis on the effect of micron sized cobalt chromium particles on L929 cell viability in the presence or absence of 10% (v/v) foetal bovine serum. A two way ANOVA were performed and the MSD was calculated using the Tukey method. Statistically significant results ($p<0.05$) are indicated by a plus sign (+). A red plus sign (+) indicated that the results in the presence of 10% (v/v) FBS induced a statistically significant reduction in the cell viability in comparison to the cells in the absence of FBS. A green plus sign (+) indicated that the results in the absence of 10% (v/v) FBS induced a statistically significant reduction in the cell viability in comparison to the cells in the presence of FBS.

5.3.2 The internalisation of nanoscale alumina and cobalt chromium particles into L929 fibroblasts in the absence or presence of foetal bovine serum

The internalisation and localisation of nanoscale alumina and CoCr particles in the presence or absence of FBS into L929 fibroblasts was investigated using TEM analysis. Due to time constraints only the nanoscale particles were tested.

5.3.2.1 Internalisation of nanoscale alumina particles into L929 fibroblasts in the absence or presence of foetal bovine serum

Based on the cell viability results (section 5.3.1) the time point of 5 days was chosen. Nanoscale alumina particles were observed within the L929 cells at all particle concentrations regardless of the presence of 10% (v/v) FBS. For the cells cultured with nanoscale alumina particles at a particle volume of 50 μm^3 per cell in the presence of serum, agglomerates of particles were observed. These agglomerates appeared to be in vesicle or vesicle-like structures with in the cytoplasm of the cells (Figure 5.8A and B). On occasion some of the particles within vesicles surrounded the nuclear membrane as shown in Figure 5.8B. Few particles were detected within the cells cultured with alumina particles at a particle volume of 5 μm^3 per cell in the presence of serum. However, some particles were observed within vesicles of the cytoplasm (Figure 5.8C and D). No particles were observed in the cell only controls (Figure 5.8E and F).

In the absence of 10% (v/v) FBS, nanoscale alumina particles were also detected within the cells as shown by the white arrows in Figure 5.9. Again the particles at all concentrations were observed in vesicles within the cytoplasm. The particles appeared as agglomerates within the vesicles. However at the particle volumes of 5 μm^3 per cell the particles were much less prevalent within the cells (Figure 5.9C and

D). No particles were observed within the cell only controls (Figure 5.9E and F). The TEM images were used to measure the diameters of the particle agglomerates within the cells (Figure 5.9). A large variation in the sizes of the particle agglomerates at any particle concentration, in the presence or absence of 10% (v/v) FBS was observed. The largest particle agglomerate of 2 µm was measured for the particles incubated in the absence of 10% (v/v) FBS at a particle volume of 5 μm^3 per cell. No statistical differences were observed between the particle agglomerate sized within the cells in the presence or absence of 10% (v/v) FBS at any particle volume tested. In addition, no statistical differences were measured between the different particle volumes used.

The presence of the alumina nanoscale particles was confirmed by EDX analysis as shown by the white arrows in Figure 5.11. Only particle like structures within vesicles were confirmed as containing alumina. The aluminium peak can clearly be observed within the EDX spectra (Figure 5.11A, spectra 1 and 2). Particle like structures which were not bound within vesicles were found to be remnants of the staining process during sample preparation (Figure 5.11B, spectrum 3). No aluminium peak was observed in the EDX spectrum; instead, the main elements detected included copper (grid material) and silica.

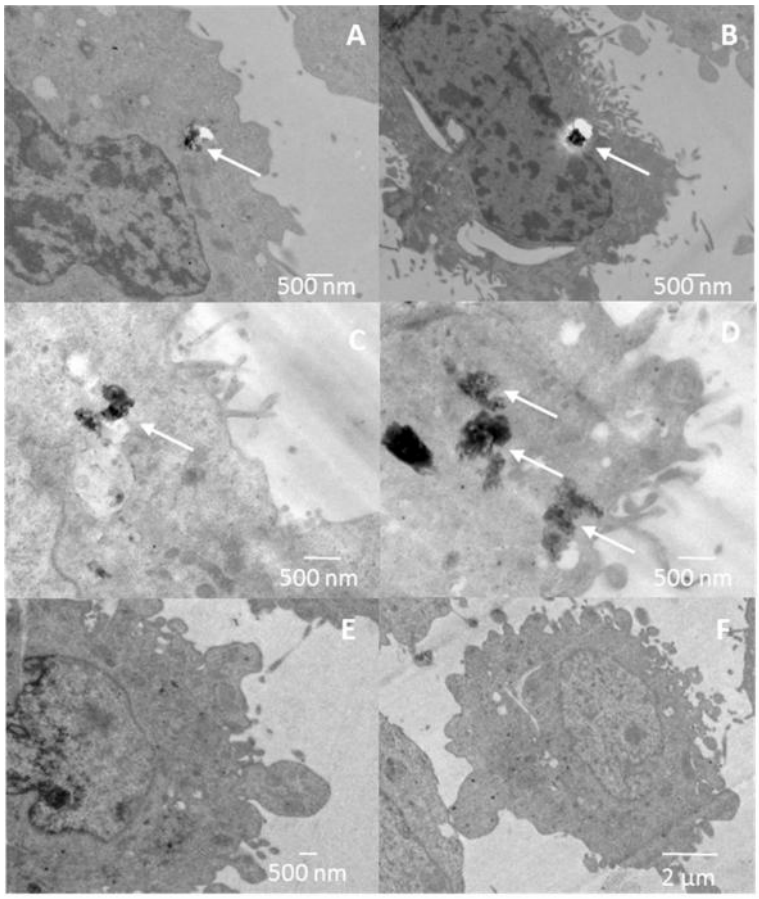

Figure 5.8 – Transmission electron microscopy analysis of alumina nanoscale particles within L929 fibroblasts cultured in the presence of foetal bovine serum. Cells were cultured in the presence of 10% (v/v) FBS and nanoscale alumina particles at particles volumes of 50, 5 and 0.5 µm^3 per cell for 5 days. Arrows indicate particles within cells. A & B – 50 µm^3 per cell. C & D – 5 µm^3 per cell. E & F – Cell only control.

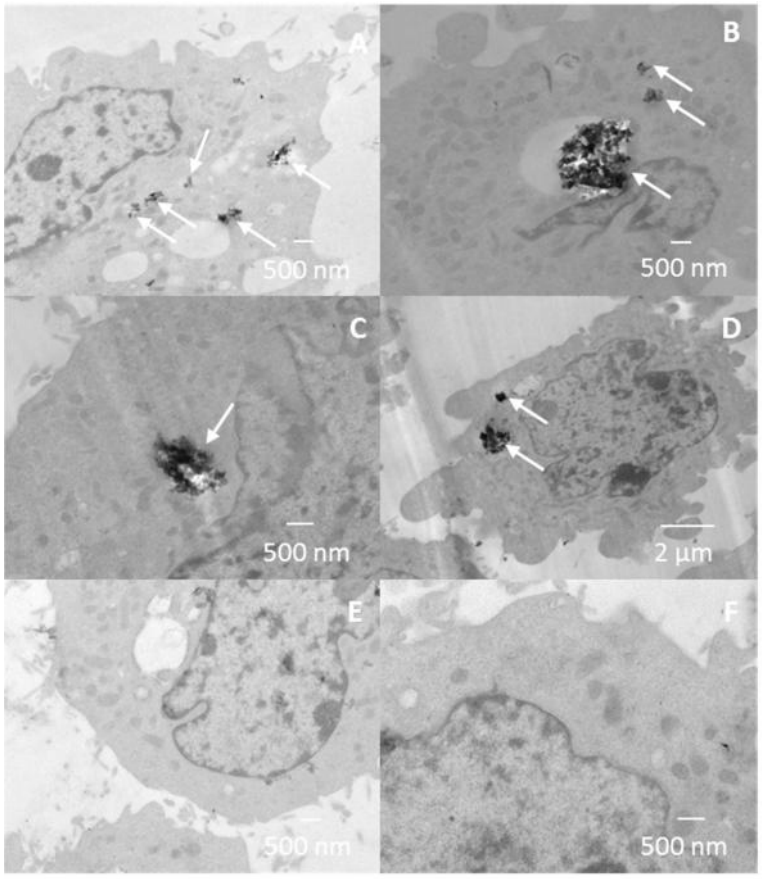

Figure 5.9 – Transmission electron microscopy analysis of nanoscale alumina particles within L929 fibroblasts cultured in the absence of foetal bovine serum. Fibroblast cells were cultured in the absence of 10% (v/v) FBS with nanoscale alumina particles at particles volumes of 50, 5 μm^3 per cell for 5 days. Arrows indicate particles within cells. A & B – 50 μm^3 per cell. C & D – 5 μm^3 per cell. E & F – Cell only control.

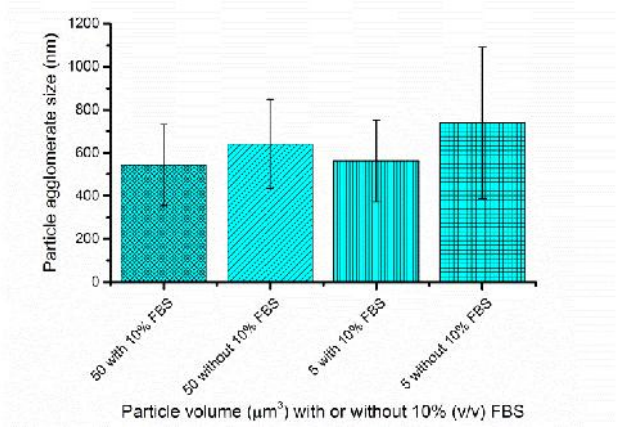

Figure 5.10 – Sizing of nanoscale alumina particle agglomerates within L929 fibroblasts. Alumina particle agglomerates within the L929 fibroblasts were sized using the corresponding TEM images and the computer software Image Pro Plus (version 6.1). Error bars represent 95% CI levels.

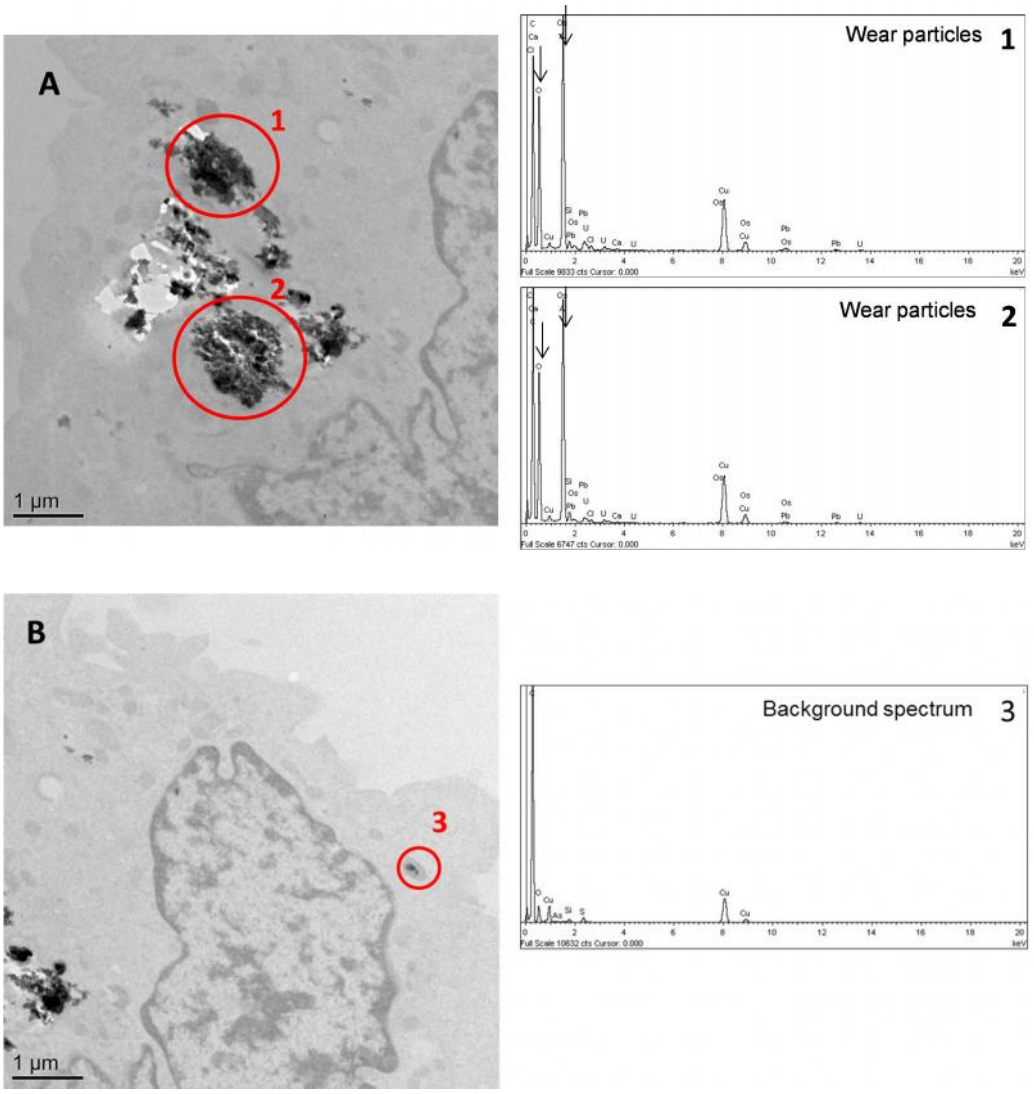

Figure 5.11 – Energy-dispersive X-ray spectroscopy of nanoscale alumina particles. L929 fibroblasts were cultured with 10% (v/v) FBS and nanoscale alumina particles at a particle volume of 50 µm^3 per cell (A) or 50 µm^3 per cell (B) for 5 days. Confirmation of particles was performed using the INCA EDX analysis system and the Tecnai F20 TEM. Example EDX plots (1 & 2) of particles within vesicles and corresponding image are displayed. Major peaks of aluminium and oxygen are indicated by black arrows. Example EDX plots (3) of staining precipitates and corresponding image is also displayed.

5.3.2.2 Internalisation of nanoscale cobalt chromium particles into L929 fibroblasts in the absence or presence of foetal bovine serum

The internalisation and localisation of nanoscale CoCr particles into L929 fibroblasts in the presence or absence of FBS was also investigated. From the cell viability results (section 5.3.1) the time point of 2 days was chosen as the largest difference

between cell viability, in the presence or absence of serum, was observed at this incubation period. In the presence of 10% (v/v) FBS, CoCr nanoscale particles were observed within vesicles in the cytoplasm of the L929 fibroblasts at all the particle volumes tested. Nanoscale CoCr particles volumes of 50 and 5 μm^3 per cell formed large agglomerates as shown by the white arrows in Figure 5.12. Furthermore for both the particle volumes of 50 and 5 μm^3 per cell, multiple vesicles containing CoCr particles were detected within the cells. Occasional vesicles containing CoCr particles were observed at the particle volume of 0.5 μm^3 per cell as shown in Figure 5.12E and F. No particles were observed in the cell only control (Figure 5.12G and H).

In the absence of 10% (v/v) FBS, the images were very similar to the cells cultured with the CoCr particles in the presence of serum. Again multiple vesicles within single cells containing CoCr nanoscale particles were observed at particle volumes of 50 and 5 μm^3 per cell as shown in Figure 5.13A – D. These vesicle-bound particles were most prevalent at the highest particle volume of 50 μm^3 per cell. However at the lower particle concentration of 0.5 μm^3 per cell, very few particles were detected within the cells (Figure 13E and F). Again, no particles were detected in the cell only control (Figure 13G and H).

The TEM images were used to measure the diameters of the particle agglomerates within the cells (Figure 5.14). The largest particle agglomerate of 2.6 µm was measured for the particles incubated in the presence of 10% (v/v) FBS at a particle volume of 50 μm^3 per cell. No statistical differences were observed between the size of the particle agglomerates, at any particle concentration tested in the presence 10% (v/v) FBS and the corresponding particle concentration in the absence of 10% (v/v) FBS. However, in the presence of 10% (v/v) FBS, the agglomerates at the particle volume of 50 μm^3 per cell were statistically different to the aggregates at the particle volume of 0.5 and 5 μm^3 per cell.

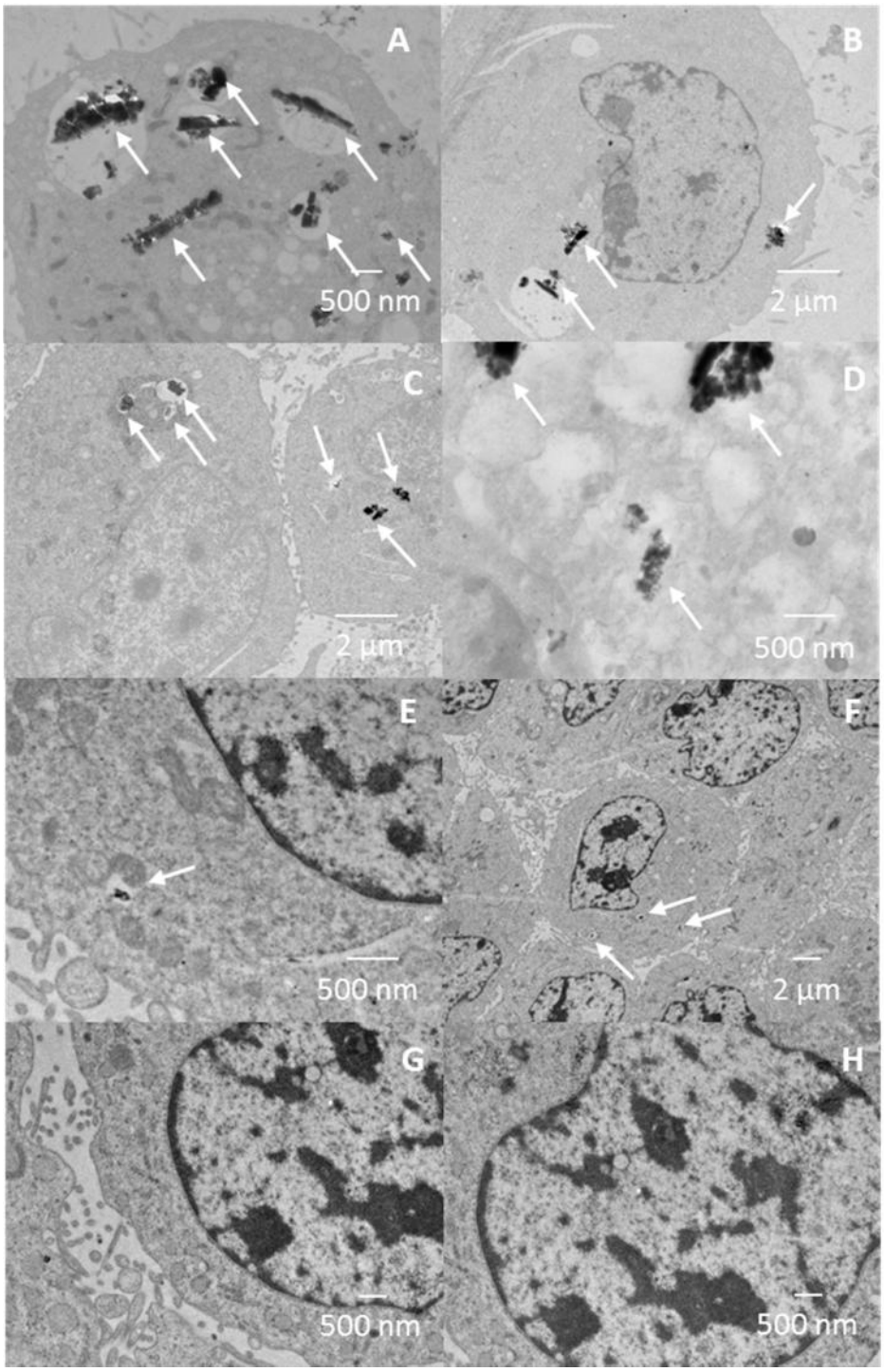

Figure 5.12 – Transmission electron microscopy analysis of nanoscale cobalt chromium particles within L929 fibroblasts cultured in the presence of foetal bovine serum. Fibroblast cells were cultured in the presence of 10% (v/v) FBS and nanoscale CoCr particles at particles volumes of 50, 5 and 0.5 μm^3 per cell. After 48 hours, the cells were harvested, fixed and stained before being imaged using TEM. White arrows indicate particles within cells. A & B – 50 μm^3 per cell. C & D – 5 μm^3 per cell. E & F – 0.5 μm^3 per cell. G & H – Cell only control.

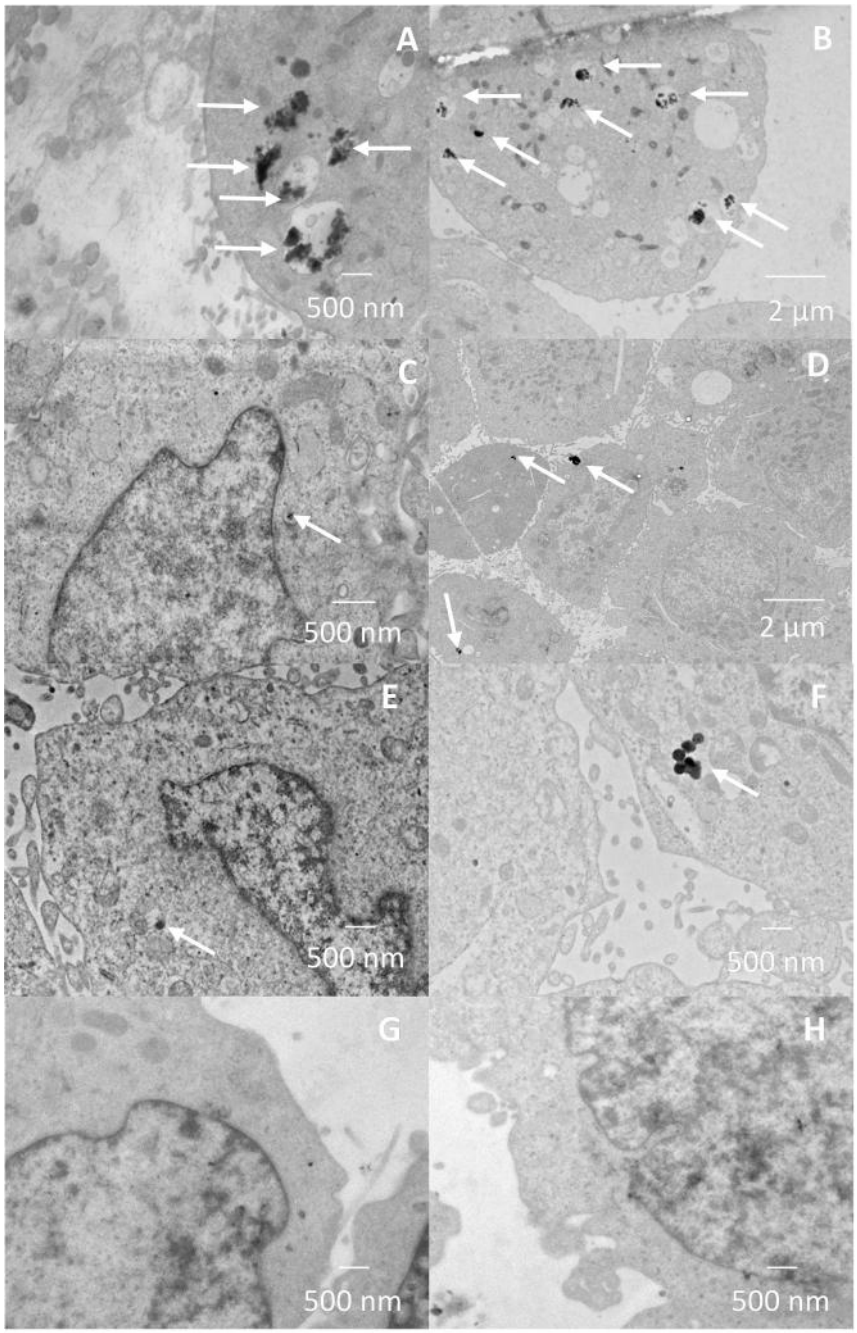

Figure 5.13 – Transmission electron microscopy analysis of nanoscale cobalt chromium particles within L929 fibroblasts cultured in the absence of foetal bovine serum. Fibroblast cells were cultured in the absence FBS and nanoscale CoCr particles at particles volumes of 50, 5 and 0.5 μm^3 per cell. After 48 hours, the cells were harvested, fixed and stained before being imaged using TEM. White arrows indicate particles within cells. A & B – 50 μm^3 per cell. C & D – 5 μm^3 per cell. E & F – 0.5 μm^3 per cell. G & H – Cell only control.

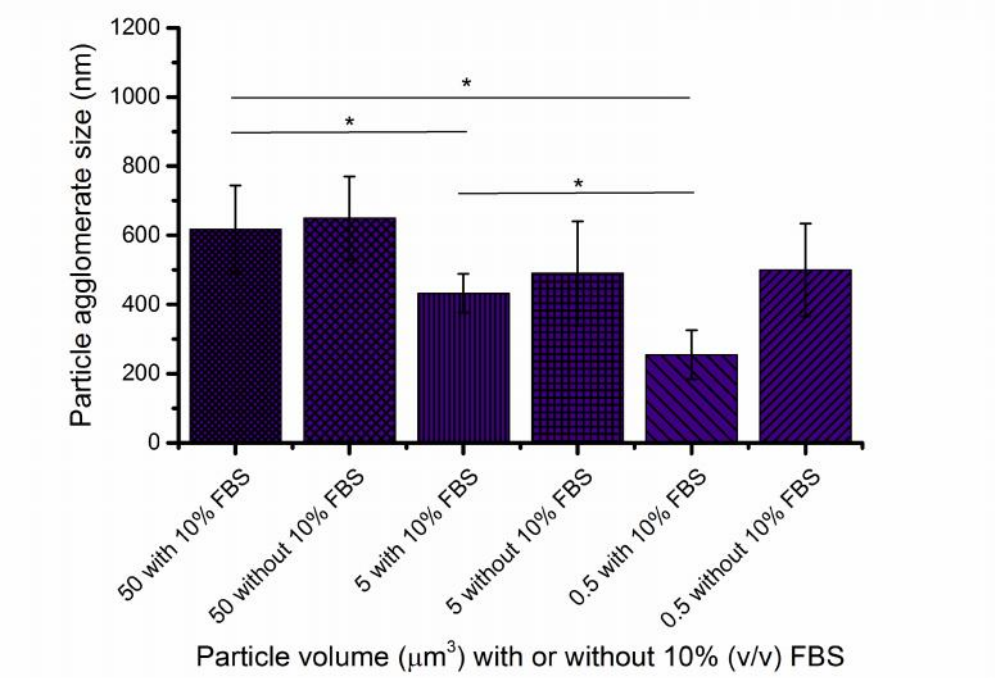

Figure 5.14 – Sizing of nanoscale cobalt chromium particle agglomerates within L929 fibroblasts. The CoCr particle agglomerates within the L929 fibroblasts were sized using the corresponding TEM images and the computer software Image Pro Plus (version 6.1). Error bars represent 95% CI levels.

The aggregates of particles within the vesicles were confirmed to be CoCr using EDX analysis, by the presence of cobalt and chromium peaks within the spectra (Figure 5.15A, spectra 1 and 2). Other peaks within the spectra, including lead are from the sample preparation process or from the copper TEM grid. Similar to the nanoscale alumina particle samples, particle like structures not within vesicles were found to not be particles but remnants of the staining process (Figure 5.15B, spectra 3). Only peaks for elements used in the sample preparation process were detected in the EDX spectrum.

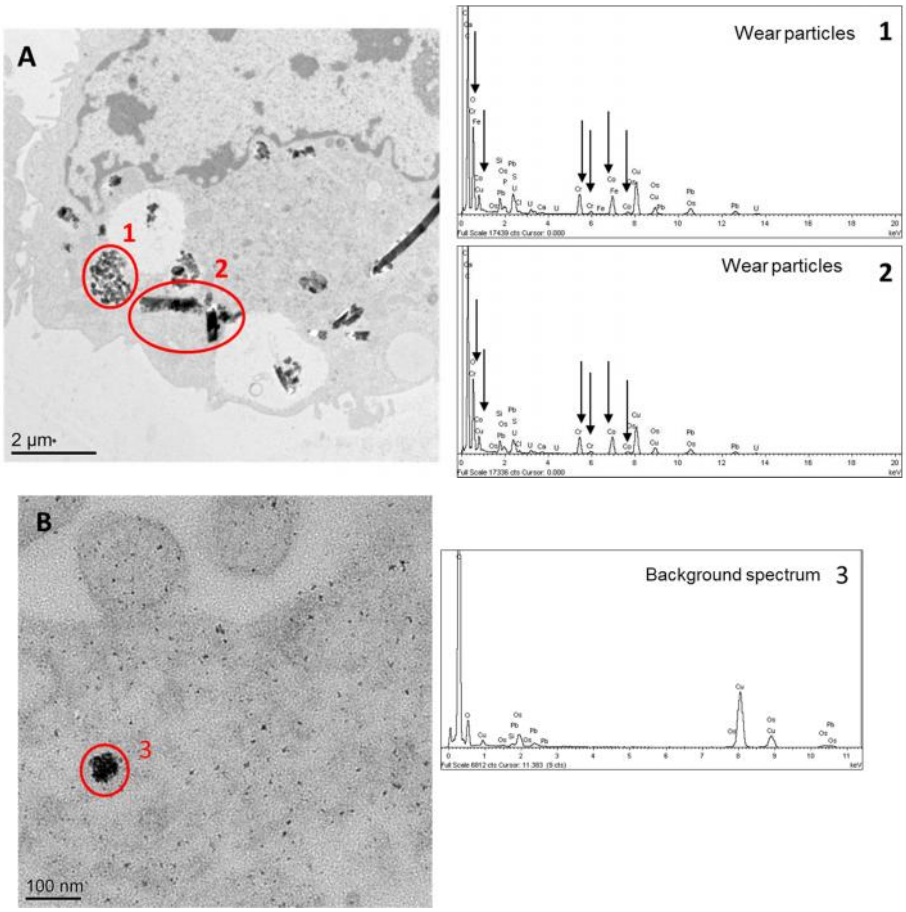

Figure 5.15 – Energy-dispersive X-ray spectroscopy of nanoscale cobalt chromium particles. L929 fibroblasts were cultured with 10% (v/v) FBS and nanoscale CoCr particles at a particle volume of 50 (A) or 0.5 (B) μm^3 per cell for 2 days. Confirmation of particles was performed using the INCA EDX analysis system and the Tecnai F20 TEM. Example EDX plots (1 & 2) of particles within vesicles and corresponding image are displayed. The black arrows indicate the element peaks of the particles. Example EDX plots (3) of staining precipitates and corresponding image is displayed.

5.3.3 The effect of particles on the vesicle leakage of a model lipid plasma membrane in the presence of foetal bovine serum

The effect of nanoscale and micron sized alumina and cobalt chromium particles on membrane integrity, in the presence of 10% (v/v) FBS, was assessed.

5.3.3.1 The effect of nanoscale and micron sized alumina particles on the vesicle leakage of a model lipid plasma membrane in the presence of foetal bovine serum

The effect of nanoscale alumina particles on membrane integrity was measured in the presence of 10% (v/v) FBS. The addition of 10% (v/v) serum alone, without any particles, induced vesicle leakage of up to 7.6% (Figure 5.16A). A dose dependent increase in the vesicle leakage was measured in the presence of serum. At the highest particle concentration of 100 $\mu g.ml^{-1}$, an average 33.5% leakage was measured, which was statistically significant in comparison to the 10% (v/v) FBS control and the lower particle concentrations of 1 and 10 $\mu g.ml^{-1}$. No statistically significant increase in vesicle leakage for nanoscale alumina particles at particle concentration of 1 and 10 $\mu g.ml^{-1}$ were measured.

The micron sized alumina particles induced less vesicle leakage in comparison to the nanoscale alumina particles (Figure 5.16B). Whilst a dose dependent increase in vesicle leakage was observed, the highest particle concentration of 100 $\mu g.ml^{-1}$ only induced 20% leakage, which was much less than the 33.5% leakage caused by the nanoscale alumina particles. However, this leakage was partly caused by the presence of the 10% (v/v) FBS. Due to sample variability, no statistically significant differences were measured in comparison to the 10% (v/v) FBS only control.

5.3.3.1.1 Quenching effects of nanoscale and micron sized alumina particles on the vesicle leakage assay

The effect of the nanoscale and micron sized alumina particles on the quenching of the fluorescent dye used in the vesicle leakage assay was assessed. The vesicles, which encapsulated an autoquenching fluorescent dye, were formed as stated in section 2.2.6.2. As described in section 2.2.6.3.3 the vesicles diluted in DMEM,

without phenol red and in the presence of 10% (v/v) FBS were first lysed using 0.1% (v/v) Triton-X 100. Incremental concentrations of the particles (1, 10 and 100 $\mu g.ml^{-1}$) were subsequently added to the vesicles and the fluorescent intensity was observed over time. The vesicle leakage from each treatment was expressed as a percentage of the Triton-X 100 (100%) reading and the baseline prior to the addition of particles represented 0% vesicle leakage.

In the presence of the nanoscale alumina particles, no significant quenching effects were measured in the presence of 10% (v/v) FBS at all the particle concentrations tested as shown in Figure 5.17A. Although there was a slight decrease in the fluorescence at the highest particle concentration of 100 $\mu g.ml^{-1}$. No significant quenching effect was observed for the micron sized alumina particles at all the particle concentrations tested (Figure 5.17B). However, the highest particle concentration of 100 $\mu g.ml^{-1}$ induced a slight increase in fluorescence.

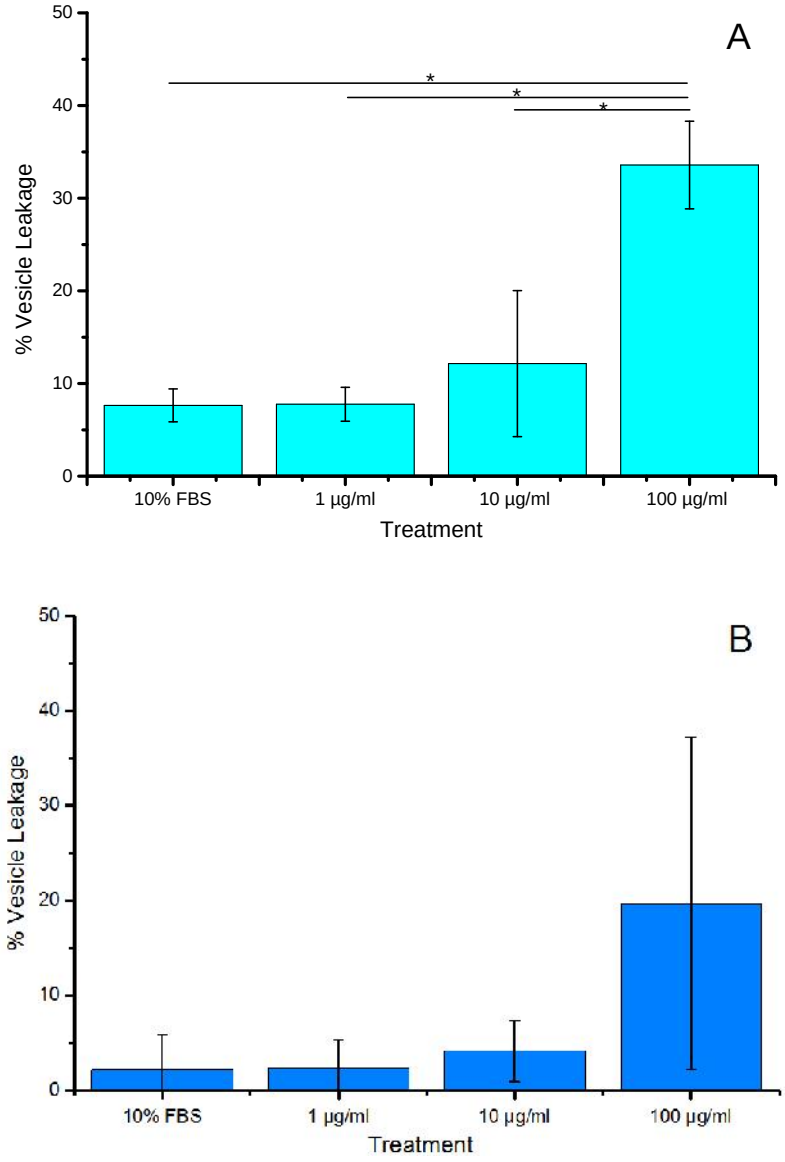

Figure 5.16 – The effect of nanoscale (A) and micron sized (B) alumina particles on vesicle leakage in the presence of foetal bovine serum. Data (n=3) was expressed as percentage vesicle leakage of the detergent Triton-X 100, which represented 100% leakage. Vesicle leakage of fluorescent dye encapsulated with vesicles was measured in real time in the presence of 10% (v/v) FBS and subsequent increasing particle concentrations (1, 10 and 100 µg.ml^{-1}). Raw data were analysed using paired t-test in comparison to FBS only control and statistically significant results ($p < 0.05$) are indicated by an asterisk (*). Error bars represented 95% confidence levels.

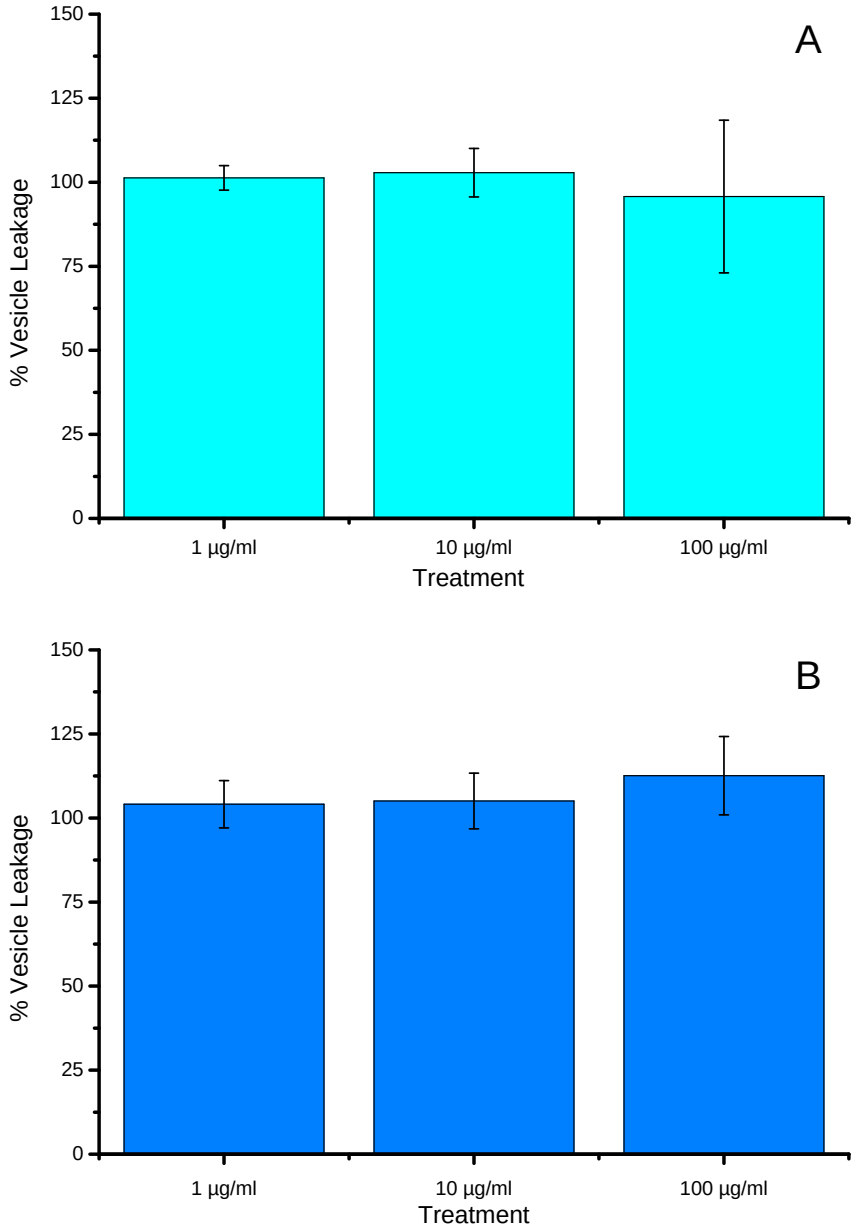

Figure 5.17 – The effect of nanoscale (A) and micron sized (B) alumina particles on the quenching of the fluorescent dye. Vesicles loaded with an autoquenching fluorescent dye were formed from lipid membranes. In the presence of 10% (v/v) FBS, the vesicles were then lysed with Triton-X 100 followed by the addition of increasing particle concentrations (1 – 100 $\mu g.ml^{-1}$). The release of fluorescent dye was measured, in real-time, using a fluorometer. Data (n=3) was expressed as percentage vesicle leakage of the detergent Triton-X 100, which represented 100% leakage. Raw data were analysed using paired t-test and statistically significant results ($p < 0.05$) are indicated by an asterisk (*). Error bars represented 95% confidence levels.

5.3.3.2 The effect of particles on the vesicle leakage of a model lipid membrane in the presence of foetal bovine serum

The effect of nanoscale CoCr particles on membrane integrity was measured in the presence of 10% (v/v) FBS. The addition of serum alone (no particles) induced vesicle leakage of up to 4% (Figure 5.18A). At the highest particle concentration of 100 $\mu g.ml^{-1}$, an average 11% leakage was measured, which was statistically significant in comparison to the 10% (v/v) FBS control and all the other particle concentrations tested. However, vesicle leakage at the highest particle concentration was approximately three fold lower than the leakage measured for nanoscale alumina particles (section 5.3.3.1)

The micron sized CoCr particles induced less vesicle leakage in comparison to the nanoscale CoCr particles (Figure 5.18B). The highest particle concentration of 100 $\mu g.ml^{-1}$ only induced an average 7% leakage. Due to sample variability, no statistically significant differences were measured in comparison to the 10% (v/v) FBS only control.

5.3.3.2.1 Quenching effects of nanoscale and micron sized cobalt chromium particles on the vesicle leakage assay

The effect of the nanoscale and micron sized CoCr particles on the quenching of the fluorescent dye used in the vesicle leakage was assessed. The vesicles, which encapsulated an autoquenching fluorescent dye, were formed as stated in section 2.2.6.3. As described in section 2.2.6.3.3 the vesicles were then diluted at least 1000 times in DMEM, without phenol red. In the presence of 10% (v/v) FBS, the vesicles were first lysed using 0.1% (v/v) Triton-X 100 and incremental concentrations of the particles (1, 10 and 100 $\mu g.ml^{-1}$) were subsequently added to the vesicles and the fluorescent intensity was observed over time. The vesicle

leakage from each treatment was expressed as a percentage of the Triton-X 100 (100%) and the baseline prior to the addition of particles represented 0% leakage.

A small quenching effect was measured in the presence of 10% (v/v) FBS for the nanoscale CoCr particles at the highest particle concentration of 100 $\mu g.ml^{-1}$. However, this was not statistically significant in comparison to of the other particle concentrations tested (Figure 5.19A). No quenching effects were observed for the lysed vesicles incubated with the micron sized CoCr particles at any of the particle concentrations tested (Figure 5.19B).

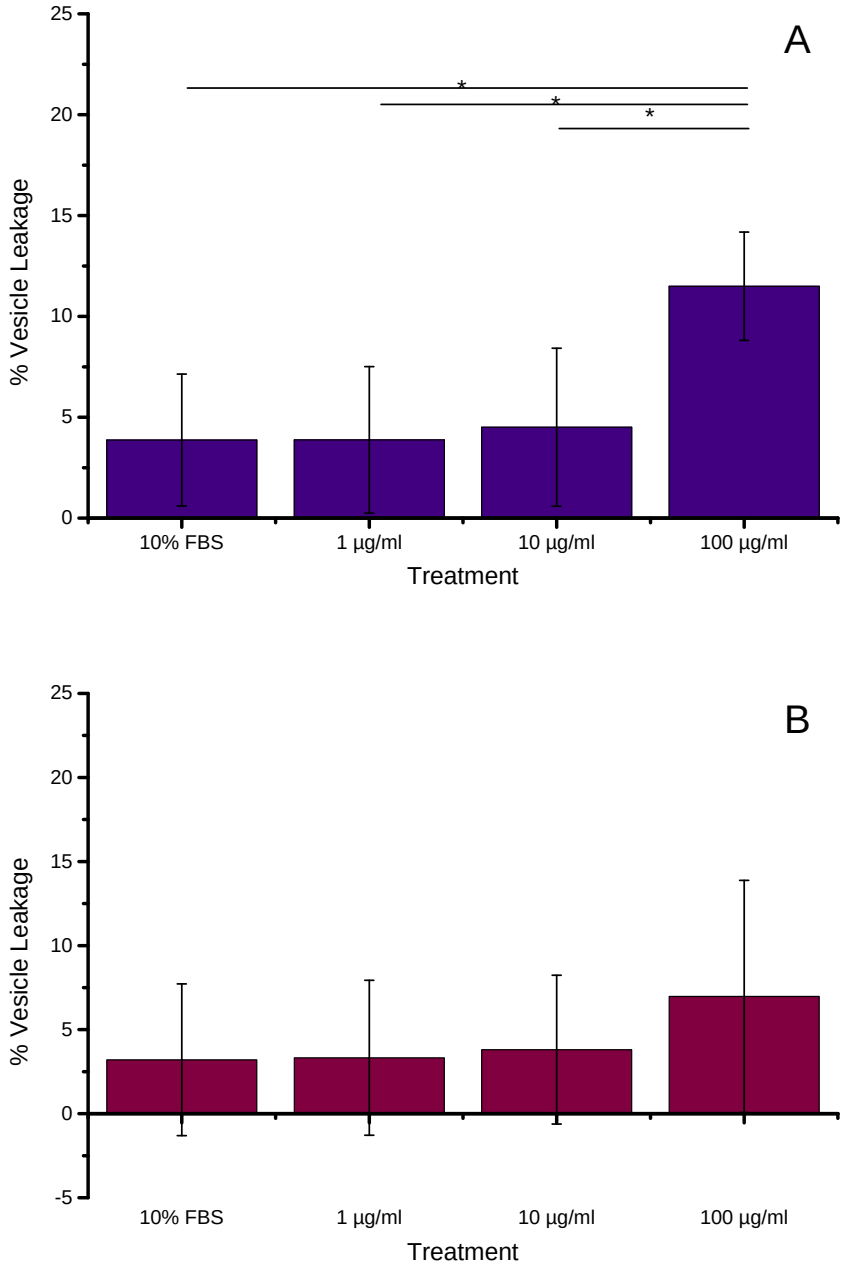

Figure 5.18 – The effect of cobalt chromium nanoscale (A) and micron sized (B) particles on vesicle leakage in the presence of foetal bovine serum. Data (n=3) is expressed as percentage vesicle leakage of the detergent Triton-X 100, which represented 100% leakage. Vesicle leakage of fluorescent dye encapsulated with vesicles was measured in real time in the presence of 10% (v/v) FBS and subsequent increasing particle concentrations (1, 10 and 100 µg.ml^{-1}). Raw data were analysed using paired t-test in comparison to FBS only control and statistically significant results ($p < 0.05$) are indicated by an asterisk (*). Error bars represented 95% confidence levels.

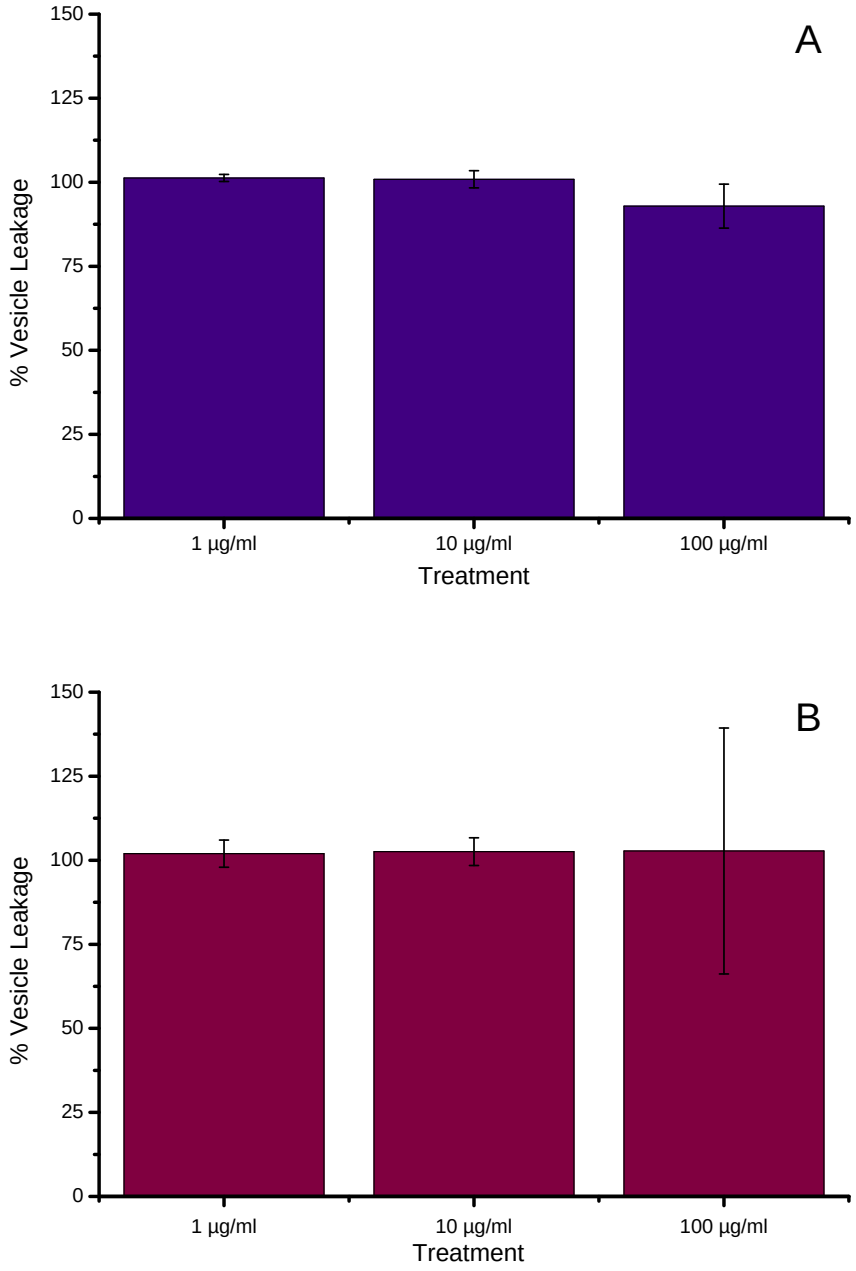

Figure 5.19 – The effect of nanoscale (A) and micron sized (B) cobalt chromium particles on the quenching of the fluorescent dye. Vesicles loaded with an autoquenching fluorescent dye were formed from lipid membranes. In the presence of 10% (v/v) FBS, the vesicles were then lysed with Triton-X 100 followed by the addition of increasing particle concentrations (1 – 100 µg.ml^{-1}). The release of fluorescent dye was measured, in real-time, using a fluorometer. Data (n=3) was expressed as percentage vesicle leakage of the detergent Triton-X 100, which represented 100% leakage. Raw data were analysed using paired t-test and statistically significant results ($p < 0.05$) are indicated by an asterisk (*). Error bars represented 95% confidence levels.

5.3.4 Investigation of the binding of particles to a solid supported bilayer lipid membrane using quartz crystal microbalance with dissipation in the presence of foetal bovine serum

The effect of the protein corona on alumina and CoCr particle interactions with the sBLM was investigated using QCM-D techniques in the presence of 10% (v/v) FBS.

5.3.4.1 Optimising the concentration of foetal bovine serum for quartz crystal microbalance with dissipation

The initial aim of this part of the study was to supplement the starting solution, DMEM, with 10% (v/v) FBS, which reflects the serum concentration used for the cell viability experiments. However, upon the addition of DMEM, supplemented with 10% (v/v) FBS to the sBLM, a large reduction in the frequency from -27 Hz to -68 Hz was observed (Figure 5.20). This was also accompanied by a sharp increase in the dissipation as shown in Figure 5.20. Furthermore, the subsequent addition of DMEM (without 10% (v/v) FBS) only induced a slight reverse in the frequency and dissipation trend. Therefore FBS had a high binding affinity to the sBLM, whereby irreversible binding occurred. Preliminary results had demonstrated no binding of CoCr nanoscale particles had occurred in the presence of 10% (v/v) FBS and it was hypothesised that the high concentration of FBS would masked any small binding events of the particles to the sBLM (Appendix C). Therefore the concentration of FBS was lowered to 0.1% (v/v) for all experiments. In order for a protein corona to form, the particles were incubated for 16 hours at 37°C with DMEM supplemented with 0.1% (v/v) FBS prior to being added to the sBLM.

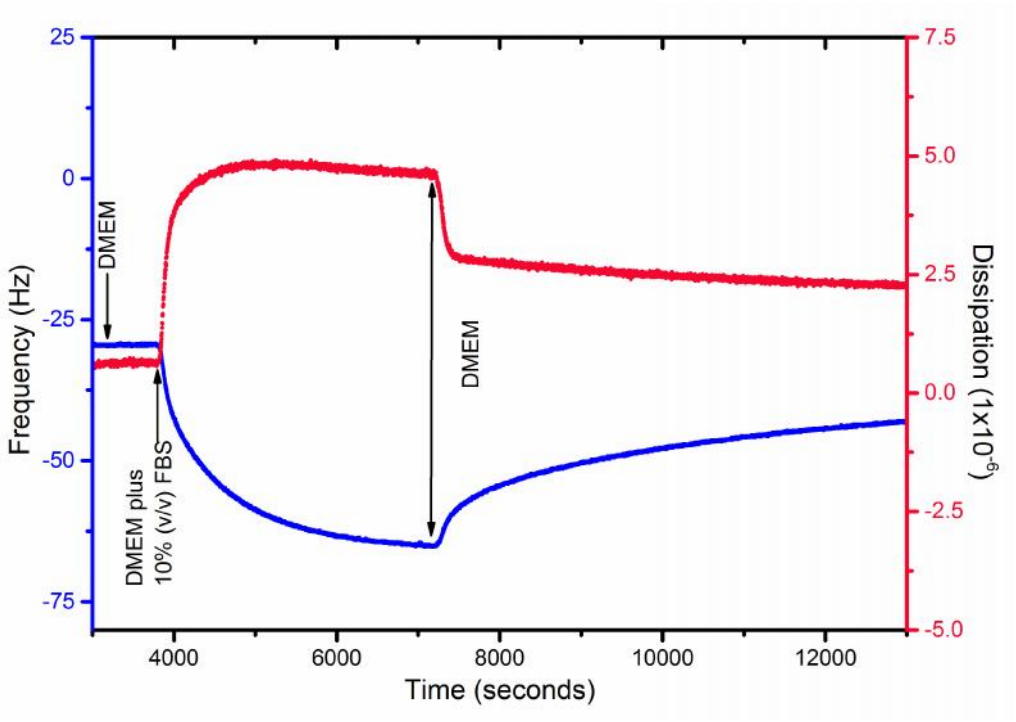

Figure 5.20 – Binding of 10% (v/v) foetal bovine serum to the solid supported bilayer lipid membrane for protein corona studies. The binding of DMEM supplemented 10% (v/v) FBS onto a sBLM was measured using QCM-D. This was followed by a DMEM only wash to establish if the binding of the serum was reversible. Changes in the frequency (blue) and dissipation (red) were measured (Ninth overtone is displayed).

5.3.4.2 The interaction of nanoscale and micron sized alumina particles with a solid supported bilayer lipid membrane using quartz crystal microbalance with dissipation in the presence of foetal bovine serum

A sBLM consisting of the model lipid membrane was formed and the starting solution of DMEM (without supplements) was added to the sBLM. For both the nanoscale and micron sized alumina particles, no changes in the frequency were observed for any of the particle concentrations tested (Figure 5.21A and 5.21B, respectively). No effect was observed for the dissipation results either, thus suggesting that no particles bonded to the sBLM at particle concentrations of 100 $\mu g.ml^{-1}$ or below.

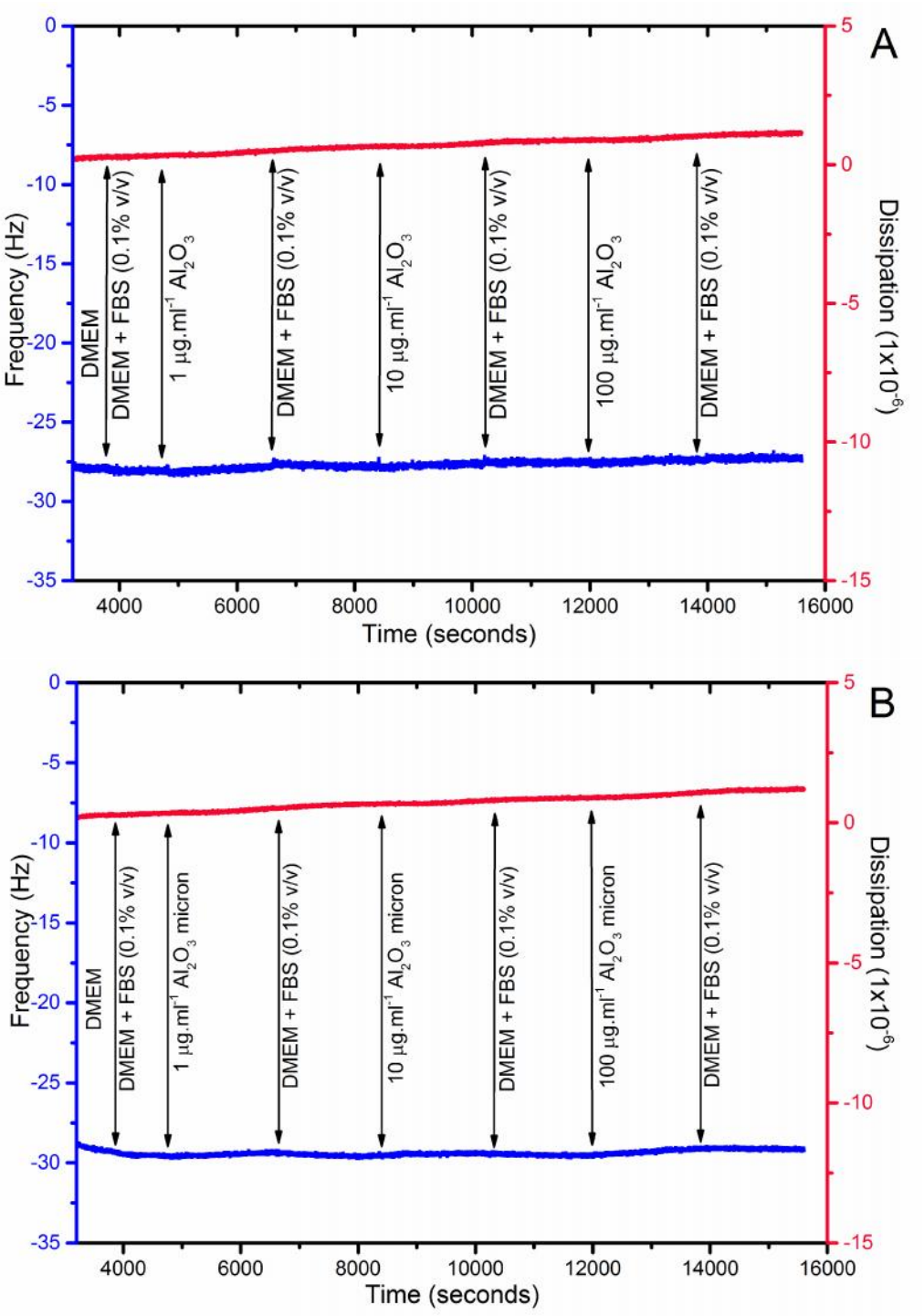

Figure 5.21 - QCM-D plot of a solid supported bilayer lipid membrane in the presence alumina nanoscale (A) and micron sized (B) particles and foetal bovine serum. A sBLM was formed in DMEM onto a crystal (not shown) followed by the addition of DMEM plus 0.1% (v/v) FBS. Incremental concentrations (1 – 100 µg.ml^{-1}) of alumina nanoscale or micron sized particles diluted in DMEM plus FBS (0.1% v/v) were added at times indicated by the arrows. Changes in the frequency (blue) and dissipation (red) were measured (Ninth overtone is displayed).

5.3.4.3 The interaction of nanoscale and micron sized cobalt chromium particles with a solid supported bilayer lipid membrane using quartz crystal microbalance with dissipation in the presence of foetal bovine serum

A stable sBLM consisting of a model lipid membrane was formed for both the CoCr nanoscale and micron sized particle QCM-D experiments (Figure 5.22A and 5.22B, respectively). Cobalt chromium nanoscale or micron sized particles diluted in DMEM plus 0.1% (v/v) FBS were added to the sBLM at incremental concentration of 1, 10 and 100 $\mu g.ml^{-1}$. The changes in frequency and dissipation were measured overtime. As also observed for the alumina particles no change in the frequency was observed for all the particle concentrations of the CoCr nanoscale and micron sized particles added to the sBLM. Similarly, no change in dissipation was measured thus suggesting that no binding of the particles to the sBLM occurred at particle concentrations tested.

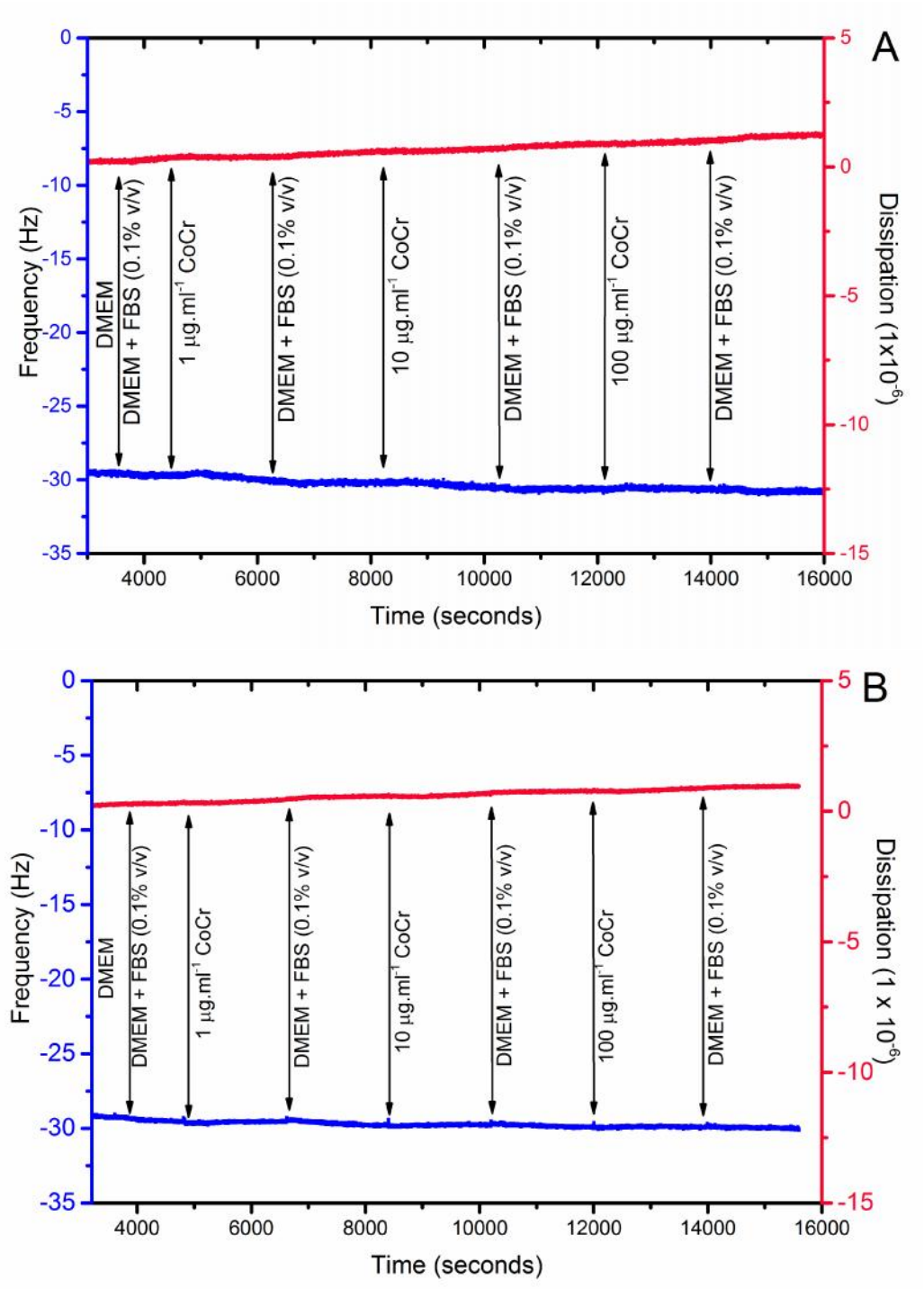

Figure 5.22 - QCM-D plot of a solid supported bilayer lipid membrane in the presence cobalt chromium nanoscale (A) and micron sized (B) particles and foetal bovine serum. A sBLM in DMEM was formed onto a quartz crystal (not shown) followed by the addition of DMEM plus 0.1% (v/v) FBS. Incremental concentrations (1 – 100 µg.ml^{-1}) of CoCr nanoscale or micron sized particles diluted in DMEM plus FBS (0.1% v/v) added at times indicated by the arrows. Changes in the frequency (blue) and dissipation (red) were measured (Ninth overtone is displayed).

5.3.5 The incorporation of isolated membrane proteins into the model lipid membrane in the presence of foetal bovine serum

To further increase the complexity of the model membrane systems used to assess alumina and CoCr particle toxicity, isolated membrane proteins were incorporated into the model lipid membrane and used for the vesicle leakage and QCM-D studies. In addition to this, the effect of the protein corona was explored by adding the particles in the presence of 10% (v/v) FBS. The isolated membrane proteins used for the vesicle leakage assays originated from U937 histiocytes and primary HFBs. In chapter four, the protein content within the membrane was optimised at 20% which was shown to enable stable bilayer formation for the QCM-D experiments.

5.3.5.1 The effect of particles on the vesicle leakage of a model lipid membrane with incorporated membrane proteins in the presence of foetal bovine serum

The effect of incorporating membrane proteins isolated from primary HFBs and U937 histiocytes on the membrane integrity in the presence of nanoscale and micron sized alumina and CoCr particles, in the presence of 10% (v/v) FBS was investigated.

5.3.5.1.1 The effect of nanoscale and micron sized alumina particles on the vesicle leakage of a model lipid membrane with incorporated membrane proteins in the presence of foetal bovine serum

In the presence of membrane proteins isolated from primary HFBs, the nanoscale alumina particles only induced vesicle leakage of 5% at the highest particle

concentration of 100 µg.ml^{-1} (Figure 5.23A). This result was statistically significant in comparison to the 10% (v/v) FBS control. However, the 10% FBS (v/v) control did not induce any overall vesicle leakage. This same trend was also observed for the nanoscale alumina particles incubated with vesicles containing U937 histiocyte membrane proteins (Figure 5.23B). The highest nanoscale alumina particle concentration of 100 µg.ml^{-1} induced 14% vesicle leakage, which was statistically significant in comparison to the 10% FBS (v/v) control. The particle concentration of 10 µg.ml^{-1} also induced a 1.2% significant vesicle leakage in comparison to the control.

A larger amount of vesicle leakage was observed for the micron sized particles in the presence of vesicles containing either human fibroblast or U937 histiocyte membrane proteins and in the presence of 10% (v/v) FBS (Figure 5.23C and D, respectively). For the micron sized alumina particles, incubated with vesicles containing human fibroblast membrane proteins, the particle concentrations of 10 and 100 µg.ml^{-1} induced a statistically significantly vesicle leakage of 1.3% and 25%, respectively. Similarly, in the presence of isolated U937 histiocytes, the micron sized alumina particles induced a statistically significant increase in vesicle leakage of 19% in comparison to the 10% FBS (v/v) control.

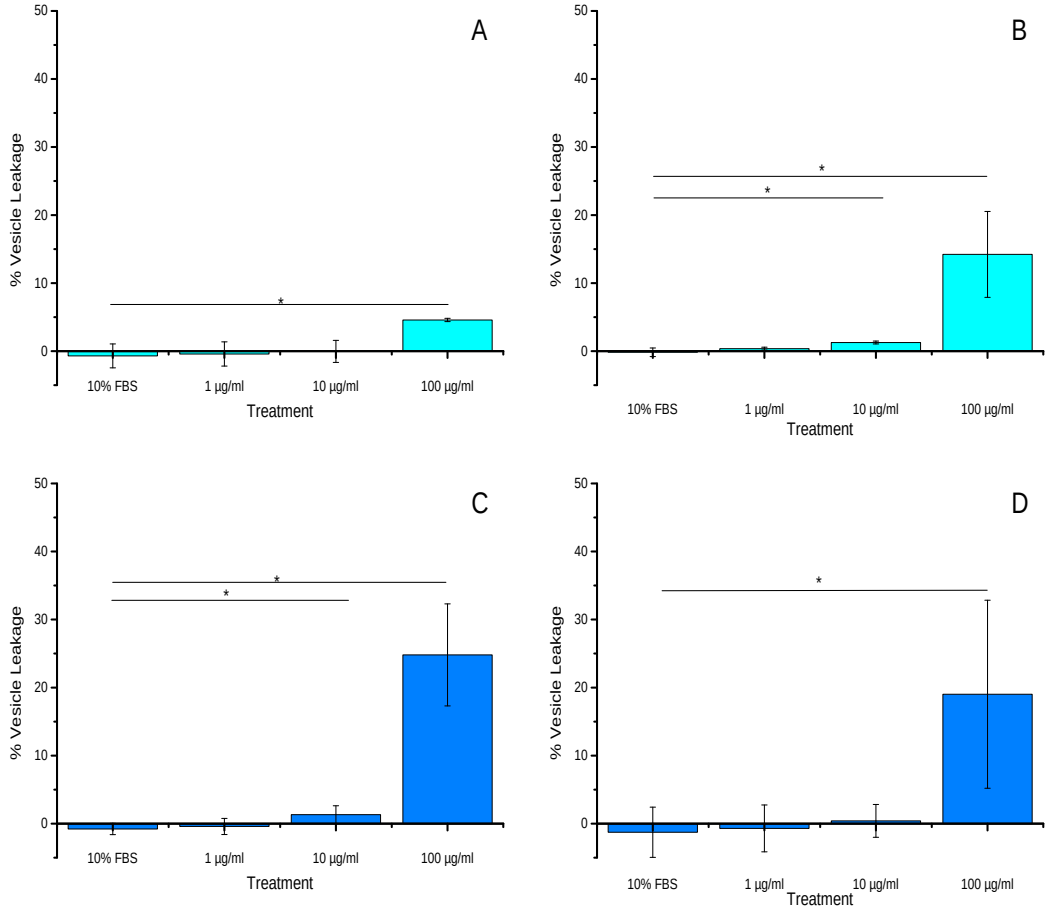

Figure 5.23 – The effect of nanoscale and micron sized alumina particles on vesicle leakage of a lipid membrane with isolated membrane proteins from primary HFBs and U937 histiocytes in the presence of foetal bovine serum. Nanoscale alumina particles were incubated with lipid vesicles consisting of 20% isolated proteins from human fibroblast membranes (A) or isolated U937 histiocytes (B). Micron sized alumina particles were incubated with lipid vesicles consisting of 20% isolated human fibroblast membrane proteins (C) or isolated U937 histiocytes (D). Data (n=3) is expressed as a percentage vesicle leakage of the detergent Triton-X 100. Vesicle leakage of on fluorescent dye encapsulated around vesicles was measured and subsequent increasing particle concentrations (1, 10 and 100 µg.ml^{-1}) in the presence of 10% (v/v) FBS. A paired t-test was performed in comparison to FBS only control and statistically significant results ($p < 0.05$) is indicated by an asterisk (*). Error bars represented 95% confidence levels.

5.3.5.1.2 The effect of nanoscale and micron sized cobalt chromium particles on the vesicle leakage of a model lipid membrane with incorporated membrane proteins in the presence of foetal bovine serum

The nanoscale CoCr particles induced 23% vesicle leakage at the highest particle concentration of 100 $\mu g.ml^{-1}$, in the presence of membrane proteins isolated from primary HFBs and 10% (v/v) FBS (Figure 5.24A). This result was statistically significant in comparison to the 10% (v/v) FBS control. In contrast, no increase in vesicle leakage was observed for all the nanoscale CoCr particle concentrations tested in the in the presence of membrane proteins isolated from U937 histiocytes (Figure 5.24B). The result for the micron sized CoCr particles at the particle concentration of 100 $\mu g.ml^{-1}$ is unexpected, suggesting that it may have been an outlier.

A small increase in the vesicle leakage was observed for the micron sized CoCr particles in the presence of vesicles containing either primary HFBs or U937 histiocyte membrane proteins (Figure 5.24C and D, respectively). For the micron sized CoCr particles, incubated with vesicles containing human fibroblast membrane proteins, the highest particle concentration of 100 $\mu g.ml^{-1}$ induced an average 6% in vesicle leakage in the presence of 10% (v/v) FBS. This result was statistically significant in comparison to the 10% (v/v) FBS control. Similarly, in the presence of isolated U937 histiocytes, the micron sized CoCr particles induced statistically significant vesicle leakage of 10% in comparison to the 10% (v/v) FBS control.

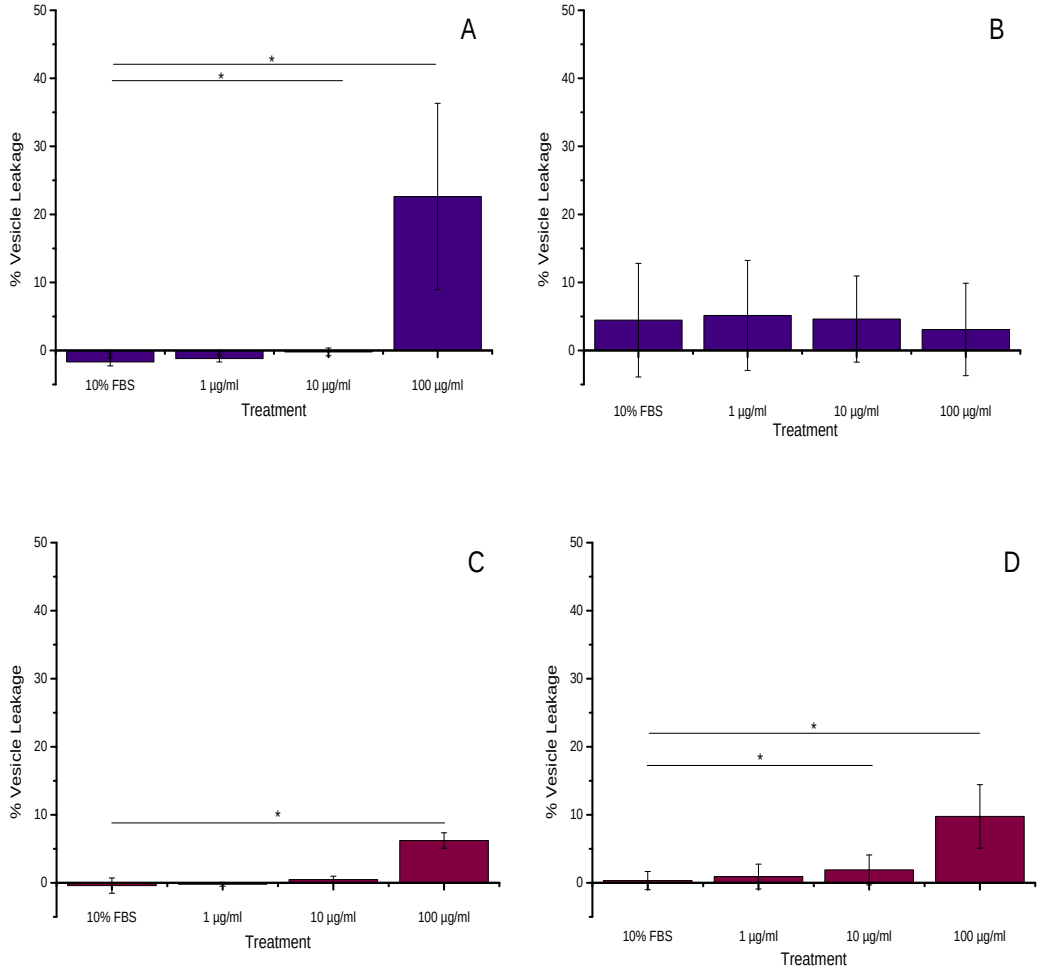

Figure 5.24 – The effect of nanoscale and micron sized cobalt chromium particles on vesicle leakage of a lipid membrane with isolated membrane proteins from primary HFBs and U937 histiocytes in the presence of foetal bovine serum. Nanoscale CoCr particles were incubated with lipid vesicles consisting of 20% isolated proteins from primary HFB membranes (A) or isolated U937 histiocytes (B). Micron sized CoCr particles were incubated with lipid vesicles consisting of 20% isolated human fibroblast membrane proteins (C) or isolated U937 histiocytes (D). Data (n=3) is expressed as a percentage vesicle leakage of the detergent Triton-X 100. Vesicle leakage of on fluorescent dye encapsulated around vesicles was measured and subsequent increasing particle concentrations (1, 10 and 100 µg.ml^{-1}) in the presence of 10% (v/v) FBS. A paired t-test was performed in comparison to FBS only control and statistically significant results ($p < 0.05$) is indicated by an asterisk (*). Error bars represent 95% confidence levels (n = 3).

5.3.6 The binding of particles to a solid supported bilayer lipid membrane with incorporated membrane proteins using quartz crystal microbalance with dissipation in the presence of foetal bovine serum

The effects of 10% (v/v) FBS on the binding of nanoscale and micron sized alumina and CoCr particles to a sBLM were investigated in the presence of isolated membrane proteins. The membrane proteins from primary HFBs were isolated and incorporated into the sBLM. Time constraints and poor yield meant that incorporation of U937 membrane proteins into sBLMs was not possible.

5.3.6.1 Nanoscale and micron sized alumina particles

A sBLM was formed on the quartz crystal surface which consisted of 20% (w/w) membrane proteins isolated from primary HFBs. The particles were incubated with DMEM supplemented with 0.1% (v/v) FBS at 37°C for 16 hours prior to being added to the sBLM. The changes in frequency and dissipation are shown in Figure 5.25A for the alumina nanoscale particles and Figure 5.25B for the micron sized alumina particles. A stable sBLM, with 20% (w/w) isolated fibroblast membrane proteins, was formed for both the nanoscale and micron sized alumina particle experiments and the changes in frequency and dissipation are shown in Figure 5.25A for and Figure 5.25B, respectively. However, variability in the frequency of the established bilayer was observed. The addition of DMEM supplemented with 0.1% (v/v) FBS lowered the frequency slightly, but no overall effect on the dissipation was measured for both experiments. Upon the addition of 1 $\mu g.ml^{-1}$ of nanoscale alumina particles, a minor decrease in the frequency was measured from -45 Hz to -50 Hz (Figure 5.25A). A further reduction in the frequency was observed when the alumina nanoscale particle concentrations of 10 and 100 $\mu g.ml^{-1}$ were added to the sBLM.

Indeed the greatest rate in frequency decrease was measured for the highest particle concentration of 100 $\mu g.ml^{-1}$ from -52 Hz to -62 Hz. Furthermore, this particle concentration also induced a large increase in the dissipation to 16×10^{-6}.

Similar results were also observed for the micron sized alumina particles (Figure 25B). A large decrease in the frequency, coupled with a larger increase in dissipation (24×10^{-6}) was measured after the addition of 100 $\mu g.ml^{-1}$ micron sized alumina particles to the sBLM. This change in the frequency and dissipation stabilised upon the addition of the DMEM supplemented with 0.1% (v/v) FBS. The binding of alumina micron sized particles to sBLM with 20% (w/w) isolated fibroblast membrane proteins, in the presence of 10% (v/v) FBS, was repeated. However, it must be noted that whilst a positive result (a reduction in frequency) was observed, the overall decrease in the frequency varied between repeats. For example the decrease in frequency for one repeat was -16 Hz, whilst a frequency of -3Hz was measured for another repeat.

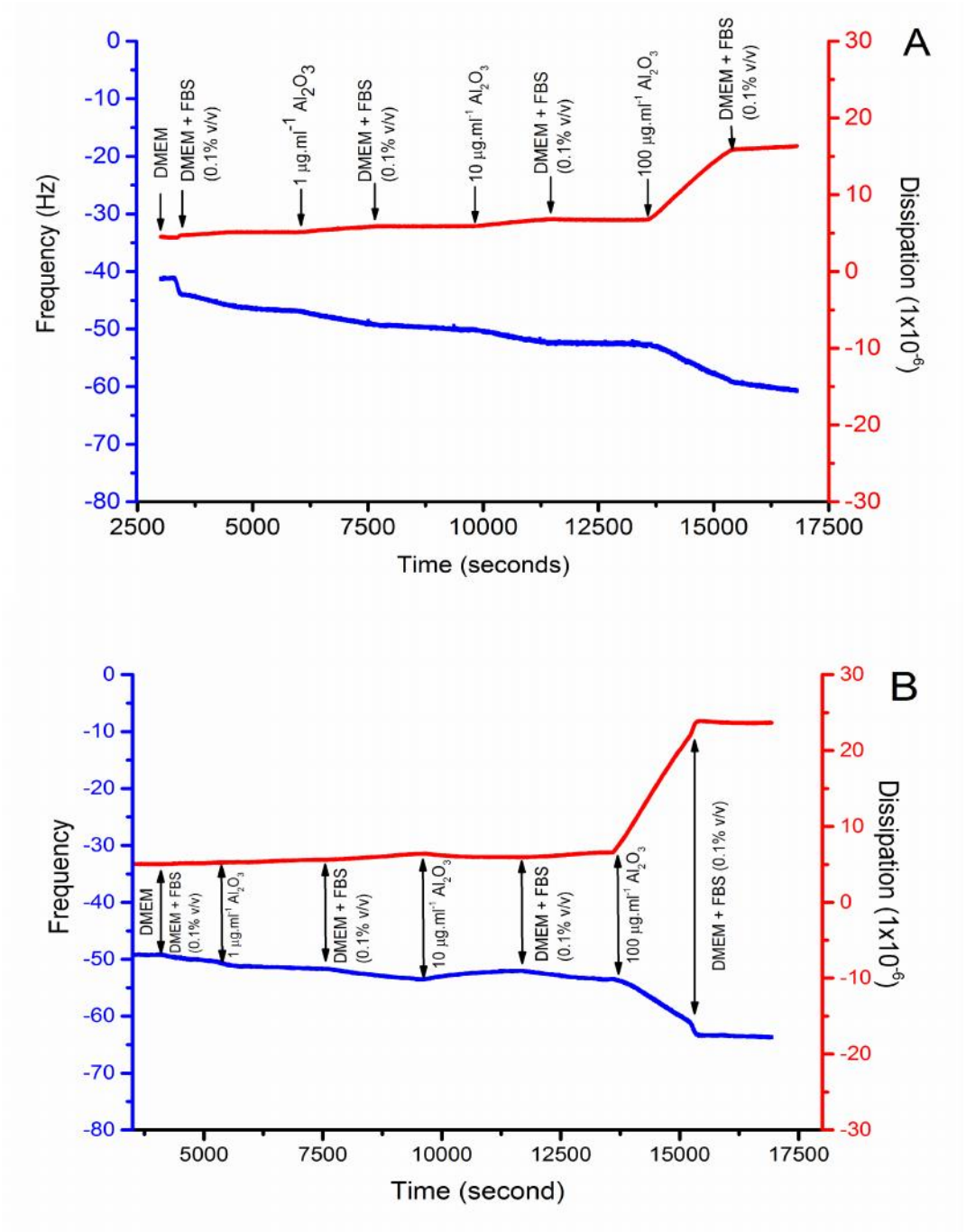

Figure 5.25 - QCM-D plot of a solid supported bilayer lipid membrane with incorporated membrane proteins in the presence nanoscale (A) and micron sized (B) alumina particles and foetal bovine serum. A sBLM with 20% isolated membrane proteins from primary HFBs was formed in DMEM onto an oscillating quartz crystal (not shown) followed by the addition of DMEM plus 0.1% (v/v) FBS. Incremental concentrations (1 – 100 µg.ml^{-1}) of alumina nanoscale or micron sized particles diluted in DMEM plus FBS (0.1% v/v) were added at times indicated by the arrows. Changes in the frequency (blue) and dissipation (red) were measured (Ninth overtone is displayed).

5.3.6.2 Nanoscale and micron sized cobalt chromium particles

A bilayer was formed consisting of 20% (w/w) isolated fibroblast membrane proteins from primary HFBs and DMEM supplemented with 0.1% (v/v) FBS was added to the sBLM, as described previously. In contrast to the alumina results, for the nanoscale (Figure 5.26A) and micron sized (Figure 5.25B) CoCr particles data, no large reduction in the frequency was observed. A minor decrease in the frequency was measured when 1 $\mu g.ml^{-1}$ of CoCr nanoscale particles was added to the sBLM. Similarly a drop in the frequency was observed at the particle concentration of 100 $\mu g.ml^{-1}$ for the micron sized CoCr particles (Figure 5.26B). However, overall no significant changes in the frequency were observed at any particle concentration.

A small increase in the dissipation was observed for the nanoscale CoCr particles, with increasing particle concentration. A much larger increase in the dissipation was measured for the micron sized CoCr particles at 100 $\mu g.ml^{-1}$ with a 6×10^{-6} increase. This increase plateaued when the DMEM supplemented with 0.1% (v/v) FBS wash was added.

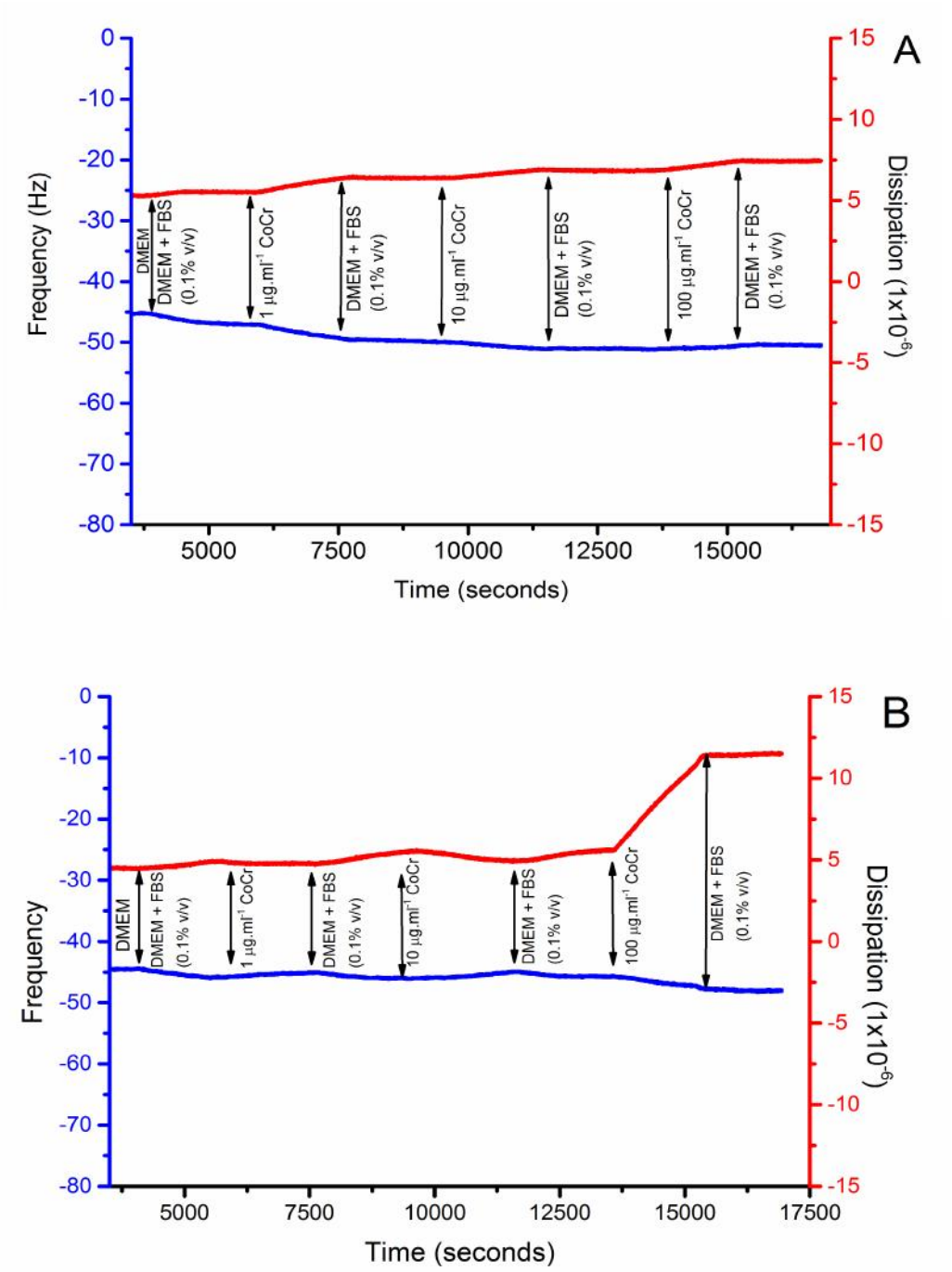

Figure 5.26 - QCM-D plot of a solid supported bilayer lipid membrane with incorporated membrane proteins in the presence nanoscale (A) and micron sized (B) cobalt chromium particles and foetal bovine serum. A sBLM with 20% isolated membrane proteins from primary HFBs was formed in DMEM onto an oscillating quartz crystal (not shown) followed by the addition of DMEM plus 0.1% (v/v) FBS. Incremental concentrations (1 – 100 µg.ml^{-1}) of CoCr nanoscale or micron sized particles diluted in DMEM plus FBS (0.1% v/v) were added at times indicated by the arrows. Changes in the frequency (blue) and dissipation (red) were measured (Ninth overtone is displayed).

5.4 Discussion

This part of the study aimed to investigate the effect of alumina and CoCr particles in the presence of 10% (v/v) FBS, to determine the effect on fibroblast cell viability, membrane integrity and binding to the cell membrane. Proteins within FBS are known to bind to surface of particles causing the formation of a protein corona (Mahmoudi *et al.* 2011). The bound proteins on the particle surface can change the surface characteristics and in turn can alter the cellular response to the particles, such as the effect on cell viability (Rauch *et al.* 2013).

Studies on the effect of the protein corona on particle toxicity *in vitro* have reported conflicting results, with some studies suggesting the presence of serum increases particle uptake and induce inflammation and cell death (Borgognoni *et al.* 2015; Cheng *et al.* 2015). However, other studies have reported the formation of protein coronae on particle surfaces generates a protective barrier, thus reducing particle binding to the cell membrane and inducing lower levels of cell death (Duan *et al.* 2015; Landgraf *et al.* 2015; Shang and Nienhaus 2015). The inconsistencies reported from these studies maybe due to the lack of standardisation between different methods (Horie *et al.* 2009). This part of the study aimed to use QCM-D and vesicle leakage assay techniques to generate a highly controlled environment in which to explore the role of serum proteins on particle interactions with the plasma membrane and how this relates to the effects on cell viability of fibroblasts.

5.4.1 The effect of the presence of foetal bovine serum on particle cell viability

The effect of nanoscale and micron sized alumina and CoCr particles on the cell viability of L929 fibroblasts in the presence or absence of 10% (v/v) FBS was investigated. This followed on from an undergraduate final year project exploring the

role of serum on the cell viability of L929 fibroblasts in the presence of CoCr and alumina particles (Moisley 2014). However, Moisley (2014) reported large variation between repeats and therefore, these series of experiments were repeated. The results from this current study revealed that nanoscale and micron sized alumina particles induced a greater reduction in the cell viability in the absence of FBS in comparison to cells cultured with 10% (v/v) FBS. These results suggest that the formation of a protein corona around the alumina nanoscale and micron sized particles reduced the cytotoxic effects.

In contrast to the alumina particle results, the absence of FBS seemed to have a positive effect on cell viability for the L929 cells cultured with CoCr particles However, it must be noted that after day 2, there was no statistically significant difference between the cell viability of the fibroblasts cultured with nanoscale CoCr particles in the absence or presence of FBS. This highlights that the effect of FBS on particle toxicity is short term and the cells may partly recover over time. Another consideration is that over the incubation period, the nanoscale CoCr particles, in the absence of FBS, could have been coated with biological materials from cell secretions or cell damage and these moieties may have modified particle uptake and effect cell viability (Lesniak *et al.* 2013).

No overall difference in the effect of serum on the cytotoxicity of micron sized CoCr particles was observed over the 5 days of culture, which was in contrast to the nanoscale CoCr results previously discussed. This suggested that for CoCr, particle size was the major factor influencing on cell viability rather than the presence or absence of FBS. Cheng *et al.* (2015) also reported that particle size had a significant effect on cell viability and particle uptake of 5, 20 and 50 nm gold nanoparticles into Raw 264.7 cells cultured in the presence or absence of serum for 24 hours. The formation of protein coronae on the larger particles caused them to be less readily internalised in comparison to the smaller particles. These authors

hypothesised that in the presence of serum, particles of different sizes bind to different domains on the cell plasma membrane. This in turn causes the particles to be internalised into the cells *via* different endocytic pathways. For example, using endocytic inhibitors, Cheng *et al.* (2015) concluded that 50 nm gold nanoparticles in the absence of serum proteins would be taken into Raw 264.7 cells *via* caveolin-mediated endocytosis. In the presence of serum, the same particles were observed to be internalised *via* scavenger receptors.

Alongside particle size, these results suggest that particle cytotoxicity in the presence of serum is dependent on particle composition. The formation of a protein corona induced more cytotoxic effects, as in the case of CoCr nanoscale particles, or alternatively reduced the effects, as seen with the alumina nanoscale and micron sized particles. Whilst no direct comparisons with the literature on CoCr and alumina particles can be made, these varying results are consistent with the reported literature on other particle types investigated in nanotoxicology studies. Overall, whilst a number of other factors are involved, such as particle size, particle composition seems to play a major role on particle cytotoxicity in the presence or absence of serum as described previously (Rauch *et al.* 2013).

The presence of serum may have influenced the release of Co and Cr ions from the nanoscale CoCr particles, which in turn could have had an effect on the cell viability. Cobalt and Cr ions have been demonstrated to significantly reduce the cell viability of macrophages and osteoblasts over time *in vitro*, suggesting that the ions as well as the particles have cytotoxic effects (Catelas *et al.* 2005; Fleury *et al.* 2006; Kwon *et al.* 2009). Hedberg *et al.* (2014) demonstrated that Co and Cr ion release from CoCr particles was greater in the presence of BSA than in the absence of BSA. Vidal and Muñoz (2011) also revealed that the pH conditions had an effect on CoCr corrosion in the presence of BSA. At pH 3, BSA had a protective effect on particle corrosion, however at neutral and alkaline conditions, BSA promoted ion release.

Furthermore, molybdenum ion release has been reported to be increased in the presence of BSA (Simoes *et al.* 2015). Therefore the rate of ions released from the nanoscale CoCr particles may be higher in the presence of serum and subsequently have a greater effect on the cell viability. In contrast when in serum free (or reduced serum) conditions, the ion release is lower and therefore the potential effect on cell viability is reduced (Hedberg and Wallinder 2014). Further it could be speculated that this phenomenon may have occurred with the micron sized CoCr particles cultured with the fibroblasts with or without FBS. It has previously been demonstrated *in vitro* that micron sized particles corrode less than nanoscale particles when internalised within cells (Papageorgiou *et al.* 2007; Brown *et al.* 2013). Therefore the effect of ion release on cell viability may be reduced in the presence of CoCr micron particles compared to nanoscale CoCr particles, which may explain why no difference in cell viability was observed in the absence or presence of FBS with micron sized CoCr particles.

One drawback of the cell viability experiments performed in this study is that the protein coronae formed on the surface of alumina and CoCr particles was not characterised. Preliminary studies of nanoscale alumina particles using dynamic light scattering (DLS) demonstrated that particle agglomeration occurred in the presence of DMEM and DMEM supplemented with 10% (v/v) FBS. However, agglomerations greater than 1 µm were formed, which is too large for accurate sizing using DLS. Further experiments could investigate particle agglomeration under different conditions this using TEM and EDX techniques, as described by Simoes *et al.* (2015). This would provide useful information on formation of protein coronae by analysing the EDX spectra for element peaks representing the particles (cobalt, chromium or molybdenum) and proteins (nitrogen). Alongside this the rate of Co and Cr ion release from the surface of clinically relevant CoCr particles could also be determined in the presence or absence of serum using inductively coupled

plasma mass spectrometry (ICP-MS). These results would highlight the potential role of ion and protein complexes and their effect on cell viability.

5.4.2 The internalisation of nanoscale alumina and cobalt chromium particles into L929 fibroblasts in the absence or presence of foetal bovine serum

Following on from the cell viability assays, the internalisation of nanoscale and micron sized alumina and CoCr particles into fibroblast cells were investigated using TEM analysis. The cell viability experiments revealed that particle composition was a major influencing factor on cell viability in the presence or absence of FBS. Therefore, the effect of the presence or absence of 10% (v/v) FBS on particle uptake was explored to provide an greater insight into the potential mechanisms involved in particle cytotoxicity and potential effects of proteins on the interactions of particles with the cell plasma membrane. For these series of experiments, due to time pressures, only the nanoscale alumina and CoCr particles were investigated as these represent particles that have been reported to be released *in vivo*.

The nanoscale alumina particles at particle volumes of 50 and 5 μm^3 per cell were observed within the fibroblasts after 5 days using TEM analysis. Due to the hardness of alumina, it was technically very difficult to successfully section particle volumes over 50 μm^3 per cell, even with a diamond blade as the presence of a high particle concentration would cause major tears in the slides. Therefore, it was not possible to analyse the highest particle volume of 500 μm^3 per cell using TEM. The time point of 5 days was chosen as the largest differences in cell viability results was observed at this time point, in the presence or absence of FBS. However, overall no differences in particle uptake were observed between the samples cultured in the presence or absence of FBS. For all samples, the alumina particles

were revealed to be within membrane bound vesicles within the cytoplasm of the cells. Further, the particles were found to form large agglomerates, regardless of whether the particles were incubated with serum or not. No statistically significant differences were measured between the particle agglomerates in the presence or absence of 10% (v/v) FBS, at any particle volume.

Similar results to the alumina particles were also observed for the L929 fibroblasts cultured with nanoscale CoCr particles. Particle volumes of 50, 5 and 0.5 μm^3 per cell were cultured with L929 fibroblasts in the presence or absence of 10% (v/v) FBS over 2 days. Again this time point was chosen as the greatest effects on cell viability results were observed at this time point, in the presence or absence of FBS. Nanoscale CoCr particles were observed in all samples in the presence and absence of serum and appeared to have formed large agglomerates. The particles were also observed within membrane bound vesicles within the cytoplasm of the cells. However, the aggregates were much larger than those observed for the alumina particles, and many cells had multiple vesicles of CoCr particles. No statistically significant differences were measured between the particle agglomerates, at each particle volume, in the presence or absence of 10% (v/v) FBS. However, in the presence of serum, at the particle volume of 50 μm^3 per cell, the particle agglomerates were statistically larger than the lower particle volumes of 5 and 0.5 μm^3 per cell. Furthermore, in the presence of serum, at the particle volume of 50 μm^3 per cell, the particle agglomerates were statistically larger than the particle volume of 0.5 μm^3 per cell.

These results demonstrated that at higher particle volumes, the particles formed larger sized agglomerates regardless of the presence of serum. However, due to time constraints of the project, it was difficult to obtain a large number of images of particles within cells to size. This was particularly difficult for the lower particle volumes of 5 and 0.5 μm^3 per cell, where as little as 10 cells were observed to have

particles within the cells. Therefore the conclusions from these results are limited and would require further quantification.

Occasional particle-like structures were observed in the cytoplasm and nucleus of the cells which were not bound within vesicles for both the alumina and CoCr samples. EDX analysis revealed that these structures, for both the alumina and CoCr samples, were precipitates from reagents used in the sample preparation process. For example a lead peak in the EDX spectra corresponded to the lead citrate used in sample preparation. This suggests that in order for the particles to be internalised within vesicles, the particles are taken up *via* an active process. Corroded, cobalt chromium wear particles, which were nearly devoid of cobalt, have previously been visualised within vesicles of the cytoplasm of macrophages isolated from the periprosthetic tissues of a patient with a CoCr alloy metal-on-metal hip resurfacing implant (Goode *et al.* 2012). Furthermore, CoCr particles have been reported to be readily taken up and found within vesicles of the cytoplasm by a variety of cells, including HFBs and macrophages *in vitro* (Lewis *et al.* 2007; Papageorgiou *et al.* 2007).

At present this study is the only study to have confirmed the internalisation of alumina nanoscale particles within fibroblasts using TEM. Hashimoto *et al* (2015) investigated the internalisation of model alumina particles into macrophages. Analysis using TEM revealed that the particles were found within the nucleus of the cells and many particle were not within vesicles. However the authors failed to confirm the presence of the particles using EDX or equivalent analysis and therefore particle uptake was not validated.

This series of experiments which investigated the internalisation of alumina and CoCr particles by fibroblasts revealed no difference in particle uptake regardless of whether the fibroblasts were cultured in the presence or absence of serum.

Interestingly, these results do not reflect the results from the cell viability experiments. Cheng *et al.* (2015) also reported inconsistencies between cell viability and cell uptake results for Raw 264.7 macrophages cultured with gold nanoparticles in the presence or absence of serum. The cell viability results revealed no difference in the cell viability in the presence of gold nanoparticles with or without serum after 24 hours. However, particles were more readily internalised into the macrophages when incubated with serum proteins. This indicated that whilst the particles could be readily taken up by the fibroblast cells, this in itself does not necessarily correlate with cell viability results. This may suggest that more downstream effects are occurring, such as ion release into the cytoplasm, or that the particles may be interacting with the cell plasma membrane differently, depending on the formation of a protein corona.

5.4.3 The effect of particles on membrane integrity and particle binding to model membranes in the presence of foetal bovine serum

As previously described, the cell viability results revealed that alumina and CoCr particle size and composition induced an effect on fibroblast viability, in the absence or presence of FBS. Nanoscale alumina and CoCr particles cultured with L929 cells in the presence and absence of serum were confirmed to be internalised within vesicles of the cytoplasm using TEM techniques. The interaction of nanoscale and micron sized alumina and CoCr particles on the interactions with the cell plasma membrane, in the presence of serum proteins, were investigated. Specifically, the effect of alumina and CoCr particles on membrane integrity and particle binding in the presence of serum was explored.

The effect of nanoscale and micron sized alumina and CoCr particles on membrane integrity, in the presence of 10% (v/v) FBS, was explored using the vesicle leakage assay. Lipid vesicles, loaded with an autoquenching dye, were incubated with particles at concentrations of 1, 10 and 100 $\mu g.ml^{-1}$. The release of fluorescent dye from any damaged vesicles over time was measured and expressed as a percentage of the positive control, Triton-X 100, which is a detergent that disrupts vesicles. A dose dependent increase in vesicle leakage was measured for the nanoscale and micron sized alumina and CoCr particles. However, only the highest dose of 100 $\mu g.ml^{-1}$ of nanoscale alumina and CoCr particles induced significant damage to the vesicles, in comparison to the FBS only control. Nevertheless, even at this highest concentration of the nanoscale alumina particles, only 33.5% vesicle leakage was measured. This particle concentration is approximately five times higher than the highest particle volume used in the cell viability assays in this study and hence, is unlikely to be the main mode of particle toxicity.

Currently there is minimal published data on the role of wear particles and the integrity of the plasma membrane, especially in the presence of serum. Papageorgiou *et al*. (2007) reported observing vesicle damage in the presence of CoCr nanoscale particles in fibroblasts. Nevertheless no vesicle damage was observed during TEM analysis of the samples used in this current study. Silica and zinc oxide nanoparticles have been reported to induce pores within the membrane of A549 lung epithelial cells (Mu *et al.* 2012; Churchman *et al.* 2013; Mu *et al.* 2014). However, the formation of these pores did not necessarily induce cell death and therefore it was hypothesised that the formation of pores within the membrane must be extensive in order to reduce cell viability. Based upon the results from this model membrane, without the incorporation of isolated membrane proteins, it is unlikely that the nanoscale and micron sized alumina and CoCr particles, regardless of type or size elicited membrane damage or that this was a major mode of toxicity.

The interaction of nanoscale and micron sized alumina and CoCr particles with a sBLM in the presence of serum were also explored. As previously discussed in section 5.3.4.1, it was revealed that the FBS rapidly and irreversibly bound to the sBLM, making analysis of any subtle particle binding events difficult to detect. Therefore, it was decided to reduce the FBS concentration to 0.1% (v/v) and to incubate the particles with the FBS, diluted in DMEM, for 16 hours at 37°C. As previously described, the formation of a protein corona is a continuous process and overtime consists of a hard and soft corona. This incubation period allowed the formation of a stable protein corona. As previously described, there is a conflicting data on the role of serum on particle interactions with the membrane and subsequent uptake. One of the major reasons for this is the inconsistency between studies, making direct comparisons difficult. A select number of reports have recommended the standardisation of *in vitro* studies on the effect of particles on the membrane. For example Horrie *et al*. (2009) recommended the pre-adsorption of particles with serum before testing, and hence this study follows this recommendation.

The nanoscale and micron sized alumina and CoCr particles demonstrated no overall binding to the sBLM in the presence of serum. As stated in chapter four, in the absence of serum, the particles had an effect on the dissipation at a particle concentration of 100 $\mu g.ml^{-1}$. However, no effect on the frequency or dissipation was observed at any of the particle concentrations tested here (1 – 100 $\mu g.ml^{-1}$). The presence of serum has also been reported to reduce nanoparticle binding to a sBLM. Lesniak *et al.* (2012) reported reduced binding of carboxylated polystyrene nanoparticles to a POPC sBLM in the presence of serum, using QCM-D. Furthermore these authors reported that the serum bound irreversibly to the sBLM, with a large decrease in the frequency. The presence of the serum may have reduced the number of non-specific interactions of the native particle surface with

the sBLM, and hence a decrease in particle binding to the membrane. Duan *et al.* (2015) reported a reduction in the interaction of graphene oxide nanoparticles with the cell membrane of A549 lung epithelial cells, again stating that the formation of a protein corona reduced the exposed surface area of the particles and reduced particle: membrane interactions. Nevertheless it must be noted that the presence of protein has been reported to promote particle uptake. For example gold nanoparticles coated in fibrinogen have been demonstrated to bind with a greater affinity to the integrin receptor Mac-1 on macrophages than when fibrinogen was not present (Deng *et al.* 2011). Therefore particles with a low binding affinity for the lipid membrane may be more likely to interact with the membrane in the presence of serum. However, the conclusions from these studies are limited and should be viewed with caution, as simplified membranes are used, often only consisting of one type of lipid. In the current study the sBLM used was more representative of the cell plasma membrane of human fibroblasts, with representative concentrations of types of lipids and the inclusion of cholesterol. Therefore it can be concluded that in the presence of serum, no overall binding to the sBLM occurred for the nanoscale and micron sized alumina and CoCr particles, and that other factors, such as the presence of specific binding sites, determine particle binding and subsequent uptake into fibroblasts.

5.4.4 The effect of particles binding to a solid supported bilayer lipid membrane with incorporated membrane proteins in the presence of foetal bovine serum

To further increase the complexity and physiological relevance of the model membrane, membrane proteins isolated from primary HFB and U937 histiocytes were incorporated into the model lipid membrane. The recovery of isolated

membrane proteins from U937 histiocytes was very low and therefore due to sample shortage and time constraints, these proteins were only used for the vesicle leakage assays. The effect of FBS in the presence of the isolated membrane proteins was explored for nanoscale and micron sized alumina and CoCr particles using vesicle leakage and QCM-D studies.

The effect of alumina and CoCr nanoscale and micron sized particles on membrane integrity, for membranes containing isolated membrane proteins from either histiocytes or fibroblasts was investigated, in the presence of 10% (v/v) FBS. The vesicle leakage assays revealed a dose dependent increase in membrane damage for vesicles containing isolated primary HFB proteins, for all particle types, in the presence of serum. With the exception of the nanoscale CoCr particles, this was observed for vesicles containing U937 isolated membrane proteins. The increase in vesicle leakage measured was much lower than the vesicle leakage measured in the absence of membrane proteins (section 5.3.3). For example 100 $\mu g.ml^{-1}$ of nanoscale alumina particles, incubated with vesicles consisting of 20% (w/w) U937 histiocyte isolated membrane proteins, induced 14% leakage. However in the absence of isolated membrane proteins, 33% vesicle leakage was measured. This suggests that the proteins provide a protective effect against particle induced membrane damage. Again, these results highlight that nanoscale and micron sized alumina and CoCr particles do not damage the membrane integrity.

The QCM-D studies were performed using a sBLM formed from 20% (w/w) isolated membrane proteins from primary HFBs. Due to the low yield of isolated membrane protein from U937 histiocytes, only primary HFB membrane proteins were investigated. Again, as described in section 5.4.3.1 the particles were incubated with 0.1% (v/v) FBS for 16 hours at 37°C to allow the proteins within the serum to coat the particles and form a protein corona. For the alumina nanoscale and micron sized particles, a reduction in the frequency, accompanied with an increase in the

dissipation was observed at the highest particle concentration of 100 $\mu g.ml^{-1}$. These observations suggested that particle binding to the sBLM occurred. These results suggest that particle size for the alumina particle had no effect on particle binding. Moreover, in order for particle binding to occur, FBS and isolated membrane proteins from primary HFBs must be present. However it must be noted that with the alumina micron sized particles interaction with the sBLM was observed, the changes in frequency and dissipation were different each time the experiment was repeated. For example a frequency change of -12 Hz was measured for one repeat, but another only measured -3 Hz. Nevertheless, this study is the first to report that the presence of serum and proteins within the plasma membrane are key factors in nanoscale and micron sized alumina particle binding to a human fibroblast model membrane. These results suggest that alumina particle binding to the plasma membrane is mediated through the interactions with the proteins within the serum, which subsequently formed a protein corona. The proteins then act as a mediator to promote particle binding to the functional groups found on the membrane proteins of the sBLM.

Nanoparticle uptake *via* membrane proteins in the presence of serum, have previously been reported for multiple cell types and particle compositions including gold, silver and zinc oxide particles (Cheng *et al.* 2015; Franchi *et al.* 2015; Shang and Nienhaus 2015). Fleisher and Payne (2014b) demonstrated that particle composition can play a key role in particle interactions with the plasma membrane. In the presence of MEM, supplemented with 10% (v/v) FBS, uptake of cationic polystyrene nanoparticles was increased in comparison to particles incubated in the absence of serum in kidney epithelial cells *in vitro*. In contrast, under the same conditions, uptake of anionic polystyrene nanoparticles was reduced. This phenomenon was observed with polystyrene particles of varying diameter and cell

type, including epithelial and macrophages (Fleischer and Payne 2014a; Fleischer and Payne 2014b).

No overall binding to the sBLM containing isolated membrane proteins was observed for the nanoscale and micron CoCr size particles, in the presence of FBS. These results are in contrast to the QCM-D results for the nanoscale and micron alumina particles. Interestingly TEM analysis observed the internalisation of nanoscale CoCr particles into fibroblasts in the absence and presence of serum, thus suggesting that the particles must interact with the membrane in order to be taken up by the cells. This could be due to the particles binding to more specific receptors which not readily available on the sBLM. Potnis *et al.* (2013) recently reported that CoCr particles were found to bind to the TLR4 receptors of macrophages *in vitro.* Therefore, more specific binding sites could be required for particle: membrane interactions to occur. Furthermore, the QCM-D experiments only observed the interactions for a short period of time of 30 minutes and this does not reflect the timescale used for the cell viability and TEM experiments. It maybe that over time the CoCr particles can bind to the membrane, however, it can be concluded that the particles do not readily bind to the membrane. The TEM results revealed that the nanoscale CoCr particles were located within vesicles of the cytoplasm of fibroblasts. Another consideration is that once the particles are internalised within the cells, the particles may induce toxic effects on the cell. Further the particles within the vesicles could bind to lysosomes. The acidic conditions of the lysosomes may promote ion release from the particles, which may induce adverse effects within the cells such as DNA damage (Parry *et al.* 2010; Sood *et al.* 2011). Initial studies demonstrated that CoCr particles at concentrations greater than 10 $\mu g.ml^{-1}$ induced membrane damage at pH 5 using the vesicle leakage assays. However the extreme pH also caused the vesicle to lyse

irrespective of the presence of CoCr. Therefore future investigations into the internalisation of CoCr particles require significant optimisation.

It would be expected that in the presence of serum, the alumina particle interactions with the model membrane would be reduced as the particles were less cytotoxic than in the absence of serum. This suggests that whilst nanoscale and micron sized alumina particles bind to the membrane in the presence of FBS and isolated membrane proteins, the serum proteins do not promote cytotoxic effects. In contrast, the nanoscale CoCr particles were observed to be more cytotoxic in the presence of serum, however no binding to the membrane was observed in the presence of serum. These results further highlight that interactions with the cell membrane and subsequent uptake in the presence or absence of serum does not necessarily correlate with the cytotoxic effects observed for fibroblasts.

Furthermore, the discrepancies between cell viability, TEM and membrane experiments may be due to the sensitivity of the membrane studies. For the vesicle leakage assay and especially for the QCM-D experiments, the testing conditions can be carefully controlled, forming a truly protein free environment. Whereas the TEM and cell viability conditions are unlikely to be completely protein free due to cell secretions. Therefore the cell viability and TEM results are likely to demonstrate the effects of reduced protein conditions. Another consideration, which may cause discrepancies in the results, is the difference in timescales between the various experiments. For example the particle incubation period with the sBLM is approximately 30 minutes for the QCM-D experiments, whereas the cell viability experiments occur over 5 days. In addition to this, the TEM and cell viability assays used a fibroblast cell line whereas the QCM-D and vesicle leakage experiments used membrane proteins isolated from primary HFBs. Franchi *et al*. (2015) demonstrated differences in particle uptake for silver and titanium dioxide particles incubated with a fibroblast cell lines and primary cells. The authors hypothesised

that different membrane proteins on the surface of the cells induced differing binding affinities. Therefore this must be taken into consideration with the current study. Future work could extend this study to explore nanoscale and micron sized alumina and CoCr particle interactions with the cell plasma membrane of more clinically relevant primary cell types. In addition the differences between phagocytic and primarily non-phagocytic cells could be investigated.

5.4.5 Conclusion

The role of FBS on nanoscale and micron sized alumina and CoCr particles were explored. In the absence of FBS, nanoscale and micron sized alumina particles were reported to significantly reduce the cell viability of fibroblasts in comparison to cell cultured in the presence of FBS. Interestingly, the opposite was observed for the CoCr nanoscale particles. However, these results did not correlate with TEM analysis as no differences in particle uptake were observed in the presence or absence of FBS for both the nanoscale alumina and CoCr particles.

The presence of serum did not induce particle binding to a sBLM for all particle types, suggesting that the formation of a protein corona reduced the potential interactions of the particles with the sBLM. Furthermore, no extensive vesicle leakage was observed in the presence of serum, even with vesicle containing isolated membrane proteins. This suggests that the mode of toxicity for both alumina and CoCr particles is not caused *via* pore formation in the plasma membrane.

Interestingly, in the presence of serum, nanoscale and micron sized alumina particles bound to a sBLM consisting of 20% (w/v) isolated fibroblast membrane proteins. This suggests that the interaction of the protein corona on the surface of the particles and the functional groups of the membrane proteins is important for

particle uptake. In contrast no overall binding was observed for the nanoscale and micron sized CoCr particles in the presence of serum and isolated membrane proteins. At present it is unclear what key factors are required to promote CoCr interaction with the membrane and subsequent uptake. Like the alumina particles results, this does not correlate with the TEM and cell viability results. This suggests that the timescales used may have an influence or that CoCr particle require more specific interactions which are beyond the complexity of the model used. Overall it can be concluded that particle size does not appear to have an effect on membrane interactions but rather particle composition is a major influencing factor. However, particle binding to the membrane does not necessarily induce cytotoxic effects within fibroblasts.

Chapter 6
Discussion

6.1 Introduction

Hard-on-hard THRs, such as metal-on-metal and alumina ceramic-on-ceramic, were perceived as attractive alternatives to conventional UHMWPE prostheses for younger, more active individuals due to the reported low wear rates (Bessette *et al.* 2003; Dowson *et al.* 2004). The use of large diameter metal-on-metal THRs and resurfacing implants were also demonstrated to theoretically improve the range of motion of the joint (Underwood *et al.* 2011). However, metal-on-metal THRs, particularly large diameter bearing prosthesis, such as the ASR implant, have been associated with adverse reactions in patients such as necrosis of periprosthetic tissue, delayed-type IV hypersensitivity reactions, and pseudotumours (Pandit *et al.* 2008; Campbell *et al.* 2010; Hart *et al.* 2012). These tissue reactions have been reported to be associated with the CoCr wear particles and associated ions released from the implants, however the severity of the adverse reactions did not necessarily correspond to the wear rate of the implant (Hart *et al.* 2012; Matthies *et al.* 2012). In contrast alumina ceramic-on-ceramic THRs have been reported to be very low wearing, even under adverse conditions such as rotational or translational malpositioning (Al-Hajjar *et al.* 2013a; Al-Hajjar *et al.* 2013b). Subsequently few adverse biological effects of ceramic-on-ceramic THRs have been reported in patients (Esposito *et al.* 2012).

In vitro studies on CoCr wear particles have revealed cytotoxic and genotoxic effects, the ability to induce inflammatory responses and oxidative stress in a variety of cell types (Tkaczyk *et al.* 2010; Behl *et al.* 2013; Brown *et al.* 2013b).In addition, at very high particle doses, not usually achieved *in vivo*, alumina wear particles have been demonstrated to be cytotoxic and genotoxic (Germain *et al.* 2003; Tsaousi *et al.* 2010). Nevertheless the number of studies on the effect of

alumina wear particles *in vitro* is very limited. This is further compounded by a number of studies not using clinically relevant wear particles in terms of size, morphology and composition (Hallab *et al.* 2000; Dalal *et al.* 2012). Therefore the mechanisms of CoCr and alumina wear particle toxicity are not fully understood.

An area of wear particle toxicity that has not been extensively investigated is the interaction and effect of wear particles on the cell plasma membrane. The cell plasma membrane plays a particularly important role in the cellular response to particles and effects whether the particles are internalised or cause membrane damage (Gill *et al.* 2012). This area of research is increasingly popular within the field of nanotoxicology, such as improving drug delivery, and a number of techniques can be employed to study the effect of wear particles on the cell plasma membrane. These include the use of biomimetic techniques of QCM-D and SPR, which provide a sensitive analysis of particle interactions with a model membrane (Dixon 2008; Mahmoudi *et al.* 2011). Furthermore, parameters such as the formation of protein coronas and the incorporation of proteins within the membrane can be investigated due to the highly controlled environment that these techniques provide (Mahmoudi *et al.* 2011).

This project aimed to investigate if nanoscale and micron sized alumina and CoCr particles were able to damage or passively pass the cell membrane with adverse consequences.

6.2 Generation and characterisation of nanoscale and micron sized alumina and cobalt chromium particles

The first objective of the study was to generate and isolate nanoscale and micron sized alumina and CoCr particles for subsequent cell and model membrane experiments in terms of particle size, morphology, and composition. These particle

properties have widely been demonstrated to affect cellular responses, such as cytokine production, genotoxic responses and cell viability (Hallab *et al.* 2010; Tsaousi *et al.* 2010; Sood *et al.* 2011; Behl *et al.* 2013; Brown *et al.* 2013b). The main findings from this current study are summarised in the following:

- Nanoscale CoCr particles were generated using a simple pin-on-plate wear simulator, which mimicked the loading and kinematics conditions of the standard gait cycle (Jin *et al.* 2000). The isolated nanoscale CoCr particles from this current study were analysed and a mode particle size of 40 – 49 was measured. Simulator studies and *ex vivo* particle studies have reported nanoscale wear particles of a similar size under standard conditions (Doorn *et al*. 1998; Firkins *et al.* 2001b; Brown *et al.* 2007; Papageorgiou *et al.* 2007).
- In order to investigate the effect of particle size on cell viability and membrane integrity, commercially available micron sized CoCr particles were used. The mode particle size was measured at 2 – 3 µm, with a mean particle size of 3.26 µm (± SD 1.30 µm). Comparable results to the findings from this study, in terms of particle size range, morphology and composition, have been reported in the published literature (Papageorgiou *et al.* 2007).
- Using sequential filtration techniques, the micron sized alumina particles were isolated from an alumina powder and a mode particle size of 400 – 449 nm, with a particle size range of 17 – 1464 nm was measured. As the particle size range fell within the micron size range, this particle stock was referred to as micron sized alumina particles to differentiate from the smaller nanoscale alumina particles. As previously described a bimodal particle size distribution has been reported for ceramic-on-ceramic THRs (Hatton *et al.* 2002).
- A commercially available alumina powder was purchased and used for the nanoscale alumina particles. The particles had a mode particle size of 30 – 39 nm, which was greater than the particle sizes in the published literature of less than 20 nm (Hatton *et al.* 2002; Tipper *et al.* 2002; Germain *et al.* 2003).

However comparisons against the micron sized alumina particles were still investigated.

- Prior to using the nanoscale and micron sized alumina and CoCr particles for the membrane experiments, the effect of the particles on cell viability was also measured. Due to the highly reactive nature of the nanoparticles, a false negative or false positive readout can be generated during cell viability experiments (Monteiro-Riviere *et al.* 2009). Therefore, more than one cell type and using a least two cell assays was used in this current study. Furthermore a particle only control was also used in all cell viability experiments to measure the potential interference of the particles with the assay. The presence of nanoscale and micron sized alumina particles were revealed to increase the MTT readouts at the highest particle volume. The particle only control corrected for this. The use of particle only controls, when assessing the effect of particles, are often not considered within the published literature (Dalal *et al.* 2012).
- Primary HFBs and a U937 histiocyte cell line were cultured with the particles as these cell types have been reported to interact and engulf the particles *in vivo*. A U937 histiocyte cell line was chosen as only a limited number of cells can be isolated from human blood and the large numbers of cells were required, particularly for the QCM-D studies and therefore it was not feasible to use PBMNCs. The ATPlite and MTT assays were used to measure the effect of the particles on cell viability.
- The nanoscale and micron sized alumina particles were observed to have limited effects on the cell viability of both U937 histiocytes and primary HFBs, using the ATPlite and MTT assays at particle volumes of 0.0005 – 500 μm^3 per cell over five days. The only significant effects on the cell viability were for the nanoscale and micron sized alumina particles were observed at the higher particle volumes. Nevertheless, as previously reported, the wear rates of ceramic-on-ceramic THRs are very low, with wear rates of 0.1 $mm^3/ 10^6$ cycles

reported under adverse conditions (Al-Hajjar *et al.* 2010). Therefore the likelihood of cells encountering particle volumes as high as those used in these experiments is very rare. Studies using commercially available alumina particles have also reported the effect of alumina particles on the viability of a number of cell types, with most studies also only reporting cytotoxic effects at high particle concentrations (Catelas *et al.* 1999; Germain *et al.* 2003; Hatton *et al.* 2003; Granchi *et al.* 2004; Gutwein and Webster 2004; Dalal *et al.* 2012).

- The nanoscale CoCr particles were observed to have significant adverse effects on primary HFB and U937 viability. Overall the results suggested that the nanoscale CoCr particles had a dose and time-dependent effect on primary HFB and U937 viability. Studies using the same pin-on-plate simulator method to generate CoCr particles reported very similar results to this current study (Germain *et al.* 2003; Brown *et al.* 2006; Papageorgiou *et al.* 2007; Bhabra *et al.* 2009; Papageorgiou *et al.* 2014).
- The micron sized CoCr particles only induced a significant reduction in the U937 and primary HFB viability at the highest particle volume dose of 50 μm^3 per cell, when assessed using the MTT assay. Micron sized CoCr particles have also been reported to have a less of an effect on cell viability of primary HFBs in comparison to nanoscale CoCr particles (Papageorgiou *et al.* 2007).

6.3 The effect of particles on the cell plasma membrane

In order to investigate the effect of nanoscale and micron size alumina and CoCr particles on the cell plasma membrane, recently developed methods within the field of nanotoxicology have been implemented. These include the use of simple vesicle leakage assays, QCM-D and SPR techniques, which have been used in this current study (Green *et al.* 2000; Cho *et al.* 2010; Mu *et al.* 2014). In an attempt to make the model membranes more clinically relevant, the composition of the model lipid

membrane employed in this study consisted of a phospholipid: cholesterol mixture similar to the composition of primary HFBs (Schroeder *et al.* 1984; Mahadik *et al.* 1994). At present this is the first instance where a model fibroblast membrane has been used to investigate particle: membrane interactions.

6.3.1 The effect of particles on the binding and integrity of a model lipid cell plasma membrane

Initially, the effects of nanoscale and micron size alumina and CoCr particles on membrane integrity were investigated using a simple vesicle leakage assay previously described in the literature (Mu *et al.* 2012). The results revealed that both the nanoscale and micron size alumina and CoCr particles induced a minor increase in the vesicle leakage of the model lipid membrane. The nanoscale and micron sized alumina particles induced a larger vesicle leakage than the nanoscale and micron size CoCr particles, whereby the highest nanoscale alumina particle concentration of 100 $\mu g.ml^{-1}$ caused a 16% increase in vesicle leakage. In addition to this the particle concentrations used in the vesicle leakage assays (up to and including 100 $\mu g.ml^{-1}$) are much higher than the volume concentrations used in the cell viability assays (approximately 25 fold higher) described in Chapter three and five and would not be observed within a clinical scenario. Therefore it is unlikely that the main modes of toxicity for nanoscale and micron size alumina and CoCr particles are direct damage to the plasma membrane and is unlikely to occur *in vivo*.

The binding of nanoscale and micron sized alumina and CoCr particles to model lipid membranes were also investigated using QCM-D. This technique has recently been implemented within the field of nanotoxicology and is highly sensitive and can measure changes in mass as low as 100 $pg.cm^{-2}$ over the crystal area. (Cho *et al.*

2010). The results for the QCM-D experiments revealed that none of the nanoscale and micron sized alumina and CoCr particles caused a significant reduction in the frequency at any particle concentrations tested. A reduction in the frequency would indicate particle binding. An example of binding to a membrane can be observed in Appendix C and section 1.6.3.2. For all particle types, a rise in the dissipation was observed with increasing particle concentration. This has been previously described by Karlsson *et al.* (2013) for copper nanoparticles in the presence of a sBLM however, no reasoning or further investigation into the increase in dissipation was provided by these authors.

To quantify the binding of the nanoscale and micron sized alumina and CoCr particles to the sBLM, the frequency and dissipation data at all overtones was modelled using the Voight model. The Voight model is commonly used for QCM-D studies of sBLMs (Voinova *et al.* 1999). The modelling outputs for the nanoscale and micron sized alumina and CoCr particles revealed that stable sBLMs had been formed. However, the second layer of the model was not characteristic of either alumina or CoCr particles. Therefore it was hypothesised that the increase in dissipation may have been caused by an intermediate layer being formed between the sBLM and the particles, known as a slippage layer (Daikhin *et al.* 2000). The presence of the slippage layer would have caused no overall change in the frequency but may have increased the dissipation outputs. However, it was not possible to model this using the Voight model as this is limited to modelling only two layers. Therefore, a complementary technique to QCM-D of SPR was used to confirm particle binding. Using the nanoscale CoCr particles as an example no particle binding was observed at the highest particle concentration tested of 100 $\mu g.ml^{-1}$ using this technique. These results suggest that the change in dissipation may have been caused by very weak interactions between particles and sBLM or, alternatively, a minor disrupting effect on the sBLM without permanent adherence of the particles.

6.3.2 The incorporation of fibroblast membrane proteins into the model lipid membrane on the binding of particles

Membrane proteins, isolated from the cell membranes of U937 histiocytes and primary HFBs were incorporated into the model lipid membrane to further increase the complexity and clinical relevance of the model. Preliminary experiments revealed that the optimal protein concentration to form a solid supported planar membrane was 20%, which was in good agreement with the literature (Dodd *et al.* 2008). This complex model membrane has not been used in literature and was considered a novel, clinically relevant model of a human fibroblast cell membrane.

The effect of nanoscale and micron sized alumina and CoCr particles on membrane integrity in the presence of membrane proteins was investigated using the vesicle leakage assay. The membrane proteins isolated from U937 histiocytes and primary HFBs were used in these experiments. For both types of isolated proteins, no extensive vesicle leakage was observed for the nanoscale and micron sized alumina and CoCr particles. This suggests that pore formation within the cell membrane is not the main mode of particle toxicity.

Nanoscale and micron sized alumina and CoCr particle interaction with the sBLM containing 20% (w/w) isolated membrane proteins was also explored. Due to low protein recovery rates from U937 histiocytes, only the proteins isolated from primary HFBs were tested. Again the results for the nanoscale and micron sized alumina and CoCr particles demonstrated no overall decrease in the frequency. Instead an increase in the dissipation was observed which was considered to indicate no or only weak particle binding to the sBLM.

6.4 The effect of serum proteins on the interaction of particles with a model lipid membrane

This part of the study aimed to investigate the effects of alumina and CoCr particles, which were cultured with in the presence of 10% (v/v) FBS, to determine the effect on fibroblast cell viability, membrane integrity and binding to the cell membrane. Currently there are a limited number of studies that have investigated the effect of serum on wear particle toxicity as described in section 1.5.4 (Hallab *et al.* 2000; Lewis *et al.* 2007; Vidal and Muñoz 2011; Hedberg and Wallinder 2014; Hashimoto and Imazato 2015). However, proteins within FBS are known to bind to the surface of particles causing the formation of a protein corona, which can in turn alter the cellular responses to the particles, such as the effect on cell viability (Mahmoudi *et al.* 2011; Rauch *et al.* 2013).

6.4.1 The effect of the presence of foetal bovine serum on particle cell viability

The results revealed that particle cytotoxicity in the presence of serum was dependent on particle composition. Nanoscale and micron sized alumina particles induced a greater reduction in the cell viability, in the absence of FBS, in comparison to cells cultured with 10% (v/v) FBS. These results suggest that the formation of a protein corona around the alumina nanoscale and micron sized particles reduced the cytotoxic effects. In contrast, the absence of FBS seemed to have a less of an effect on cell viability for the L929 cells cultured with CoCr particles at 48 hours. However by day 5, this effect was no longer apparent, suggesting that the effects were short term and the cells may partly recover over time. No differences in the effect of serum on the cytotoxicity of micron sized CoCr particles were observed over the 5 days of culture. This suggested that for CoCr,

particle size was the another major factor influencing on cell viability rather than the presence or absence of FBS, whereby the nanoscale CoCr particles were more cytotoxic than the micron sized particles. The influence of particle size in the presence of serum has also been described in the literature for gold nanoparticle uptake into Raw 264.7 macrophage cells. The formation of protein coronae was reported to decrease particle uptake with increasing particle size (Cheng *et al.* 2015).

6.4.2 The internalisation of nanoscale alumina and cobalt chromium particles into L929 fibroblasts in the presence or absence of foetal bovine serum

The internalisation of nanoscale alumina and CoCr particles into fibroblast cells was investigated using TEM analysis. Based upon the results obtained in Chapter five, particle volumes and time points which caused a significant reduction in cell viability were selected. Nanoscale alumina particles at particle volumes of 50 and 5 μm^3 per cell were cultured with L929 fibroblasts with or without 10% (v/v) FBS for 5 days. Nanoscale CoCr particles at particle volumes of 50 and 5 μm^3 per cell were cultured with L929 fibroblasts with or without 10% (v/v) FBS for 2 days. For both particle types, at all particle doses tested, no differences in particle uptake were observed between the samples cultured in the presence or absence of FBS. For all samples, the particles were revealed to have formed aggregates within membrane bound vesicles within the cytoplasm of the cells.

Interestingly, these results do not reflect the results from the cell viability experiments. Cheng *et al.* (2015) also reported inconsistencies between cell viability and cell uptake results for Raw 264.7 macrophages cultured with gold nanoparticles, in the presence or absence of serum. The cell viability results

revealed no difference in the cell viability in the presence of gold nanoparticles with or without serum after 24 hours. However, particles were more readily internalised into the macrophages when incubated with serum proteins. This indicated that whilst the particles could be readily taken up by the fibroblast cells, this in itself does not necessarily correlate with cell death.

6.4.3 The effect of particles on membrane integrity and particle binding to model membranes in the presence of foetal bovine serum

The effect of nanoscale and micron sized alumina and CoCr particles on membrane integrity, in the presence of 10% (v/v) FBS, was explored using the vesicle leakage assay. Only the highest doses of 100 $\mu g.ml^{-1}$ of nanoscale alumina and CoCr particles induced significant damage to the vesicles, in comparison to the FBS only control, again highlighting that it is unlikely to be the main mode of particle toxicity. The formation of these pores did not necessarily induce cell death and therefore it was hypothesised that the formation of pores within the membrane was not extensive enough to reduce cell viability.

Particle binding to a sBLM in the presence of serum was also investigated. However, FBS rapidly and irreversibly bound to the sBLM, making analysis of any subtle particle binding events difficult to detect. This also demonstrated that the QCM-D and model membrane used were able to measure membrane binding. Therefore, it was decided to reduce the FBS concentration to 0.1% (v/v) and to incubate the particles with the FBS, in DMEM, for 16 hours at 37°C prior to the membrane experiments. The nanoscale and micron sized alumina and CoCr particles demonstrated no overall binding to the sBLM in the presence of serum. This has also been reported within the literature. For example, Lesniak *et al.* (2012)

reported reduced binding of carboxylated polystyrene nanoparticles to a POPC sBLM in the presence of serum, using QCM-D. It is hypothesised that the serum binding to the membrane reduces the available sites of interactions of the membrane for the particles to bind to.

6.4.4 The effect of particles binding to a solid supported bilayer lipid membrane with incorporated membrane proteins in the presence of foetal bovine serum

Membrane proteins isolated from primary HFB and U937 histiocytes were incorporated into the model lipid membrane to investigate particle effects on membrane integrity and binding. Due to the low recovery rates and time constraints, the isolated membrane proteins from U937 histiocytes were only used for the vesicle leakage assays. Therefore only proteins from HFBs were used for the QCM-D experiments.

The vesicle leakage assays revealed minor increases in membrane damage for vesicles containing isolated primary HFB proteins, for all particle types, in the presence of 10% (v/v) FBS. However the membrane damage induced by the particles was low and required particle concentrations much greater than those observed within the clinical scenario. Again, these results highlighted that nanoscale and micron sized alumina and CoCr particles did not damage the membrane integrity.

The QCM-D studies were performed using a sBLM formed from 20% (w/w) isolated membrane proteins from primary HFBs. The particles were incubated with 0.1% (v/v) FBS for 16 hours at 37°C, to allow the proteins within the serum to coat the particles and form a protein corona prior to the start of the QCM-D experiments. For the alumina nanoscale and micron sized particles, a reduction in the frequency,

accompanied with an increase in the dissipation was observed at the highest particle concentration of 100 $\mu g.ml^{-1}$. These observations suggested that particle binding to the sBLM occurred in the presence of FBS and isolated membrane proteins from primary HFBs. However, it must be noted that with the alumina micron sized particle interaction with the sBLM was observed, the changes in frequency and dissipation were different each time the experiment was repeated. For example a frequency change of -12 Hz was measured in one experiment, but another only -3 Hz was measured in another. This could be caused by variation in the structure of the proteins incorporated in the membrane between each repeat.

Nanoparticle binding *via* membrane proteins in the presence of serum, has previously been reported for multiple cell types and particle compositions including gold, silver and zinc oxide particles (Cheng *et al.* 2015; Franchi *et al.* 2015; Shang and Nienhaus 2015). This phenomenon was observed with polystyrene particles of varying diameter and cell type, including in epithelial and macrophages (Fleischer and Payne 2014a; Fleischer and Payne 2014b).

No overall binding to the sBLM containing isolated membrane proteins was observed for the nanoscale and micron CoCr size particles, in the presence of FBS. Interestingly TEM analysis observed the internalisation of CoCr nanoscale particles into fibroblasts in the absence and presence of serum, thus suggesting that the particles must interact with the membrane in order to be taken up by the cells. Possible reasons for the lack of binding include the particles binding to more specific receptors, which are not readily available in the sBLM. Potnis *et al.* (2013) recently reported that CoCr particles were found to bind to the TLR4 receptors of macrophages *in vitro.* Therefore, more specific binding sites could be required for particle: membrane interactions to occur. Furthermore, the QCM-D experiments only observed the interactions for a short period of time of 30 minutes and this does not reflect the timescale used for the cell viability and TEM experiments. It maybe

that overtime the CoCr particles can bind to the membrane, however, it can be concluded that the particles do not readily bind to the membrane.

Furthermore, the discrepancies between cell viability, TEM and membrane experiments may be due to the sensitivity of the membrane studies. For the vesicle leakage assay and especially for the QCM-D experiments, the testing conditions can be carefully controlled, forming a truly serum free environment. Whereas the TEM and cell viability conditions are unlikely to be completely protein free due to cell secretions. Therefore the cell viability and TEM results are likely to demonstrate the effects of reduced serum conditions, rather than serum free conditions.

6.5 Novelty of current study

The following novel approaches were used in this current study to investigate the interaction of particles with the model membrane, which are summarised in the following:

- The effect of nanoscale and micron sized alumina and CoCr particles on membrane damage using the vesicle leakage assay has not been investigated previously.
- The interactions of nanoscale and micron sized alumina and CoCr particles with a model membrane using QCM-D.
- The use of a membrane model, which represents the membrane composition of fibroblasts has not been studied previously.
- The incorporation of membrane proteins into the model membrane and subsequent effects on particle induced membrane damage or particle binding have not been studied in the context of nanoscale and micron sized alumina and CoCr particles.

- Similarly, the presence of serum on the model membrane and subsequent effects on particle induced membrane damage or particle binding have not been studied in the context of nanoscale and micron sized alumina and CoCr particles.

6.6 Limitations of current study

There are a number of limitations and proposed future experiments, which were beyond the scope and time frame of this present study. One such limitation is the use of commercially available nanoscale and micron sized alumina particles within this present study. Due to the low wear rates of ceramic-on-ceramic bearings, currently there is no isolation protocol which would isolate sufficient volumes of particles for the cell membrane experiments. Therefore, it was not feasible to isolate particles from simulator lubricant. However, for completeness it would have been ideal to compare the results with particles isolated from serum lubricant. Furthermore, different alumina composites are currently used in the manufacture of ceramic-on-ceramic THRs and include ATZ and ZTA (Stewart *et al.* 2003; Stewart 2010). Future studies could investigate the effect of the different alumina composites on membrane interactions to determine if there are any differences. No significant differences have been observed between alumina and zirconia particles on the macrophage viability, however it would be interesting to determine if this is also reflected in subsequent membrane studies (Catelas *et al.* 1999).

A limitation of the cell viability assays is that the effect of Co and Cr ions was not separately investigated. Ions are known to be released from the bearing surface and wear particles and have been reported to be cytotoxic, even at physiological relevant levels (Bhabra *et al.* 2009; Andrews *et al.* 2011; Goode *et al.* 2012; Brown *et al.* 2013a; Posada *et al.* 2014). However, the current study only investigated CoCr particles and therefore, it cannot be determined if the reduction in cell viability

was caused by the particles, the release of ions into the surrounding culture medium, or a combination of both. In addition to this, the effect of ions in the presence of a protein corona could be investigated. The formation of a protein corona on CoCr particles has been associated with the accelerated release of ions into the surrounding medium (Simoes *et al.* 2015). The release of ions from the CoCr particles could also be assessed, using TEM and EDX analysis, to determine if the presence of serum promotes ion release as described by Simoes *et al.* (2015).

Another limitation of this present study was that the particles were not confirmed to be endotoxin free. The nanoscale and micron sized alumina and CoCr particles were sterilised, using a hot air oven at 190°C for 4 hours, which has been demonstrated to reliably produce endotoxin free particles (Brown *et al.* 2006; Sood *et al.* 2011; Papageorgiou *et al.* 2014). However, for completeness it would have been ideal to have confirmed this.

One of the major limitations of the QCM-D and vesicle leakage studies is that the timings of the experiments did not reflect the timings used in the cell viability assays as it is not possible to perform the membrane experiments over a period of days. Therefore it is difficult to directly compare the results from the membrane studies with the cell viability or internalisation experiments from Chapter three and five, respectively. As previously mentioned, the concentration of FBS had to be reduced from 10% (v/v) to 0.1% (v/v) for the protein corona membrane experiments. This was due to the FBS binding to the membrane and possibly inhibiting any binding occurring. Ideally, the membrane experiments would have been performed in the presence of 10% (v/v) FBS to make comparisons with the cell studies easier. Furthermore the sensitivity of the QCM-D method meant that it was difficult in some instances to determine if particle: membrane interactions were occurring or were due to a possible artefact.

6.7 Future studies

Future studies on certain aspects of this current study could be implemented to improve the design of the experiments and to further investigate the potential effect of nanoscale and micron sized alumina and CoCr particles on membrane toxicity.

The findings from this present study revealed that nanoscale alumina and CoCr particles were internalised into L929 fibroblasts in the presence or absence of 10% (v/v) FBS. It is not known the proportion of particles were internalised by the cells. However, these results did not correlate with the cell viability assays of Chapter five, which suggested that the presence of 10% (v/v) FBS affects the viability of L929 fibroblasts cultured with the particles. Future studies could investigate this further and one proposed idea is to explore more closely the localisation of the particles within the cells. This could highlight the potential mechanisms of particle toxicity once inside the cells. In the case of the CoCr particles, if they were located within the lysosomes of the cells, the acidic environment could promote ion release, which could be a possible mode of toxicity once internalised. One possible method to explore this hypothesis would be to use specific gold-labelled antibodies for lysosome or other organelles, which could be observed using TEM (Kuo 2007). Confirmation of particle localisation as well as antibody binding could be confirmed using EDX analysis as described in Chapter five.

The results from Chapter five revealed that in the presence of 10% (v/v) FBS, nanoscale and micron sized alumina particles bound to a tethered membrane containing membrane proteins, using QCM-D. These results suggested that in order for alumina particle binding to occur, both 10% (v/v) FBS and membrane proteins were required. However, this was only observed at very high concentrations, much greater than those generated under normal conditions by ceramic-on-ceramic THRs. Future studies could further investigate the potential particle: protein interactions. The formation of a protein corona could be confirmed

by analysing particles in the presence or absence of 10% (v/v) FBS using dynamic light scattering methods as described by Churchman *et al.* (2013). The main proteins within the protein corona could also be analysed using a method adapted from Fleischer and Payne (2014a). In brief, repeated centrifugation steps are performed on the particles incubated with 10% (v/v) FBS. The supernatant would be loaded onto a polyacrylamide gel for analysis using electrophoresis and a Coomassie protein stain performed. The molecular weight of the protein band can be compared to commonly found proteins within FBS to determine which proteins bound to the particles. For example the presence of albumin corresponds to a protein band at 66 kDa. For proteins still bound to the particle surface a SDS wash could be used to solubilise the proteins for further electrophoresis analysis.

Another future study would be to determine if the nanoscale and micron sized alumina and CoCr particles are actively taken up into cells. As previously stated, the nanoscale alumina and CoCr particles were observed within the cytoplasm of L929 fibroblasts using TEM, However to establish if the particle were taken up *via* an active process, the cells could be cultured with the particles at 4°C, as described by Mu *et al.* (2012). This drop in temperature would prevent any active cell uptake to occur. The cells cultured with the particles could then be prepared for TEM analysis as described in Chapter five and if the particles were no longer located within the cells or are significant reduced in number, then the particles are more likely to be actively taken up. Alongside this the use of specific inhibitors of different types of endocytosis, such as clathrin- and caveolae-mediated endocytosis could be used as described by Rejman *et al.* (2004) to determine the uptake mechanism of the particles.

This present study was unable to determine the specific factors required for nanoscale and micron sized CoCr particles to interact with the model lipid membrane. The CoCr particles were demonstrated to be internalised within L929

fibroblasts. However, the interactions with the membrane were not apparent using the techniques employed in this study. The interaction of CoCr particles with membrane proteins isolated from primary HFBs were only assessed using QCM-D. A limitation of the QCM-D experiments employed in Chapter five is that the orientation and composition of the proteins within the membrane were not considered and it is possible that the binding sites for the CoCr particles were not readily available. However, cell specific responses and particle interactions with membrane proteins isolated from L929 fibroblasts and U937 histiocytes could also be investigated. Indeed, TLR-4 receptors have been associated with CoCr particle induced inflammation, suggesting CoCr particle binding to the membrane is limited to specific proteins (Potnis *et al.* 2013). This is a particularly interesting area of research and could be a potentially important factor in CoCr particle toxicity in patients. The binding of CoCr particles to the TLR-4 receptor or other specific membrane receptors could be investigated using the QCM-D and vesicle leakage methods used in this current study. The TLR-4 could be isolated and incorporated in the model membrane and the effect on particle: membrane interactions could be measured *via* QCM-D. The environment during QCM-D experiments can be tightly controlled and the addition of certain factors can be investigated. This is particularly advantageous in comparison to *in vitro* cell studies whereby the environment in which the cells are cultured in the presence of the particles can be affected by other compounding factors. For example, investigating the effect of serum on cell viability and forming a truly serum-free environment as described previously.

Another proposed method is to investigate CoCr particle interactions with the plasma cell membrane using QCM-D methods in conjunction with other techniques. Whilst QCM-D is highly sensitive, this can make analysis of data particularly challenging. Therefore techniques such as atomic force microscopy and SPR could be used to provide a greater insight into the interaction of particles with the cell plasma membrane (Mahmoudi *et al.* 2011). Dual-Polarization Interferometry (DPI)

with QCM-D has also been used to investigate protein binding and the combination of techniques have allowed the measurement of surface coverage, layer structural parameters, water content, and viscoelastic properties of the protein layers (Escorihuela *et al.* 2015). The combination of DPI and QCM-D could be used to study particle: membrane interactions as the use of DPI can provide details on structural changes to the membrane (Escorihuela *et al.* 2015).

6.8 Conclusion

This study aimed to investigate if alumina and CoCr particles were able to damage or passively pass the cell membrane with adverse consequences. Nanoscale and micron sized alumina and CoCr particles were characterised using SEM, EDX and cell viability assays. Using QCM-D techniques the nanoscale and micron sized alumina and CoCr particles were revealed to not significantly bind to model lipid bilayers which mimicked the composition of the phospholipid membrane of fibroblasts. Using vesicle leakage assays, the particles were also observed to not induce membrane damage, even in the presence of 10% (v/v) FBS and the inclusion of membrane proteins within the model membrane.

Nevertheless differences in the cell viability of L929 fibroblasts cultured with alumina and CoCr particles was observed in the absence of serum. Nanoscale alumina and micron sized alumina particles in the absence of 10% (v/v) FBS, were revealed to have more of an effect on the cell viability in comparison to cells cultured in the presence of serum. Interestingly, the opposite was observed for CoCr particles, whereby the presence of 10% (v/v) FBS caused a more detrimental effect on cell viability. However, TEM analysis of sectioned cells cultured with nanoscale alumina and CoCr particles revealed no differences in particle uptake in the presence or absence of serum.

Further analysis using QCM-D and a lipid membrane containing fibroblast membrane proteins revealed that nanoscale and micron sized alumina particles did bind to the model membrane. This suggests that the formation of a protein corona and the presence of membrane proteins are integral for alumina particle binding, regardless of particle size. Furthermore, the effect on cell viability did not correlate to membrane binding. In contrast no particle binding was observed for the nanoscale and micron sized CoCr particles, thus suggesting that particle composition rather than size has a greater impact on the series of experiments used in this present study. Further investigation is required to determine how the CoCr particles interact with the cell plasma membrane and elicit cytotoxic effects.

6.8.1 Main conclusions

- Nanoscale and micron sized alumina and CoCr particles caused a reduction in viability of U937 and primary HFBs.
- Nanoscale and micron sized alumina and CoCr particles did not extensively damage the model membrane by producing pores within the membrane, even in presence of 10% (v/v) FBS.
- Nanoscale alumina and CoCr particles were internalised within L929 fibroblasts, at particle volumes of 5 μm^3 and 0.5 μm^3 per cell, respectively. This suggested that the particles do interact with the membrane in order to be taken up by the cells.
- No or weak interactions were detected for nanoscale and micron sized CoCr particles to model membranes of increasing complexity and in presence of 10% (v/v) FBS.
- Nanoscale and micron sized alumina particles were demonstrated to interact with the model membranes, consisting of 20% (v/v) isolated membrane proteins and in the presence of 10% (v/v) FBS at particle

concentrations of 10 and 100 μg.ml^{-1}. This key finding demonstrated that in order for alumina particles to interact with the cell membrane, a protein corona must form around the particles.

- Nanoscale and micron sized alumina and CoCr particles did not cause damage to the membrane and therefore do not contribute directly to particle toxicity.

References

Affatato, S., Taddei, P., Cartnignato, S., Modena, E. and Toni, A. 2012. Severe damage of alumina-on-alumina hip implants: Wear assessments at a microscopic level. *Journal of the European Ceramic Society*. **32**(14), pp.3647-3657.

Al-Hajjar, M., Fisher, J., Tipper, J.L., Williams, S. and Jennings, L.M. 2013a. Wear of 36-mm BIOLOX (R) delta ceramic-on-ceramic bearing in total hip replacements under edge loading conditions. *Proceedings of the Institution of Mechanical Engineers Part H-Journal of Engineering in Medicine*. **227**(H5), pp.535-542.

Al-Hajjar, M., Fisher, J., Williams, S., Tipper, J.L. and Jennings, L.M. 2013b. Effect of femoral head size on the wear of metal on metal bearings in total hip replacements under adverse edge-loading conditions. *Journal of Biomedical Materials Research Part B-Applied Biomaterials*. **101**B(2), pp.213-222.

Al-Hajjar, M., Jennings, L.M., Begand, S., Oberbach, T., Delfosse, D. and Fisher, J. 2013c. Wear of novel ceramic-on-ceramic bearings under adverse and clinically relevant hip simulator conditions. *Journal of Biomedical Materials Research Part B-Applied Biomaterials*. **101**(8), pp.1456-1462.

Al-Hajjar, M., Leslie, I.J., Tipper, J., Williams, S., Fisher, J. and Jennings, L.M. 2010. Effect of cup inclination angle during microseparation and rim loading on the wear of BIOLOX (R) delta ceramic-on-ceramic total hip replacement. *Journal of Biomedical Materials Research Part B-Applied Biomaterials.* **95B**(2), pp.263-268.

Alexander, J. and Aaseth, J. 1995. Uptake of chromate in human red-blood-cells and isolated rat-liver cells - the role of the anion carrier. *Analyst.* **120**(3), pp.931-933.

Amanatullah, D.F., Landa, J., Strauss, E.J., Garino, J.P., Kim, S.H. and Di Cesare, P.E. 2011. Comparison of surgical outcomes and implant wear between ceramic-ceramic and ceramic-polyethylene articulations in total hip arthroplasty. *Journal of Arthroplasty.* **26**(6), pp.72-77.

Andrews, R.E., Shah, K.M., Wilkinson, J.M. and Gartland, A. 2011. Effects of cobalt and chromium ions at clinically equivalent concentrations after metal-on-metal hip replacement on human osteoblasts and osteoclasts: Implications for skeletal health. *Bone*. **49**(4), pp.717-723.

Bagchi, D., Stohs, S.J., Downs, B.W., Bagchi, M. and Preuss, H.G. 2002. Cytotoxicity and oxidative mechanisms of different forms of chromium. *Toxicology.* **180**(1), pp.5-22.

Baldwin, E.L., Byl, J.a.W. and Osheroff, N. 2004. Cobalt enhances DNA cleavage mediated by human topoisomerase II alpha in vitro and in cultured cells. *Biochemistry*. **43**(3), pp.728-735.

Baxmann, M., Jauch, S.Y., Schilling, C., Blömer, W., Grupp, T.M. and Morlock, M.M. 2013. The influence of contact conditions and micromotions on the fretting behavior of modular titanium alloy taper connections. *Medical Engineering & Physics.* **35**(5), pp.676-683.

Behl, B., Papageorgiou, I., Brown, C., Hall, R., Tipper, J.L., Fisher, J. and Ingham, E. 2013. Biological effects of cobalt-chromium nanoparticles and ions on dural fibroblasts and dural epithelial cells. *Biomaterials.* **34**(14), pp.3547-3558.

Bell, D. and Garratt-Reed, A. 2003. Energy Dispersive X-ray Analysis in the Electron Microscope. Oxford: BIOS Science Publishing.

Berry, D. and Lieberman, J. 2013. *Surgery of the Hip.* Amsterdam: Elsevier Health Sciences.

Bessette, B., Fassier, F., Tanzer, M. and Brooks, C. 2003. Total hip arthroplasty in patients younger than 21 years: a minimum 10-year follow-up. Canadian *Journal of Surgery*. **46**(4), pp.257-262.

Bhabra, G., Sood, A., Fisher, B., Cartwright, L., Saunders, M., Evans, W.H., Surprenant, A., Lopez-Castejon, G., Mann, S., Davis, S.A., Hails, L.A., Ingham, E., Verkade, P., Lane, J., Heesom, K., Newson, R. and Case, C.P. 2009. Nanoparticles can cause DNA damage across a cellular barrier. *Nature Nanotechnology.* **4**(12), pp.876-883.

Billi, F., Benya, P., Kavanaugh, A., Adams, J., Ebramzadeh, E. and Mckellop, H. 2012a. The John Charnley Award: An Accurate and Sensitive Method to Separate, Display, and Characterize Wear Debris: Part 1: Polyethylene Particles. *Clinical Orthopaedics and Related Research.* **470**(2), pp.329-338.

Billi, F., Benya, P., Kavanaugh, A., Adams, J., Mckellop, H. and Ebramzadeh, E. 2012b. The John Charnley Award: An Accurate and Extremely Sensitive Method to

Separate, Display, and Characterize Wear Debris Part 2: Metal and Ceramic Particles. *Clinical Orthopaedics and Related Research*. **470**(2), pp.339-350.

Billi, F. and Campbell, P. 2010. Nanotoxicology of metal wear particles in total joint arthroplasty: a review of current concepts. *Journal of Applied Biomaterials & Biomechanics.* **8**(1), pp.1-6.

Blumenfeld, T.J., Bargar, W.L. and Campbell, P.A. 2010. A painful metal-on-metal total hip arthroplasty: a diagnostic dilemma. *The Journal of Arthroplasty.* **25**(7), pp.1168-1172.

Borgognoni, C.F., Mormann, M., Qu, Y., Schafer, M., Langer, K., Ozturk, C., Wagner, S., Chen, C.Y., Zhao, Y.L., Fuchs, H. and Riehemann, K. 2015. Reaction of human macrophages on protein corona covered TiO_2 nanoparticles. *Nanomedicine-Nanotechnology Biology and Medicine.* **11**(2), pp.275-282.

Brown, C., Fisher, J. and Ingham, E. 2006. Biological effects of clinically relevant wear particles from metal-on-metal hip prostheses. *Proceedings of the Institution of Mechanical Engineers Part H-Journal of Engineering in Medicine.* **220**(H2), pp.355-369.

Brown, C., Lacharme-Lora, L., Mukonoweshuro, B., Sood, A., Newson, R.B., Fisher, J., Case, C.P. and Ingham, E. 2013. Consequences of exposure to peri-articular injections of micro- and nano-particulate cobalt-chromium alloy. *Biomaterials.* **34**(34), pp.8564-8580.

Brown, C., Williams, S., Tipper, J.L., Fisher, J. and Ingham, E. 2007. Characterisation of wear particles produced by metal on metal and ceramic on metal hip prostheses under standard and microseparation simulation. *Journal of Materials Science-Materials in Medicine.* **18**(5), pp.819-827.

Caicedo, M.S., Samelko, L., Mcallister, K., Jacobs, J.J. and Hallab, N.J. 2013. Increasing both CoCrMo-alloy particle size and surface irregularity induces increased macrophage inflammasome activation in vitro potentially through lysosomal destabilization mechanisms. *Journal of Orthopaedic Research.* **31**(10), pp.1633-1642.

Campbell, P., Ebramzadeh, E., Nelson, S., Takamura, K., De Smet, K. and Amstutz, H.C. 2010. Histological Features of Pseudotumor-like Tissues From Metal-on-Metal Hips. *Clinical Orthopaedics and Related Research.* **468**(9), pp.2321-2327.

Canton, I. and Battaglia, G. 2012. Endocytosis at the nanoscale. *Chemical Society Reviews.* **41**(7), pp.2718-2739.

Case, C.P., Langkamer, V.G., James, C., Palmer, M.R., Kemp, A.J., Heap, P.F. and Solomon, L. 1994. Widespread dissemination of metal debris from implants. *Journal of Bone and Joint Surgery-British Volume.* **76B**(5), pp.701-712.

Castellanos, M.I., Zenses, A.S., Grau, A., Rodriguez-Cabello, J.C., Gil, F.J., Manero, J.M. and Pegueroles, M. 2015. Biofunctionalization of REDV elastin-like recombinamers improves endothelialization on CoCr alloy surfaces for cardiovascular applications. *Colloids and Surfaces B-Biointerfaces*. **127**, pp.22-32.

Catalani, S., Leone, R., Rizzetti, M.C., Padovani, A. and Apostoli, P. 2011. The role of albumin in human toxicology of cobalt: contribution from a clinical case. *ISRN Hematol*. 2011, 690620.

Catelas, I. 2011. New insights into wear and biological effects of metal-on-metal bearings. *Journal of Bone and Joint Surgery-American Volume*. **93A**(12), pp.1158-1158.

Catelas, I., Bobyn, J.D., Medley, J.B., Krygier, J.J., Zukor, D.J., Petit, A. and Huk, O.L. 2001a. Effects of digestion protocols on the isolation and characterization of metal-metal wear particles. I. Analysis of particle size and shape. *Journal of Biomedical Materials Research.* **55**(3), pp.320-329.

Catelas, I., Bobyn, J.D., Medley, J.J., Zukor, D.J., Petit, A. and Huk, O.L. 2001b. Effects of digestion protocols on the isolation and characterization of metal-metal wear particles. II. Analysis of ion release and particle composition. *Journal of Biomedical Materials Research*. **55**(3), pp.330-337.

Catelas, I., Petit, A., Marchand, R., Zukor, D.J., Yahia, L.H. and Huk, O.L. 1999. Cytotoxicity and macrophage cytokine release induced by ceramic and polyethylene particles in vitro. *Journal of Bone and Joint Surgery-British Volume*. **81B**(3), pp.516-521.

Catelas, I., Petit, A., Vali, H., Fragiskatos, C., Meilleur, R., Zukor, D.J., Antoniou, J. and Huk, O.L. 2005. Quantitative analysis of macrophage apoptosis vs. necrosis induced by cobalt and chromium ions in vitro. *Biomaterials.* **26**(15), pp.2441-2453.

Catelas, I., Petit, A., Zukor, D.J. and Huk, O.L. 2001c. Cytotoxic and apoptotic effects of cobalt and chromium ions on J774 macrophages - Implication of caspase-3 in the apoptotic pathway. Journal of Materials Science-Materials in Medicine. **12**(10-12), pp.949-953.

Caton, J. and Prudhon, J.L. 2011. Over 25 years survival after Charnley's total hip arthroplasty. *International Orthopaedics*. **35**(2), pp.185-188.

Champion, J.A., Katare, Y.K. and Mitragotri, S. 2007. Making polymeric micro- and nanoparticles of complex shapes. *Proceedings of the National Academy of Sciences of the United States of America*. **104**(29), pp.11901-11904.

Charnley, J. and Cupic, Z. 1973. Nine and ten year results of low-friction arthroplasty of hip. *Clinical Orthopaedics and Related Research*. **95**(1), pp.9-25.

Cheng, X., Tian, X., Wu, A., Li, J., Tian, J., Chong, Y., Chai, Z., Zhao, Y., Chen, C. and Ge, C. 2015. Protein Corona Influences Cellular Uptake of Gold Nanoparticles by Phagocytic and Nonphagocytic Cells in a Size-Dependent Manner. *ACS Appl Mater Interfaces*. **7**(37), pp.20568-20575.

Cho, N.J., Frank, C.W., Kasemo, B. and Hook, F. 2010. Quartz crystal microbalance with dissipation monitoring of supported lipid bilayers on various substrates. *Nature Protocols*. **5**(6), pp.1096-1106.

Churchman, A.H., Wallace, R., Milne, S.J., Brown, A.P., Brydson, R. and Beales, P.A. 2013. Serum albumin enhances the membrane activity of ZnO nanoparticles. *Chemical Communications*. **49**(39), pp.4172-4174.

Clarke, I.C., Good, V., Williams, P., Schroeder, D., Anissian, L., Stark, A., Oonishi, H., Schuldies, J. and Gustafson, G. 2000. Ultra-low wear rates for rigid-on-rigid bearings in total hip replacements. *Proceedings of the Institution of Mechanical Engineers Part H-Journal of Engineering in Medicine*. **214**(H4), pp.331-347.

Colognato, R., Bonelli, A., Ponti, J., Farina, M., Bergamaschi, E., Sabbioni, E. and Migliore, L. 2008. Comparative genotoxicity of cobalt nanoparticles and ions on human peripheral leukocytes in vitro. *Mutagenesis*. **23**(5), pp.377-382.

Cooper, H.J., Della Valle, C.J., Berger, R.A., Tetreault, M., Paprosky, W.G., Sporer, S.M. and Jacobs, J.J. 2012. Corrosion at the Head-Neck Taper as a Cause for Adverse

Local Tissue Reactions After Total Hip Arthroplasty. *Journal of Bone and Joint Surgery-American Volume*. **94A**(18), pp.1655-1661.

Crouch, S.P.M., Kozlowski, R., Slater, K.J. and Fletcher, J. 1993. The use of ATP bioluminescence as a measure of cell-proliferation and cytotoxicity. *Journal of Immunological Methods*. **160**(1), pp.81-88.

D'antonio, J.A., Capello, W.N. and Naughton, M. 2012. Ceramic Bearings for Total Hip Arthroplasty Have High Survivorship at 10 Years. *Clinical Orthopaedics and Related Research.* **470**(2), pp.373-381.

Dai, Q., Yan, Y., Ang, C., Kempe, K., Kamphuis, M., Dodds, S. and Caruso, F. 2015. Monoclonal antibody-functionalized multilayered particles: targetingcancer cells in the presence of protein coronas. *ACS Nano*. **9**(3), pp.2876-2885.

Daikhin, L., Gileadi, E., Tsionsky, V., Urbakh, M. and Zilberman, G. 2000. Slippage at adsorbate-electrolyte interface. Response of electrochemical quartz crystal microbalance to adsorption. *Electrochimica Acta*. **45**(22-23), pp.3615-3621.

Dalal, A., Pawar, V., Mcallister, K., Weaver, C. and Hallab, N.J. 2012. Orthopedic implant cobalt-alloy particles produce greater toxicity and inflammatory cytokines than titanium alloy and zirconium alloy-based particles in vitro, in human osteoblasts, fibroblasts, and macrophages. *Journal of Biomedical Materials Research Part A.* **100A**(8), pp.2147-2158.

Davda, K., Lali, F.V., Sampson, B., Skinner, J.A. and Hart, A.J. 2011. An analysis of metal ion levels in the joint fluid of symptomatic patients with metal-onmetal hip replacements. *Journal of Bone and Joint Surgery-British Volume*. **93B**(6), pp.738-745.

Davies, A.P., Willert, H.G., Campbell, P.A., Learmonth, I.D. and Case, C.P. 2005. An unusual lymphocytic perivascular infiltration in tissues around contemporary metal-on-metal joint replacements. *Journal of Bone and Joint Surgery-American Volume.* **87A**(1), pp.18-27.

De Haan, R., Pattyn, C., Gill, H.S., Murray, D.W., Campbell, P.A. and De Smet, K. 2008. Correlation between inclination of the acetabular component and metal ion levels in metal-on-metal hip resurfacing replacement. *Journal of Bone and Joint Surgery-British Volume.* **90B**(10), pp.1291-1297.

De Smet, K., De Haan, R., Calistri, A., Campbell, P.A., Ebramzadeh, E., Pattyn, C. and Gill, H.S. 2008. Metal Ion Measurement as a Diagnostic Tool to Identify Problems with Metal-on-Metal Hip Resurfacing. *Journal of Bone and Joint Surgery-American Volume*. **90A**, pp.202-208.

Deng, Z.J., Liang, M.T., Monteiro, M., Toth, I. and Minchin, R.F. 2011. Nanoparticle-induced unfolding of fibrinogen promotes Mac-1 receptor activation and inflammation. *Nature Nanotechnology*. **6**(1), pp.39-44.

Dixon, M.C. 2008. Quartz crystal microbalance with dissipation monitoring: enabling real-time characterization of biological materials and their interactions. *Journal of Biomolecular Techniques*. **19**(3), pp.151-158.

Dodd, C.E., Johnson, B.R.G., Jeuken, L.J.C., Bugg, T.D.H., Bushby, R.J. and Evans, S.D. 2008. Native E. coli inner membrane incorporation in solid-supported lipid bilayer membranes. *Biointerphases*. **3**(2), pp.FA59-FA67.

Doorn, P.F., Campbell, P.A., Worrall, J., Benya, P.D., Mckellop, H.A. and Amstutz, H.C. 1998. Metal wear particle characterization from metal on metal total hip replacements: Transmission electron microscopy study of periprosthetic tissues and isolated particles. *Journal of Biomedical Materials Research.* **42**(1), pp.103-111.

Dowson, D., Hardaker, C., Flett, M. and Isaac, G.H. 2004a. A hip joint simulator study of the performance of metal-on-metal joints - Part I: The role of materials. *Journal of Arthroplasty*. **19**(8), pp.118-123.

Dowson, D., Hardaker, C., Flett, M. and Isaac, G.H. 2004b. A hip joint simulator study of the performance of metal-on-metal joints - Part II: Design. *Journal of Arthroplasty.* **19**(8), pp.124-130.

Dowson, D. and Jin, Z.M. 2006. Metal-on-metal hip joint tribology. *Proceedings of the Institution of Mechanical Engineers Part H-Journal of Engineering in Medicine. 220*(H2), pp.107-118.

Duan, G., Kang, S.G., Tian, X., Garate, J.A., Zhao, L., Ge, C. and Zhou, R. 2015. Protein corona mitigates the cytotoxicity of graphene oxide by reducing its physical interaction with cell membrane. *Nanoscale.* **7**(37), pp.15214-15224.

Dunstan, E., Ladon, D., Whittingharn-Jones, P., Carrington, R. and Briggs, T.W. 2008. Chromosomal aberrations in the peripheral blood of patients with metal-on-metal hip bearings. *Journal of Bone and Joint Surgery-American Volume.* **90A**(3), pp.517-522.

Engh, C.A., Jr., Stepniewski, A.S., Ginn, S.D., Beykirch, S.E., Sychterz-Terefenko, C.J., Hopper, R.H., Jr. and Engh, C.A. 2006. A randomized prospective evaluation of outcomes after total hip arthroplasty using cross-linked marathon and non-cross-linked Enduron polyethylene liners. *Journal of Arthroplasty*. **21**(6), pp.17-25.

Engh Jr, C.A., Ho, H., Engh, C.A., Hamilton, W.G. and Fricka, K.B. 2010. Metal-on-metal total hip arthroplasty adverse local tissue reaction. *Seminars in Arthroplasty*. **21**(1), pp.19-23.

Escorihuela, J., Gonzalez-Martinez, M.A., Lopez-Paz, J.L., Puchades, R., Maquieira, A. and Gimenez-Romero, D. 2015. Dual-Polarization Interferometry: A Novel Technique To Light up the Nanomolecular World. *Chemical Reviews.* **115**(1), pp.265-294.

Esposito, C., Maclean, F., Campbell, P., Walter, W.L., Walter, W.K. and Bonar, S.F. 2013. Periprosthetic Tissues From Third Generation Alumina-on-Alumina Total Hip Arthroplasties. *Journal of Arthroplasty*. **28**(5), pp.860-866.

Esposito, C.I., Walter, W.L., Roques, A., Tuke, M.A., Zicat, B.A., Walsh, W.R. and Walter, W.K. 2012. Wear in alumina-on-alumina ceramic total hip replacements: a retrieval analysis of edge loading. *The Journal of Bone and Joint Surgery. British Volume*. **94**(7), pp.901-907.

Figgitt, M., Newson, R., Leslie, I.J., Fisher, J., Ingham, E. and Case, C.P. 2010. The genotoxicity of physiological concentrations of chromium (Cr(III) and Cr(VI)) and cobalt (Co(II)): An in vitro study. *Mutation Research/Fundamental and Molecular Mechanisms of Mutagenesis*. **688**(1–2), pp.53-61.

Firkins, P.J , Tipper, J.L., Ingham, E., Stone, M.H., Farrar, R., Fisher, J. 2001a. Influence of simulator kinematics on the wear of metal-on-metal hip prostheses. *Proceedings of the Institution Of Mechanical Engineers Part H-Journal of Engineering in Medicine.* **215**, pp 119-121.

Firkins, P.J., Tipper, J.L., Saadatzadeh, M.R., Ingham, E., Stone, M.H., Farrar, R. and Fisher, J. 2001b. Quantitative analysis of wear and wear debris from metal-on-metal

hip prostheses tested in a physiological hip joint simulator. *Bio-Medical Materials and Engineering.* **11**(2), pp.143-157.

Fisher, J. 1994. Wear of ultra high molecular weight polyethylene in total artificial joints. *Current Orthopaedics*. **8**(1), pp.164 - 169.

Fisher, J. 2011. Bioengineering reasons for the failure of metal-on-metal hip prostheses. An engineer's perspective. *Journal of Bone and Joint Surgery-British Volume.* **93B**(8), pp.1001-1004.

Fleischer, C.C. and Payne, C.K. 2014a. Nanoparticle-cell interactions: molecular structure of the protein corona and cellular outcomes. *Acc Chem Res.* **47**(8), pp.2651-2659.

Fleischer, C.C. and Payne, C.K. 2014b. Secondary structure of corona proteins determines the cell surface receptors used by nanoparticles. *J Phys Chem B.* **118**(49), pp.14017-14026.

Fleury, C., Petit, A., Mwale, F., Antoniou, J., Zukor, D.J., Tabrizian, M. and Huk, O.L. 2006. Effect of cobalt and chromium ions on human MG-63 osteoblasts in vitro: Morphology, cytotoxicity, and oxidative stress. *Biomaterials.* **27**(18), pp.3351-3360.

Franchi, L.P., Manshian, B.B., De Souza, T.A., Soenen, S.J., Matsubara, E.Y., Rosolen, J.M. and Takahashi, C.S. 2015. Cyto- and genotoxic effects of metallic nanoparticles in untransformed human fibroblast. *Toxicol In Vitro*. **29**(7), pp.1319-1331.

Fuller, K., Murphy, C., Kirstein, B., Fox, S.W. and Chambers, T.J. 2002. TNFa potently activates osteoclasts, through a direct action independent of and strongly synergistic with RANKL. *Endocrinology.* **143**(3), pp.1108-1118.

Garcia-Cimbrelo' E. Martinez-Sayanes, J. M., Minuesa, A., Munuera, L. 1996. Mittelmeier ceramic—ceramic prosthesis after 10 years. *The Journal of Arthroplasty*. **11**(7), pp 773-781.

Geraghty, R. J., Capes-Davis, A., Davis, J. M., Downward, J., Freshney, R., Knezevic, I., Lovell-Badge, R., Masters, R., Meredith, J., Stacey, G. N., Thraves, P., Vias, M. 2014. Guidelines for the use of cell lines in biomedical research. *British Journal of Cancer*. **111,** pp 1021–1046

Germain, M.A., Hatton, A., Williams, S., Matthews, J.B., Stone, M.H., Fisher, J. and Ingham, E. 2003. Comparison of the cytotoxicity of clinically relevant cobalt-chromium and alumina ceramic wear particles in vitro. *Biomaterials.* **24**(3), pp.469-479.

Gill, H.S., Grammatopoulos, G., Adshead, S., Tsialogiannis, E. and Tsiridis, E. 2012. Molecular and immune toxicity of CoCr nanoparticles in MoM hip arthroplasty. *Trends in Molecular Medicine*. **18**(3), pp.145-155.

Gillespie, W.J., Frampton, C.M.A., Henderson, R.J. and Ryan, P.M. 1988. The incidence of cancer following total hip-replacement. *Journal of Bone and Joint Surgery-British Volume.* **70**(4), pp.539-542.

Glaser, D., Komistek, R.D., Cates, H.E. and Mahfouz, M.R. 2008. Clicking and Squeaking: In Vivo Correlation of Sound and Separation for Different Bearing Surfaces. *Journal of Bone and Joint Surgery-American Volume*. **90A**, pp.112-120.

Goldberg, J.R. and Gilbert, J.L. 2003. In vitro corrosion testing of modular hip tapers. *Journal of Biomedical Materials Research Part B-Applied Biomaterials*. **64B**(2), pp.78-93.

Goode, A.E., Perkins, J.M., Sandison, A., Karunakaran, C., Cheng, H., Wall, D., Skinner, J.A., Hart, A.J., Porter, A.E., Mccomb, D.W. and Ryan, M.P. 2012. Chemical speciation of nanoparticles surrounding metal-on-metal hips. *Chemical Communications*. **48**(67), pp.8335-8337.

Grammatopoulos, G., Pandit, H., Kwon, Y.M., Gundle, R., Mclardy-Smith, P., Beard, D.J., Murray, D.W. and Gill, H.S. 2009. Hip resurfacings revised for inflammatory pseudotumour have a poor outcome. *Journal of Bone and Joint Surgery-British Volume.* **91B**(8), pp.1019-1024.

Granchi, D., Cenni, E., Ciapetti, G., Savarino, L., Stea, S., Gamberini, S., Gori, A. and Pizzoferrato, A. 1998. Cell death induced by metal ions: necrosis or apoptosis? *Journal of Materials Science-Materials in Medicine*. **9**(1), pp.31-37.

Granchi, D., Ciapetti, G., Amato, I., Pagani, S., Cenni, E., Savarino, L., Avnet, S., Peris, J.L., Pellacani, A., Baldini, N. and Giunti, A. 2004. The influence of alumina and ultra-high molecular weight polyethylene particles on osteoblast-osteoclast cooperation. *Biomaterials*. **25**(18), pp.4037-4045.

Granchi, D., Ciapetti, G., Stea, S., Savarino, L., Filippini, F., Sudanese, A., Zinghi, G. and Montanaro, L. 1999. Cytokine release in mononuclear cells of patients with Co-Cr hip prosthesis. *Biomaterials*. **20**(12), pp.1079-1086.

Green, R.J., Frazier, R.A., Shakesheff, K.M., Davies, M.C., Roberts, C.J. and Tendler, S.J.B. 2000. Surface plasmon resonance analysis of dynamic biological interactions with biomaterials. *Biomaterials.* **21**(18), pp.1823-1835.

Green, T.R., Fisher, J., Stone, M., Wroblewski, B.M. and Ingham, E. 1998. Polyethylene particles of a 'critical size' are necessary for the induction of cytokines by macrophages in vitro. *Biomaterials*. **19**(24), pp.2297-2302.

Gutwein, L.G. and Webster, T.J. 2004. Increased viable osteoblast density in the presence of nanophase compared to conventional alumina and titania particles. *Biomaterials.* **25**(18), pp.4175-4183.

Haddad, F. S., Thakrar, R. R., Hart, A. J., Skinner, J. A., Nargol, A., Nolan, J. F., Gill, H. S., Murray, D. W., Blom, A. W., Case, P. 2011. Metal-on-metal bearings: The evidence so far. *Journal of Bone and Joint Surgery-British Volume.* **93B**(5), pp 572-579.

Hallab, N., J. Jacobs, J. and Black, J. 2000a. Hypersensitivity to metallic biomaterials: a review of leukocyte migration inhibition assays. *Biomaterials.* **21**(13), pp.1301-1314.

Hallab, N., Mikecz, K., Vermes, C., Skipor, A. and Jacobs, J. 2000b. Differential lymphocyte reactivity to serum-derived metal–protein complexes produced from cobalt-based and titanium-based implant alloy degradation. *Journal Of Biomedical Materials Research*. **56**(3), pp.427-436.

Hallab, N.J., Anderson, S., Caicedo, M., Skipor, A., Campbell, P. and Jacobs, J.J. 2004. Immune responses correlate with serum-metal in metal-on-metal hip arthroplasty. *The Journal of Arthroplasty.* **19**(8), pp.88-93.

Hallab, N.J., Caicedo, M., Epstein, R., Mcallister, K. and Jacobs, J.J. 2010. In vitro reactivity to implant metals demonstrates a person-dependent association with both T-Cell and B-Cell activation. *Journal of Biomedical Materials Research Part A.* **92A**(2), pp.667-682.

Hannouche, D., Nich, C., Bizot, P., Meunier, A., Nizard, R., Sedel, L. 2003. Fractures of ceramic bearings. *Clinical Orthopaedics And Related Research*. **417**, pp. 19–26

Hart, A.J., Sabah, S., Henckel, J., Lewis, A., Cobb, J., Sampson, B., Mitchell, A. and Skinner, J.A. 2009. The painful metal-on-metal hip resurfacing. *Journal of Bone and Joint Surgery-British Volume.* **91B**(6), pp.738-744.

Hart, A.J., Satchithananda, K., Liddle, A.D., Sabah, S.A., Mcrobbie, D., Henckel, J., Cobb, J.P., Skinner, J.A. and Mitchell, A.W. 2012. Pseudotumors in Association with Well-Functioning Metal-on-Metal Hip Prostheses A Case-Control Study Using Three-Dimensional Computed Tomography and Magnetic Resonance Imaging. *Journal of Bone and Joint Surgery-American Volume.* **94A**(4), pp.317-325.

Hashimoto, M. and Imazato, S. 2015. Cytotoxic and genotoxic characterization of aluminum and silicon oxide nanoparticles in macrophages. *Dental Materials.* **31**(5), pp.556-564.

Hatton, A., Nevelos, J.E., Matthews, J.B., Fisher, J. and Ingham, E. 2003. Effects of clinically relevant alumina ceramic wear particles on TNF-alpha production by human peripheral blood mononuclear phagocytes. *Biomaterials.* **24**(7), pp.1193-1204.

Hatton, A., Nevelos, J.E., Nevelos, A.A., Banks, R.E., Fisher, J. and Ingham, E. 2002. Alumina-alumina artificial hip joints. Part I: a histological analysis and characterisation of wear debris by laser capture microdissection of tissues retrieved at revision. *Biomaterials.* **23**(16), pp.3429-3440.

Hauptfleisch, J., Pandit, H., Grammatopoulos, G., Gill, H.S., Murray, D.W. and Ostlere, S. 2012. A MRI classification of periprosthetic soft tissue masses (pseudotumours) associated with metal-on-metal resurfacing hip arthroplasty. *Skeletal Radiology*. **41**(2), pp.149-155.

Hedberg, Y. and Wallinder, O. 2014. Metal release and speciation of released chromium from a biomedical CoCrMo alloy into simulated physiologically relevant solutions. *J Biomed Mater Res B Appl Biomater*. **102**(4), pp.693-699.

Holding, C.A., Findlay, D.M., Stamenkov, R., Neale, S.D., Lucas, H., Dharmapatni, A.S.S.K., Callary, S.A., Shrestha, K.R., Atkins, G.J., Howie, D.W. and Haynes, D.R. 2006. The correlation of RANK, RANKL and TNF alpha expression with bone loss

volume and polyethylene wear debris around hip implants. *Biomaterials.* **27**(30), pp.5212-5219.

Horie, M., Nishio, K., Fujita, K., Endoh, S., Miyauchi, A., Saito, Y., Iwahashi, H., Yamamoto, K., Murayama, H., Nakano, H., Nanashima, N., Niki, E. and Yoshida, Y. 2009. Protein adsorption of ultrafine metal oxide and its influence on cytotoxicity toward cultured cells. *Chemical Research in Toxicology*. **22**(3), pp.543-553.

Hu, Z.Y., Zhang, H.Y., Zhang, Y., Wu, R.A. and Zou, H.F. 2014. Nanoparticle size matters in the formation of plasma protein coronas on Fe3O4 nanoparticles. *Colloids and Surfaces B-Biointerfaces*. **121**, pp.354-361.

Ingham, E. and Fisher, J. 2000. Biological reactions to wear debris in total joint replacement. *Proceedings of the Institution of Mechanical Engineers Part H-Journal of Engineering in Medicine*. **214**(H1), pp.21-37.

Ingham, E. and Fisher, J. 2005. The role of macrophages in osteolysis of total joint replacement. *Biomaterials*. **26**(11), pp.1271-1286.

Isaac, G.H., Thompson, J., Williams, S. and Fisher, J. 2006. Metal-on-metal bearings surfaces: materials, manufacture, design, optimization, and alternatives. *Proceedings of the Institution of Mechanical Engineers Part H-Journal of Engineering in Medicine*. **220**(H2), pp.119-133.

Janeway, C., Travers, P., Walport, M. and Shlomchik, M. 2005. Immunobiology. New York: Garland Science Publishing.

Jarrett, C.A., Ranawat, A.S., Bruzzone, M., Blum, Y.C., Rodriguez, J.A. and Ranawat, C.S. 2009. The Squeaking Hip: A Phenomenon of Ceramic-on-Ceramic Total Hip Arthroplasty. *Journal of Bone and Joint Surgery-American Volume*. **91A**(6), pp.1344-1349.

Jin, Z.M., Dowson, D. and Fisher, J. 1997. Analysis of fluid film lubrication in artificial hip joint replacements with surfaces of high elastic modulus. *Proceedings of the Institution of Mechanical Engineers Part H-Journal of Engineering in Medicine*. **211**(3), pp.247-256.

Jin, Z.M., Firkins, P., Farrar, R. and Fisher, J. 2000. Analysis and modelling of wear of cobalt-chrome alloys in a pin-on-plate test for a metal-on-metal total hip replacement.

Proceedings of the Institution of Mechanical Engineers Part H-Journal of Engineering in Medicine. **214**(H6), pp.559-568.

Jin, Z.M., Stone, M., Ingham, E. and Fisher, J. 2006. Biotribology. *Current Orthopaedics.* **20**(1), pp.32-40.

Jing, Y., Trfna, H., Persson, M., Kasemo, B. and Svedhem, S. 2014. Formation of supported lipid bilayers on silica: relation to lipid phase transition temperature and liposome size *Soft Matter*. **10**, pp 187 – 195.

Joyce, T.J., Langton, D.J. and Nargol, A.V.F. 2011. A study of the wear of explanted metal-on-metal resurfacing hip prostheses. *Tribology International*. **44**(5), pp.517-522.

Karlsson, H.L., Cronholm, P., Hedberg, Y., Tornberg, M., De Battice, L., Svedhem, S. and Wallinder, I.O. 2013. Cell membrane damage and protein interaction induced by copper containing nanoparticles--importance of the metal release process. *Toxicology.* **313**(1), pp.59-69.

Kaufman, A.M., Alabre, C.I., Rubash, H.E. and Shanbhag, A.S. 2008. Human macrophage response to UHMWPE, TiAlV, CoCr, and alumina particles: Analysis of multiple cytokines using protein arrays. *Journal of Biomedical Materials Research Part A*. **84A**(2), pp.464-474.

Korovessis, P., Petsinis, G., Repanti, M. and Repantis, T. 2006. Metallosis after contemporary metal-on-metal total hip arthroplasty - Five to nine-year follow-up. *Journal of Bone and Joint Surgery-American Volume*. **88A**(6), pp.1183-1191.

Kroll, A., Pillukat, M.H., Hahn, D. and Schnekenburger, J. 2009. Current in vitro methods in nanoparticle risk assessment: Limitations and challenges. European *Journal of Pharmaceutics and Biopharmaceutics*. **72**(2), pp.370-377.

Krpetic, Z., Porta, F., Caneva, E., Dal Santo, V. and Scari, G. 2010. Phagocytosis of Biocompatible Gold Nanoparticles. *Langmuir*. **26**(18), pp.14799-14805.

Krug, H.F. and Wick, P. 2011. Nanotoxicology: An Interdisciplinary Challenge. *Angewandte Chemie-International Edition*. **50**(6), pp.1260-1278.

Kubo, K., Clarke, I.C., Sorimachi, T., Williams, P.A., Donaldson, T.K., and Yamamato, K. 2009. Aggressive 3rd-body wear challenge to highly cross-linked polyethylene: A hip simulator model. *Wear.* **267**(5-8), pp.734-742.

Kunze, A., Zach, M., Svedhem, S. and Kasemo, B. 2011. Electrodeless QCM-D for lipid bilayer applications. *Biosensors & Bioelectronics*. **26**(5), pp.1833-1838.

Kuo, J. 2007. Electron microscopy, methods and protocols. 2nd Edition ed. Totowa, U.S.A: Humana Press.

Kwon, Y.-M., Ostlere, S.J., Mclardy-Smith, P., Athanasou, N.A., Gill, H.S. and Murray, D.W. 2011. "Asymptomatic" pseudotumors after metal-on-metal hip resurfacing arthroplasty. *Journal of Arthroplasty*. **26**(4), pp.511-518.

Kwon, Y.M., Glyn-Jones, S., Simpson, D.J., Kamali, A., Mclardy-Smith, P., Gill, H.S. and Murray, D.W. 2010. Analysis of wear of retrieved metal-on-metal hip resurfacing implants revised due to pseudotumours. *Journal of Bone and Joint Surgery-British Volume.* **92B**(3), pp.356-361.

Kwon, Y.M., Xia, Z., Glyn-Jones, S., Beard, D., Gill, H.S. and Murray, D.W. 2009. Dose-dependent cytotoxicity of clinically relevant cobalt nanoparticles and ions on macrophages in vitro. *Biomedical Materials*. **4**(2), pp.1-8.

Lalmohamed, A., MacGregor, A. J., de Vries, F., Leufkens, H. G. M., van Staa, T. 2013. Patterns of Risk of Cancer in Patients with Metal-onMetal Hip Replacements versus Other Bearing Surface Types: A Record Linkage Study between a Prospective Joint Registry and General Practice Electronic Health Records in England. *Plos One* **8**(7), pp 1 - 8

Landgraf, L., Christner, C., Storck, W., Schick, I., Krumbein, I., Dahring, H., Haedicke, K., Heinz-Herrmann, K., Teichgraber, U., Reichenbach, J.R., Tremel, W., Tenzer, S. and Hilger, I. 2015. A plasma protein corona enhances the biocompatibility of Au Fe3O4 Janus particles. *Biomaterials*. **68**, pp.77-88.

Langton, D.J., Jameson, S.S., Joyce, T.J., Gandhi, J.N., Sidaginamale, R., Mereddy, P., Lord, J. and Nargol, A.V.F. 2011. Accelerating failure rate of the ASR total hip replacement. J*ournal of Bone and Joint Surgery-British Volume.* **93B**(8), pp.1011-1016.

Langton, D.J., Jameson, S.S., Joyce, T.J., Hallab, N.J., Natu, S. and Nargol, A.V.F. 2010. Early failure of metal-on-metal bearings in hip resurfacing and large-diameter total hip replacement. A consequence of excess wear. *Journal of Bone and Joint Surgery-British Volume*. **92B**(1), pp.38-46.

Leslie, I., Williams, S., Isaac, G., Hatto, P., Ingham, E. and Fisher, J. 2013. Wear of surface-engineered metal-on-metal bearings for hip prostheses under adverse conditions with the head loading on the rim of the cup. *Proceedings of the Institution of Mechanical Engineers Part H-Journal of Engineering in Medicine.* **227**(H4), pp.345-349.

Leslie, I.J., Williams, S., Isaac, G., Ingham, E. and Fisher, J. 2009. High cup angle and microseparation increase the wear of hip surface replacements. *Clinical Orthopaedics and Related Research*. **467**(9), pp.2259-2265.

Lesniak, A., Fenaroli, F., Monopoli, M.R., Aberg, C., Dawson, K.A. and Salvati, A. 2012. Effects of the presence or absence of a protein corona on silica nanoparticle uptake and impact on cells. *ACS Nano*. **6**(7), pp.5845-5857.

Lesniak, A., Salvati, A., Santos-Martinez, M.J., Radomski, M.W., Dawson, K.A. and Aberg, C. 2013. Nanoparticle adhesion to the cell membrane and its effect on nanoparticle uptake efficiency. *J Am Chem Soc*. **135**(4), pp.1438-1444.

Lewis, A.C., Ladon, D., Heard, P.J., Peto, L. and Learmonth, I. 2007. The role of the surface chemistry of CoCr alloy particles in the phagocytosis and DNA damage of fibroblast cells. *Journal of Biomedical Materials Research Part A.* **82A**(2), pp.363-372.

Liu, A.Q., Richards, L., Bladen, C.L., Ingham, E., Fisher, J. and Tipper, J.L. 2015. The biological response to nanometre-sized polymer particles. *Acta Biomaterialia*. **23**, pp.38-51.

Lloyd, D.R., Carmichael, P.L. and Phillips, D.H. 1998. Comparison of the formation of 8-hydroxy-2 ’-deoxyguanosine and single- and double-strand breaks in DNA mediated by Fenton reactions. *Chemical Research in Toxicology.* **11**(5), pp.420-427.

Lombardi, A.V., Mallory, T.H., Dennis, D.A., Komistek, R.D., Fada, R.A. and Northcut, E.J. 2000. An in vivo determination of total hip arthroplasty pistoning during activity. *Journal of Arthroplasty*. **15**(6), pp.702-709.

Lord, J.K., Langton, D.J., Nargol, A.V.F. and Joyce, T.J. 2011. Volumetric wear assessment of failed metal-on-metal hip resurfacing prostheses. *Wear.* **272**(1), pp.79-87.

Lu, F., Royle, M., Lali, F.V., Hart, A.J., Collins, S., Housden, J. and Shelton, J.C. 2012. Simple isolation method for the bulk isolation of wear particles from metal on metal bearing surfaces generated in a hip simulator test. *Journal of Materials Science-Materials in Medicine*. **23**(4), pp.891-901.

Ma, Z.F., Bai, J. and Jiang, X.E. 2015. Monitoring of the enzymatic degradation of protein corona and evaluating the accompanying cytotoxicity of nanoparticles. *ACS Applied Materials & Interfaces.* **7**(32), pp.17614-17622.

Madl, A. K., Liong, M., Kovochich, M., Finley, B. L., Paustenbach, D. J., Oberdörster, G. 2015. Toxicology of wear particles of cobalt-chromium alloy metal-on-metal hip implants Part I: Physicochemical properties in patient and simulator studies. *Nanomedicine: Nanotechnology, Biology, and Medicine.* **11**, pp.1201-1215.

Mahadik, S.P., Mukherjee, S., Correnti, E.E., Kelkar, H.S., Wakade, C.G., Costa, R.M. and Scheffer, R. 1994. Plasma-membrane phospholipid and cholesterol distribution of skin fibroblasts from drug-naive patients at the onset of psychosis. *Schizophrenia Research*. **13**(3), pp.239-247.

Mahendra, G., Pandit, H., Kliskey, K., Murray, D., Gill, H.S. and Athanasou, N. 2009. Necrotic and inflammatory changes in metal-on-metal resurfacing hip arthroplasties Relation to implant failure and pseudotumor formation. *Acta Orthopaedica.* **80**(6), pp.653-659.

Mahmoudi, M., Lynch, I., Ejtehadi, M.R., Monopoli, M.P., Bombelli, F.B. and Laurent, S. 2011. Protein-Nanoparticle Interactions: Opportunities and Challenges. *Chemical Reviews*. **111**(9), pp.5610-5637.

Mall, N.A., Nunley, R.M., Zhu, J.J., Maloney, W.J., Barrack, R.L. and Clohisy, J.C. 2011. The incidence of acetabular osteolysis in young patients with conventional versus highly crosslinked polyethylene. *Clinical Orthopaedics and Related Research.* **469**(2), pp.372-381.

Malmström, J., Agheli, H., Kingshott, P. and Sutherland, D. 2007. Viscoelastic modelling of highly hydrated laminin layers at homogeneous and nanostructured

surfaces: quantification of protein layer properties using QCM-D and SPR. *Langmuir.* **23**(19), pp.9760-9768.

Masui, T., Sakano, S., Hasegawa, Y., Warashina, H. and Ishiguro, N. 2005. Expression of inflammatory cytokines, RANKL and OPG induced by titanium, cobalt-chromium and polyethylene particles. *Biomaterials.* **26**(14), pp.1695-1702.

Matthews, J., Green, T., Stone, M., Wroblewski, M., Fisher, J. and Ingham, E. 2000. Comparison of the response of primary human peripheral blood mononuclear phagocytes from different donors to challenge with model polyethylene particles of known size and dose. Biomaterials. **21**(20), pp.2033 - 2044.

Matthies, A.K., Skinner, J.A., Osmani, H., Henckel, J. and Hart, A.J. 2012. Pseudotumors are common in well-positioned low-wearing metal-on-metal hips. *Clinical Orthopaedics and Related Research*. **470**(7), pp.1895-1906.

Mbeh, D.A., Akhavan, O., Javanbakht, T., Mahmoudi, M. and Yahia, L.H. 2014. Cytotoxicity of protein corona-graphene oxide nanoribbons on human epithelial cells. *Applied Surface Science*. **320**, pp.596-601.

Mcdonnell, J.M. 2001. Surface plasmon resonance: towards an understanding of the mechanisms of biological molecular recognition. *Current Opinion in Chemical Biology.* **5**(5), pp.572-577.

McKellop, H., Park, S., Chiesa, R., Doorn, P., Lu, B., Normand, P., Grigoris, P., Amstutz, H. 1996 In vivo wear of 3 types of metal on metal hip prostheses during two decades of use. *Clinical Orthopaedics and Related Research.* **3298**, pp 128-140.

McMinn, D. 2012. The Birmingham Hip Resurfacing. [Online]. [Accessed 25th September]. Available from: http://www.mcminncentre.co.uk/birmingham-hip-resurfacing.html

Merritt, K. and Brown, S. A. 1995. Release of hexavalent chromium from corrosion of stainless steel and cobalt-chromium alloys. *Journal of Biomedical Materials Research.* **29**, pp 627-633.

Metikos-Hukovic, M. and Babic, R. 2007. Passivation and corrosion behaviours of cobalt and cobalt-chromium-molybdenum alloy. *Corrosion Science*. **49**(9), pp.3570-3579.

Meyer, H., Mueller, T., Goldau, G., Chamaon, K., Ruetschi, M. and Lohmann, C.H. 2012. Corrosion at the cone/taper interface leads to failure of large-diameter metal-on-metal total hip arthroplasties. *Clinical Orthopaedics and Related Research*. **470**(11), pp.3101-3108.

MHRA. 2010. Medical Device Alert: All metal-on-metal (MoM) hip replacements. [Online]. [Accessed 20th September 2015]. Available from: http://www.mhra.gov.uk/home/groups/dts-bs/documents/medicaldevicealert/con079162.pdf

MHRA. 2012. Medical Device Alert: All metal-on-metal (MoM) hip replacements (MDA/2012/036) [Online]. [Accessed 20th September]. Available from: http://www.mhra.gov.uk/home/groups/dts-bs/documents/medicaldevicealert/con155767.pdf

MHRA. 2015. Medical Safety Alert - Metal-on-metal (MoM) hip replacements - guidance on implantation and patient management. [Online]. [Accessed 5th November 2015]. Available from: https://www.gov.uk/drug-device-alerts/metal-on-metal-mom-hip-replacements-guidance-on-implantation-and-patient-management

Mirshafiee, V., Kim, R., Park, S., Mahmoudi, M. and Kraft, M.L. 2015. Impact of protein pre-coating on the protein corona composition and nanoparticle cellular uptake. *Biomaterials.* **75**, pp.295-304.

Mislick, K.A. and Baldeschwieler, J.D. 1996. Evidence for the role of proteoglycans in cation-mediated gene transfer. *Proceedings of the National Academy of Sciences of the United States of America*. **93**(22), pp.12349-12354.

Moisley, K. 2014. The effect of protein coronae of alumina and cobalt chromium wear particle cytotoxicity. BSc thesis, University of Leeds.

Monteiro-Riviere, N.A., Inman, A.O. and Zhang, L.W. 2009. Limitations and relative utility of screening assays to assess engineered nanoparticle toxicity in a human cell line. *Toxicology and Applied Pharmacology*. **234**(2), pp.222-235.

Morlock, M., Nassutt, R., Janssen, R., Willmann, G. and Honl, M. 2001. Mismatched wear couple zirconium oxide and aluminum oxide in total hip arthroplasty. *Journal of Arthroplasty*. **16**(8), pp.1071-1074.

Morlock, M., Bishop, N., Stahmer, F., Zustin, J., Breer, S., Sauter, G. Hahn, M., Krause, M., Rüther, W., Amling, M. Reasons for failure of hip resurfacing implants. A failure analysis based on 250 revision specimens *Orthopade,* **37** pp. 695-703.

Moyer, T. P. and Sierra, R. (Mayo Medical Laboratories) 2011. Evaluation of Metal-on-Metal Wear of Orthopedic Implants — Role of Serum Chromium and Cobalt Analysis. [Online]. [Acessed 10th February 2017]. Available from: http://www.mayomedicallaboratories.com/media/articles/features/metal-ortho/metal-ortho-implants.pdf

Mu, Q., Hondow, N., Kreminski, L., Brown, A., Jeuken, L. and Routledge, M. 2012. Mechanism of cellular uptake of genotoxic silica nanoparticles. *Particle and Fibre Toxicology*. **9**, pp.1-29.

Mu, Q.S., David, C.A., Galceran, J., Rey-Castro, C., Krzeminski, L., Wallace, R., Bamiduro, F., Milne, S.J., Hondow, N.S., Brydson, R., Vizcay-Barrena, G., Routledge, M.N., Jeuken, L.J.C. and Brown, A.P. 2014. Systematic investigation of the physicochemical factors that contribute to the toxicity of ZnO nanoparticles. *Chemical Research in Toxicology*. **27**(4), pp.558-567.

Natu, S., Sidaginamale, R.P., Gandhi, J., Langton, D.J. and Nargol, A.V.F. 2012. Adverse reactions to metal debris: histopathological features of periprosthetic soft tissue reactions seen in association with failed metal on metal hip arthroplasties. *Journal of Clinical Pathology*. **65**(5), pp.409-418.

Naumann, R.L.C., Nowak, C. and Knoll, W. 2011. Proteins in biomimetic membranes: promises and facts. *Soft Matter*. **7**(20), pp.9535-9548.

Nel, A.E., Madler, L., Velegol, D., Xia, T., Hoek, E.M.V., Somasundaran, P., Klaessig, F., Castranova, V. and Thompson, M. 2009. Understanding biophysicochemical interactions at the nano-bio interface. *Nature Materials.* **8**(7), pp.543-557.

Nevelos, J., Ingham, E., Doyle, C., Streicher, R., Nevelos, A., Walter, W. and Fisher, J. 2000. Microseparation of the centers of alumina-alumina artificial hip joints during simulator testing produces clinically relevant wear rates and patterns. *Journal of Arthroplasty*. **15**(6), pp.793-795.

Nevelos, J.E., Ingham, E., Doyle, C., Fisher, J. and Nevelos, A.B. 1999. Analysis of retrieved alumina ceramic components from Mittelmeier total hip prostheses. *Biomaterials*. **20**(19), pp.1833-1840.

Nevelos, J.E., Ingham, E., Doyle, C., Nevelos, A.B. and Fisher, J. 2001. The influence of acetabular cup angle on the wear of "BIOLOX Forte" alumina ceramic bearing couples in a hip joint simulator. *Journal of Materials Science-Materials in Medicine*. **12**(2), pp.141-144.

Niche, C., Ali, E.-H.S., Hannouche, D., Nizard, R., Witvoet, J., Sedel, L. and Bizot, P. 2006. Long-term results of alumina-on-alumina hip arthroplasty for osteonecrosis. *Clinical Orthopaedics and Related Research*. **442**, pp.283-283.

NJR. 2011. National Joint Registry for England and Wales, 8th annual report [Online]. [Accessed 23rd August 2012]. Available from: http://www.njrcentre.org.uk/NjrCentre/Portals/0/Documents/NJR%208th%20Annual%20Report%202011.pdf

NJR. 2015. National Joint Registry for England and Wales, 12th annual report. [Online]. [Accessed 23rd August 2016]. Available from: http://www.njrcentre.org.uk/njrcentre/Portals/0/Documents/England/Reports/12th%20annual%20report/NJR%20Online%20Annual%20Report%202015.pdf

O'Brien, T. 2003. Complexities of chromium carcinogenesis: role of cellular response, repair and recovery mechanisms. *Mutation Research/Fundamental and Molecular Mechanisms of Mutagenesis.* **533**(1-2), pp.3-36.

Oberdorster, G., Stone, V. and Donaldson, K. 2007. Toxicology of nanoparticles: A historical perspective. *Nanotoxicology.* **1**(1), pp.2-25.

Olsson, A.L.J., Van Der Mei, H.C., Johannsmann, D., Busscher, H.J. and Sharma, P.K. 2012. Probing Colloid-Substratum Contact Stiffness by Acoustic Sensing in a Liquid Phase. *Analytical Chemistry*. **84**(10), pp.4504-4512.

Owen, D.H., Russell, N.C., Smith, P.N. and Walter, W.L. 2014. An estimation of the incidence of squeaking and revision surgery for squeaking in ceramic-on-ceramic total hip replacement A meta-analysis and report from the australian orthopaedic association national joint registry. *Bone & Joint Journal*. **96B**(2), pp.181-187.

Pandit, H., Glyn-Jones, S., Mclardy-Smith, P., Gundle, R., Whitwell, D., Gibbons, C.L.M., Ostlere, S., Athanasou, N., Gill, H.S. and Murray, D.W. 2008. Pseudotumours associated with metal-onmetal hip resurfacings. *Journal of Bone and Joint Surgery-British Volume*. **90B**(7), pp.847-851.

Papageorgiou, I., Abberton, T., Fuller, M., Tipper, J.L., Fisher, J. and Ingham, E. 2014. Biological effects of clinically relevant cocr nanoparticles in the dura mater: An organ culture study. *Nanomaterials*. **4**(2), pp.485-504.

Papageorgiou, I., Brown, C., Schins, R., Singh, S., Newson, R., Davis, S., Fisher, J., Ingham, E. and Case, C.P. 2007a. The effect of nano- and micron-sized particles of cobalt-chromium alloy on human fibroblasts in vitro. *Biomaterials*. **28**(19), pp.2946-2958.

Papageorgiou, I., Yin, Z.R., Ladon, D., Baird, D., Lewis, A.C., Sood, A., Newson, R., Learmonth, I.D. and Case, C.P. 2007b. Genotoxic effects of particles of surgical cobalt chrome alloy on human cells of different age in vitro. *Mutation Research-Fundamental and Molecular Mechanisms of Mutagenesis*. **619**(1-2), pp.45-58.

Parry, M.C., Bhabra, G., Sood, A., Machado, F., Cartwright, L., Saunders, M., Ingham, E., Newson, R., Blom, A.W. and Case, C.P. 2010. Thresholds for indirect DNA damage across cellular barriers for orthopaedic biomaterials. *Biomaterials*. **31**(16), pp.4477-4483.

Pearson, M.J., Williams, R.L., Floyd, H., Bodansky, D., Grover, L.M., Davis, E.T. and Lord, J.M. 2015. The effects of cobalt-chromium-molybdenum wear debris in vitro on serum cytokine profiles and T cell repertoire. *Biomaterials.* **67**, pp.232-239.

Peng, L., Zhang, H.W., Zhou, Y.F., Li, W.B., Jiang, P., Zhang, Y.E. and Song, K.G. 2015. TNF-alpha suppression and osteoprotegerin overexpression inhibits wear debris-induced inflammation and osteoclastogenesis in vitro. International *Journal of Artificial Organs*. **38**(10), pp.565-571.

Petit, A., Mwale, F., Tkaczyk, C., Antoniou, J., Zukor, D.J. and Huk, O.L. 2005. Induction of protein oxidation by cobalt and chromium ions in human U937 macrophages. *Biomaterials*. **26**(21), pp.4416-4422.

Petit, A., Mwale, F., Tkaczyk, C., Antoniou, J., Zukor, D.J. and Huk, O.L. 2006. Cobalt and chromium ions induce nitration of proteins in human U937 macrophages in vitro. *Journal of Biomedical Materials Research Part A*. **79A**(3), pp.599-605.

Polyzois, I., Nikolopoulos, D., Michos, I., Patsouris, E. and Theocharis, S. 2012. Local and systemic toxicity of nanoscale debris particles in total hip arthroplasty. *Journal of Applied Toxicology*. **32**(4), pp.255-269.

Posada, O.M., Gilmour, D., Tate, R.J. and Grant, M.H. 2014. CoCr wear particles generated from CoCr alloy metal-on-metal hip replacements, and cobalt ions stimulate apoptosis and expression of general toxicology-related genes in monocyte-like U937 cells. *Toxicology and Applied Pharmacology*. **281**(1), pp.125-135.

Posada, O.M., Tate, R.J. and Grant, M.H. 2015a. Effects of CoCr metal wear debris generated from metal-on-metal hip implants and Co ions on human monocyte-like U937 cells. *Toxicology in Vitro*. **29**(2), pp.271-280.

Posada, O.M., Tate, R.J. and Grant, M.H. 2015b. Toxicity of cobalt-chromium nanoparticles released from a resurfacing hip implant and cobalt ions on primary human lymphocytes in vitro. *Journal of Applied Toxicology*. **35**(6), pp.614-622.

Potnis, P.A., Dutta, D.K. and Wood, S.C. 2013. Toll-like receptor 4 signaling pathway mediates proinflammatory immune response to cobalt-alloy particles. *Cell Immunol*. **282**(1), pp.53-65.

Pozzi, D., Caracciolo, G., Capriotti, A.L., Cavaliere, C., La Barbera, G., Anchordoquy, T.J. and Lagana, A. 2015. Surface chemistry and serum type both determine the nanoparticle-protein corona. *Journal of Proteomics*. **119**, pp.209-217.

Raikar, U.S., Tangod, V.B., Mastiholi, B.M. and Fulari, V.J. 2011. Fluorescence quenching using plasmonic gold nanoparticles. *Optics Communications*. **284**(19), pp.4761-4765.

Rauch, J., Kolch, W., Laurent, S. and Mahmoudi, M. 2013. Big signals from small particles: regulation of cell signaling pathways by nanoparticles. *Chem Rev*. **113**(5), pp.3391-3406.

Rehmer, A., Bishop, N.E. and Morlock, M.M. 2012. Influence of assembly procedure and material combination on the strength of the taper connection at the head–neck junction of modular hip endoprostheses. *Clinical Biomechanics*. **27**(1), pp.77-83.

Rejman, J., Oberle, V., Zuhorn, I.S. and Hoekstra, D. 2004. Size-dependent internalization of particles via the pathways of clathrin-and caveolae-mediated endocytosis. *Biochemical Journal*. **377**, pp.159-169.

Renner, L., Faschingbauer, M., Schmidt-Braekling, T. and Boettner, F. 2016. Cobalt serum levels differ in well functioning Birmingham resurfacing and Birmingham modular THA. *Archives of Orthopaedic and Trauma Surgery*. **136**(5), pp.715-721.

Richter, R.P., Berat, R. and Brisson, A.R. 2006. Formation of solid-supported lipid bilayers: An integrated view. *Langmuir*. **22**(8), pp.3497-3505.

Rieker, C.B., Kottig, P., Schon, R., Windler, M. and Wyss, U.P. 1998. Clinical wear performance of metal-on-metal hip arthroplasties. *Alternative Bearing Surfaces in Total Joint Replacement*. pp.144-156.

Riordan, J., Alon, N., Buchwald, M. 1979. Plasma membrane lipids of human diploid fibroblasts from normal individuals and patients with cystic fibrosis. *Biochimica et Biophysics Acta*. **574**, pp.39-47.

Rose, S.F., Weaver, C.L., Fenwick, S.A., Horner, A. and Pawar, V.D. 2012. The effect of diffusion hardened oxidized zirconium wear debris on cell viability and inflammation-An in vitro study. *Journal of Biomedical Materials Research Part B-Applied Biomaterials*. **100B**(5), pp.1359-1368.

Roualdes, O., Duclos, M.E., Gutknecht, D., Frappart, L., Chevalier, J. and Hartmann, D.J. 2010. In vitro and in vivo evaluation of an alumina-zirconia composite for arthroplasty applications. *Biomaterials.* **31**(8), pp.2043-2054.

Sampson, B. and Hart, A. 2012. Clinical usefulness of blood metal measurements to assess the failure of metal-on-metal hip implants. *Annals of Clinical Biochemistry*. **49**, pp.118-131.

Sargeant, A. and Goswami, T. 2007. Hip implants – Paper VI – Ion concentrations. *Materials & Design*. **28**(1), pp.155-171.

Sariali, E., Lazennec, J.Y., Khiami, F. and Catonne, Y. 2009. Mathematical evaluation of jumping distance in total hip arthroplasty Influence of abduction angle, femoral head offset, and head diameter. *Acta Orthopaedica*. **80**(3), pp.277-282.

Sariali, E., Veysi, V. and Stewart, T. 2008. Biomechanics of the human hip - consequences for total hip replacement. *Current Orthopaedics*. **22**(6), pp.371-375.

Sauerbrey, G. 1959. Verwendung von schwingquarzen zur wagung dunner schichten und zur mikrowagung. *Zeitschrift Fur Physik*. **155**(2), pp.206-222.

Schmalzried, T.P. and Callaghan, J.J. 1999. Wear in total hip and knee replacements. *Journal of Bone and Joint Surgery-American Volume*. **81A**(1), pp.115-136.

Schroeder, F., Goetz, I. and Roberts, E. 1984. Age-related alterations in cultured human fibroblast membrane-structure and function. *Mechanisms of Ageing and Development*. **25**(3), pp.365-389.

Serro, A.P., Degiampietro, K., Colaco, R. and Saramago, B. 2010. Adsorption of albumin and sodium hyaluronate on UHMWPE: A QCM-D and AFM study. *Colloids and Surfaces B-Biointerfaces*. **78**(1), pp.1-7.

Shang, L. and Nienhaus, G.U. 2015. Metal nanoclusters: Protein corona formation and implications for biological applications. *Int J Biochem Cell Biol*. **75**, pp.175-179.

Shishido, T., Yamamoto, K., Tanaka, S., Masaoka, T., Clarke, I.C. and Williams, P. 2006. A study for a retrieved implant of ceramic-on-ceramic total hip arthroplasty. *Journal of Arthroplasty*. **21**(2), pp.294-298.

Sidaginamale, R. P., Joyce, T. J., Lord, J. K., Jefferson, R., Blain, P. G., Nargol, A. V. F., Langton D. J. 2013. Blood metal ion testing is an effective screening tool to identify poorly performing metal-on-metal bearing surfaces. *Bone & Joint Research.* **2**(5), pp 84-95.

Sieber, H.P., Rieker, C.B. and Kottig, P. 1999. Analysis of 118 second-generation metal-on-metal retrieved hip implants. *Journal of Bone and Joint Surgery-British Volume*. **81B**(1), pp.46-50.

Simoes, T., Brown, A., Milne, S. and R., B. 2015. Bovine serum albumin binding to CoCrMo nanoparticles and the influence on dissolution. *Journal of Physics: Conference Series.* **644**, pp.1-4.

Simonsen, L.O., Brown, A.M., Harbak, H., Kristensen, B.I. and Bennekou, P. 2011. Cobalt uptake and binding in human red blood cells. *Blood Cells, Molecules, and Diseases.* **46**(4), pp.266-276.

Singh, G., Nuechtern, J.V., Meyer, H., Fiedler, G.M., Awiszus, F., Junk-Jantsch, S., Bruegel, M., Pflueger, G. and Lohmann, C.H. 2015. Particle characterisation and cytokine expression in failed small-diameter metal-on-metal total hip arthroplasties. *Bone & Joint Journal*. **97B**(7), pp.917-923.

Smith, I.O., Baumann, M.J. and Mccabe, L.R. 2004. Electrostatic interactions as a predictor for osteoblast attachment to biomaterials. *J Biomed Mater Res A.* **70**(3), pp.436-441.

Smith, S.L., Dowson, D. and Goldsmith, A.a.J. 2001. The effect of femoral head diameter upon lubrication and wear of metal-on-metal total hip replacements. *Proceedings of the Institution of Mechanical Engineers Part H-Journal of Engineering in Medicine*. **215**(H2), pp.161-170.

Soenen, S.J., Rivera-Gil, P., Montenegro, J.-M., Parak, W.J., De Smedt, S.C. and Braeckmans, K. 2011. Cellular toxicity of inorganic nanoparticles: Common aspects and guidelines for improved nanotoxicity evaluation. *Nano Today*. **6**(5), pp.446-465.

Sood, A., Salih, S., Roh, D., Lacharme-Lora, L., Parry, M., Hardiman, B., Keehan, R., Grummer, R., Winterhager, E., Gokhale, P.J., Andrews, P.W., Abbott, C., Forbes, K., Westwood, M., Aplin, J.D., Ingham, E., Papageorgiou, I., Berry, M., Liu, J., Dick, A.D., Garland, R.J., Williams, N., Singh, R., Simon, A.K., Lewis, M., Ham, J., Roger, L., Baird, D.M., Crompton, L.A., Caldwell, M.A., Swalwell, H., Birch-Machin, M., Lopez-Castejon, G., Randall, A., Lin, H., Suleiman, M.S., Evans, W.H., Newson, R. and Case, C.P. 2011. Signalling of DNA damage and cytokines across cell barriers exposed to nanoparticles depends on barrier thickness. *Nature Nanotechnology*. **6**(12), pp.824-833.

Stewart, T.D. 2010. Tribology of artificial joints. *Orthopaedics and Trauma.* **24**(6), pp.435-440.

Stewart, T.D., Tipper, J.L., Insley, G., Streicher, R.M., Ingham, E. and Fisher, J. 2003. Long-term wear of ceramic matrix composite materials for hip prostheses under severe swing phase microseparation. *Journal of Biomedical Materials Research Part B-Applied Biomaterials.* **66B**(2), pp.567-573.

Stockert, J.C., Blazquez-Castro, A., Canete, M., Horobin, R.W. and Villanueva, A. 2012. MTT assay for cell viability: Intracellular localization of the formazan product is in lipid droplets. *Acta Histochemica*. **114**(8), pp.785-796.

Tipper, J.L., Hatton, A., Nevelos, J.E., Ingham, E., Doyle, C., Streicher, R., Nevelos, A.B. and Fisher, J. 2002. Alumina-alumina artificial hip joints. Part II: Characterisation of the wear debris from in vitro hip joint simulations. *Biomaterials.* **23**(16), pp.3441-3448.

Tkaczyk, C., Huk, O.L., Mwale, F., Antoniou, J., Zukor, D.J., Petit, A. and Tabrizian, M. 2009. The molecular structure of complexes formed by chromium or cobalt ions in simulated physiological fluids. *Biomaterials.* **30**(4), pp.460-467.

Tkaczyk, C., Huk, O.L., Mwale, F., Antoniou, J., Zukor, D.J., Petit, A. and Tabrizian, M. 2010. Effect of chromium and cobalt ions on the expression of antioxidant enzymes in human U937 macrophage-like cells. *Journal of Biomedical Materials Research Part A.* **94A**(2), pp.419-425.

Trindade, M.C.D., Lind, M., Sun, D., Schurman, D.J., Goodman, S.B. and Smith, R.L. 2001. In vitro reaction to orthopaedic biomaterials by macrophages and lymphocytes isolated from patients undergoing revision surgery. *Biomaterials*. **22**(3), pp.253-259.

Tsaousi, A., Jones, E. and Case, C.P. 2010. The in vitro genotoxicity of orthopaedic ceramic (Al2O3) and metal (CoCr alloy) particles. *Mutation Research-Genetic Toxicology and Environmental Mutagenesis*. **697**(1-2), pp.1-9.

Underwood, R., Matthies, A., Cann, P., Skinner, J.A. and Hart, A.J. 2011. A comparison of explanted Articular Surface Replacement and Birmingham Hip Resurfacing components. *Journal of Bone and Joint Surgery-British Volume.* **93B**(9), pp.1169-1177.

Unger, R. E., Krump-Konvalinkova, V., Peters, K., Kirkpatrick, C.J. 2002. In Vitro Expression of the Endothelial Phenotype: Comparative Study of Primary Isolated Cells

and Cell Lines, Including the Novel Cell Line HPMEC-ST1.6R. *Microvascular Research.* **64**, pp 384–397.

Urban, R.M., Tomlinson, M.J., Hall, D.J. and Jacobs, J.J. 2004. Accumulation in liver and spleen of metal particles generated at nonbearing surfaces in hip arthroplasty. *Journal of Arthroplasty*. **19**(8), pp.94-101.

Van Der Veen, H.C., Reininga, I.H.F., Zijlstra, W.P., Boomsma, M.F., Bulstra, S.K. and Van Raay, J. 2015. Pseudotumour incidence, cobalt levels and clinical outcome after large head metal-on-metal and conventional metal-on-polyethylene total hip arthroplasty mid-term results of a randomised controlled trial. *Bone & Joint Journal*. **97B**(11), pp.1481-1487.

Vassiliou, K., Scholes, S.C. and Unsworth, A. 2007. Laboratory studies on the tribology of hard bearing hip prostheses: ceramic on ceramic and metal on metal. *Proceedings of the Institution of Mechanical Engineers Part H-Journal of Engineering in Medicine*. **221**(H1), pp.11-20.

Vidal, V. and Muñoz, I. 2011. Effect of physico-chemical properties of simulated body fluids on the electrochemical behaviour of CoCrMo alloy. *Electrochimica Acta*. **56**(24), pp.8239-8248.

Vincent, J.B. and Love, S. 2012. The binding and transport of alternative metals by transferrin. *Biochim Biophys Acta.* 1**820**(3), pp.362-378.

Virtanen, S., Milosev, I., Gomez-Barrena, E., Trebse, R., Salo, J. and Konttinen, Y.T. 2008. Special modes of corrosion under physiological and simulated physiological conditions. *Acta Biomaterialia*. **4**(3), pp.468-476.

Visuri, T., Pulkkinen, P., Paavolainen, P. and Pukkala, E. 2010. Cancer risk is not increased after conventional hip arthroplasty A nationwide study from the Finnish Arthroplasty Register with follow-up of 24,636 patients for a mean of 13 years. *Acta Orthopaedica*. **81**(1), pp.77-81.

Voet, D., Voet, J. and Pratt, C. 2013. Principles of Biochemistry. 4th edition ed. Hoboken: John Wiley & Sons Inc.

Voinova, M.V., Rodahl, M., Jonson, M. and Kasemo, B. 1999. Viscoelastic acoustic response of layered polymer films at fluid-solid interfaces: Continuum mechanics approach. *Physica Scripta*. **59**(5), pp.391-396.

Walter, L.R., Marel, E., Harbury, R. and Wearne, J. 2008. Distribution of chromium and cobalt ions in various blood fractions after resurfacing hip arthroplasty. *Journal of Arthroplasty*. **23**(6), pp.814-821.

Wei, Z.C., Chen, L.M., Thompson, D.M. and Montoya, L.D. 2014. Effect of particle size on in vitro cytotoxicity of titania and alumina nanoparticles. *Journal of Experimental Nanoscience*. **9**(6), pp.625-638.

Willert, H.G., Buchhorn, G., Gobel, D., Koster, G., Schaffner, S., Schenk, R. and Semlitsch, M. 1996. Wear behavior and histopathology of classic cemented metal on metal hip endoprostheses. *Clinical Orthopaedics and Related Research.* **329**, pp.160-186.

Willert, H.G., Buchhorn, G.H., Fayyazi, A., Flury, R., Windler, M., Koster, G. and Lohmann, C.H. 2005. Metal-on-metal bearings and hypersensitivity in patients with artificial hip joints - A clinical and histomorphological study. *Journal of Bone and Joint Surgery-American Volume.* **87A**(1), pp.28-36.

Williams, S., Al-Hajjar, M., Isaac, G.H. and Fisher, J. 2013. Comparison of ceramic-on-metal and metal-on-metal hip prostheses under adverse conditions. *Journal of Biomedical Materials Research Part B-Applied Biomaterials.* **101B**(5), pp.770-775.

Williams, S., Leslie, I., Isaac, G., Jin, Z., Ingham, E. and Fisher, J. 2008. Tribology and wear of metal-on-metal hip prostheses: Influence of cup angle and head position. *Journal of Bone and Joint Surgery-American Volume*. **90A**, pp.111-117.

Williams, S., Schepers, A., Isaac, G., Hardaker, C., Ingham, E., Van Der Jagt, D., Breckon, A. and Fisher, J. 2007. The 2007 Otto Aufranc Award - Ceramic-on-metal hip arthroplasties - A comparative in vitro and in vivo study. *Clinical Orthopaedics and Related Research*. **465**, pp.23-32.

Williams, S., Tipper, J.L., Ingham, E., Stone, M.H. and Fisher, J. 2003. In vitro analysis of the wear, wear debris and biological activity of surface-engineered coatings for use in metal-on-metal total hip replacements. *Proceedings of the Institution of Mechanical Engineers. Part H, Journal of Engineering in Medicine*. **217**(3), pp.155-163.

Witkiewicz-Kucharczyk, A. and Bal, W. 2006. Damage of zinc fingers in DNA repair proteins, a novel molecular mechanism in carcinogenesis. *Toxicology Letters.* **162**(1), pp.29-42.

Xia, Z., Kwon, Y.-M., Mehmood, S., Downing, C., Jurkschat, K. and Murray, D.W. 2011. Characterization of metal-wear nanoparticles in pseudotumor following metal-on-metal hip resurfacing. *Nanomedicine-Nanotechnology Biology and Medicine*. **7**(6), pp.674-681.

Yamamoto, A., Honma, R., Sumita, M. and Hanawa, T. 2004. Cytotoxicity evaluation of ceramic particles of different sizes and shapes. *Journal of Biomedical Materials Research Part A*. **68A**(2), pp.244-256.

Yan, Y., Gause, K.T., Kamphuis, M.M.J., Ang, C.S., O'brien-Simpson, N.M., Lenzo, J.C., Reynolds, E.C., Nice, E.C. and Caruso, F. 2013. Differential Roles of the Protein Corona in the Cellular Uptake of Nanoporous Polymer Particles by Monocyte and Macrophage Cell Lines. *ACS Nano*. **7**(12), pp.10960-10970.

Yan, Y., Neville, A. and Dowson, D. 2006. Understanding the role of corrosion in the degradation of metal-on-metal implants. *Proceedings of the Institution of Mechanical Engineers Part H-Journal of Engineering in Medicine*. **220**(H2), pp.173-181.

Yoshida, K., Morita, M. and Mishina, H. 2003. Cytotoxicity of metal and ceramic particles in different sizes*. International Journal Series C-Mechanical Systems Machine Elements and Manufacturing*. **46**(4), pp.1284-1289.

Zhang, S., Nelson, A. and Beales, P. A. 2012. Freezing or wrapping: The role of particle size in the mechanism of nanoparticle–biomembrane interaction. *Langmuir.* **28**(35), pp 12831–12837.

Appendix A

General Materials

Table 1: Chemicals & reagents used throughout this study

Chemical	Catalogue number	Supplier
3-(4,5-dimethylthiazol-2-yl)-2, 5-diphenyltetrazolium bromide (MTT)	M2128	Sigma-Aldrich, Irvine, U.K.
3-(N-morpholino) propanesulfonic acid (MOPS)	M0289	Sigma-Aldrich, Irvine, U.K.
Adenosine triphosphate (ATP) luminescence assay detection kit (ATP-lite assay)	6016947	Perkin-Elmer, Cambridge, U.K.
Bicinchoninic protein assay kit	23225	Thermo Fisher Scientific, Langenselbold, Germany
Calcium chloride ($CaCl_2$)	BP510-100	Fisher Scientific, Loughborough, U.K.
Camptothecin	C9911	Sigma-Aldrich, Irvine, U.K.
Carbon dioxide	UN1030	Boc, Leeds, UK.
Carboxylfluorescein (CF)	21877	Sigma-Aldrich, Irvine, U.K.
Chloroform	C2432	Sigma-Aldrich, Irvine, U.K.
"Complete" protease inhibitor tablets	1836145	Roche, Mannheim, Germany
Detergent (multi-purpose)	0001	Teepol, Dublin, Ireland.
Dimethyl sulphoxide (DMSO)	D26650	Sigma-Aldrich, Irvine, U.K.
Dithiothreitol (DTT)	Plus one 17-1318-01	G.E. Healthcare, Piscataway, U.S.A.
Dulbecco's modified eagles medium (DMEM) without L- glutamine	D6546	Sigma-Aldrich, Irvine, U.K.
Dulbecco's modified eagles medium (DMEM) without phenol red	BC12-(17F)	Lonza, Castleford, U.K.
Dulbecco's phosphate buffer solution (DPBS) without Ca^{2+}/Mg^{2+}	D8537	Sigma-Aldrich, Irvine, U.K.
Dulbecco's phosphate buffer tablets	BR0014G	Oxoid, Basingstoke, U.K.

Chemical	Catalogue number	Supplier
Ethanol, absolute	E/0650DE/17	Thermo Fisher Scientific, Langenselbold, Germany.
Ethylenediaminetetraacetic acid (EDTA)	E/P140/53	Fisher Scientific, Loughborough, U.K.
Foetal bovine serum (FBS)	EU-000	Sigma-Aldrich, Irvine, U.K.
Hydrochloric acid (HCl) (12 M)	H/1200/PB17	Thermo Fisher Scientific Ltd, Langenselbold, Germany.
Isopropanol	10722295	Fisher Scientific, Loughborough, U.K.
L-glutamine (200 mM)	G7513	Sigma-Aldrich, Irvine, U.K.
Methanol	GPS1004-G	Atom Scientific Ltd., Manchester, U.K.
Nitrogen Gas	UN1066	Boc, Leeds, U.K.
Penicillin (5000 U)/ Streptomycin (5 mg.ml^{-1})	P4458	Sigma-Aldrich, Irvine, U.K.
Phenylmethanesulfonylfluoride (PMSF)	P7626	Sigma-Aldrich, Irvine, U.K.
Roswell Park Memorial Institute (RPMI) 1640 medium	R0883	Sigma-Aldrich, Irvine, U.K.
Sodium dodecyl sulphate (SDS)	L3771	Sigma-Aldrich, Irvine, U.K.
Sodium hydroxide	S8045	Sigma-Aldrich, Irvine, U.K.
Sodium sulphate	239313	Sigma-Aldrich, Irvine, U.K.
Sterile water	UKF7114	Baxter
Sucrose	57-50-1	Melford Laboratories Ltd., Ipswich, U.K.
Trigene	TR106	MediChem International, Sevenoaks, U.K.
Tris	32005	Melford Laboratories Ltd., Ipswich, U.K.
Triton X-100	9002-93-1	Sigma-Aldrich, Irvine, U.K.

Chemical	Catalogue number	Supplier
Trypsin- EDTA	T3924	Sigma-Aldrich, Irvine, U.K.

Table 2: Computer software used throughout this study

Computer software	Version	Supplier
AMT602 TEM imaging software	6	Advanced Microscopy Techniques, Bury St. Edmunds, U.K.
AZtec EDX analysis software	2	Oxford Instruments, Abington, U.K.
BIAevaluation SPR analysis software	3.1	BIAcore
FL Win Lab	4.0	Perkin Elmer, Cambridge, U.K.
Image Pro-Plus particle characterisation software	6.1	Media Cybernetics
Microsoft Office	2010	Microsoft, Redmond, U.S.A.
MikroWin 2000 Luminescence plate reader software	-	Microtek Laborsysteme GmBH, Overath, Germany
Origin Software	8	OriginLab Corporation, Northampton, U.S.A
Q soft software	4.1	Biolin Scientific, Stockholm, Sweden
Q tools modelling software	3.1	Biolin Scientific, Stockholm, Sweden
ScanIt MSS	2.1	AmsterCHEM, Almería, Spain.
Spekwin 32	1.71.6.1	Spekwin 32, Berchtesgaden, Germany

Table 3: General consumables and plasticware used throughout this study

Equipment	Model	Supplier
Automatic pipette tip (5 ml)	0030.089.669	Eppendorf, Stevenage, U.K.

Equipment	Model	Supplier
Bijous	856412-2	Scientific Laboratory Supplies Ltd., Nottingham, U.K.
Cell culture flasks	T75 cm^2: 156499 T175 cm^2: 156472 T25 cm^2: 156367	Thermo Fisher Scientific Ltd, Langenselbold, Germany.
Cell scraper	541070	Greiner Bio-One, Stonehouse, U.K.
Column, G-25 size exclusion column	17-0853-01	GE Healthcare, Chalfort, U.K.
Cyrovials	72.380.992	Sarstedt Ltd. Leicester, U.K.
Eppendorf tubes (1.5 ml)	72.690	Sarstedt Ltd. Leicester, U.K.
Extruder filter support	610014	Avanti Polar Lipids, Inc. Alabaster, U.S.A.
Falcon tubes, sterile (15 & 50 ml)	15 ml: 62.547.254 50 ml: 62.554.502	Sarstedt Ltd. Leicester, U.K.
Filter unit, sterile, single use (0.22 µm)	SLGPM33RS	Merck Millipore, Cork, Ireland.
Glass 8 well slides	803711	Thermo Fisher Scientific Ltd, Langenselbold, Germany.
Inoculation loops (sterile)	731171	Greiner Bio-one, Stonehouse, U.K.
Microplate adhesive sealing film	6050195	PerkinElmer, Windsor, U.K.
Microplates, Nunc® (96-well, flat bottom)	167008	Thermo Fisher Scientific Ltd, Langenselbold, Germany.
Microplates, Nunc® (96-well,U-shaped bottom)	167008	Thermo Fisher Scientific Ltd, Langenselbold, Germany.
Optiplate™ plate	96well	PerkinElmer, Windsor, U.K.
Pasteur pipettes	6121681	VWR International, Radnor, U.S.A
Pipette tips (10 µl, 20 µl, 200 µl, 1000 µl)	10 µl: S112-3810 20 µl: S1122 - 1830 200 µl: S1122-8810 1000 µl: S1122-1830	Starlab, Ahrensburg, Germany

Equipment	Model	Supplier
Polycarbonate filter membranes (0.015 µm, 0.1 µm, 0.4 µm, 0.8 µm, 1 µm, 10 µm)	Cyclopore™ Track Etch Membrane 0.015 µm: 110601 0.1 µm: 7060-4701 0.4 µm: 7060-2504 0.8 µm: 7060-2508 1 µm: 111110 10 µm: 111115	Whatman, Maidstone, U.K.
Polycarbonate thin walled ultracentrifuge tubes (14 ml)	331302	Beckmann Coulter, High Wycombe, U.K.
Serological pipette tips	5 ml: 86.1253.001 10 ml: 86.1254.001 25 ml: 86.1685.001	Sigma-Aldrich, Irvine, U.K.
Sterile containers	60 ml: 13E17RA024 150 ml: 15D45RD004 250 ml: 15F39RD014	Scientific Laboratory Supplies Ltd., Nottingham, U.K.
Universals	0991055-1	Scientific Laboratory Supplies Ltd., Nottingham, U.K.

Table 4: General equipment used throughout this study

Equipment	Model	Supplier
Automatic pipette dispenser	Multipette® stream	Eppendorf Ltd, Stevenage, U.K.
Automatic Pipette (Pipetboy®)	Ergo One®	Starlab, Milton Keynes, U.K.
Balance (Accuracy: 10 µg)	XP205	Mettler-Toledo Ltd, Leicester, U.K.
Balance (Accuracy: 1 µg)	AT21	Mettler-Toledo Ltd, Leicester, U.K.
Ball bearing homogeniser	Isobiotec	Isobiotec, Heidelberg, Germany
Extruder	610023	Avanti Polar Lipids, Inc. Alabaster, Alabama, U.K.
Bench top centrifuge	5415R	Eppendorf Ltd, Stevenage, U.K.
Carbon sputter coater	Q150TE	Quorum Technologies Ltd, Lewes, U.K.

Equipment	Model	Supplier
Cell culture centrifuge	MSE Mistral 3000i	MSE Scientific Instruments, London, U.K.
Class I laminar flow hood	-	Bassaire, Southampton, U.K.
Class II laminar flow hood	Herasafe HS18	Heraeus Instruments, Hanau, Germany
Dessicator, vacuum	DWA215	SciLabware Ltd., Stone, U.K.
Distilled water reservoir and filter	ELGA, Reservoir 75l	ELGA, High Wycombe, U.K.
Energy-dispersive X-ray spectroscopy (EDX) for both SEM and TEM analysis	Inca EDX system	Oxford Instruments, Abington, U.K.
Extruder	610023	Avanti Polar Lipids, Inc. Alabaster, Alabama, U.K.
Fluorescent plate reader	Multiskan Spectrum	Thermo Labsystems, Helsinki, Finland.
Fluorescence spectrometer	LS 55	Perkin-Elmer, Cambridge, U.K
Freezer (-20°C)	Electrolux	Jencons Plc, East Grinstead, U.K.
Freezer (-80°C)	MDF-U2086S	Sanyo, Watford, U.K.
Fridge	Electrolux ER8817C	Jencons Plc, East Grinstead, U.K.
Fume hood	-	Whitely Fume Extraction Solutions Ltd, Bradford, U.K.
Haemocytometer	Neubauer Improved	Optik Labor, Lancing, U.K.
High speed centrifuge	Sorvall® Evolution RC	Kendo Laboratory Products, Lagenselbold, Germany.
High speed centrifuge rotor	Sorvall® Evolution RC (SS-34)	Kendo Laboratory Products, Lagenselbold, Germany.
Human class II laminar flow hood	NU-437-600E	Nuaire
Infra-red heat lamp	A-138P	Philips®, Gilford, U.K.
Ion stream	Stat-Attack 1B-8	Amersham International Ltd., Amersham, U.K.
Light microscope	CK40	Olympus Optical Company, London, U.K.

Equipment	Model	Supplier
Luminescent plate reader	Chameleon	Hidex, Turku, Finland
Magnetic stirrer	Stuart SB161	Scientific Laboratory Supplies Ltd., Nottingham, U.K.
Microbalance (Accuracy: 1 µg)	AT21 Mettler	Sarotorius, Goettingen, Germany
Oven (hot air)	OMT225	Genlab, Widnes, U.K.
Peristaltic pump	ISM935	IDEX Health & Science GmbH, Wertheim, Germany
pH metre	Jenway 3010	VWR International
Pipettes (10 µl, 20 µl, 200 µl, 1000 µl)	Finnpipette®	Thermo Labsystems, Franklin, U.S.A.
Plate reader, absorbance	Multiskan Spectrum	Thermo Labsystems, Franklin, U.S.A.
Plate shaker	Vari-Shaker®	Dynatech Ltd., Billinghurst, U.K.
Quartz crystals (silicon dioxide coated)	QSX303	Biolin Scientific, Stockholm, Sweden
Quartz crystal microbalance with dissipation	E4 series	Biolin Scientific, Stockholm, Sweden
Quartz glass cuvette (10 x 4 mm)	109.004F-QS	Hellma® Analytics, Southend-On-Sea, U.K.
Scanning electron microscope	Leo 1530	LEO Electron Microscopy Limited, Cambridge, U.K.
Sputter Coater and thickness monitor	B7341 & B7348, respectively	Agar Scientific Limited, Stanstead, U.K.
Transmission electron microscope	Jeol 1400	Jeol, Peabody, U.S.A.
Transmission electron microscope (for EDX analysis)	FEI Tecnai TF20	FEI, Hillsboro, USA
Ultracentirfuge	Optima L-90K	Beckmann Coulter, High Wycombe, U.K.
Ultracentrifuge rotar	SW40	Beckmann Coulter, High Wycombe, U.K.
Ultrapure distilled water reservoir	QEARD00R1	Merck Millipore, Cork, Ireland.

Equipment	Model	Supplier
Ultrasonicator	XB3	Grant Instruments Ltd., Shepreth, U.K.
UV – Ozone cleaning system	T10X10/0ES/E	UVOS Inc. Montgomeryville, U.S.A.
Vacuum pump	113Gc11BT4	Edwards, Clevedon, U.K.
Vortexer	Topmix FB15024	Fisher Scientific, Loroughborough, U.K.
Water bath	NE2-D	Clifton, Weston-Super-Mare, U.K.

Table 5: General Glassware used throughout this study

Equipment	Model	Supplier
25 mm glass filtration apparatus	16306	Sarotorius, Goettingen, Germany
47 mm glass filtration apparatus set	25710545	Duran Group, Wertheim am Main, Germany
Glass bijous	-	Faculty of Biological Sciences, University of Leeds, Leeds, U.K.
Glass Duran bottes with caps and pouring ring	100 ml: 21801245 500 ml: 21801365 1000 ml: 21801545	Duran Group, Wertheim am Main, Germany
Glass round bottom, short neck, flask and stopcock adaptor	Flask: FR500/3S Adaptor: MF11/3/SC	SciLabware Ltd., Stone, U.K.
Glass syringe (0.2 ml)	1359-01/02	Avanti Polar Lipids, Inc. Alabaster, Alabama, U.K.
Glass syringe (1 ml)	81365	Avanti Polar Lipids, Inc. Alabaster, Alabama, U.K.
Glass universals	-	Faculty of Biological Sciences, University of Leeds, Leeds, U.K.
Glass vials (1.75 ml)	T101/V1	CamLab, Cambridge, U.K.
Glass vials (14 ml)	T102/V2	CamLab, Cambridge, U.K.

Appendix B

Calculating particle volumes

Cobalt chromium

Density of CoCr = 7.7 $g.cm^{-3}$ (Behl *et al.* 2013)

7.7 grams in 1 cm^3
7.7 x 10^{-12} grams in 1 μm^3
3.85 x 10^{-10} grams in 50 μm^3
3.85 x 10^{-4} µg in 50 μm^3 per cell

Therefore for 1 x 10^4 cells per well:
3.85 µg of particles is required to give a particle volume of 50 μm^3 per well.

Alumina wear particles

Density of alumina particles = 3.9 $g.cm^{-3}$ (according to manufacturer's specification: PlasmaChem, Germany and Cermatec, Germany).

3.9 grams in 1 cm^3
3.9 x 10^{-12} grams in 1 μm^3
1.95 x 10^{-9} grams in 500 μm^3
1.95 x 10^{-3} µg in 500 μm^3 per cell

Therefore for 1 x 10^4 cells per well:
19.5 µg of particles is required to give a particle volume of 500 μm^3 per well.

Appendix C

Quartz microbalance with dissipation preliminary results for solid supported bilayer lipid membrane in the presence of 10% (v/v) FBS

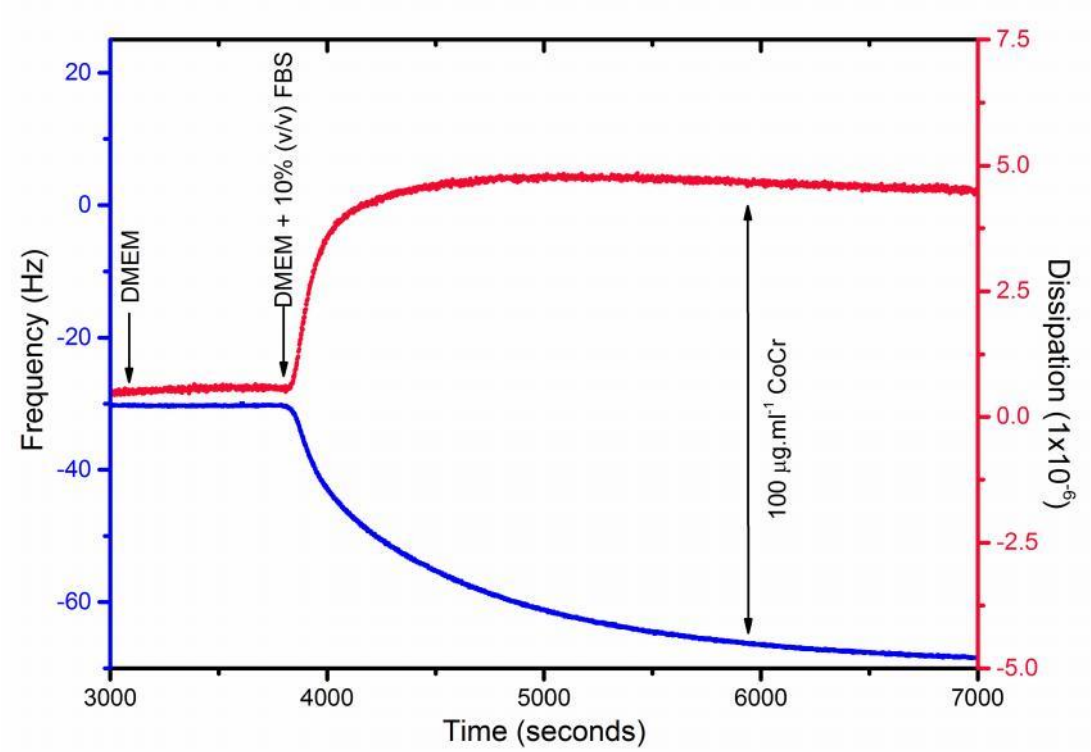

QCM-D plot of a solid supported bilayer lipid membrane in the presence nanoscale cobalt chromium particles and foetal bovine serum. A sBLM was formed in DMEM onto an oscillating quartz crystal followed by the addition of DMEM plus 10% (v/v) FBS. of CoCr nanoscale particles, at a concentration of 100 µg.ml^{-1} were diluted in DMEM plus FBS (10% v/v) were added at the time indicated by the arrows. Changes in the frequency (blue) and dissipation (red) were measured (ninth overtone is displayed).